

# Harvesting energy from high up

## Final report

Group 1

Technische Universiteit Delft



This page is intentionally left blank

# Harvesting energy from high up

## Final report

by

## Group 1

Tuesday January 28, 2020  
Delft (the Netherlands)

Project members:	T. P. S. (Thomas) Arblaster	4482468
	X. F. (Xander) van Beurden	4377001
	H.H.J. (Erik Jan) de Goeijen	4494784
	L. M. (Linde) de Klerk	4375904
	T. S. (Thomas) Lokken	4449282
	P. (Pranav) Madabhushi	4542894
	A. D. P. (Daam) Schoon	4561465
	M. G. M. (Mart) van de Ven	4456505
	W. A. J. G. (Wesley) de Vries	4296869
	R. M. (Richelle) Vrouwes	4285573
	C. F. (Caroline) van Winkel	4538226
Project duration:	November 11, 2019 – January 31, 2020	
Staff members:	Dr. S. J. Garcia	TU Delft, Tutor
	Dr. Ir. V. S. V. Dhanisetty	TU Delft, Coach
	G. Gonzalez Saiz MSc	TU Delft, Coach
	Dr. Ir. E. Mooij	TU Delft, OSCC
	Ir. J. M. Melkert	TU Delft, Course manager

Current version: 1.0

Version	Date	Rationale
1.0	22-01-2020	Draft

# Preface

This report is written in fulfillment of the Design Synthesis Exercise of the BSc Aerospace Engineering at TU Delft. From November 2019 to January 2020, the group has worked full-time to design a system that can harvest energy above the clouds. The project was executed under supervision of Dr. S.J. Garcia of TU Delft. Furthermore, it was mentored by Dr. V.S.V. Dhanisetty and G. Gonzalez Saiz, MSc. We thank them for their quick and accurate help throughout the entire project.

The *Baseline Report* (Arblaster et al. 2019a) shows an initial study in the field of energy harvesting and the setup of the project. After this, a trade-off process from three preliminary ideas to one design was fully worked out, in the *Midterm Report* (Arblaster et al. 2019b). Now, this report will focus on the design of the energy harvesting system, and will provide a description of the process which should follow to reach a full deployment phase.

We are thankful for all the help we received from various departments, both within and outside of TU Delft. In particular we want to thank Dr. R. Schmehl of TU Delft for all his help in exploring the field of airborne wind energy and for bringing us into contact with his various contacts all over the world. His quick and extensive reactions to all our questions have brought us to the point where we are today.

Within TU Delft, we received assistance of Dr.ir. E. Mooij for the Systems Engineering and Project Management, ir. J.A. Melkert for legal restrictions, Dr. C. Lettieri for thermodynamics and condensation, Dr. W.A.A.M. Bierbooms for wind speeds in the troposphere, Dr.ir. O. Isabella for insight into current developments in photovoltaics, ir. D. Eijkelhof for airborne wind energy gliders, Dr. M.B. Zaayer for rotor design, Dr. C.A. Infante Ferreira for wind energy, and Dr.ir. R. Merino-Martínez for noise from propellers. Their help is much appreciated.

Outside of TU Delft, a lot of assistance was provided by researchers and companies. In particular, we want to thank Dr. J.F. Guillemoles for his help in solar panel and solar balloon design, Dr. A. Cherubini for his help in the take-off procedure, KitePower for their help in understanding kites and generators, KiteSwarms for their assistance in understanding multiple-glider systems and ir. R. Leuthold for her help regarding the interference between gliders in the air.

Our appreciation holds for everyone who supported us, in big or small matters, or somehow contributed to our project. Without the help and support from all of you, we could not have made it.

# Executive overview

## Project objectives and requirements

The discussion concerning the world-wide energy transition has been surrounded by a continuously recurring problem in the Netherlands: the lack of available area due to a high population density. This project contributes to this transition by designing a system which can provide Delft University of Technology (TU Delft) with all its electricity demands by harvesting energy from renewable sources, all while operating above the clouds – limiting the impact of the system on ground activities – and placing a focus on the application of sustainable materials (Garcia 2019). Harvesting energy above the clouds also brings advantages regarding the amount of energy that can be captured, as wind speeds and solar intensity are higher above the lower-layer clouds, which are located 2 km above the ground.

The goal of the project, the mission need statement (MNS) and the goal of the project team, the project objective statement (POS) are:

- MNS: To provide TU Delft with its energy demands by using an environmentally-sustainable flying energy-harvesting station operating above the low-level clouds.
- POS: To win the symposium by designing an environmentally-sustainable flying energy-harvesting station that operates above the low-level clouds and feeds the TU Delft's energy demands, with 11 students in 10 weeks.

The product to be designed is an energy harvesting system that operates above the clouds. There are several base requirements that drive the design of the system (Garcia 2019): it shall be safe for humans and other species in its environment; it shall only use renewable resources in its production and operation (although it is specified that other resources are acceptable in the structure if it is shown that renewable options are unfeasible); and it shall be able to supply sufficient energy to meet the energy demands of TU Delft. The cost efficiency of the system shall be such that a life-cycle analysis shall indicate a return on investment within 10 years. Finally, the design shall be able to fly year round and be more efficient than existing (ground-based) energy farms of comparable cost and surface area.

## Trade-off summary

Three system concepts were created and traded off to find the final concept. These three concepts were a free-floating solar balloon, a tethered glider generating electricity on the ground and a tethered wind turbine generating electricity in air. Within each of the three concepts several design possibilities were traded off based on power density, energy transfer, scalability, feasibility, controllability, RAMS, sustainability and cost. The three concepts derived from this were traded off based on flight performance, operations, energy, structures and materials, risk and sustainability. Design option two, the tethered glider generating electricity on the ground, performed best in all trade-off criteria, therefore being selected as the final concept.

## The final concept

The layout of the glider generating electricity on the ground and tether of concept were elaborated on. A twin fuselage glider was chosen, as it relieves the bending stress of the wing. Also the landing gear can be stored in the fuselages.

As tether drag is the main source of aerodynamic drag, a promising way of reducing it was selected. A stationary tether will be split at high altitude in two moving cables connected to gliders, a Y-tether. To

generate enough energy for the TU Delft requires 19 of these systems, so 38 gliders. To reduce ground space, a circular runway around each drum will be used for take-off and landing.

## **Sustainable development strategy**

As this project is fundamentally concerned with sustainability, a robust sustainable development strategy is required. The project aims to contribute to sustainability by offering a measure to lower the emission of greenhouse gasses to meet energy demands in a way that is both cost efficient and resource efficient. As was established in the *Midterm Report* (Arblaster et al. 2019b) and the *Baseline Report* (Arblaster et al. 2019a) before it, the sustainability of the airborne energy-harvesting system will be evaluated in two ways: its environmental footprint (EF) through life-cycle assessment (LCA) and its direct impact on its surroundings.

As such, there is a lot of discussion surrounding sustainability in the chapters about the siting of the system and about its life-cycle assessment. However, because of the holistic nature sustainability has for this project, it is frequently incorporated in other chapters too: production, material choice, etcetera.

## **Technical risk assessment**

Many risks were identified, assessed, and mitigated. This is important in the selection of the optimal design, as well as for the general well-being of the project. The assessment was performed on two parameters: the likelihood of the risk and the impact it could have. Both are measured on a four-point scale. Likelihood ranges from remote (1), improbable (2), and possible (3), to probable (4). Impact ranges from acceptable (1), tolerable (2), and critical (3), to catastrophic (4). Different types of risks have been identified generally and for each specific design, like design, manufacturing, operational, end-of-life, and sustainability and legal risks. The highly-problematic risk – those with a score of six or above, so (2,4), (3,3), (4,2), (3,4), (4,3), or (4,4) – are mitigated.

## **Technical analysis of the tethers**

Considering the length of the tether, sag could not be neglected. Sag computations were done to analyse the performance of the tether material chosen. More dense and weak materials sag more. In the end, Dyneema was selected as the tether material. It is not sustainable, which is a pro of banana fibre, the alternative. Banana fibre would however require a thicker and heavier tether, which would make the design unfeasible. Icephobic coating is needed to maintain correct material properties during operation. A parachute is added to the cable as an emergency feature.

The drag force on the tether was calculated for the stationary and Y-part of the tether. Using a drag coefficient of 1 and correcting for the increased length of the stationary tether due to sag, the aerodynamic force on the cable in the wind direction is 0.45 kN and the force in downwards direction is 1.2 kN. Neglecting the sag for the Y-tether gives a drag of 16 kN for each Y-tether. If no Y-tethers were used, but the cable would turn as a whole, the drag would be five times higher.

## **Technical analysis of the gliders**

Performance analysis showed that a 60 m<sup>2</sup> wing is optimal. A larger wing area was considered since it means that more lift can be generated, however the structure will become heavier, therefore corresponding bending loads will become larger. The aspect ratio is determined to be 12, due to the fact that it is a good balance between low induced drag and roll response: both are very important for the design. The taper ratio is chosen to be equal to 0.4, due to the high Oswald efficiency factor of 1. With middle section of 20% of the wing span, this resulted in a mean aerodynamic chord of 2.385 m and a root and tip chord of 2.942 m and 1.177 m. The angle of attack that the aircraft will encounter the most is 3°, therefore this is used to optimize the wing. Due to the low mach number no sweep angle is required. Additionally, no dihedral angle is required as engines are not mounted on the front of the wing, but on the fuselage. No angle of

twist is applied, as this will decrease the lift properties to such an amount that the used software did not converge anymore. It is however recommended to apply an angle of twist to decrease tip stall.

Using XFLR5 the airfoil was designed using an optimization with 3D analysis. This airfoil had the Makani M600 airfoil (MRevE-v2) as baseline, from which after iterations EHAC mod. 1 was designed. Seven additional iterations yielded EHAC mod. 5 as best airfoil, which was renamed to EHAC8431. EHAC8431, where the numbers follow the same terminology as NACA 4-series, is an airfoil with high camber and high thickness. Analytical and numerical analysis were performed for the wing at an altitude of 3000 m with a mach number of 0.267. This resulted in a discrepancy of 0% between the  $C_L - \alpha$ -plots and 12,5% between the drag polars. An analytical analysis is also performed for the full aircraft drag, where the zero lift drag coefficient is equal to 0.026. Both numerical plots can be seen in figures 1a and 1b. Flow separation started at 12° at the tips and trailing edge, where trailing edge stall is preferred over leading edge stall due to its gradual behaviour. From visual analysis it can indeed be confirmed that the taper ratio of 0.4 resulted in a elliptical lift distribution.

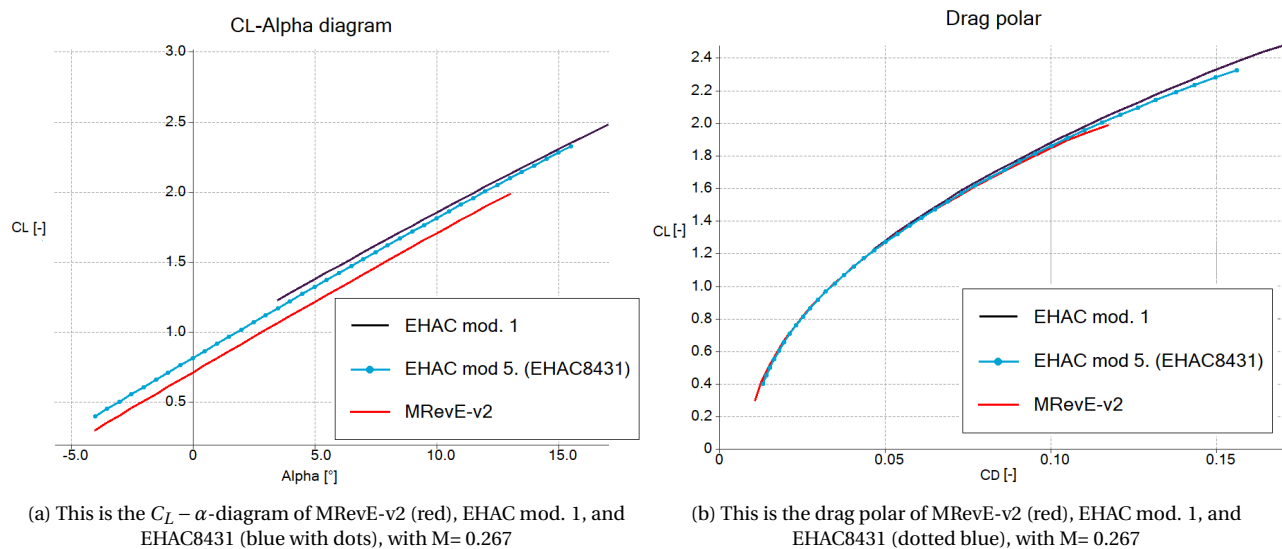


Figure 1: Results of the numerical analysis in two diagrams.

Control surfaces were scaled using reference aircraft. From the tether, glider drag, and weight, the required take-off thrust was calculated. A safety factor of three was implemented to account for all other possible sources of drag. With a propeller efficiency of 85% from literature, 600 kW of engine power would be required for take-off. Two retractable propellers will be used for the take-off propulsion and the generation of power for the on-board battery during the reel-in phase. The on-board control and communication software and hardware require 20 kW and the landing gear 1 kW, according to literature. This gives a total required on-board power of 621 kW.

The flight path is optimised for maximum net cycle power, by combining scripts on structures, materials, flight path and wing. It results in an operating altitude of 3,000 m, leading to a power output during reel-out phase of 635 kW. Reel-out time is 233 seconds and reel-in phase is 32 seconds. Weather influences could decrease lift by 24% and drag could increase by 108%. This should be mitigated by active heating or coatings. For the take-off and landing an on-board propulsion system is needed. The propellers of this will be used to generate the on-board energy during the reel-in phase. For take-off, a circular take-off path is taken, using the tether.

The structure will consist mainly of wing box structures. It will be made of carbon fiber + PEEK resin and has to be 2 mm thick to cope with the loads. A weight estimation reveals the glider would weigh 3.333 kg. A VECTOR autopilot is used for all flight operations.

A sensitivity analysis is performed on the glider parameters by changing input values to the optimiza-

Table 1: Results of sensitivity analysis after changing some of the input variables slightly

Inputs/Outputs	Weight per glider	Power per system	Flight path radius
#Gliders per system (2, 3, 4)	(0%, -8.64%, -21.0%)	(0%, +20.9%, +13.4%)	(0%, +44.4%, +71.7%)
Aspect ratio (10, 12, 14)	(-6.9% , 0%, +12.2%)	(N.A. , 0%, +8.5%)	(N.A. , 0%, +10.5%)
Surface area (60, 65, 70 m <sup>2</sup> )	(0%, +13.6%, +29.6%)	(0%, +7.4%, +14.6%)	(0%, +5.2%, +9.7%)
Altitude (2.5, 3, 3.5 km)	(-6.2%, 0%, N.A.)	(-27.7%, 0%, N.A.)	(-6.9% , 0%, N.A.)

Table 2: Optimised system parameters

Parameters	Symbol	Value	Units
Apparent wind speed magnitude	$V_a$	87.72	m/s
Average operating altitude	-	3000	m
Tether reel-out speed	$V_{reel, out}$	3.44	m/s
Wind speed	$V_w$	11.47	m/s
Tether elevation angle at ground station	$\theta$	40	°
Glider elevation angle at Y-connection	$\beta$	20	°
Power generated at each ground station	$P_{drum}$	635,042	W
Flight path radius	$R_{flight}$	466.5	m
Total tether mass	$m_{tether}$	2,292	kg
Lift generated by each glider	$L_{glider}$	228,981	N
Tether force at connection to glider	$F_{tether}$	106,518	N
Tether diameter	$D_{tether}$	1.49	cm
Tether length	$L_{tether}$	4,809	m
Number of units	$n_{sys}$	19	-
Duration of reel-out phase	$t_{out}$	232	s
Duration of reel-in phase	$t_{in}$	32	s
Length of reeled tether	$l_{reel}$	800	m
Spacing between ground stations	$d_u$	1,296	m
Radius of runway	$r_{runway}$	300	m
Mass of each glider	$m_{glider}$	3,333	kg
Diameter of fuselage	$d_{fuselage}$	106	cm
Nominal angle of attack	$\alpha_{nom}$	2	°

tions scripts. These result in the output percentage-wise changes shown in table 1. It is important to note that scaling the system down or putting it at higher altitude quickly can lead to the system not being able to stay airborne. No extreme changes were seen by changing the inputs a little.

All of these considerations and optimizations lead to one optimised system, of which the parameters are shown in table 2.

## Technical analysis of the ground station

The ground station consists of three drums and a generator, for each system. The winch that is going to be used is the AWE winch from FEcreate<sup>1</sup> due to its high reel-in speed. This results in a power needed for the winch of 5.58 kW. This consequently results in a net power (without generator) of 557.5 kW. A permanent magnet synchronous generator is used due to its high power efficiency. Furthermore, AC-DC-AC converters are used to obtain fixed current frequency with variable wind speeds. Lastly, the generator has an efficiency of 97%. All in all, the average net power during one cycle (one reel-in and one reel-out phase)

<sup>1</sup><https://fcreate.com/> [cited 16 January 2020]

equals 541 kW.

To connect the system to TU Delft, it needs to be connected to the 380 kV connection in Ens. A high voltage transformers can be bought of the shelf and have efficiencies close to 100%.

## Placement of the system and its impacts

There are many requirements relating to the placement of the system. The energy farm should be located close to a high-voltage grid connection, outside of range of no-fly zones, and the gliders must not fly into Natura 2000 areas (which was expanded here to include all important bird areas). Additionally, areas with a low population density are strongly preferred over more populated areas. From these restrictions, an area within the Noordoostpolder – in the province of Flevoland – was selected. The exact location spans between the villages of Ens and Marknesse. This area was chosen because of its proximity to the high-voltage grid connection east of Ens, while avoiding a lot of tourist attractions in the Noordoostpolder without any gliders entering the nearby important bird areas. The ground stations are positioned such as to prevent collisions between tethers, while keeping a minimum distance of 1 km from residential areas (with only two coming within 1.5 km), resulting in a swept area of 78.1 km<sup>2</sup>.

Two categories of impacts were considered for this placing: societal and ecological impact. Besides the visual impact of the system (for which the tourist destinations mentioned earlier are significant), the main impact that was identified is noise pollution. Noise generation from aircraft is an increasingly pressing topic and something this project will have to deal with too. Using the day-evening-night sound pressure level ( $L_{den}$ ) regulations of the Netherlands (meaning the system should stay under 47 dBA), it was estimated that – on an average day – no more than two movements (take-offs or landings) could take place from the ground stations nearest to residential areas. Given that the gliders should remain airborne unless for scheduled maintenance, this should be sufficient. However, it is clear that noise should play a key role in the further design of the gliders.

The impact of the system on its local ecology was also addressed. In doing so, it was discovered that – due to a number of important bird areas being in close proximity to the energy farm – there would be a substantial collision risk. This must be mitigated by marking the tether in bright colours, improving the ability of birds to avoid the system. This in turn creates a barrier effect, meaning birds are hindered in their regular flight paths, requiring them to expend more energy than they would otherwise. However, given the limited area of the system, combined with the distance between tethers, this impact is expected to be acceptable. Other ecological impacts were considered to be minor or negligible.

## Operations and logistics

The reliability has been approximated by means of a failure mode, effect, and criticality analysis (FMECA). The FMECA is build up from the fault tree analysis, which is the top down analysis performed for the reliability of the system. From the reliability analysis the most critical item of the system was determined, which is the tether.

To properly analyse the maintainability of the system more data is required. When the data has been acquired for the maintainability a more thorough analysis can be performed. The goal of this analysis would be to determine to optimum maintenance interval to reduce the cost on maintenance as much as possible.

The availability follows from the maintainability and reliability. Unfortunately, without the data to perform a proper maintainability analysis no accurate availability analysis could be performed.

In order to quantify the safety of each failure mode, the failure mode had to be rated on severity. Based on severity and failure rate the failure mode was rated for safety. From this analysis, the most important mitigation methods are:

1. Ensure strong network security to minimise hacking risk of the system
2. Secure possible overwrite to prevent hostile take over of harming surroundings

### 3. Maintain strict protocol concerning personnel on landing strips

To reduce waste and cost, when parts require maintenance they are sent to a repair facility to be placed on a different system once repaired. This requires a storage sufficient to accommodate for plenty of parts.

Possible complications involving the system maintenance require adequate storage for entire aircraft in the approximate area surrounding the operational area. Between the location of the operational area and factory adequate infrastructure must be in place to support transportation of a single unit. A team must be present for the take-off process.

The harvested energy will be directly transferred to the grid. Only an energy storage facility is located at the harvesting site, in the form of a lithium-ion battery. The energy stored in this battery can be used in case of emergency. It contains 79.7 kWh, which is enough energy to run the office located at the harvesting site and for communication with the gliders for 24 hours.

## Production plan

The production plan includes the manufacturing, assembly, and integration plan (MAI plan). The MAI plan gives a time ordered outline of the activities required to construct the product from its constituent parts (Garcia 2019).

Figure 2 shows the production plan of the final design. The red, horizontal, arrow represents the main assembly line. Sub-assembly lines are added to the main assembly line at specific moments, some can be one simultaneously. In order to make the final assembly, sub-assemblies need to be produced. Some of those sub-assemblies can not be made straight from the parts, but will require a sub-sub-assembly step. In the design, there is the possibility to manufacture or buy parts. The energy that is required for the production of the systems, will be compensated by the renewable energy harvested by the systems when in operation.

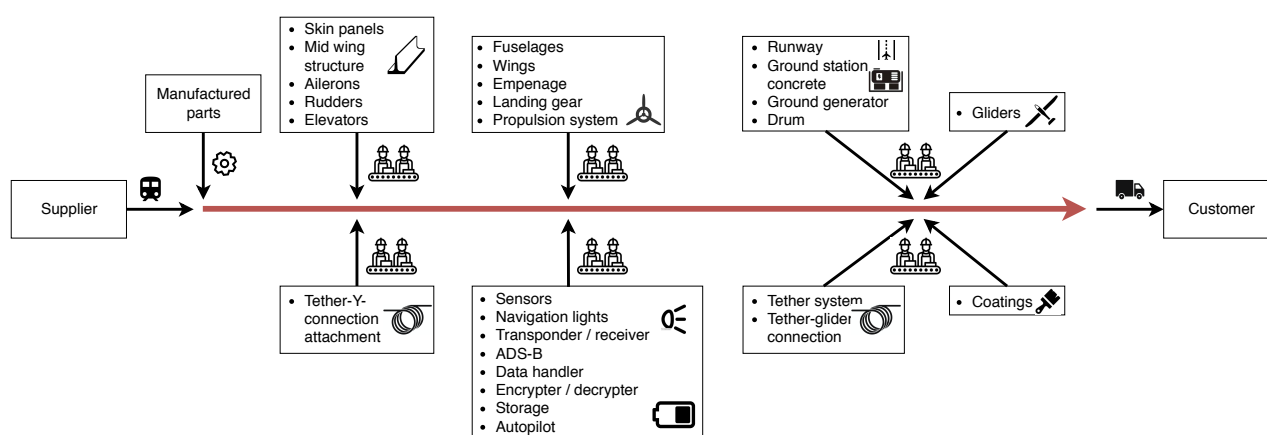


Figure 2: Production plan

## Life-cycle assessment

A rough life-cycle assessment (LCA) was performed to estimate the environmental footprint of the full energy farm, specifically looking into the global warming potential over 100 years (GWP100a) of the exhausts associated with it. These calculations revealed that, by far, the most influential elements are the degradation of the tether, which must be replaced regularly, as well as the construction of the runways. Using values based on literature, it was revealed that the system could be engineered to have a GPW100a as low as 25.4 gCO<sub>2</sub>-eq/kWh, with recommendations for further improvements. This is in the same ballpark as onshore wind (20.85 gCO<sub>2</sub>-eq/kWh), but towards the higher side. This means that, all other things being equal, current onshore technology should be preferred above airborne wind energy.

However, given the relative flexibility in placement of AWES and the reliability of high-altitude wind speeds, this is certainly not a death sentence for the further development of this project. Additionally, the potential areas for improvement are abundantly clear. Given a more ecological runway, or entirely different take-off procedure – possibly in combination with a higher lifetime for (the non-reeled section of) the tether – the current system could already outperform conventional wind parks.

## Cost analysis

To identify the cost elements of the post-DSE project, a cost breakdown structure was made. The cost associated with the project were divided in two main categories: direct cost and indirect cost. After identifying the cost elements, sub-elements were identified. Each sub-category may have an investment cost and a yearly cost associated with it.

After identifying all cost a total investment cost of €62,883,653.87, and a yearly cost once the system is operational is €3,971,648.50 were found. As energy prices are expected to rise by 13% by 2030, TU Delft will spend €10,001,630 on energy each year. When operating, €6,029,981.50 can be saved each year. Using the yearly savings and the investment cost, the return of investment is 10.43 years.

## Market analysis

The name of the company will be Greenhyve as this gets the company's ambition across and includes what sets the system apart of other airborne wind energy systems.

Currently, the Netherlands will be a good starting market as there is a high demand for low area-requiring renewable energy systems. With a good prospective of beating conventional wind energy systems in the future, there is a good chance Greenhyve will overtake the offshore wind energy market of wind turbines.

With European Union investments, the future market for Greenhyve will lay in less prosperous inland European countries or European countries without much coastline. Once the system outperforms wind turbines, European countries with coastline will also provide good opportunity for system deployment.

## Post-DSE phase

The project design & development logic for the post-DSE period is described. This comprises the steps which need to be taken to bring the product to the market. It gives a good indication of the specialisms and resources needed for the follow-up steps. The project design & development logic is given in figure 3.

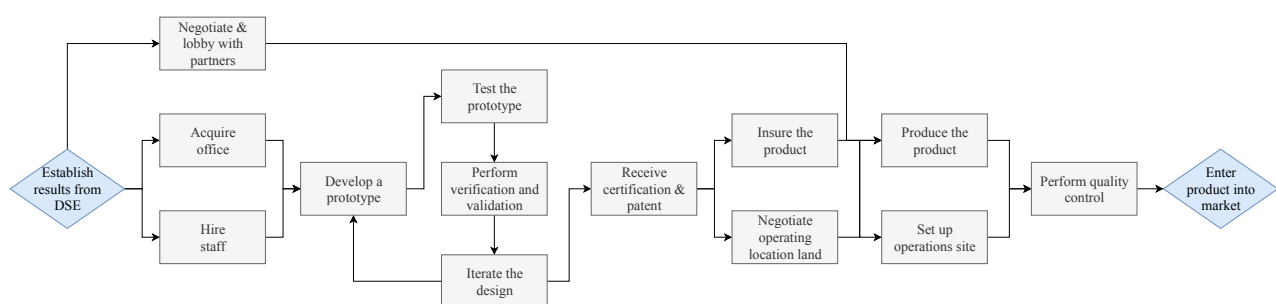


Figure 3: Flow diagram of tasks to be completed after the DSE.

## Requirement compliance matrix

Multiple requirements were determined which have to be met by the designed system. However, at an early stage some requirements were identified as being important to the system, but were later discovered to be beyond the scope of this study.

The mission requirements are considered to be the most important. All three, stated below, have been

met in the design of the system. EHAC-MIS-01 is met, since the system produces 38 MWh above the TU Delft energy needs, daily. As the system flies above 2 km, EHAC-MIS-03 and EHAC-MIS-04 are both met.

- **EHAC-MIS-01:** The system shall provide the TU Delft with its yearly energy needs.
- **EHAC-MIS-03:** The system shall be located above the clouds.
- **EHAC-MIS-04:** The system shall be able to fly.

There are six requirements which have not been met, these are stated and explained below.

- **EHAC-SH-11-01:** The system shall be constructed using renewable materials only: Due to low TRL and currently insufficient material characteristics, it has been decided that for now, non-renewable materials are used to benefit the production of green energy.
- **EHAC-SH-11-08:** The system shall produce more energy than others of comparable surface area: As onshore wind turbines require less ground space than the glider systems, and they produce a higher output power, the glider system will not generate more power than an existing energy harvesting system with comparable surface area.
- **EHAC-SH-11-09:** The system shall have a smaller environmental footprint than methods on the ground surface of comparable costs: The global warming potential of the system is higher than that for a standardised model of onshore wind turbines. Given that they generate energy at comparable costs, it can be concluded that energy from a conventional wind farm is more sustainable than energy from this design.
- **EHAC-SH-04-01:** The system shall be sited 1 km away from mitigation paths of birds: Since the ideal position for the energy was decided to be in the Noordoostpolder, a lot of important bird areas are nearby. These areas are a popular winter destination to tens of thousands of birds each year. Although the system is located nearby migration routes, the ecological impact of the system can be mitigated in various ways.
- **EHAC-SH-06-01:** The system shall fit within the municipality's destination plan: The municipality's destination plan is difficult to change, and there is a low chance that the people living in the area will agree to making place for the harvesting site.
- **EHAC-SH-09-05:** The system shall have an impact more than 100 m away from buildings and crowds of people: As the system will be built in a place where houses are located, it can not be ensured that the place of impact in case of system failure will have a distance of at least 100 m away from buildings or people.

## Conclusion and recommendations for further research

The goal of the project was to have a set of airborne energy systems that would provide enough energy to power the TU Delft's yearly energy demands. This set of systems were aptly named 'Greenhyve'. Each unit within the Greenhyve consists of; three drums, a generator, a circular runway, a Y-tether, and two gliders. The average power generated by each unit is 541.2 kW. For the first 20 years its life, TU Delft would have to pay 10 euro cents per kWh. After 20 years, the cost of energy production would drop to 6 cents per kWh, which is comparable to onshore wind farms. High costs of repairs and maintenance have been accounted for (equivalent to nearly 3 new gliders per year), so the system is guaranteed to operate at peak performance even after 20 years. The ethos of this project was sustainability. The project produces continuous environmentally sustainable energy, and the glider was partially built with sustainable materials. Greenhyve can establish itself not only as an industry leader in airborne energy production, but also a household name.

There are details of the system that need further investigation or opportunities to increase the performance. One of them is to do more research on tether vibrations, as a lot is still unknown on the behaviour of tethers at such high altitude. The glider partly consists of non-renewable materials as they were the only ones that could cope with the requirements. Further investigation on renewables could help in there. An

assymetrical glider would make sense as most of its flight is in constant turning. For the ground station it is important to reduce the amount of runways so that multiple systems can use the same runways. Control and certification should be done in detail, to ensure safe flight above inhabited lands.

# Contents

<b>1</b>	<b>Introduction</b>	<b>4</b>	7.11	Verification . . . . .	64
<b>2</b>	<b>Requirements overview</b>	<b>5</b>	7.12	Conclusions. . . . .	65
2.1	User requirements . . . . .	5	7.13	Recommendations . . . . .	67
2.2	Global picture of the system. . . . .	5	<b>8</b>	<b>Technical analysis of the ground station</b>	<b>70</b>
2.3	Functional analysis. . . . .	5	8.1	Ground station model . . . . .	70
2.4	Requirements overview . . . . .	6	8.2	Performance . . . . .	72
<b>3</b>	<b>Trade-off summary</b>	<b>7</b>	8.3	Anchoring. . . . .	72
3.1	System concepts . . . . .	7	8.4	Area needed for ground station . . . . .	72
3.2	Concept trade-off . . . . .	8	8.5	Sensitivity Analysis and Verification . . . . .	73
3.3	Defining the final design. . . . .	8	8.6	Conclusions. . . . .	73
<b>4</b>	<b>Sustainable development strategy</b>	<b>10</b>	8.7	Recommendations . . . . .	73
4.1	Contribution to sustainability. . . . .	10	<b>9</b>	<b>Placement and local impacts of the system</b>	<b>74</b>
4.2	Assessment of sustainability requirements . . . . .	10	9.1	Spacing of ground stations . . . . .	74
<b>5</b>	<b>Technical risk assessment</b>	<b>12</b>	9.2	Horizontal positioning of the system . . . . .	75
5.1	Identification and assessment of technical risks . . . . .	12	9.3	Impact of the system on residents . . . . .	77
5.2	Risk mitigation . . . . .	14	9.4	Impact of the system on ecology . . . . .	80
<b>6</b>	<b>Technical analysis of the tethers</b>	<b>18</b>	9.5	Recommendations . . . . .	82
6.1	Tether model . . . . .	18	<b>10</b>	<b>Operations and logistics</b>	<b>84</b>
6.2	Material selection . . . . .	21	10.1	Maintenance plan and replacement of parts . . . . .	84
6.3	Friction, durability, and weather performance . . . . .	24	10.2	Reliability . . . . .	84
6.4	Emergency procedures . . . . .	27	10.3	Maintainability. . . . .	85
6.5	Aerodynamics . . . . .	28	10.4	Availability . . . . .	86
6.6	Verification . . . . .	29	10.5	Safety . . . . .	86
6.7	Conclusions. . . . .	29	10.6	Effect of RAMS on the design . . . . .	87
6.8	Recommendations . . . . .	29	10.7	Communication systems . . . . .	87
<b>7</b>	<b>Technical analysis of the gliders</b>	<b>31</b>	10.8	Tether replacement . . . . .	90
7.1	Assumptions . . . . .	32	10.9	Logistics. . . . .	90
7.2	Wing layout . . . . .	33	10.10	Energy storage . . . . .	92
7.3	Glider layout . . . . .	45	10.11	Electrical block diagram . . . . .	94
7.4	Flight performance of tethered rigid kites . . . . .	48	10.12	Scalability of the system . . . . .	95
7.5	Performance analysis . . . . .	53	10.13	Logistics flow diagram . . . . .	95
7.6	On-board control subsystem . . . . .	56	10.14	Verification . . . . .	95
7.7	Power budget . . . . .	57	10.15	Conclusions. . . . .	95
7.8	Material selection . . . . .	57	10.16	Recommendations . . . . .	96
7.9	Structural analysis . . . . .	58	<b>11</b>	<b>Production plan</b>	<b>97</b>
7.10	Sensitivity analysis . . . . .	63	<b>12</b>	<b>Life-cycle assessment</b>	<b>99</b>
			12.1	System boundary. . . . .	99
			12.2	Resource use and emissions profile. . . . .	99

12.3	Impact assessment . . . . .	100	<b>17</b>	<b>Verification procedure</b>	<b>113</b>
12.4	End-of-life . . . . .	101	<b>18</b>	<b>Conclusion and recommendations for further research</b>	<b>115</b>
12.5	Conclusion . . . . .	101	18.1	Conclusion . . . . .	115
12.6	Recommendations . . . . .	102	18.2	Recommendations . . . . .	118
<b>13</b>	<b>Cost analysis</b>	<b>103</b>	<b>A</b>	<b>Functional flow diagram</b>	<b>124</b>
13.1	Cost breakdown structure . . . . .	103	<b>B</b>	<b>Functional breakdown structure</b>	<b>126</b>
13.2	Operational profit and return of investment . . . . .	103	<b>C</b>	<b>Fault Tree Analysis</b>	<b>127</b>
<b>14</b>	<b>Market analysis</b>	<b>106</b>	<b>D</b>	<b>FMECA</b>	<b>131</b>
14.1	Branding . . . . .	106	<b>E</b>	<b>Logistics flow diagram</b>	<b>132</b>
14.2	Current market . . . . .	106	<b>F</b>	<b>Cost breakdown structure</b>	<b>133</b>
14.3	Market opportunities . . . . .	107	<b>G</b>	<b>Project Gantt chart</b>	<b>134</b>
<b>15</b>	<b>Post-DSE phase</b>	<b>108</b>	<b>H</b>	<b>Technical drawing glider</b>	<b>135</b>
15.1	Design & development logic . . . . .	108			
15.2	Project Gantt chart . . . . .	108			
<b>16</b>	<b>Requirement compliance matrix</b>	<b>109</b>			

# Lists of abbreviations & symbols

AC	Alternating current	HMPE	high-modulus polyethylene
ACM	Authority for Consumers & Markets	IEA	International Energy Agency
ADS-B	Automatic dependent surveillance-broadcast	IF	Interference factor
AWE	Airborne wind energy	ILT	Human Environment and Transport Inspectorate
AWES	Airborne wind energy system	ISO	International Organisation for Standardization
BSc	Bachelor of Science	KNMI	Royal Netherlands Meteorological Institute
c.g.	Center of gravity	LCA	Life-cycle assessment
CAES	Compressed-air energy storage	LCN	Load classification number
CFD	Computational fluid dynamics	LE	Leading edge
CO <sub>2</sub> -eq	Carbon dioxide equivalent	LG	Landing gear
DC	Direct current	LLT	Prandtl lifting line theory
D&D	Design and development	LVNL	Air Traffic Control the Netherlands
DFIG	Double-fed induction generator	MAI plan	Maintenance, assembly, integration plan
DSE	Design Synthesis Exercise	MDT	Mean downtime for maintenance
DSO	Distribution system operators	MNS	Mission need statement
e.g.	Exempli gratia	MPMT	Mean preventive maintenance time
EASA	European Union Aviation Safety Agency	MR	Manufacturing risk
EC	European Commission	MTBM	Mean time between maintenance
EF	Environmental footprint	MTBM <sub>u</sub>	Mean time between unscheduled maintenance
EHAC	Energy harvesting above the clouds	MTBM <sub>s</sub>	Mean time between scheduled maintenance
EIB	European Investment Bank	MTOW	Maximum take-off weight
EM	Electric motor	MTTM	Mean time to maintain
EOLR	End-of-life-risk	MTTR	Mean time to repair
ERO	Emergency response officer	NASA	National Aeronautics and Space Administration
EU	European Union	NECP	National Energy & Climate Plans
EVA	Ethylene vinyl acetate	OBB	On-board battery
FBD	Free body diagram	OBC	On-board communication
FBS	Functional breakdown structure	OEW	Operational empty weight
FEM	Finite elements method	OLC	Obstructive light control
FF	Component form factor	Ops	Operations
FFD	Functional flow diagram	OR	Operation risk
FMECA	Failure mode, effect, and criticality analysis	PBL	Netherlands Environmental Assessment Agency
FP	Flight performance	PEEK	Polyether ether ketone
FTA	Fault tree analysis	PEF	Product Environmental Footprint
GC	Ground communication	PMG	Permanent magnet generator
GG	Ground generator	PM/SE	Project management and systems engineering
GNSS	Global navigation satellite system		
GPS	Global positioning system		
GWP	Global warming potential		
GWP100a	Global warming potential over a period of 100 years		
HAP	High-altitude platforms		

POS	Project objective statement
PS	Polystyreen
PSH	Pumped-storage hydroelectricity
PVC	Polyvinyl chloride
PVF	Polyvinyl fluoride
RAMS	Reliability, availability, maintainability, and safety
RF	Radio frequency
RPAS	Remotely-piloted aircraft systems
SH	Stakeholder
SLR	Sustainability and legal risk
SMES	Superconducting magnetic energy storage
S&M	Structures and materials
TRL	Technology readiness level
TSE	Energy Top Sector
TSO	Transmission system operators
TU Delft	Delft University of Technology
TU/e	Eindhoven University of Technology
UAV	Unmanned aerial vehicle
UV	Ultraviolet
USA	United States of America
USD	United States Dollars
V&V	Verification and validation
w.r.t.	With respect to
WBS	Work breakdown structure
WFD	Work flow diagram

Symbol	Description	Unit
$\alpha$	Angle of attack	[°]
$\alpha$	Failure mode ratio	[-]
$\beta$	Compressibility factor	[-]
$\beta$	Failure probability	[-]
$\beta$	Mean flight position with respect to the ground	[°]
$\beta$	Side slip angle	[°]
$\beta_0$	Angle of the tether with respect to the ground	[°]
$\beta_1$	Angle of the tether with respect to the glider	[°]
$\gamma$	Ratio of specific heat	[-]
$\Gamma$	Dihedral angle	[°]
$\epsilon$	Downwash angle	[°]
$\eta$	Airfoil efficiency factor	[-]
$\eta$	Efficiency	[-]
$\theta$	Azimuth angle	[°]
$\lambda$	Tangential velocity factor	[-]
$\lambda$	Taper ratio	[-]
$\lambda$	Wavelength	[m]
$\lambda_p$	Failure rate	[-]
$\Lambda$	Sweep angle	[rad]
$\Lambda_{LE}$	Leading edge sweep angle	[°]
$\mu$	Dynamic viscosity of the fluid	[kg/m/s]

$\rho$	Density	[kg/m <sup>3</sup> ]
$\rho_{el}$	Resistivity	[ $\Omega \cdot m$ ]
$\sigma$	Stress	[N/m <sup>2</sup> ]
$\phi$	Operation angle	[°]
$\phi$	Wing twist	[°]
$\phi_r$	Glider roll angle	[°]
$\chi$	Course angle	[°]
$\omega$	Rotational speed	[rad/s]
$a$	Speed of sound	[m/s]
$A$	Area	[m <sup>2</sup> ]
$AR$	Aspect ratio	[-]
$A_a$	Achieved availability	[-]
$A_i$	Inherent availability	[-]
$A_o$	Operational availability	[-]
$b$	Wing span	[m]
$c_{wingbox}$	Width of the wingbox	[m]
$C$	Chord length	[m]
$C$	Glider speed	[m/s]
$C$	Tether length incl. sag	[m]
$C_d$	Drag-coefficient in 2D	[-]
$C_D$	Drag-coefficient in 3D	[-]
$C_{D_0}$	Drag-coefficient in 3D at zero lift	[-]
$C_f$	Skin friction coefficient	[-]
$C_l$	Lift-coefficient in 2D	[-]
$C_L$	Lift-coefficient in 3D	[-]
$C_{L\alpha}$	Lift-coefficient in 3D per angle of attack	[-]
$C_m$	Criticality for a failure mode	[-]
$C_p$	Cost of preventive maintenance	[€]
$C_p$	Pressure coefficient	[-]
$C_t$	Thrust coefficient	[-]
$C_v$	Cost of unscheduled maintenance	[€]
$d$	Diameter	[m]
$d_u$	Ground distance between units	[m]
$D$	Drag	[m]
$D$	Rotor diameter	[m]
$e$	Efficiency factor	[-]
$E$	Energy	[Wh]
$f$	Frequency	[Hz]
$f_{fuselage}$	Fuselage slenderness factor	[-]
$F$	Force	[N]
$F_{tether}$	Tether force	[N]
$FF$	Form factor	[-]
$g$	Gravitational acceleration	[m/s <sup>2</sup> ]
$h$	Altitude	[m]
$H$	Horizontal tether tension	[N]
$H_{2\pi}$	Altitude gain/ loss after one revolution	[m]
$I$	Current	[A]
$I$	Moment of Inertia	[m]

$IF$	Interference factor	[-]	$T$	Torsion	[Nm]
$k$	Generator constant		$T_0$	Tether tension at ground station	[N]
$k$	Surface smoothness coefficient	[-]	$T_1$	Tether tension at top of tether	[N]
$k$	Rotor constant	[-]	$U$	Voltage	[V]
$K_1$	Tether sag integration constant	[-]	$\nu$	Opening angle of the operational envelope	[°]
$K_2$	Tether sag integration constant	[-]	$\nu_a$	Apparent wind speed	[m/s]
$K_{\epsilon_\Lambda}$	Downwash constant including sweep	[-]	$\nu_{k,\tau}$	Tangential kite velocity	[m/s]
$K_{\epsilon_\Lambda=0}$	Downwash constant for 0 sweep	[-]	$\nu_{k,r}$	Radial kite velocity	[m/s]
$K_q$	Integration constant	[N/m <sup>2</sup> ]	$\nu_w$	Wind speed	[m/s]
$l$	Length	[m]	$V$	Velocity	[m/s]
$l_s$	Segment length tether	[m]	$V$	Volume	[m <sup>3</sup> ]
$l_{yt}$	Affected length Y-tether	[m]	$V_a$	Apparent velocity	[m/s]
$L$	Lift	[N]	$V_{TO}$	Apparent take-off speed	[m/s]
$L$	Rotor length	[m]	$V_w$	Wind velocity	[m/s]
$L$	Horizontal operating distance	[m]	$w$	Weight per unit length	[N/m]
$L$	A-weighted sound pressure level	[dBA]	$W$	Weight	[N]
$L_{den}$	Day-evening-night sound pressure level	[dBA]	$W/S$	Wing loading	[N/m <sup>2</sup> ]
$L/D$	Lift-over-drag ratio	[-]	$x$	Untapered wing span ratio	[-]
$m$	Mass	[kg]	$x/c$	Horizontal position on airfoil with respect to leading edge	[%]
$m_{tv}$	Distance between the horizontal tailplane and the vortex shed plane as a fraction of half-wing span	[-]			
$M$	Mach number	[-]			
$M$	Moment	[Nm]			
$n$	Number of	[-]			
$N$	Number of full rotations	[-]			
$P$	Power	[W]			
$q$	Distributed load strength	[N/m]			
$q$	Local lift load	[N/m]			
$q_{drag}$	Local drag load	[N/m]			
$r$	Distance	[m]			
$r$	Distance aerodynamic center wing to tail as fraction of half-wing span	[-]			
$R$	Radius	[m]			
$R$	Specific gas constant	[g/mol]			
$Re$	Reynolds number	[-]			
$R(t)$	Probability the system has not failed	[-]			
$S$	Shear	[Pa]			
$S$	Surface area	[m <sup>2</sup> ]			
$SF$	Safety factor	[-]			
$t$	Thickness	[m]			
$t$	Time	[s]			
$T$	Temperature	[K]			
$T$	Thrust	[N]			
$T$	Time	[s]			

# Introduction

The need for humanity to decrease its burden on the environment is abundantly clear. In the twenty-first century, a sizable portion of this struggle has been devoted to transitioning away from energy sources based on fossil fuels, towards renewable sources. However, the transition towards green and sustainable energy causes challenges for the grid, by introducing a high dependency on weather conditions. The answer to the challenge of reliable sustainable energy could be right above your head: above the planetary boundary layer, strong and reliable winds can be found. However, harvesting these winds is not straightforward. Towers as tall as a few hundreds of meters are expensive and require enormous foundations. That is where the field of airborne wind energy comes into play.

In fulfillment of the BSc Aerospace Engineering at TU Delft, our group consisting of 11 students took on the challenge to design a device that can harvest energy above the clouds. Earlier progresses described in the *Baseline Report* (Arblaster et al. 2019a) and the *Midterm Report* (Arblaster et al. 2019b) give an overview of steps taken so far. The choice has fallen on designing an airborne wind energy system capable of powering TU Delft by using tethered gliders.

The goal of the project in the form of a mission need statement (MNS) and the goal of the project team, the project objective statement (POS), are:

- MNS: To provide TU Delft with its energy demands by using an environmentally-sustainable flying energy-harvesting station operating above the low-level clouds.
- POS: To win the symposium by designing an environmentally-sustainable flying energy-harvesting station that operates above the low-level clouds and feeds the TU Delft's energy demands, with 11 students in 10 weeks.

This report presents the design of the system, from sizing to detailed calculations on critical system parts. The designed system shall have some characteristics of existing systems like Ampyx<sup>1</sup> and KiteSwarms<sup>2</sup>, but will harvest energy at much higher altitudes: above two kilometers. This operating altitude adjustment poses many additional challenges in the design of the system. Next to the design, surrounding business and management matters will be discussed, to give a broad overview of the feasibility of such a system.

In chapters 2 to 3, the previous steps will be recapped and the requirements of the design are (re)introduced in chapter. Next, the technical analysis can start with analyzing the tether (chapter 6), the glider (chapter 7) and the ground station (chapter 8).

A wide array of factors must be considered in the development of this project. Once technical parameters are established, the report will continue with topics such as the placement of the system in chapter 9, followed by operations and logistics in chapter 10. A production plan is established in chapter 11, while a life-cycle assessment, cost analysis, and market analysis can be found in chapters 12 to 14. Additionally, the post-DSE development of the project is given further form in chapter 15.

In chapters 16 and 17, the current design is evaluated based on the analyses performed so far. The sensitivity to design inputs is evaluated, requirements compliance is checked, and verification and validation procedures explained. Finally, conclusions and recommendations are given in chapter 18.

<sup>1</sup><https://www.ampyxpower.com/> [cited 20 January 2020]

<sup>2</sup><https://kiteswarms.com/> [cited 20 January 2020]

## Requirements overview

This report deals with the design of an airborne wind energy system. This system is constrained in several ways, while also having certain goals it tries to achieve. This chapter reiterates several of the established requirements, while also exploring the further functioning of the system.

The scope of this chapter ranges from the user requirements, treated in section 2.1, to a global picture of the system, found in section 2.2, a functional analysis in 2.3 and the requirements that will drive the design in 2.4.

### 2.1. User requirements

The product to be designed is an energy harvesting system that operates above the clouds. There are several base requirements that dictate the system : it shall be safe for humans and other species in its environment; it shall only use renewable resources in its production and operation (although it is specified that other resources are acceptable in the structure if it is shown that renewable options are unfeasible); and it shall be able to supply sufficient energy to meet the energy demands of TU Delft (Garcia 2019). The cost efficiency of the system shall be such that a life-cycle analysis shall indicate a return on investment within 10 years. Finally, the design shall be able to fly year round and be more efficient than existing (ground-based) energy farms of comparable cost and surface area.

### 2.2. Global picture of the system

This project is prompted by the ongoing energy transition. In this process, there is a focus on producing energy from renewable (infinite) sources that do not directly lead to massive production of greenhouse gasses. This has resulted in energy sources such as wind power, solar power, geothermal energy, and hydroelectricity being heavily developed and funded. Nowadays, there are energy farms on the ground and at sea. However, the energy production of conventional solar or wind energy farms are limited by the presence of clouds and wind speeds respectively. This limitation could be alleviated by taking the production of energy to the skies.

The requirements listed in section 2.1 depict a clear picture of what the output of the system shall be: an amount of energy sufficient to meet the energy demand of TU Delft. However, how this goal will be achieved is left in the open. Because of this challenge, the scope of exploration will reach outside of commercially available technologies to also include the potential up-scaling of more lab-scale technologies. It is possible, and even expected, that a combination of technologies will be chosen to harvest energy.

### 2.3. Functional analysis

The functional analysis consists of two parts. Firstly, all system functions are determined from a flow diagram considering all of its operational phases. The functional flow helps creating the bigger picture of all aspects of the functions involved. Once the bigger picture is established, a more in-depth analysis is performed to create the functional breakdown structure. The functional breakdown structure takes the functions from the flow diagram and adds an extra layer of depth by demonstrating the functions involved within the bigger function.

### 2.3.1. Functional flow diagram

Since the baseline report no significant changes have been made in the functional flow diagram except for the operational phase. The functional flow diagram for the operational phase can be found in appendix A. The functional flow diagram from the *Baseline Report* (Arblaster et al. 2019a) is the final functional flow diagram for the other phases.

### 2.3.2. Functional breakdown structure

Very little functional blocks have been changed since the *Baseline Report* (Arblaster et al. 2019a), as they still cover the content pretty well. The biggest change made was a division in production tasks, dividing the preparation of the assembly from the assembly itself. The functional breakdown structure can be found in appendix B.

## 2.4. Requirements overview

From the functional analysis the requirements can be derived. The mission, stakeholder, and system requirements were determined in the *Baseline report* (Arblaster et al. 2019a). At this point of the design, no further requirements can be set, as a system like this has not been designed before. Without a reference system, more specific requirements are not possible to define within reason. The main requirements that will drive the design, however, will be discussed here.

The mission requirements define the goal of this project and are therefore the most important requirements to design for. The mission requirements are the following:

- **EHAC-MIS-01:** The system shall provide the TU Delft with its yearly energy needs.
- **EHAC-MIS-03:** The system shall be located above the clouds.
- **EHAC-MIS-04:** The system shall be able to fly.

These requirements are also reflected in the mission need statement (MNS) and project objective statement (POS) of the project:

- MNS: To provide TU Delft with its energy demands by using an environmentally-sustainable flying energy-harvesting station operating above the low-level clouds.
- POS: To win the symposium by designing an environmentally-sustainable flying energy-harvesting station that operates above the low-level clouds and feeds the TU Delft's energy demands, with 11 students in 10 weeks.

Other requirements that the project is focused around are mainly to do with sustainability. The requirement that the product will be designed most for is EHAC-SH-11-01: the system shall be constructed using renewable materials only. This requirement for this project means that the design will be focused on currently available renewable materials. All materials will be chosen by first investigating possible renewable materials. Any non-renewable materials can only enter the design if the renewable materials prove to be either insufficient in material properties or less sustainable considering durability of the material.

Similarly, the requirements that the system shall be safe for humans and birds (EHAC-SH-11-06, EHAC-SH-11-07), will likely drive the placement of the system, while the grid operator will drive the energy delivery system of the system. Another requirement that must be designed for is efficiency, both in cost and surface area (EHAC-SH-11-03, EHAC-SH-11-08). These requirements were kept in mind during the trade-off phase of the project, and should therefore be met, though the system will always be designed with these efficiencies in mind. The complete list of requirements (including if they have been met) is presented in chapter 16.

## Trade-off summary

In the first phase of the project different design options were established. As a starting point, the project objectives and requirements were determined together with the stakeholders. Brainstorming resulted in a design option tree where ten top-level concepts rolled out. These were evaluated by back-of-the-envelope calculations and more in-depth literature study in order to reduce the ten top-level concepts to three system concepts (Arblaster et al. 2019a). This chapter discusses the trade-off that was made that led to the final concept. Section 3.1 describes the inner trade-off method that was performed for each of the three system concepts in order to finalise its concept lay-out. Section 3.2 elaborates on the final trade-off method leading to the final concept. How the final design is defined can be found in section 3.3.

### 3.1. System concepts

The design option tree in combination with further analysis resulted into three system concepts where the energy harvesting method, flight method and method of energy transfer were determined. Based on the criteria itemised below, an inner trade-off was made for all three system concepts to establish a final configuration.

- Power density
- Energy transfer
- Scalability
- Feasibility
- Controllability
- Reliability
- Availability
- Maintainability
- Safety
- Sustainability
- Cost

Figure 3.1 gives an overview of the three system concepts that resulted from the inner trade-off where its specific lay-out now was determined.

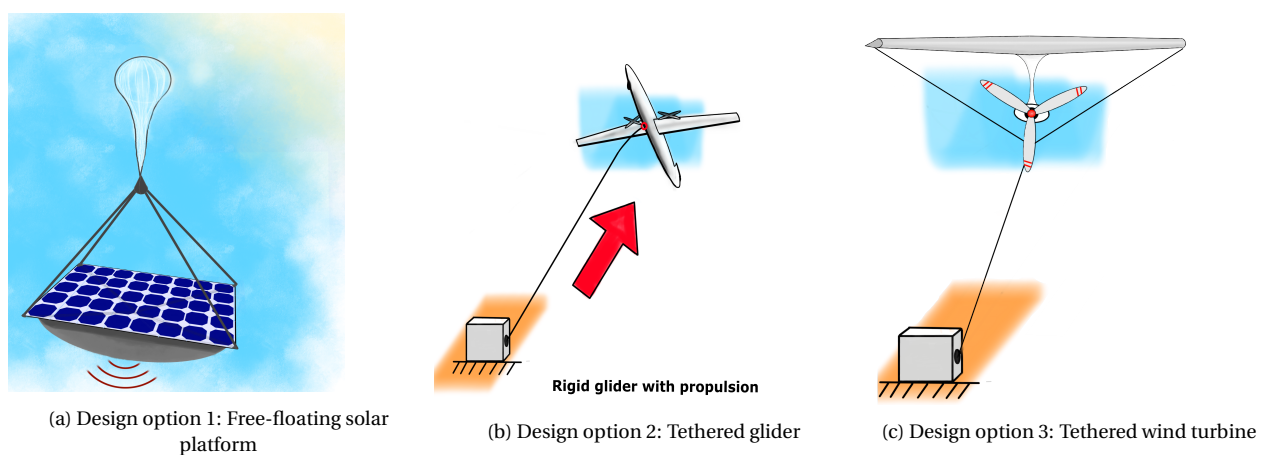


Figure 3.1: The designs selected to enter the trade-off (Arblaster et al. 2019b)

Figure 3.1a shows a free-floating solar balloon harvesting solar energy and transferring it back to Earth via micro-wave transmission. Figure 3.1b shows a tethered glider that is flying cross-wind to generate lift

which causes the tether to reel-out a drum attached to a generator in order to generate electricity. The third design showed in figure 3.1c shows a tethered wind turbine, flying in the wind head-on. This design transfers energy back to the ground via an electric cable.

### 3.2. Concept trade-off

For the final trade-off, the subsystems were evaluated. For each subsystem, the inner trade-off was executed by the team designing it. The inner trade-off lead to a final concept entering the final trade-off for each of the three system concepts. A sensitivity analysis was performed to ensure that the outcome was reliable even though some of the parameters being different than expected. To perform the final trade-off, weights have been assigned to the different criteria, which add up to 100. As the main object of this project is the energy production, this was given the highest weight factor. Besides, an important requirement of the client is sustainability and availability and safety of the system, within operations (ops), are of great importance and thus are granted a weight of 20%. Risk of the entire life-cycle, structures and materials (S&M), and flight performance (FP) are of less importance and correspondingly weighted with flight performance having the lowest weight since the system must be able to fly by definition.

Table 3.1: Trade summary table (Arblaster et al. 2019b)

Concept	FP, 5	Ops, 20	Energy, 30	S&M, 10	Risk, 15	Sustainability, 20	Total
Design 1	2.6	3.0	2.1	3.1	3.0	2.1	2.5
Design 2	3.6	3.5	2.6	3.8	3.8	3.9	3.4
Design 3	3.1	2.9	2.1	1.2	2.3	3.3	2.5

For the sensitivity analysis only the weights can be evaluated which were subject to previous sensitivity analysis. As can be seen in table 3.1, design 2 scores the highest grade for each trade-off criterion. Therefore, design option 2 is the final concept that will be analysed in detail in this report. Figure 3.1b gives a general overview of the system.

### 3.3. Defining the final design

The final concept is going to be a rigid tethered glider with an on-board control system, as shown in figure 3.2. This will be designed in the form of a wind harvesting farm, with multiple harvesting systems operating. One system will consist of two gliders, a tether, a generator and three drums (for tether replacement). For some of these components specific design decisions are made. These are stated below.

First of all, the glider is further investigated. The decision is made to give each glider a twin fuselage, as this has several notable advantages compared to a single fuselage. The biggest advantage is that the fuselages provide space to store the main landing gear, and will have the landing gear spaced at an appropriate distance from each other. The fuselages are not required to hold a significant amount of payload since only the necessary on-board systems are carried. So, these fuselages can each be slender, resulting in favourable aerodynamic performance. Furthermore, the fuselages relief bending moment from the wing and increase the rolling stability.

Next, the tether is looked at. The tether will be a Y-tether. It is decided that instead of one glider per system there will be two gliders per system flying crosswind on a Y-tether. This will significantly reduce the tether drag created by movement of the tether. The longest part of the tether will be stationary and only the

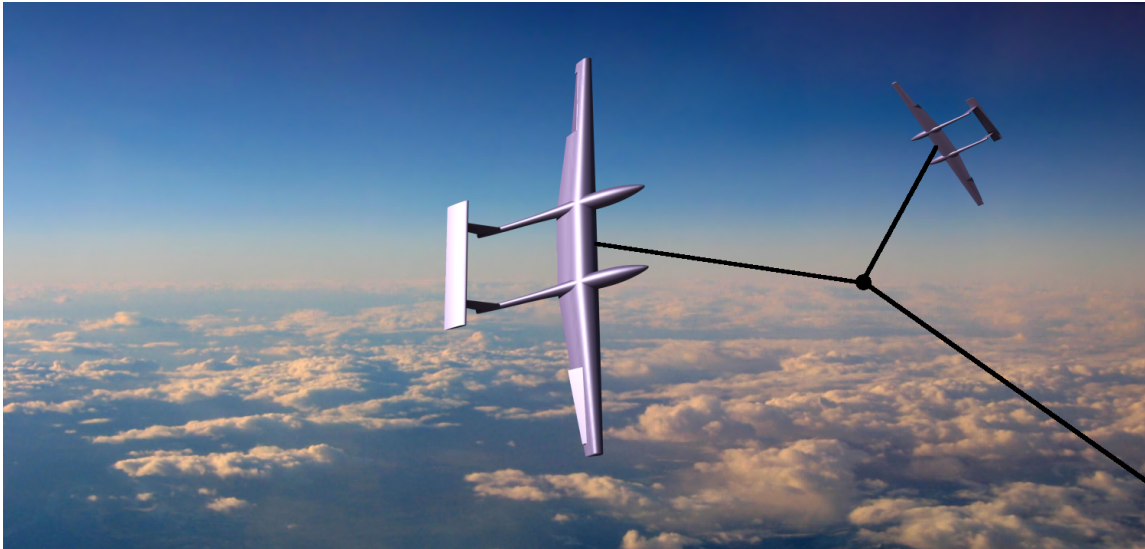


Figure 3.2: Final concept

upper part of the tether, to which the gliders are connected, will be rotating (Schmehl et al. 2013, p. 11). The amount of systems needed can be scaled up to reach the desired amount of energy for the TU Delft.

Furthermore, every system requires its own generator, and three drums for the tether replacement. The drum will reel the tether in and out during operation, where the generator will generate the actual energy. To transfer the energy to the grid a transformer is needed to transform the energy to the high-voltage required for the grid.

## Sustainable development strategy

In this chapter, the sustainability development strategy of the project within the scope of the DSE is reiterated. Further in this report, sustainability is expanded in several areas to accentuate areas which should be kept in mind during further development.

Although generally, environmental strategy should be concerned with the reduction of waste and improvement of manufacturing efficiency (discussed in chapter 11), as well as the recycling of end-of-life products (chiefly discussed in chapter 12), the environmental scope of this project is also deeply concerned with the impacts the system has on its direct environments.

Section 4.2 elaborates on where these sections are located, relating them to the sustainability-related requirements which were formulated at earlier stages. But first, the contribution this system can have to sustainability is discussed in section 4.1.

### 4.1. Contribution to sustainability

As the effects of climate change take hold across the globe – showing no signs of slowing down – the need for energy sources that do not depend on fossil fuels is becoming increasingly critical. Mitigating climate change by lowering greenhouse gas emissions is vital, but other motivations are also abundant, including the reduction of pollution and geopolitical reasons (European Commission 2011).

By exploiting renewable energy sources, the airborne energy-harvesting system has a significant step-up compared to other energy sources, but it is important to recognise that it still burdens its environment to some degree. However, if the requirements of this project – presented shortly in section 4.2 – are met, the system would be demonstrably more sustainable than current renewable energy harvesting methods.

Apart from meeting the requirements relating to sustainability, this project incorporates sustainable development through all design stages in one way or another. For example, this includes investigating the waste and the efficiency during the manufacturing process, as well as the recycling of end-of-life products.

These efforts combined will not result in a system that is entirely independent of non-renewable, finite resources, nor a system that operates in full harmony with its natural surroundings. Yet, if the results of this project are promising, the large-scale implementation of airborne energy harvesting would have profound effects on the relation of humanity with its home planet. The environmental footprint of the energy demands of humanity (or at least, that of TU Delft) would reduce drastically.

### 4.2. Assessment of sustainability requirements

In the *Baseline Report* (Arblaster et al. 2019a), the stakeholder requirements were established. Those relating to sustainability are repeated in table 4.1. Sustainability has many aspects, so these requirements must be assessed in a variety of ways. This is done at several times throughout this report, with an overview being provided in the requirement compliance matrix of chapter 16.

Requirement EHAC-SH-11-01 was evaluated as being driving; non-renewable materials are also acceptable if no renewable options are available. That requirement EHAC-SH-11-02 is fulfilled is natural, as the energy being harvested to the grid is purely a result of exploiting wind speeds. In the same vein, the current design complies with requirements EHAC-SH-04-04, EHAC-SH-04-05, and EHAC-SH-04-06.

The requirements relating to local habitats (EHAC-SH-11-06, EHAC-SH-04-01, EHAC-SH-04-02, and EHAC-SH-04-03) are heavily influenced by where the system will be sited. As such, they will be discussed in chap-

Table 4.1: Selected stakeholder requirements which relate to sustainability (Arblaster et al. 2019a)

Stakeholder	Identifier	Stakeholder requirement
Primary customer: TU Delft	EHAC-SH-11-01	The system shall be constructed using renewable materials only.
	EHAC-SH-11-02	The system shall harvest renewable energy.
	EHAC-SH-11-06	The system shall be safe for birds.
	EHAC-SH-11-07	The system shall be safe for humans.
	EHAC-SH-11-09	The system shall have a smaller environmental footprint than methods on the ground surface of comparable costs.
Environmental organisations	EHAC-SH-04-01	The system shall be sited 1 km away from migration paths of birds.
	EHAC-SH-04-02	The system shall meet the drop shadow regulations.
	EHAC-SH-04-03	The system shall not be placed in a Natura 2000 area.
	EHAC-SH-04-04	The system shall not produce any greenhouse gasses.
	EHAC-SH-04-05	The system shall not produce any harmful radiation.
	EHAC-SH-04-06	The system shall not produce any toxic byproducts.
Residents	EHAC-SH-09-01	The system shall meet the light pollution regulations.
	EHAC-SH-09-02	The system shall meet the noise pollution regulations.
	EHAC-SH-09-03	The system shall meet the visual pollution regulations.

ter 9. The same holds true for the requirements concerning the local human population (EHAC-SH-11-07, EHAC-SH-09-01, EHAC-SH-09-02, and EHAC-SH-09-03).

It was also established that, for the project to be a success, the system should harvest energy with a lower environmental footprint than methods on the ground of comparable cost. Requirement EHAC-SH-11-09 is evaluated in chapter 12 by performing a life-cycle assessment.

## Technical risk assessment

This chapter deals with the identification, assessment, and mitigation of technical risks. This is both important in the selection of the optimal design, as for the general well-being of the project.

Risks are assessed using two values: the likelihood of the risk and the impact it could have. Both are measured on a four-point scale. Likelihood ranges from remote (1), improbable (2), and possible (3) to probable (4). Impact ranges from acceptable (1), tolerable (2), and critical (3) to catastrophic (4).

Highly problematic risks – those with a score of seven or above, so (3, 4), (4,3), or (4, 4) – are mitigated in section 5.2. This results in an updated likelihood-impact matrix.

### 5.1. Identification and assessment of technical risks

This section identifies technical risks across five main categories. Every risk is given an identifying code, relating to its type and whether it is a general risk (GEN) or a specific design risk (DES). The risks associated with a project are inexhaustible, but all main sources of risk should be accounted for here. All identified risks are displayed in a likelihood-impact matrix in table 5.2. Only the high problematic general risks are stated below, a complete overview of the general risks can be found in the Midterm Report (Arblaster et al. 2019b). All the design specific risks are stated.

#### 5.1.1. Design risks

- DR-GEN-01 Mission target is revealed to be infeasible (2, 4): It is possible that the results of this project show that the mission requirements cannot be met.
- DR-GEN-03 Final analysis of cost reveals a design flaw (3, 3): Early cost estimations might be incomplete when re-evaluated at a later stage.
- DR-GEN-05 Inaccurate ground station estimations (3, 3): A robust ground station is required for a successful mission.
- DR-GEN-06 Connection to grid is infeasible (2, 4): This affects what power outputs are possible.
- DR-GEN-08 Unreliable design methods (3, 4): Airborne energy-harvesting is still at an early stage.
- DR-GEN-10 Reliance on low-TRL technologies (4, 2): The feasibility of the project greatly depends on the development of novel technologies.
- DR-GEN-11 Insufficient literature on novel technologies (4, 3): The technologies required might not be broadly investigated yet.
- DR-DES-01 Incorrect glider sizing (1, 2): Gliders are familiar terrain.
- DR-DES-02 Incorrect tether assumptions (3, 2): The required length of the tether is a highly conceptual element. The assumptions made associated with its design are therefore unreliable.
- DR-DES-03 Incorrect estimation of glider power (3, 3): Power estimates of AWES vary greatly and might be unreliable.
- DR-DES-04 Insufficient literature on high-altitude AWES (3, 3): AWES – especially high-altitude AWES – have only been studied up to a certain level.
- DR-DES-05 Insufficient literature on take-off procedure (3, 3): Circular take-off has only been studied up to a certain level.
- DR-DES-06 Incorrect drum sizing (2, 3): Affects the power output.
- DR-DES-07 Incorrect generator sizing (2, 3): Affects the power output.

### 5.1.2. Manufacturing risks

- MR-GEN-10 Inspection errors (2, 4): A significant fault being missed during inspection could result in a dangerous situation.
- MR-DES-01 Glider assembly (1, 3): Faulty assembly might cause failure.
- MR-DES-02 Subsystem assembly (1, 3): See MR-DES-01.

### 5.1.3. Operations risks

- OR-GEN-01 Loss of communication (3, 3): Operations heavily rely on constant communication.
- OR-GEN-02 Structural degradation (environment) (4, 2): The environment will be a driving factor in the structures of the system.
- OR-GEN-03 Structural degradation (fatigue) (4, 2): Fatigue is likely to play a vital role in maintenance.
- OR-GEN-06 Sensor failure (3, 3): Operations such as the autopilot could fail.
- OR-GEN-08 Bird-strike/other object (3, 3): The structures and flight performance of the system must not be compromised.
- OR-GEN-10 Parts inaccessible for maintenance (3, 3): Life-cycle goals could become compromised.
- OR-GEN-13 Termination of funding (2, 4): Would likely require the project to be terminated.
- OR-DES-01 Tether structural failure (2, 4): Especially a large concern regarding safety.
- OR-DES-02 System tampered with (1, 4): An amount of ground-level security will be required.
- OR-DES-03 Glider structural failure (1, 4): Especially a large concern regarding safety.
- OR-DES-04 System hijacked (1, 4): This would result in an enormous safety problem.
- OR-DES-05 Glider wake interference (3, 2): Reduced glider performance.
- OR-DES-06 Drum failure (2, 3): No energy generation.
- OR-DES-07 Generator failure (2, 3): See OR-DES-06.

### 5.1.4. End-of-life risks

- EOLR-GEN-08 Reusing worn out materials (2, 4): Reusability might not be appropriate.
- EOLR-DES-01 Magnetic disturbance (1, 2): Magnets of the generator could affect other equipment.
- EOLR-DES-02 Non recyclable material (4, 3): The material requirements needed may not be possible in a recyclable form.

### 5.1.5. Sustainability and legal risks

- SLR-GEN-04 Habitat disturbance (3, 3): Requirements EHAC-SH-11-06, EHAC-SH-04-01, EHAC-SH-04-02, and EHAC-SH-04-03 (Arblaster et al. 2019a) must be met.
- SLR-GEN-06 Ecologically sensitive site (2, 4): See SLR-GEN-04.
- SLR-GEN-07 Resident disturbance (3,3): Requirements EHAC-SH-09-01, EHAC-SH-09-02, and EHAC-SH-09-03 (Arblaster et al. 2019a) must be met.
- SLR-GEN-08 Airspace unavailability (4, 4): Airspace above the Netherlands is very restrictive, but a vital requirement for this project.
- SLR-GEN-09 Ground area unavailability (2, 4): Should there not be a suitable location for the ground station and area needed around it, the project would fail.
- SLR-GEN-10 Restrictive grid regulations (3, 3): The system might be limited to a large degree to what grid operators allow.
- SLR-DES-01 Wildlife mortality due to tether (4, 2): This demonstrably is an issue (Schmehl 2018, p. 693), but should be mitigated as much as possible.
- SLR-DES-02 Wildlife mortality due to glider (4, 2): See SLR-DES-01.
- SLR-DES-03 Restrictive UAV regulations (4, 4): This will hinder operations.
- SLR-DES-04 Noise pollution (2, 2): Requirement EHAC-SH-09-02 (Arblaster et al. 2019a) must be met.

### 5.1.6. Pre-mitigation likelihood-impact matrix

All risks identified in this section are aggregated in table 5.1, according to their likelihood and impact. To make a clear distinction between the general and the design risks, the design risks are printed in italics.

Table 5.1: Pre-mitigation technical risks shown in a likelihood-impact matrix

I / L	Remote (1)	Improbable (2)	Possible (3)	Probable (4)
<b>Catastrophic (4)</b>	<i>OR-DES-02</i> <i>OR-DES-03</i>	DR-GEN-01 DR-GEN-06 MR-GEN-10 OR-GEN-13 EOLR-GEN-08 SLR-GEN-06 SLR-GEN-09 <i>OR-DES-01</i>	<b>DR-GEN-08</b>	<b>SLR-GEN-08</b> <i>SLR-DES-03</i>
<b>Critical (3)</b>	SLR-GEN-03 <i>MR-DES-01</i> <i>MR-DES-02</i>	DR-GEN-02 OR-GEN-09 SLR-GEN-01 SLR-GEN-02 SLR-GEN-05 SLR-GEN-11 <i>DR-DES-06</i> <i>DR-DES-07</i> <i>OR-DES-06</i> <i>OR-DES-07</i>	DR-GEN-03 DR-GEN-04 DR-GEN-05 OR-GEN-01 OR-GEN-06 OR-GEN-08 OR-GEN-10 SLR-GEN-04 SLR-GEN-07 SLR-GEN-10 <i>DR-DES-03</i> <i>DR-DES-04</i> <i>DR-DES-05</i>	<b>DR-GEN-11</b> <i>EOLR-DES-02</i>
<b>Tolerable (2)</b>	<b>MR-GEN-07</b>	DR-GEN-07 MR-GEN-02 MR-GEN-06 MR-GEN-09 OR-GEN-05 EOLR-GEN-01 <i>SLR-DES-04</i>	DR-GEN-09 OR-GEN-04 EOLR-GEN-02 EOLR-GEN-05 EOLR-GEN-06 <i>DR-DES-02</i>	DR-GEN-10 OR-GEN-02 OR-GEN-03 <i>SLR-DES-01</i> <i>SLR-DES-02</i>
<b>Acceptable (1)</b>		MR-GEN-11 EOLR-GEN-04 EOLR-GEN-07 <i>DR-DES-01</i> <i>EOLR-DES-01</i>	MR-GEN-01 MR-GEN-03 MR-GEN-04 MR-GEN-05 MR-GEN-08 OR-GEN-11 OR-GEN-12	OR-GEN-07

## 5.2. Risk mitigation

As can be seen in section 5.1, several risks have a combined score of six or greater (e.g. possible and catastrophic). These pose too great of a threat to the project and must be mitigated. How this will be approached will be discussed in this section. The results of the mitigation are shown in a new likelihood-impact matrix in table 5.2. Again, to make a clear distinction between the general and the design risks, the design risks are printed in italics.

Five highly-problematic risks are identified as too big of a threat as they have a score of seven or more and must therefore first be mitigated: DR-GEN-08 Unreliable design methods, DR-GEN-11 Insufficient literature on novel technologies, SLR-GEN-08 Airspace unavailability, SLR-DES-03 Restrictive UAV regulations and EOLR-DES-02 Non recyclable material.

Unreliable design methods (DR-GEN-08) can be mitigated by using extensive verification and validation, especially by using various different design methods to verify the others. This way the likelihood of using unreliable design methods is lowered. In addition, the impact of the use of unreliable design methods will be lower, as the discrepancies will be less after comparison with other models.

DR-GEN-11 can be mitigated by the use of experts. Though the team may not be able to find the necessary literature, experts can point the team to the right direction. This way, the impact on the design of

the project is lowered, as the team will not be stuck on literature study as long. Additionally, the likelihood of insufficient literature will be lowered, as experts will provide us with more literature.

Airspace unavailability (SLR-GEN-08) is a great threat to the execution project. However, the client has specified that this project is meant to be a technological feasibility study, rather than a legal feasibility study. This means that, although it is probable that airspace is restricted, the project can tolerate this. If the product were to be taken to the execution phase, extensive lobbying would have to be done to make the project work legally as well, which would be aided by promising energy yields.

Restrictive UAV regulations (SLR-DES-03) will hinder the operation of the project. This risk is mitigated by placing the harvesting site at a location where it will have a minimal impact on its surroundings. More information on this can be found in chapter 9. The right permits will be requested to be able to operate the system.

Non recyclable materials (EOLR-DES-02) will prevent the system from being completely recycled. Though this is a requirement for the project, the primary mission is to provide energy. Therefore, at this point the material properties of sustainable materials may be insufficient, but developments in the field will be watched closely to switch to sustainable materials as soon as possible.

Also, risks with a score of six (4,2), (3,3), (2,4) will be mitigated. The post-mitigation risk map is shown in table 5.2

- Mission target is revealed to be infeasible (DR-GEN-01) can result in the possibility that the mission requirements will not be met. To mitigate this risk a safety factor on the energy demand is set, to make sure the system will generate more energy than is consumed.
- Final analysis of cost reveals design flaw (DR-GEN-03), this can be mitigated by negotiations regarding development costs. The project should have a return of investment of 10 years according to requirement EHAC-SH-11-04 (Arblaster et al. 2019a), which is the reason for this risk. However, after negotiations with the client this requirement is flexible to 15 or even 20 years, therefore lowering the likelihood. Additionally, costs can be lowered by waiting with the development until another party develops the technologies needed. This way, development costs can be reduced, so the impact is lowered as well.
- Inaccurate ground station estimations (DR-GEN-05) can cause an infeasible ground station to be chosen for the designed system. This risk is mitigated by doing in-depth research in different type of ground stations. Also, the ground station will be tested before the system will be working.
- Connection to the grid is infeasible (DR-GEN-06) can cause problems since it might affect the power outputs. This risk is mitigated by placing the harvest site close to a grid connection, and a transformer is used to transform the energy to the required voltage for the grid.
- Reliance on low-TRL technologies (DR-GEN-10) makes the system dependent of the development of these technologies over the years. This risk is mitigated by putting the lower-TRL technologies as recommendations.
- Incorrect estimation of glider power (DR-DES-03) might cause great variations in the estimated power output. This risk is mitigated in the same way as DR-GEN-01.
- Insufficient literature on high-altitude AWES (DR-DES-04) and insufficient literature on take-off procedure (DR-DES-05) are mitigated by informing experts on these subjects.
- Inspection errors (MR-GEN-10) will be mitigated by making sure that during inspection the system is checked by two different inspectors, to reduce the change of a significant fault being missed.
- Loss of communication (OR-GEN-01) and sensor failure (OR-GEN-06) are mitigated by doing regular maintenance. Also machine learning can be implemented in order to replace parts just before failure occurs.
- Structural degradation (environment) (OR-GEN-02) is mitigated by putting a coating on the surface area directly in contact with the environment.

- Structural degradation (fatigue) (OR-GEN-03) is mitigated by using a safety factor on the desired material properties chosen for the design. This ensures that the structure will hold until the planned maintenance.
- Bird-strike/other object (OR-GEN-08) is mitigated by placing the systems in a non-important bird area and placing markers around the tether to make it more visible to birds.
- Parts inaccessible for maintenance (OR-GEN-10) is mitigated by assembling the system in such a way that it is easily maintainable.
- Termination of funding (OR-GEN-13) is mitigated by being independent of third parties.
- Tether structural failure (OR-DES-01) is mitigated by replacing the tether regularly.
- Reusing worn out materials (EOLR-GEN-08) creates the possibility that reusability might not be appropriate. This risk can be mitigated by making sure parts are replaced in time to still be able to reuse the materials of the broken part.
- Habitat disturbance (SLR-GEN-04), ecologically sensitive site (SLR-GEN-06), wildlife mortality due to tether (SLR-DES-01) and wildlife mortality due to glider (SLR-DES-02) are mitigated in the same way as OR-GEN-08.
- Resident disturbance (SLR-GEN-07) and ground area unavailability (SLR-GEN-09) are mitigated by placing the harvesting site in an area of the Netherlands with a low population density.
- Restrictive grid regulations (SLR-GEN-10) is mitigated by researching existing wind harvesting farms, and operating in a similar way. Which will allow the designed harvesting system to supply energy to the grid.

Table 5.2: Post-mitigation technical risks shown in a likelihood-impact matrix

I / L	Remote (1)	Improbable (2)	Possible (3)	Probable (4)
<b>Catastrophic (4)</b>	DR-GEN-01 OR-DES-01 OR-DES-02 OR-DES-03			
<b>Critical (3)</b>	SLR-GEN-03 MR-GEN-10 OR-GEN-01 OR-GEN-06 OR-GEN-08 SLR-GEN-04 SLR-GEN-07 SLR-GEN-10 MR-DES-01 MR-DES-02 DR-DES-03 DR-DES-04	DR-GEN-02 DR-GEN-03 DR-GEN-08 OR-GEN-09 SLR-GEN-01 SLR-GEN-02 SLR-GEN-05 SLR-GEN-11 EOLR-GEN-08 DR-DES-06 DR-DES-07 OR-DES-06 OR-DES-07 SLR-DES-03		
<b>Tolerable (2)</b>	MR-GEN-07 DR-GEN-06 OR-GEN-10	DR-GEN-05 DR-GEN-07 MR-GEN-02 MR-GEN-06 MR-GEN-09 OR-GEN-05 EOLR-GEN-01 SLR-GEN-06 SLR-GEN-09 OR-GEN-02 OR-GEN-03 SLR-DES-04 EOLR-DES-02 SLR-DES-01 SLR-DES-02	DR-GEN-09 DR-GEN-11 OR-GEN-04 EOLR-GEN-02 EOLR-GEN-05 EOLR-GEN-06 DR-GEN-10 SLR-GEN-08 DR-DES-02 OR-DES-05	
<b>Acceptable (1)</b>	OR-GEN-13	MR-GEN-11 EOLR-GEN-04 EOLR-GEN-07 DR-DES-01 EOLR-DES-01	MR-GEN-01 MR-GEN-03 MR-GEN-04 MR-GEN-05 MR-GEN-08 OR-GEN-11 OR-GEN-12	OR-GEN-07

## Technical analysis of the tethers

One of the most driving and innovative subsystems of the design is the tether. Bringing tethers from the ground to a few kilometers in the air is something that is not regularly done. As it is so big, it will experience sag, and thus it is not straightforward to make a model of it. This process will be described in section 6.1. The rotating y-connection and tether replacement will be discussed in sections 6.1.4 and 10.8. Of course, a material selection for the tether is necessary, which will be done in section 6.2. The friction, durability and weather performance is discussed in 6.2. Emergency for the tether and aerodynamics are discussed in sections 6.4 and 6.5. The chapter will be concluded with verification, conclusions and recommendations. Most calculations used in this chapter will include numbers as inputs which are calculated in a big optimization with all different departments involved. Therefore some input numbers will be used which will be explained later in the report. A final overview of numbers, including tethers, can be seen in table 7.11.

### 6.1. Tether model

A model of the tether is necessary to calculate the performance of the entire system. The tether model is based on sag, vibrations and it is split in different segments and connections.

#### 6.1.1. Tether sag

The longest part of the tether, from the ground station until the y-connection, will likely encounter tether sag due to its own weight. For this problem, catenary cable approximations are used (Kumarasena et al. 2005). The main variables in these approximations are shown in figure 6.1.

$$y = \frac{H}{w} \cosh\left(\frac{w}{H}x + K_1\right) + K_2 \quad (6.1)$$

The main inputs of these approximations are the horizontal tether tension,  $H$ , the operating altitude  $h$ , the horizontal operating distance  $L$  (which can be found using the altitude and the elevation angle  $\beta$ ), and the weight per unit length of the tether. Equation 6.1 determines the y-coordinates of the sagged rope under its own weight and a horizontal load.  $K_1$  and  $K_2$  are integration constants that can be found by evaluating equation 6.1 at the boundary conditions (0,0) and (L,h), resulting in equations 6.2 and 6.3. The tether length required to account for the sag can then be computed using equation 6.4 (Kumarasena et al. 2005).

$$K_1 = \operatorname{arcsinh}\left(\frac{wh}{2H \sinh\left(\frac{wL}{2H}\right)}\right) - \frac{wL}{2H} \quad (6.2)$$

$$K_2 = -\frac{H}{w} \cosh(K_1) \quad (6.3)$$

$$C = \frac{H}{w} \left( \sinh\left(\frac{wL}{H} + K_1\right) - \sinh(K_1) \right) \quad (6.4)$$

Due to the sag, the angle the tether makes with the generator and the angle it makes with the glider will not be equal to the angle the glider makes with respect to the ground and the generator ( $\beta$ ). Ideally, the glider will be pulling the tether tangential to the tether at the glider connection point,  $\beta_1$ . Additionally, it must be verified that the tether shall not drag over ground, so  $\beta_0$  must be larger than zero.  $\beta_0$  and  $\beta_1$  can be found using equations 6.5 and 6.6 respectively.

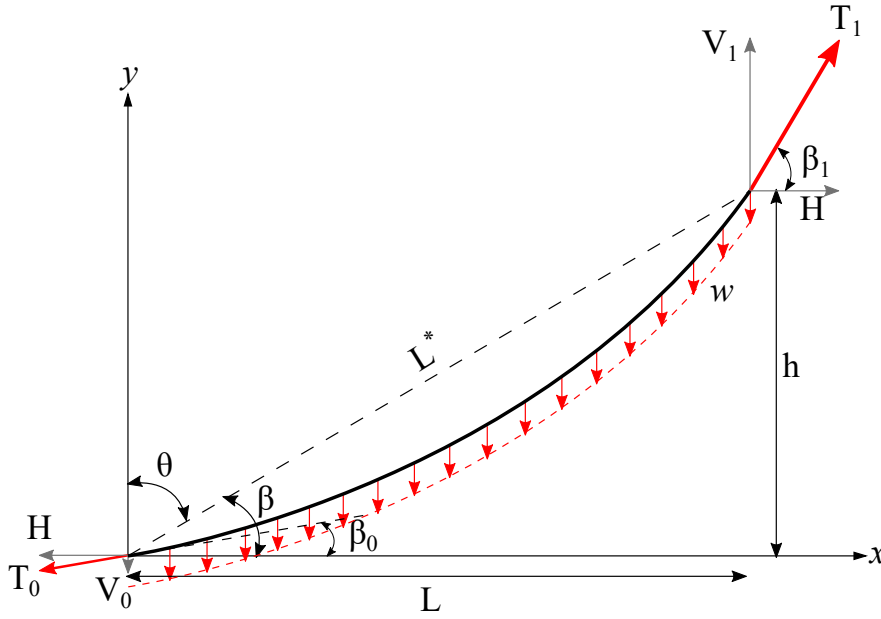


Figure 6.1: The parameters for the catenary cable approximations

$$\beta_0 = \arctan(\sinh(K_1)) \quad (6.5)$$

$$\beta_1 = \arctan\left(\sinh\left(\frac{wL}{H} + K_1\right)\right) \quad (6.6)$$

In the case of the glider, it is known what the lift force is and at what angle this lift force is generated. This means that  $T_1$  and an ideal  $\beta_1$  are known, as well as the operating altitude  $h$ . The elevation angle  $\beta$  is still unknown, but the script runs for different values of  $\beta$  until a value of  $\beta_1$  is achieved equivalent to the angle of the lift. After computing  $\beta_0$  and also using  $H$ , the tension force at the generator ( $T_0$ ) can be found by using trigonometry. The same equations can be used for the tether sag beyond the Y-connection.

Depending on the material properties (tensile strength and density) the cable may sag more or less. The top of the tether experiences the highest tension (as can also be seen from figure 6.1), because the top will experience tension due to the lift force and the weight of the cable. The cable dimensions are found using the definition of average normal stress (equation 6.7), as the cable can only be loaded in tension. Here,  $A$  is the cross sectional area of the cable, which can be found by rearranging equation 6.7 and using the ultimate strength or yield strength of the chosen material. A safety factor of five is applied to ensure the tether will not fail even during the worst of conditions and wind gusts. This safety factor is further elaborated in section 6.3. Using the density of the material, the weight per unit length can be found and used in the catenary cable approximations.

$$\sigma = \frac{T_1}{A} \quad (6.7)$$

### 6.1.2. Tether vibrations

Some substantial factors for vibrations in the tether are vortex-induced vibrations, galloping due to ice accumulation and the motions due to fluctuating tether tensions and lengths (Schmehl 2018, p. 29).

Vortex-induced vibrations are caused by the vortex shedding of the wind around the tether. These vibrations are generally low amplitude, high frequency vibrations. The tether for this project will be several kilometers long, which means that the wind speeds and directions will vary along the tether. This means

that vortex-induced vibrations will have a local cause glider instabilities. Nonetheless, these low amplitude vibrations can still increase tether drag by up to 300% (Schmehl 2018, p. 29).

Another concern is ice formation along the tether causing galloping, a type of vibration caused by non-circular cross sections. Galloping is a high amplitude, low frequency vibration and can increase drag by up to 210% (Schmehl 2018, p. 29). As this type of vibration is not as predictable and has larger amplitudes, the tether should be designed to (passively, or even actively) shed ice to prevent galloping from occurring.

Fluctuating altitudes and speeds of the gliders produce fluctuating tension in the tethers (Kumarasena et al. 2005). The difference in tension on the tether, will create either an increase, or decrease in sag, inducing vibrations on the tether.

As the energy will be harvested by reeling in and out the tether, the length of the tether will constantly change. This tether length change will not only induce vibrations on the tether, but also constantly change the natural frequency of the tether.

As stated, the natural frequency and therefore the vibrations of the tether will constantly change due to the fluctuating tension and length of the tether. Due to a shortage of literature that was found, it has been chosen to assume that the tether drag will increase by 300% due to vortex-induced vibrations and 210% by galloping.

### 6.1.3. Segments

For this model it was assumed that the tether is made of one continuous segment of constant thickness. However, as the top of the tether carries higher loads (as it must also carry its own weight), one could consider tapering the tether to become thinner towards the ground. This would make the tether lighter, therefore making the system more efficient. The bottom of the tether, however, wears relatively fast. A thicker tether there could be of use to account for this tether wear. Additionally, weaving a cable that decreases (or increases) in diameter without structurally adding a weakness in the tether can prove to be difficult. Therefore, at this stage of the development of the system, it has been decided to not have different tether segments other than those mentioned in the upcoming sections.

### 6.1.4. Connections

#### Tether to glider connection

As can be seen in table 7.11, the net tether force at the connection to the glider is equal to 106.8 kN. As the tether is connected to the glider, the connection between them needs to be able to withstand that force as well. The tether force  $F_{tether}$  will be higher when taking into consideration a load factor.

To search for an existing system that can withstand the force, it has been looked at the connection of the winch tow to a glider. Different types of connections exist, but the strongest can only withstand 10 kN (Corporaal 2017), which is lower than the required 106.8 kN and thus not feasible.

Next, the tailhook of a fighter jet was looked into. The tailhook is often used to secure the aircraft to the ground and prevent its motion during high power tests (Yoon 2007). An F-16 has an engine thrust class of 13,000 kg, thus a throttle force of around 130 kN<sup>1</sup>. As this connection handles lower forces than the tether-glider connection should withstand, but comes close, it is assumed that the tether-glider connection will have the same shape as the tailhook mechanism, but thicker to make it stronger. Looking at the strongest materials available, and taking the CO<sub>2</sub> footprint into account, it has been chosen to use a stainless steel alloy with martensitic as the material for the connection mechanism (Granta Design Limited 2019).

#### Tether to drum connection

The connection at the ground station between the drum and the tether will be determined by the chosen drum. Most likely, the tether has to be pulled through the drum to prevent it from loosening up.

---

<sup>1</sup><https://www.lockheedmartin.com/en-us/products/f-16.html> [cited 6 January 2020]

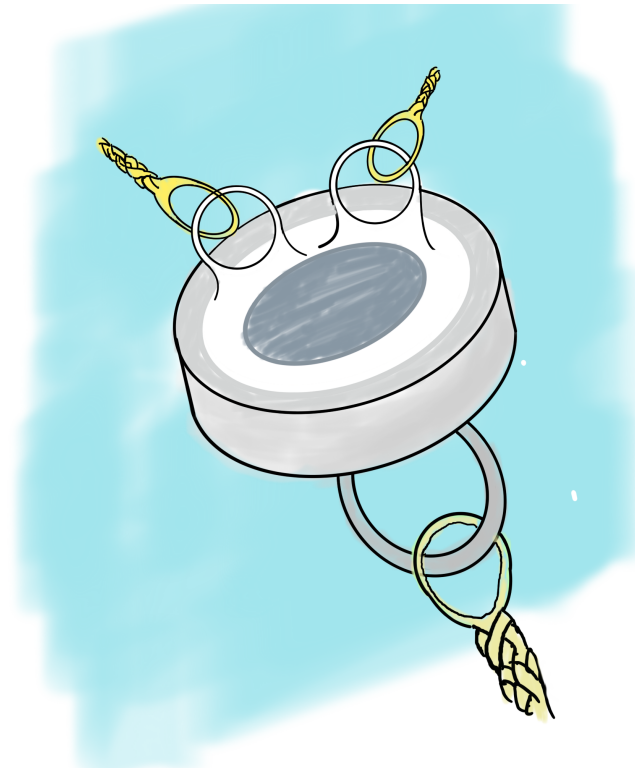


Figure 6.2: Sketch of Y-connection

### Y-connection

As the system involves two gliders both attached to the stationary cable, there has to be a connection point at which the two glider cables and the long stationary cable come together. The interface between those has to be designed. The interface needs to withstand the tensile forces generated by the gliders. Furthermore it needs to allow for free rotation. As the rotation is continuous in 360°, a ball bearing is needed to provide for this rotation. The ball bearing shall have one cable attachment on the downside of the bearing, and two cable attachments on the upper side of the bearing. It should withstand a basic dynamic load rating of 364 kN, which would accommodate for a safety factor of 2. The model 51160 M of SKF<sup>2</sup> will be able to support this requirement. Tethers will be connected using mounted rings on the bearing and an eye made by splicing the cable together after the eye is made. This does not allow for easy replacement, as the tether has to be spliced again. It is therefore vital that the bearing does not have to be replaced too often. Thus, quality of the bearing is important, especially for the high tensile loading. In order to reduce tear and wear, the ball bearing will have to be prepared as specified by SKF. A sketch is provided in figure 6.2 to support the story.

## 6.2. Material selection

With a tether model in place, available materials can be investigated to find a suitable match. The material must have a low density and high tensile strength, but also be quite durable. This section investigates two main options: banana fibre and Dyneema SK75.

### 6.2.1. Banana fibre

Since requirement EHAC-SH-11-01 dictates that the system must use renewable materials whenever possible, bio-based fibres are investigated to construct the tether rope. An overview of available fibres (both

<sup>2</sup><https://www.skf.com/ph/products/rolling-bearings/ball-bearings/thrust-ball-bearings/productid-51160%20M> [cited 19 December 2020]

synthetic and bio-based) is shown in figure 6.3, of which a selection have been labeled.

As can be seen, banana fibre performs the best in tension of all natural fibres. Kenaf fibre has a density about 20% lower, which is favourable, but its considerably lower yield strength (on average about 50% lower), makes this a worse choice overall. Several synthetic fibres outperform banana fibre, most notable of which is polyethylene – this is the material Dyneema cables are made out of, which are traditionally used in airborne wind energy applications.

Given the emphasis on sustainability and requirement EHAC-SH-11-01, banana fibre will be investigated. However, this comes with the implication that available literature is scarce. Virtually all available literature on the design of AWES assumes the use of high-modules polyethylene tethers (Schmehl et al. 2013; Schmehl 2018, p. 410, 42). How banana fibre can be used to create a satisfactory tether will therefore prove to be challenging.

Research has shown that banana fibre is able to perform between  $-50^{\circ}\text{C}$  and  $130^{\circ}\text{C}$  (Granta Design Limited 2019), meaning it is appropriate for this outdoor application, even at high altitudes. Additionally, it can perform under exposure to water, but the material is flammable (Granta Design Limited 2019), which forms a risk that should be mitigated.

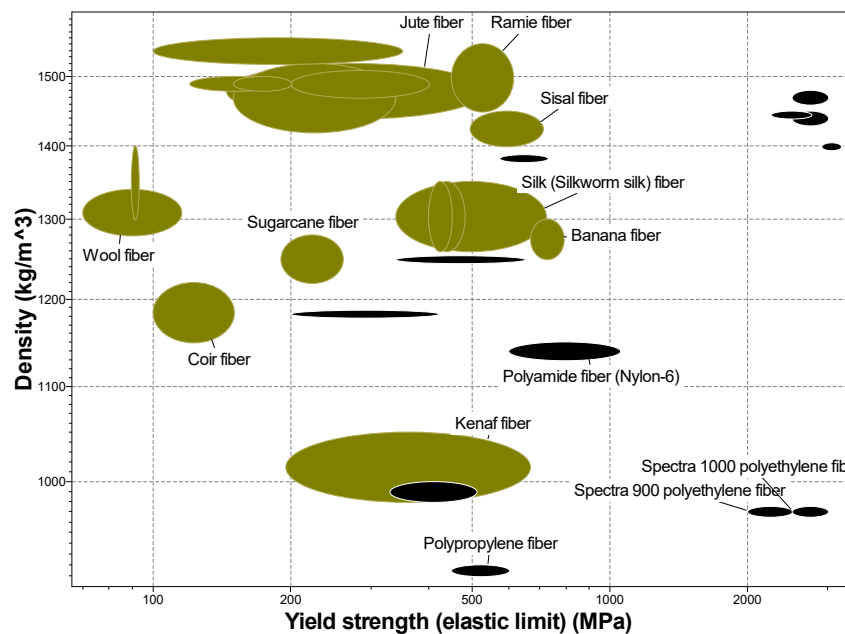


Figure 6.3: Available fibres – natural (green) and synthetic (black) – as a function of their yield strength and density (Granta Design Limited 2019)

### Treating banana fibre

The hydrophilic nature of natural fibres is particularly disadvantageous, as this means the weight of the tether could increase drastically as it absorbs atmospheric moisture or precipitation. One way of decreasing this effect is by treating the fibres with Sodium Hydroxide (NaOH), which removes impurities from the fibre surface, decreases moisture absorption. This procedure reduces the mass and tensile strength of the fibres, so low concentrations of NaOH are needed (below 1%). This results in fibres which absorb an average maximum of 11% of their weight in moisture (Doshi 2017) – this is still a lot considering the importance of weight and frost resistance in this application. This treatment also makes the fibres more flexible, making braiding them easier. How the fibres will be braided and what effect this has on tensile performance is discussed in sub-subsection 6.2.1.

### Weaving banana fibre

The performance of individual fibres differs greatly from the performance of a woven rope. Entire industries are dedicated to study of ropes and weaving techniques. The detailed know-how of this field required to design a high-performance banana-fibre rope is not something attainable during the duration of this project. Therefore, the performance of familiar ropes will be analysed and utilised: the properties of Dyneema ropes of various sizes are known<sup>3</sup>, as are the properties of Dyneema SK78 fibres<sup>4</sup>, of which these ropes are made. 12-strand braided ropes are commonly applied in AWES, due to them being torque neutral; they won't untwist under stress (Schmehl et al. 2013, p. 567).

By analysing the density and strength of the fibre and of ropes of different diameters, a correlation can be found between the strength of a rope and what amount of fibre that it requires. Figure 6.4 shows how, as the thickness of 12-strand rope increases, its performance increasingly deviates from that of pure strands of fibre. Note that ropes with a thickness larger than 10 cm in diameter were not taken into account, as such a thick rope would in no case be desirable with an airborne application in mind.

The relation by which the weight of the rope increases by rope cross-sectional area has been found to be a constant factor of 2.847, as expressed in equation 6.8, where  $m$  – the masses – are expressed in kg. 'Solid fibre' refers to a hypothetical single-fibre rope with the same tensile strength as the 12-strand rope. It is assumed that the density of the rope is the same as the density of the 'solid fibre'.

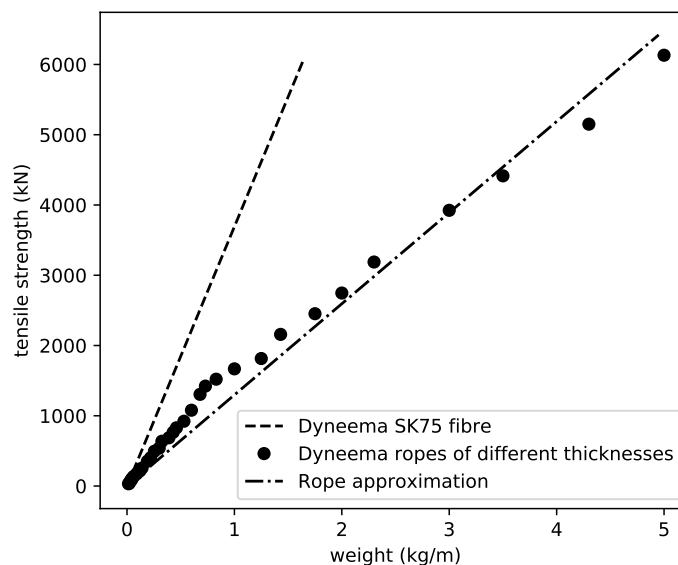


Figure 6.4: Difference in performance between SK75 fibre and Dyneema ropes of various thicknesses

$$m_{12\text{-strand rope}} = 2.847 m_{\text{solid fibre}} \quad (6.8)$$

The tensile loads the rope will experience cannot feasibly be supported using a rope made purely of banana fibre when this relation is taken into account. Using the equations found in subsection 6.1.1, a banana fibre rope will always hit the ground at the desired operational angles. Therefore, a stronger fibre must be added to achieve the desired properties. However, as was established from figure 6.3, there are no natural fibres which outperforms banana fibre in its tensile strength relative to its density, meaning an artificial fibre must be used.

<sup>3</sup><http://www.shipserv.com/ShipServ/pages/attachments/214394/Dynamica%20Ropes%202012%20brochure.pdf> [cited 13 January 2020]

<sup>4</sup><https://www.pelicanrope.com/pdfs/Dyneema-Comprehensive-factsheet-UHMWPE.pdf> [cited 10 January 2020]

As the approach to analysing the tether reaches far beyond the tensile performance of the rope, the choice is made to use a readily-available rope for these analyses. This rope will unfortunately not have an ideal life-cycle, but will allow for the further analyses this project calls for. Recommendations for the further investigation of the ideal tether material can be found in section 6.8.

### 6.2.2. Dyneema fibre

As was already mentioned in the analysis of banana fibre in subsection 6.2.1, the performance of Dyneema is not only well-known, but the best-performing material for this application. Because of these characteristics – and because it has been concluded that no natural fibre can sustain the necessary loads while exhibiting acceptable sag characteristics – a Dyneema rope will be used for further analysis of the system. This assumption leaves a lot of room for investigation in renewable ropes.

However, for the time being, the use of Dyneema greatly simplifies further analysis. Whereas the durability of banana fibre has only been scarcely studied, notably including the abrasion resistance (Doshi 2017), a range of durability factors for Dyneema are known, including abrasion resistance, fatigue resistance, UV resistance, and moisture resistance (Schmehl et al. 2013, p. 542).

## 6.3. Friction, durability, and weather performance

Each section of the tether will experience its own wear. This will range from its exposure to the weather, including UV radiation and precipitation; to the loading cycles it experiences; to the wear associated with the reeling of the tether around itself. This section investigates these effects and what can be done to improve the performance and durability of the tether.

### 6.3.1. Durability and weather performance of upper sections

The sections of the tether above the hook are continuously exposed to atmospheric conditions during operations. This brings with it UV degradation, as well as constant exposure to moisture. Additionally, as with the entire tether, constantly-changing forces reel the tether in and out, causing fatigue.

The degradation of a Dyneema cable has been previously modeled (Schmehl et al. 2013, p. 542) to reveal its lifespan for different design factors. In this example, a rope of 8 cm diameter is used. This might not be the case for this application. However, since the material is the same and the factors are unitless, it is assumed these numbers can be carried over. The degradation factors for the tether are shown in table 6.1.

For the purpose of this report, these factors are assumed to be linear; e.g. as the table shows a performance of 90% the performance of the original rope after 500 hours due to abrasion, after another 500 hours of the same abrasive forces, the rope is assumed to operate at 81% ( $= 90\% \cdot 90\%$ ) of the original strength.

The one number which can be analysed in some detail is the fatigue factor, which is based on the duration of a manoeuvre. Compared to the four figure-eight manoeuvres the reference makes, the gliders each perform one circle every 33 seconds – a difference of factor 2.2, which will be used to change the operating time to reach a given fatigue factor. Additionally, it is unclear whether the reel-in phase of the cycle is taken into account in the example given (Schmehl et al. 2013, p. 542) – to be on the safe side, this report will assume it is.

Another factor which could deviate from the reference case is the weather degradation. The tether used in this case will experience more extreme conditions due to its altitude. Upcoming subsections in the section will deal with this. However, to what degree the degradation factor will be higher or lower than a tether low to the ground is not known. Under the assumption the preventive measures compensate the more extreme conditions, the same value is used, noting that further research is required.

Using these performance factors over time, a design factor can be created for a desired lifespan; i.e. for a given duration of operation, the factor by which the load the tether must be able to bear must be multiplied to find the required initial strength of the tether. For this, a safety factor, dynamic factor, and asymmetric factor are needed. These are taken to be 1.5, 1.1, and 1.2, respectively (Schmehl et al. 2013,

Table 6.1: Used set of degradation factors (Schmehl et al. 2013, p. 542)

HMPE Dyneema rope	Joint efficiency	Abrasion	Fatigue	Moisture	UV exposure
Durability factor	0.80	0.90	0.75	1.00	0.80
Est. operating time [hrs]	n.a.	500	2200	n.a.	1050

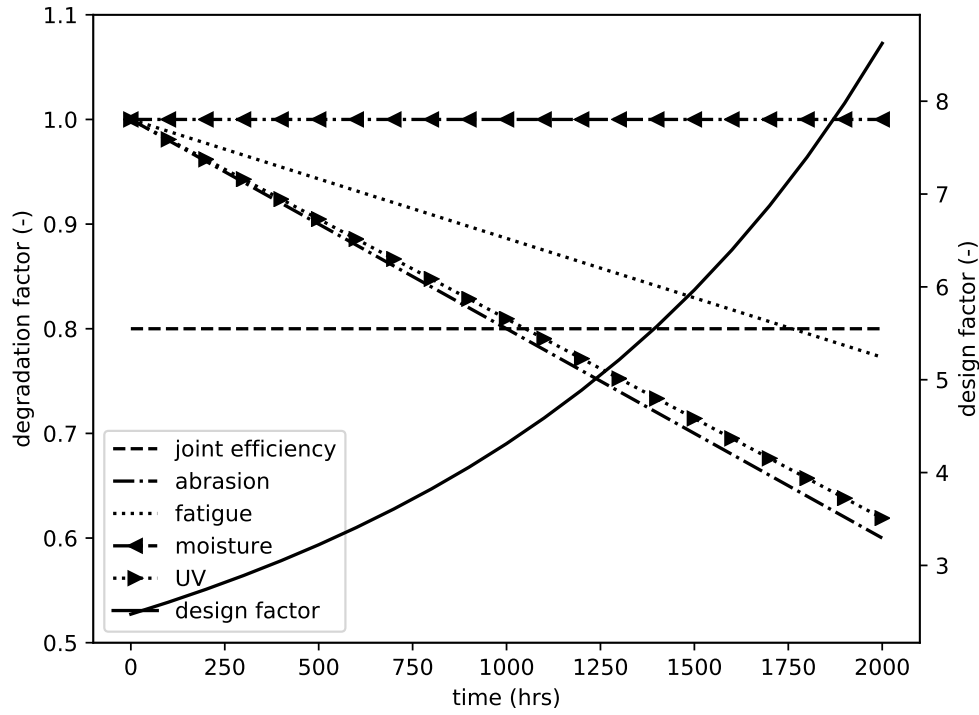


Figure 6.5: Degradation factors for the tether over time with associated design factor

p. 543). Multiplying these factors together and dividing by the product of all degradation factors at each time step results in figure 6.5. This graph reveals that for a lifespan of 24 hours, a design factor of 2.5 is required, while a design factor of 5.0 leads to a lifespan of 1225 hours (51 days).

Judging by figure 6.5, it is clear that, with a higher desired lifespan, the increase in design factor results in diminishing returns. Because of this, a design factor of 5.0 was chosen, striking a balance between a the lifespan of the tether and its structural/aerodynamic performance.

### 6.3.2. Durability and friction of reeled section

During each pumping cycle, the gliders first reel out the tether – generating electricity by spinning the drum – after which the tether is reeled in again, expending some of the generated energy. Because of the varying load the tether experiences at each point as it is wound around the drum, the tether will experience fatigue wear. The length of the cycle (circa 800 m of tether being reeled out/in) also requires winding the tether being reeled around the drum across several layers, which brings considerable abrasive wear into the picture.

Investigating the performance of multilayered ropes is part of tribology – a multidisciplinary field based in material science, physics, chemistry, and engineering, to name a few – and has been intensively investigated for the purpose of lifting loads (e.g. in mining, shipping, or off-shore drilling). However, these applications use wire rope, usually made of steel, to carry loads of many tonnes (Yu-xing et al. 2016). These scenarios differ rather crucially from the aerospace applications used in airborne wind energy.

Although it is well-established through experience that tether wear is an important factor to consider

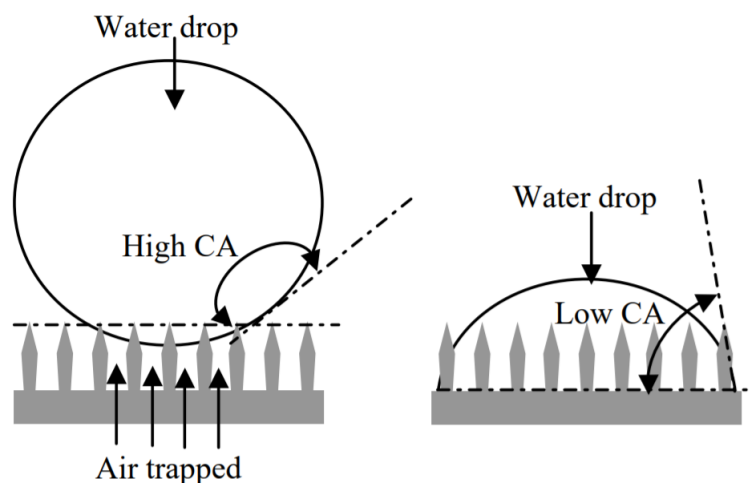


Figure 6.6: Visualisation of the contact angle (CA), from (Volat et al. 2005)

(Schmehl 2018, p. 645, 655, 720), it appears no detailed analysis of the guidance and wear of tethers being reeled has been done (Schmehl 2018, p. 453). This makes it difficult to design for the durability and wear of this part of the tether. For the purpose of this project, it is valuable to obtain some idea of how often the tether should be replaced and what can be done to improve its lifespan.

It has been claimed that a design factor of 3.0 would result in a rope that can be in service for up to a year (Schmehl 2018, p. 453), but this seems to be in blatant contradiction to the analysis performed in subsection 6.3.1, where a design factor of 5.0 results in a tether that lasts just 51 days. Ignoring this discrepancy, the main takeaway from current experiences is that the sheath guiding the tether to and from the drum must turn smoothly, or the lifespan of the tether could be reduced to a few days (Schmehl 2018, p. 477). Additionally, temperature could play an influential role in this section of the tether.

Because of the contradicting numbers found in literature, presumably resulting in a pessimistic estimation in 6.3.1, the lifespan for this section will be assumed to be similar for the purpose of further analysis (using a design factor of 5.0 and a lifespan of 51 days). During later design phases, these assumptions must be critically evaluated, which must certainly include rigorous testing under representative conditions.

### 6.3.3. Considering freezing temperatures

The effects examined in subsection 6.3.1 are incomplete, they do not include the high-altitude effects the tether experiences; at the operational altitude, temperatures are commonly freezing, meaning the formation of ice on the tether seems inevitable. As active de-icing is unlikely for these tether lengths and materials, mainly passive anti-icing coatings are considered.

The freezing of water that has adhered to the tether poses the problem of vibrations and additional weight of the tether. Therefore, anti-icing coatings and de-icing must be considered. The first step of anti-icing is to prevent water from adhering to the tether. Two factors that will affect the hydrophobicity of a coating are the contact angle and the roll angle. The contact angle defines the angle between the surface and a water droplet, as shown in figure 6.6. The roll angle is defined by the angle of the surface at which the droplet starts to slide. For a hydrophobic coating, a high contact angle and a low roll angle is desired (Volat et al. 2005).

Two options for the tether hydrophobic coating exist: hydrophobic chemicals and topology coatings. In chemical modification, the tether is sprayed with hydrophobic fluids that have for example a carboxylic or silane attachment to the surface. They then have a long "tail" of for example hydrocarbons<sup>5</sup>.

Topology coatings create small structures that trap air, such that when a water droplet falls on it, it

<sup>5</sup>Dr. S.J. Garcia, private communication, 14 January 2020

barely makes contact with the surface and the air pressure prevents it from seeping through the gaps. However, water vapour could still adhere to the surface and freeze<sup>5</sup>. A recent study (Jiang et al. 2018) has shown the possibility of using silicon carbide and carbon nanotubes for both passive anti-icing and active de-icing. The study uses the silicon carbide for the passive anti-icing using the methods described above, while the carbon nanotubes are used for their photothermal properties. The carbon nanotubes will heat up under near-infrared (808 nm) irradiation, thereby de-icing the surface.

One limitation of icephobic coatings is that the particles used are often toxic. Many coatings are applied as sprays with nano-sized particles that could be harmful for the environment. However, these kinds of coatings are necessary, regardless of the material chosen for the tether. Therefore, this harmful coating is unavoidable.

Another limitation of any type of super hydrophobic and/or icephobic coating is its durability and the effects of tension on the coatings. How the coatings are affected by continuously being reeled in and out is something that must be investigated. Similarly, how the coatings react to the continuous tension in the cable is a valuable parameter. As there currently is little to no research on this application of icephobic coatings, further testing of different coatings should be performed before a decision can be made.

## 6.4. Emergency procedures

A tether of over 4 km long poses some safety concerns when operating up to an altitude of 3 km. Should a tether fail, safety procedures shall be in place to ensure the system as a whole does not fail catastrophically. The main concern is the impact of the tether should it be disconnected from the gliders and fall from the sky.

For sailplanes, a parachute is integrated into the cable such that when the cable is in tension, the parachute is stretched out and does not affect the cable too much. However, when the cable is released from the sailplane, the cable is no longer in tension, so the parachutes deploy naturally. This concept is clarified in figure 6.7. Though this system works well for sailplanes, the tether for this system carries substantially higher loads, which the parachute would have to carry as well. Therefore, an active deployment is chosen at the Y-connection of the tether (at approximately 3km altitude). Then, if one tether fails at a glider, the other glider shall release its tether as well, and the tethers will fall. This initiates the deployment of the parachute, guiding the tether down at the speed that the generator can reel in the tether.

$$mg = \frac{1}{2} C_d \rho V^2 S \quad (6.9)$$

The parachute shall generate enough drag to overcome the weight of the tether. The drag coefficient for a typical parachute is approximately 1.75<sup>6</sup>. Assuming a tether mass of approximately 2,300 kg (taken from chapter 7), a constant air density of 1.225 m/s<sup>2</sup>, and a maximum reel speed of 20 m/s (so approximately 12.8 m/s vertically for an operation angle of 40°), the minimum surface area of the parachute can be computed using equation 6.9. For these values a surface area of 128.5 m<sup>2</sup> (diameter of 6.4 m) is required for a safe reeling in of the tether.

As the tether is being reeled in, the mass the parachute has to carry becomes lower as well, so the parachute is soon oversized. However, the heavier tether is, the more danger it poses to the environment, so having an oversized parachute is a safety measure. Additionally, considering the fact that the parachute will take some time before being deployed, this oversized parachute can only be good. These emergency procedures are for safety reasons only, so the power it consumes to reel the tether in is not considered. Using a reel speed of 20 m/s and a tether length of 3,600 m, the whole tether will be reeled in safely within 3 minutes.

To ensure the parachute will not fail, the parachute must be able to be deployed also in cold conditions. This means the parachute may not freeze shut. This may require active heating, or similar icephobic coatings as the tether must have. This would have to be investigated further.

<sup>6</sup><https://www.grc.nasa.gov/www/k-12/VirtualAero/BottleRocket/airplane/rktvrecv.html> [cited 10 January 2020]



Figure 6.7: The cable parachute of a sailplane cable (Corporaal 2017)

## 6.5. Aerodynamics

An analytical model was used to calculate the tether drag. Based on general assumptions. Only the drag was incorporated, as the friction is negligible compared to the drag. The  $C_d$  is the drag coefficient of the tether, this is assumed to be 1 (Schmehl 2018, p. 38).

The tether was divided into small elements of which each individual contribution to the drag was calculated according to equation 6.10. The drag of the elements was added together to find the total tether drag.

$$D = \frac{1}{2} C_d \rho V^2 d_{tether} l_{element} \quad (6.10)$$

To find the advantage of using two gliders attached to one tether, the aerodynamic drag of the moving tethers (upper tethers) has to be compared to the stationary part of the tether. Tether sag is important, but the stationary cable length only increases from 4,667 m to without sag to 4,800 m with sag. The upper tethers are shorter. Based on this knowledge, the drag of the upper tether was calculated, based on several assumptions.

- skin friction is neglected
- no cable sag for the upper tethers
- the air density is constant and equal to that at the average altitude of the gliders
- the  $C_d$  is the drag coefficient of the tether, this is assumed to be 1 (Schmehl 2018, p. 38)
- constant apparent speed of the glider

The angle between the two tethers is set at  $60^\circ$ . Together with the data stated in table 7.11, which resulted from several iterations, this leads to a drag of 16 kN per cable.

For the stationary tether the force in negative vertical direction and pushing force in wind speed direction are calculated. The calculations were performed on a tether without sag and the results were scaled to get the drag with sag based on several assumptions.

- altitude differences due to sag w.r.t. to a rigid cable are neglected
- drag scales linearly with the increase in cable length due to sag

With the data stated in table 7.11, which resulted from several iterations, this leads to a force of 0.45 kN in the direction of the wind speed and 1.2 kN downwards. These forces are negligible with respect to the aerodynamic drag of the upper tethers. Wind and other loads would cause the stationary tether to move and increase the aerodynamic forces on it. However, when the forces would multiply several times, they are still negligible with respect to the aerodynamic drag of the upper tethers.

Finally the drag when the entire cable would turn was calculated. With the data stated in table 7.11, which resulted from several iterations, this would lead to a drag of 76.5 kN, some five times higher than the Y-configuration and leading to a power output of 0 W, as the gliders could not maintain flight. This proves that using a Y-tether connection is the way to go to harvest wind energy above the clouds.

Tether vibrations were excluded from the calculations, as it is completely unclear how to implement them. Experimental data of short tethers showed that the drag could enlarge from 210% up to 510% as stated in subsection 6.1.2. It is unclear though, how this test data can be applied to the glider design, which has longer tethers at a higher altitude and speed. If the increase in drag is as high as mentioned, the gliders would no longer be able to fly and generate power. Still, aerodynamic improvements in cable technology might lead to power output increases of up to three times (Cherubini et al. 2015). This could counteract the drag increase due to vibrations to a large extent. Testing the design in real life circumstances is the only way to implement the tether improved aerodynamics and vibrations, which is outside of the scope of this project.

## 6.6. Verification

Verification of the tether sag computations was done by first verifying the catenary cable equations. The source of the equations (Federal Highway Administration of the USA) is reliable, and cites a journal paper from *Transactions of the American Society of Civil Engineers* for these equations. These equations are used for the stay cables of bridges mainly, but bridges are at this point of the development of this project one of the closest comparisons.

Once the equations are verified, the code written for the tether sag must be verified. The code was written in multiple definitions, thereby making the code simpler to verify. Other than using the engineering intuition, the computations were verified by hand. Plots and print functions were also used to visualise the results for mid-way calculations to verify that all inputs and outputs of the definitions were consistent and plausible. Further verification of the tether sag cannot be performed, as similar tethers do not exist, so no comparable data is available.

Verification of the tether drag calculations was done with hand calculations, comparing the drag at the elements at the lowest and upper part of the cable. Also hand calculations were performed on a generalisation of the entire cable in order to verify the order of magnitude of the outcomes of the integration of the cable segments in the code.

## 6.7. Conclusions

The Y-connection of the tether will exist of the thrust ball bearing with a basic dynamic load rating of 364 kN, which would accommodate for a safety factor of 2. The model 51160 M of SKF will be able to support this requirement.

Dyneema was selected as the tether material. It is not sustainable, which is a pro of banana fibre, the alternative. Banana fibre would however require a thicker and heavier tether, which would make the design unfeasible. Hydrophobic coating is needed to maintain correct material properties during operation. A parachute is added to the cable as an emergency feature.

The aerodynamic drag of each Y-tether is 16 kN in the negative direction of the tangential flight speed. The aerodynamic forces on the stationary cable are 0.45 kN in positive wind direction and 1.2 kN downwards. If the entire tether would move instead of just the Y-tethers, the drag increases by 400%. This would lead to no power output.

An overview of all numbers and variables calculated in the optimization is given in table 7.11.

## 6.8. Recommendations

Some research on the tether was out of the scope of this project, or exceeded its limitations in another way. Several recommendations are listed in the subsections below for further research.

### **6.8.1. Tether aerodynamics**

Active vibration counteraction on the tether might be needed, as well as thinner or more aerodynamically shaped tethers. To simulate this, a numerical model will be needed for verification purposes.

### **6.8.2. Tether material**

At the outset, banana fibre was heavily investigated as a possible material to use for the tether, as it is the natural fibre with the best tensile properties, as well as having a favourable density. However, it became clear that a rope made purely from banana fibre would not be feasible. This can be attributed – at least in part – to the method used to obtain the properties of a rope from pure fibre. This is a limited view into the field of rope making, where it is not uncommon to construct ropes combining several materials, e.g. using one as a core.

It does appear that banana fibre can be incorporated in the tether of an AWES, but basic 12-strand braiding methods would not suffice. In further research, the incorporation of other materials in combination with banana fibre could result in a more sustainable solution. However, it must be noted that concerns of durability should remain important.

### **6.8.3. Tether durability**

No tests were performed during this project. Therefore, it is often not known how accurate certain factors are for this particular application. The coatings used could outperform or underperform the estimations here, with serious effects on the financial and maintenance aspects of this project. Additionally, it could be the case that tether vibrations have a significant impact here too, as it influences abrasion and fatigue. Durability is something that could effect the feasibility of the design, so further investigating these areas should be a priority.

## Technical analysis of the gliders

The glider is a type of rigid kite, which can be modelled in a multitude of ways. There were four main focus points the group focused on when designing the glider; wing sizing, glider sizing, flight performance, structural performance. As established in chapter 3, each unit will consist of two gliders in coordinated flight with each other. Such a glider consists of twin fuselages connecting to a main wing and an empennage.

With an initial estimate of the flight conditions, the wing and airfoil could be designed. The wing planform and its corresponding airfoils were designed using the class I and II estimations, and with the help of XFLR5's numerical simulations. Analytical methods (e.g. DATCOM method) and numerical methods (i.e. XFLR5) were used to determine the optimal wing characteristics needed for the next steps of the glider design process; lift coefficient ( $C_L$ ), drag coefficient ( $C_D$ ), Lift over drag ratio (L/D), wing surface area (S), and aspect ratio (AR). With the wing designed, the structural analysis of the wing was conducted in order to find the weight of the wing group structure. The wing was discretised, and the various stresses were calculated. Furthermore, build materials for the glider were also chosen to withstand the loads and be as light as possible. With this, the weight of the wing would be known. Class II estimations use the wing group weight parameters to determine the glider weight and the centre of gravity (c.g.). These values can be applied into the flight performance model to determine the apparent wind speed, total cycle power, and the flight path. These parameters (e.g. apparent wind speed) are, in turn, inputs for the first two steps of the glider design. Finally, the take-off and landing methods are elaborated on, based on the parameters obtained from the previous steps of the glider design. With a working iterative design process, sensitivity analysis was performed on the model. Verification and validation procedures are outlined at the end of the chapter.

The design of a glider is an iterative one, which means that the calculations done for individual subsystems cannot be done with isolated values. It is evident that the wing would affect the glider sizing, which would in turn affect the flight performance. The flight performance would output values would differ from the initial conditions assumed when sizing the wing, and thus the first iteration would take place. It is important to note that if values are taken from chapters proceeding this chapter, or preceding chapters take values from this chapter, those chapters are part of the numerical model's iteration. The iteration process is visualised in figure 7.1, where the different codes are shown with their interrelations.

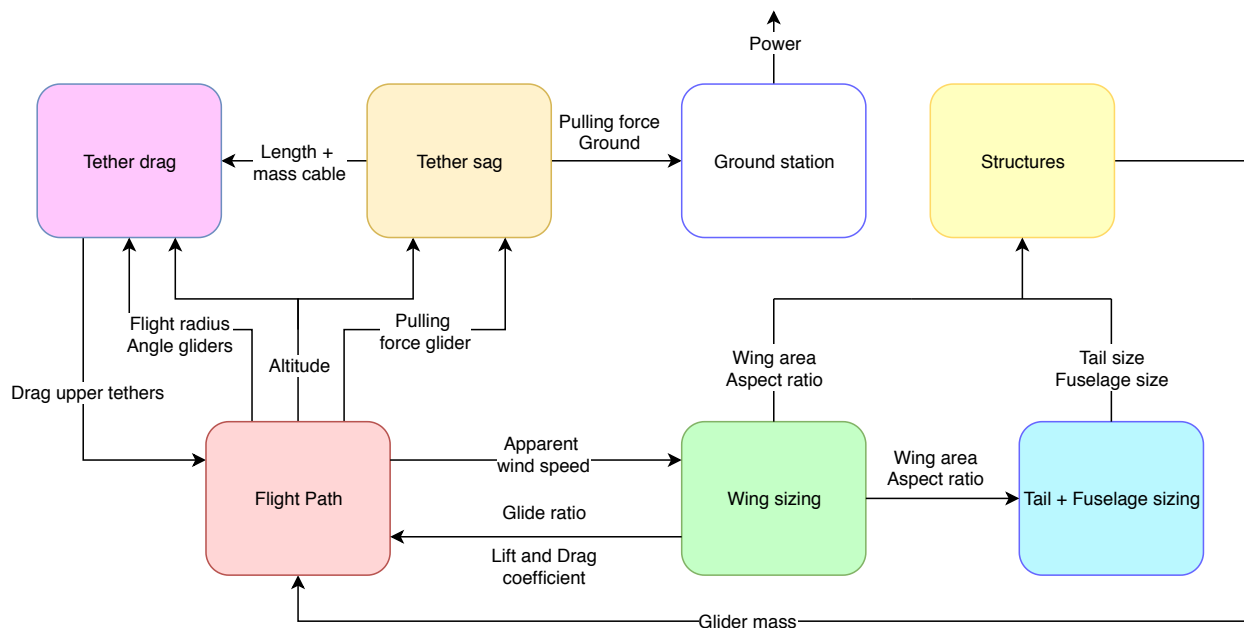


Figure 7.1: Flowchart of the iterative process

## 7.1. Assumptions

For the analysis in this chapter some assumptions were made. The most important assumptions are shown in the enumeration below:

- **Wind speed is always in horizontal direction.** The majority of the wind velocity is horizontal, in the x-direction. Since the glider mainly moves in the y-z-plane, the wind speeds in this plane are negligible compared to the wind speed vectors in the y-z-plane. Therefore, the wind speed is assumed to be horizontal.
- **The Coriolis force is neglected in this analysis.** The Coriolis effect on wind speeds are taken into account within model by using experimental average wind speed data. The Coriolis force caused by the rotation of the Earth can be neglected as the glider system is tethered to the ground station, making it a single unit.
- **The Earth is assumed to be flat.** For the altitude ranges of 2-12 km, the effect of gravity negligibly changes when the curvature is accounted for. Furthermore, the system does not cover a large enough ground distance for the curvature of the earth to affect calculations. Therefore there are no changes in results due to this assumption.
- **Drag is only minimized in flying direction.**
- **The difference between the modified Prandtl lifting line theory (LLT) which takes viscosity into account and is used for the numerical analysis in XFLR5 and a panel method is used where the surface of the wing are divided into panels, is small.** This statement is analysed in the sensitivity analysis.
- **XFLR5 produces proper results for high Reynolds number analyses.** This will create inaccuracies for the results of the numerical model. However, it can not be measured how large these inaccuracies are. Furthermore, the numerical model is verified by the analytical model, and thus any potential large discrepancies will be observed.
- **The wing is made of smoothly molded composites.**
- **25% of the flow over the fuselage is laminar, 50% of the flow over the wing is laminar, the remainder is turbulent.**
- **The tail resembles most closely an H-tail, like an A-10 Warthog.** This is used to calculate the zero-

lift drag by using the interference factor resembling an H-tail. No significant inaccuracies will result from this.

- **The interference effect between gliders can be neglected.** The wake effect has no measurable influence on the aerodynamic performance of both gliders. Unlike conventional aircraft, the gliders will be flying cross wind. So the wind speed vector would be orthogonal to the plane that the glider wake would take place in. The wake would be blown away by the wind before the second gets affected by it. The more gliders there are on a tether, the more prevalent this effect becomes. Furthermore, there is insufficient research into this effect at this moment in time<sup>1</sup>.
- **The direction of the radial speed of the glider is in the direction of the tether as if there was no sag.** The analysis of the glider is done as an isolated unit. The effect of tether forces are implemented as forces acting on the glider. Assuming that at the point of glider-tether connection, the tether is perpendicular to the surface of the glider. This is a valid assumption, as the tether sag will be minimal between the Y-connection and the glider.
- **In order to determine the flight path radius, the apparent wind speed is equal to the circular glider speed.** Centripetal forces are involved when maintaining a circular flight path. The velocity of the glider is usually the dominant factor in the apparent wind speed and contributes to approximately 98% of the apparent wind speed value. Hence, it is possible to approximate the glider speed as the apparent wind speed, as it would even provide a form of a safety factor for the flight path radius.
- **The flight path is in perfect circles.** The flight path is in a circle for the following reasons; no tangling of cables, tension at the Y-connection, and vibrations. The figure of eight is a popular flight path shape for airborne wind energy systems, however those are for single glider-tether configurations only. Having a figure of eight could cause cable tangling and potential collision unless the autopilot system is sophisticated enough to prevent it. Secondly, the gliders generate a vertical force to pull the tether, but also horizontal forces. These horizontal forces are cancelled out by each other's counter motions. The more axes of symmetry the flight path has, the more likely the resultant horizontal forces would cancel out. A circle, with infinitely many axes of symmetry, partially contributes to the force equilibrium. Finally, it is possible to maintain tension, without tangles, and with symmetry (e.g. an oval shape). However, this would involve changing the angle between the gliders constantly. While this in theory is feasible, it would move the Y-connection constantly, creating extra unnecessary vibrations within the tether.
- **The angle between the upper tethers is always constant.** As mentioned before, having varying upper tether angles would cause the Y-tether to move in the air (wobble) and create additional vibrations within the cable, which would result in extra drag. The autopilot needs to be very refined to accommodate for these angles.
- **Both gliders experience the same aerodynamic conditions at the same time.** The average altitude, measured at the point of the Y-connection, is assumed to be the atmospheric conditions for both gliders. The incremental fluctuations of altitude have a negligible effect on the atmospheric pressure, air density, temperature, and wind speeds. For the first three parameters, they affect the aerodynamic performance of the wing, which is taken into account by the numerical simulations. Wind speeds do not alter enough to drastically change the value of apparent wind speed, as the glider speed is usually an order of magnitude higher than the wind speed.

## 7.2. Wing layout

In this section the wing layout will be discussed. First the wing planform will be defined, then the airfoil will be determined after which aerodynamic analysis can be performed for the wing.

---

<sup>1</sup>R. Leuthold, private communication, 5 December 2019

### 7.2.1. Wing planform

The wing planform consists for example of the wing area, aspect ratio, taper ratio, sweep angle and twist angle, but also the use of winglets.

The wing area is initially assumed to range between 20 and 100 m<sup>2</sup>. Eventually, optimization from performance analysis showed that a 60 m<sup>2</sup> wing area is optimal. A larger wing area means that more lift can be generated, but also that the drag of the glider is increased. Furthermore, the weight of the aircraft greatly increases with wing area. After iteration with section 7.4, it was found that lower surface areas would not be able to generate as much lift to pull on the cable and generate energy.

Aspect ratios are usually lower for faster flying aircraft and higher for slow flying aircraft. Aspect ratios are quite important for keeping induced drag low (Oliviero 2017b), which has its largest effect at low speeds. The flying system should have a good balance between low induced drag and roll response, because it needs to turn constantly for an optimal harvesting trajectory. This means that initial values for the iteration process should preferably be around the range of 7 to 12. The upper bound of this range has less drag but also less controllability.

After iteration with section 7.9, an aspect ratio of 12 was found to be optimal, because higher aspect ratios would induce bending loads which are too large and lower aspect ratios would create too much induced drag.

With the surface area and aspect ratio the span could be determined. The span is equal to 26.83 m from tip to tip.

The taper ratio is chosen to be equal to the optimal number of 0.4, creating a quasi-elliptical lift distribution and this allows for a high Oswald efficiency factor reducing the drag. This taper ratio does however increase structural loads, which means more weight should be added to the aircraft in terms of structures. However for this initial analysis it is a good estimate.

As there will be two fuselages attached to the wing, the wing was split up into three parts: in a tapered - untapered - tapered configuration. An untapered part in the wing is used between the two fuselages, so that the vortices from wing-fuselage interaction cancel each other, therefore reducing the drag. Based on class I sizing estimates a value of 20% of the wing span is chosen to be straight. Therefore  $x$  in equation 7.1 is equal to 0.2, resulting in a straight part of 5.4 m.

$$C_{root} = \sqrt{\frac{S}{AR} \frac{0.5}{0.35 + 0.15x}} \quad (7.1)$$

Using the root chord ( $C_{root}$ ) and the taper ratio, the tip chord could be determined. These chords are equal to 2.942 m and 1.177 m, which resulted in a mean aerodynamic chord of 2.385 m.

According to section 7.4, the flight path an angle of 3 ° is the angle of attack that the aircraft will encounter most often during its lifetime. Therefore this value is picked to optimize the airfoil for.

The wing sweep angle reduces the maximum lift coefficient while increasing the structural weight due to a larger moment being generated. Additionally the apparent Mach number is decreased which is important to stay below the drag divergence Mach number. Fortunately, the Mach number of the system is much lower than 0.7 and therefore no sweep is required.

Usually dihedral angle is required for clearance for the engines and has an effect on controllability of the aircraft. As the engines are not mounted on the wing, but on the fuselage, a dihedral angle is not required.

Because stall usually starts from the tips for a tapered wing, a wing twist angle could be required to keep the tips from stalling. A wing twist angle of 5 ° will however decrease the lift properties to such an amount that the used software, XFLR5, will not converge anymore. Therefore for this initial analysis a wing twist angle of 0 ° was used. Stall from the tips, rendering the ailerons ineffective, can be countered via this solution.

The wing planform can be seen in figure 7.2, the dimensions can be seen in figure H.1 in appendix H.

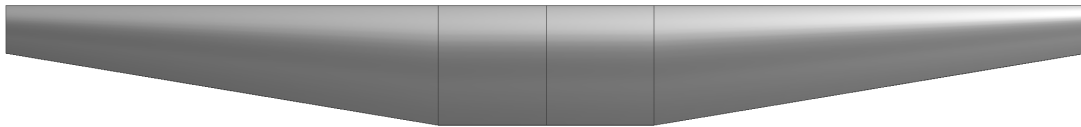


Figure 7.2: Top-view of the wing planform for the analysis in XFLR5. The top of the image is the leading edge while the bottom is the trailing edge.

A table with all of the parameters can be found in table 7.1, where they are used for analysis.

### 7.2.2. Airfoil parameters

For the airfoil selection first a 2D and then a 3D model was produced. In this sub-section, the most important parameters of airfoil design will be discussed. Then the wing planform will be discussed which is required for the analysis of the 3D model. From the 3D model an optimal airfoil could be found, of which the characteristics will be given.

Thick airfoils have advantages and disadvantages. The advantages for thick airfoils are a higher lift coefficient and gradual trailing edge stall characteristics. Disadvantages of airfoils with a larger thickness to chord ratio are that the airflow stays in contact with the surface for a longer distance, generating more friction drag. Additionally the associated form drag is higher, due to earlier flow separation. From a structural point of view, thicker airfoils have got a higher moment of inertia and will cope with bending loads better.

The location of maximum thickness is also of importance as it is related to the point of maximum pressure. The further forward it is positioned, the higher maximum lift coefficient and the lower the drag increase. The disadvantages of placing the location of maximum thickness more forward are a higher minimum drag and a lower critical Mach number.

Increasing camber leads to the wing being able to generate more lift at an angle of attack of  $0^\circ$  and also increasing the amount of lift generated for the same amount of drag. Camber also increases the pitching moment of the airfoil, which does have a larger effect on the tail.

For the maximum camber position, the advantage is when placing the maximum camber position more forward, maximum lift coefficient increases: which is essential for the system to generate energy. Unfortunately a more forward camber position decreases stall characteristics as the stall is a less gradual transition.

### 7.2.3. Airfoil design from 3D-analysis in XFLR5

Looking at contemporary designs from airborne wind energy companies, some designs could be reverse-engineered. Images published by Makani of their M600 were reverse-engineered and smoothed with the help of Javafoil: MRevE-v2 (Eijkelfhof 2019). Due to the nature of Javafoil a version of their airfoil had to be modelled where additional camber compensates for the lack of a possibility to model high-lift devices. Makani and Ampyx both use high lift devices in order to increase the produced lift, therefore this is taken into account in this analysis as well for verification reasons.

From the *Midterm Report* (Arblaster et al. 2019b), airfoil S7075 was used for initial calculations. The MRevE-v2 airfoil was compared with GOE244, GOE421, GOE435, GOE523, and MH150 but MRevE-v2 turned out to be the best option. Therefore it served as a baseline from which S7075 was optimized. Using XFLR5 (Deperrois, A. 2019), first 2D plots were produced of the airfoils. These plots do not take into account 3D effects like tip-vortices, therefore this airfoil was given dimensions and modelled into a wing. XFLR5 determined the values for  $C_L$ ,  $C_D$ , and  $C_L/C_D$  based on different angles of attack. In order to produce these 3D values from a 2D airfoil, wing planform was specified. For this the values in table 7.1 were taken from sub-section 7.2.1:

With these parameters, 3D-analysis could be performed on the wing with the aforementioned seven airfoils. This analysis takes into account viscous flows with a non-linear modified Prandtl lifting line theory

Table 7.1: Parameters for XFLR5 3D analysis

Parameter	Description	Value	Unit
S	Surface area	60	$m^2$
AR	Aspect ratio	12	-
$\alpha$	Angle of attack	3	$^\circ$
$\Lambda_{LE}$	Sweep angle	0	$^\circ$
$\Gamma$	Dihedral angle	0	$^\circ$
$\phi_{aero}$	Wing twist	0	$^\circ$
$\lambda$	Taper ratio	0.4	-
$C_{root}$	Root chord	2.942	m
$C_{tip}$	Tip chord	1.177	m
b	Wing span	26.83	m
	No fin		
	No elevator		
M	Mach number	0.267	-
h	Altitude	3,000	m

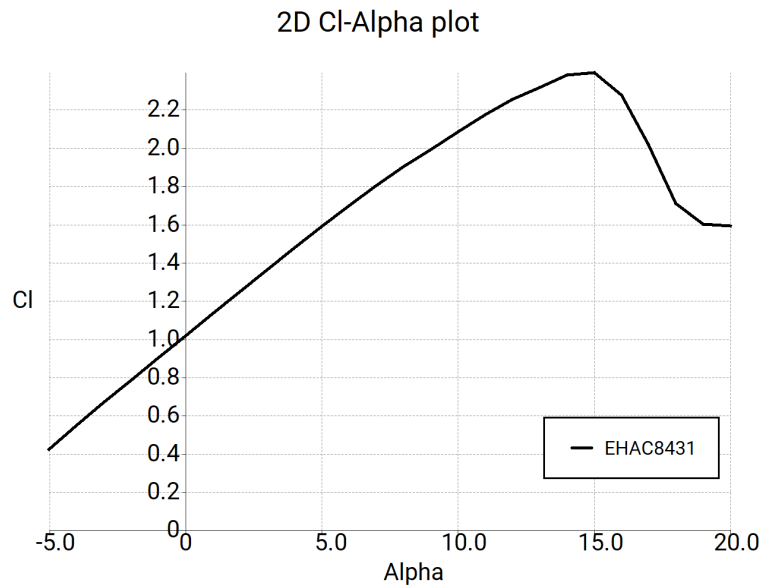
(LLT). The classic LLT is linear and viscous effects are not taken into account, though in this analysis a non-linear LLT has been implemented based on the NACA technical note 1269 (1947)<sup>2</sup>. It should be noted that the non-linear LLT does have some limitations as convergence is not a robust process, therefore angles of attack with full stall occurring cannot be analysed properly. Additionally, sweep and dihedral angles are not used in the calculation of the lift distribution<sup>2</sup>.

This analysis yielded MReVE-v2 as the best airfoil, which was then adjusted to seek even better properties. MReVE-v2, was modified seven times in an iterative process where two parameters were adjusted at the same time. From these seven modified versions, the fifth turned out to have the most favourable properties: high  $C_{L\alpha}$ ,  $C_L$ ,  $C_L/C_D$ , and thickness. The high thickness is important for the structural analysis, in order to cope with the large bending moment from the large wing loading. More on the structural analysis can be found in section 7.9. This airfoil will be referred to as EHAC8431 from now on. The 2D  $C_l - \alpha$  plot of this airfoil is given in figure 7.3.

<sup>2</sup><http://www.xflr5.tech/xflr5.htm> [cited 28 December 2019]

Table 7.2: In this table the most important properties of the EHAC8431 airfoil can be found.

Thickness [%]	$x_{t_{max}}/c$ [%]	Camber [%]	$x_{max.camber}/c$ [%]
31.45	27.51	8.07	36.11

Figure 7.3: The 2D  $C_l - \alpha$  plot of EHAC8431.

The EHAC8431 follows the NACA 4-digit naming, resulting from its camber of 8.07% at 36.11% of the airfoil in x-direction. The maximum thickness is equal to 31.45 and occurs at 27.51% of the airfoil. This can be seen in table 7.2. The airfoil is visualised in figure 7.5

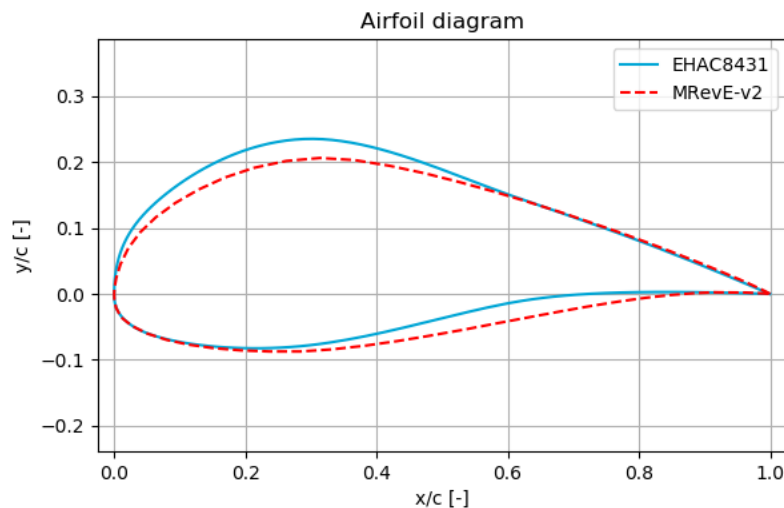


Figure 7.4: The optimized EHAC8431 airfoil and the baseline airfoil MRevE-v2 plotted in a dimensionless diagram. With the blue line EHAC8431 is depicted, while the striped red line shows the airfoil of MRevE-v2.

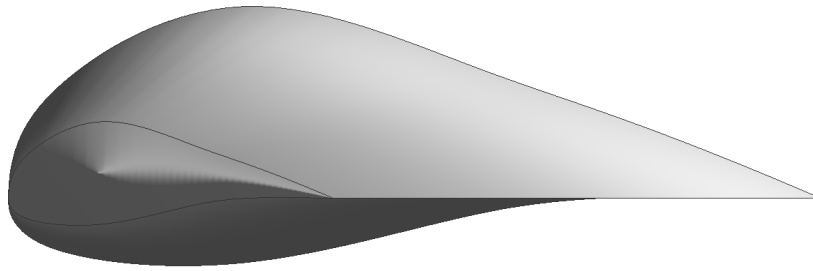


Figure 7.5: This is the left side-view of the wing, with the airfoils EHAC8431 clearly visible. The left side of the image is the leading edge, while the right side is the trailing edge. The reader is encouraged to compare current figure with figure 7.4 for clarity.

### 7.2.4. Numerical model for lift and drag of the aircraft

From section 7.2.3 it became clear that eight airfoils were analysed, where the best airfoil went through seven design iterations. Of these iterations, EHAC8431 yielded the best results as can be seen from figures 7.6, 7.7 and 7.8. MRevE-v2 shows full stall behaviour at  $13^\circ$ , while this may be in the operating range, especially during take-off. Additionally, from inspection EHAC8431 has a much higher  $C_L$  while only sacrificing a relatively small amount of  $C_L/C_D$ . A twist angle at the tips could mitigate this problem and give EHAC8431 even better properties, as this will shift the  $C_L/C_D - \alpha$  to the right until the maximum is reached at the mean angle of attack during the flight path. The  $C_L - \alpha$ ,  $C_L/C_D - \alpha$ , and the drag polar of the baseline MRevE-v2, EHAC mod. 1 and EHAC mod. 5 (EHAC8431) are shown in respectively figure 7.6, 7.7, and 7.8. From figure 7.7, it can be seen that the lift-over-drag ratio is actually optimised at  $-3^\circ$  angle of attack. However the lift coefficient at this angle of attack is too low to generate the lift required to generate power and stay airborne.

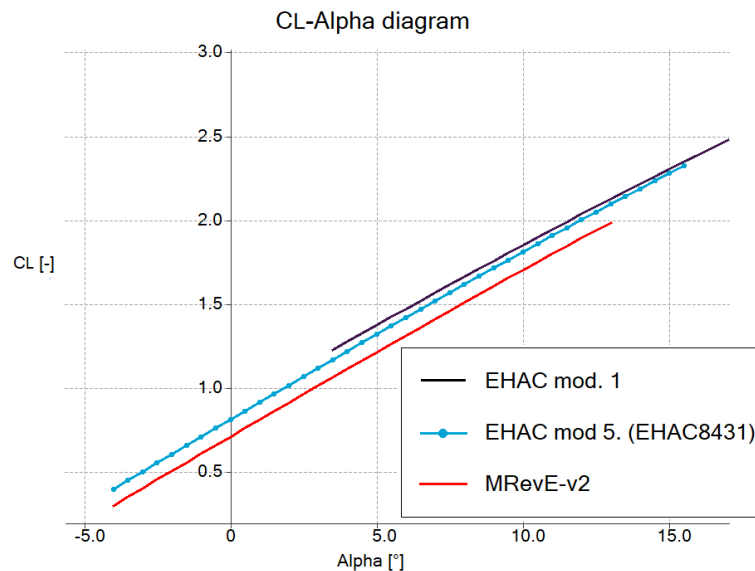


Figure 7.6: This is the  $C_L - \alpha$ -diagram of MRevE-v2 (red), EHAC mod. 1, and EHAC8431 (blue with dots), with  $M = 0.267$

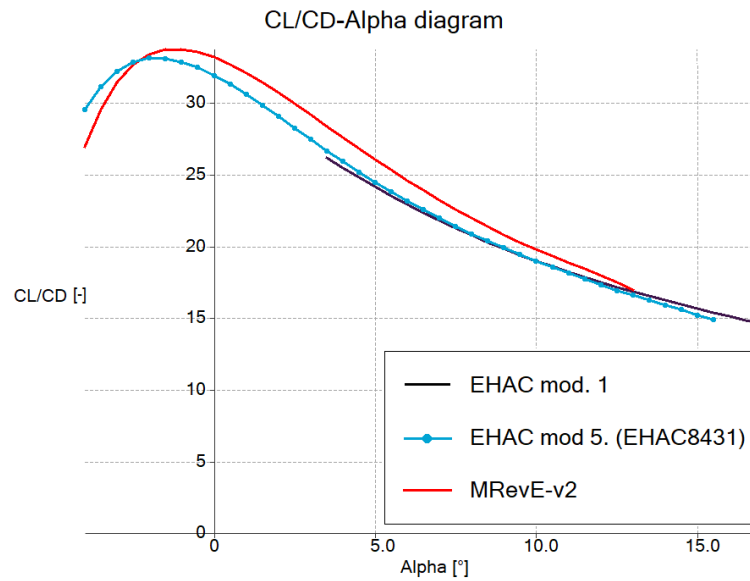


Figure 7.7: This is the  $C_L/C_D - \alpha$ -diagram of MRevE-v2 (red), EHAC mod. 1, and EHAC8431 (blue with dots), with  $M = 0.267$

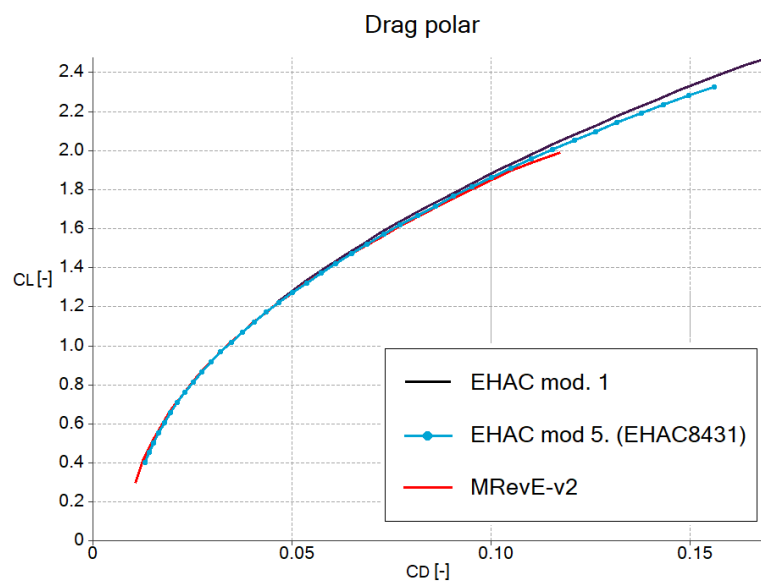


Figure 7.8: This is the drag polar of MRevE-v2 (red), EHAC mod. 1, and EHAC8431 (dotted blue), with  $M = 0.267$

From XFLR5, the  $C_L/C_D$  was determined for each angle of attack. At the operational angle of attack of  $3^\circ$  a  $C_L/C_D$  of 27.4 for the wing only was obtained.

From visualisations of the numerical model, it can indeed be seen that induced drag increases the zero-lift drag as vortices are visible and the assumption that a taper ratio of 0.4 produces a quasi-elliptical lift distribution is also true. This can be visualised in figure 7.9.

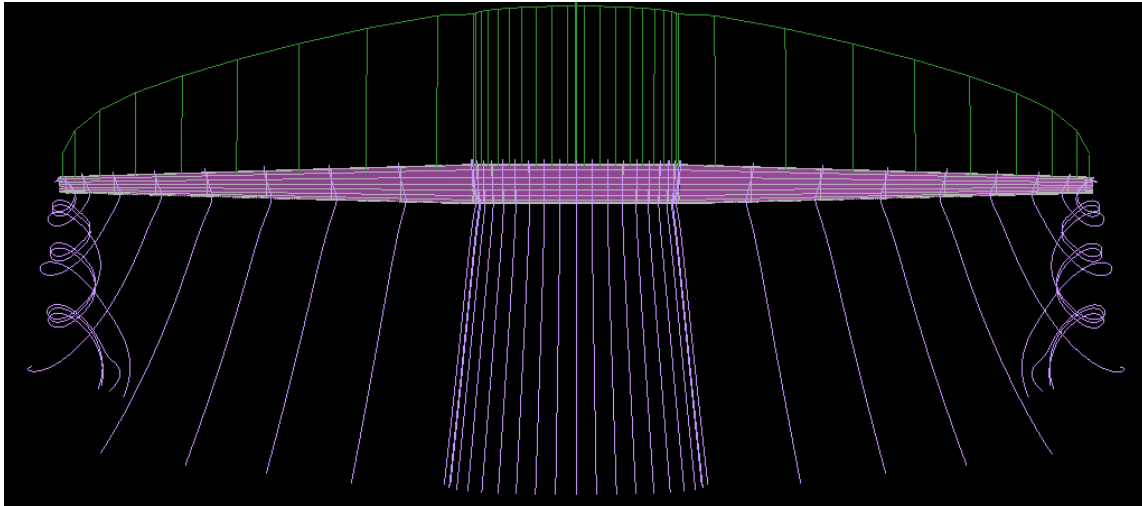


Figure 7.9: The quasi-elliptical lift distribution (in green) on top of the wing and formation of tip vortices at  $\alpha = 3^\circ$  with  $M = 0.267$  (in pink).

### 7.2.5. Analytical model for lift and drag of the aircraft

The lift of the wing and drag of the wing and aircraft from the analytical model are determined in this subsection.

#### Reynolds and Mach number

Because airfoil behaviour depends the effect of viscosity ( $\mu$ ) and compressibility, the Reynolds number (Re), Mach number (M), and angle of attack were determined.

$$Re = \frac{\rho V x_{mac}}{\mu} \quad (7.2)$$

The Reynolds number is determined using equation 7.2, with the initial value of density  $\rho$  equal to the density at 2 km altitude (based on the International Standard Atmosphere [ISA]), apparent airspeed  $V$  equal to 87.7 m/s (which resulted from iterating with 100 m/s in 7.4),  $\mu$  the fluid dynamic viscosity, and  $x_{mac}$  equal to the mean aerodynamic chord length in meters. Which results in a Reynolds number of  $12.2 \cdot 10^6$  [-]. The Mach number is calculated as in equation 7.3.

$$M = \frac{V}{\sqrt{\gamma RT}} \quad (7.3)$$

The speed of sound consisting of the square root of gamma (ratio of specific heats for air, equal to 1.4),  $R$  (specific gas constant, equal to 287.05), and  $T$  (temperature at 3 km altitude based on the ISA, equal to 269 K). The Mach number to be used for the analysis is equal to 0.267 [-] and corresponds to a speed of 87.7 m/s.

#### Lift coefficient

The lift of the wing is determined by the well-known simple relation as shown in equation 7.4. In this equation  $\beta$  is the side slip angle and  $\mu$  is the dynamic viscosity of air. The  $C_L$  is equal to the value at an angle of attack of  $3^\circ$ , as this is close to the nominal value that the aircraft will fly on. Using the DATCOM method the change of  $C_L$  per angle of attack ( $C_{L_\alpha}$ ) can be determined via equation 7.5. This results in a  $C_{L_\alpha}$  of 0.1 [1/°]. For this method errors are larger for unswept wings, than for swept wings (Oliviero 2017a).

$$L = \frac{1}{2} \rho V^2 C_L S \quad (7.4)$$

Table 7.3: Table containing parameters for the fast estimation of the zero lift drag

Aircraft component	$C_{D_c}$	$A_c$
Wing	0.007	Wing reference area (60 $m^2$ )
Fuselage (multi-engine)	0.008	Maximum frontal area fuselage (1.6 $m^2$ )
Tail (horizontal and vertical)	0.008	Horizontal and vertical tail reference area (14.8 and 3.18 $m^2$ )
$C_{D_{misc}}$	Add 15% to $C_{D_0}$	

$$C_{L_\alpha} = \frac{2\pi AR}{2 + \sqrt{4 + \left(\frac{AR\beta}{\eta}\right)^2 \left(1 + \frac{\tan\Lambda_{0.5c}^2}{\beta^2}\right)}} \quad (7.5)$$

$$A > \frac{4}{(C_1 + 1) \cos \lambda_{LE}} \quad (7.6)$$

$$C_{L_{max}} = \left[ \frac{C_{L_{max}}}{C_{l_{max}}} \right] C_{l_{max}} + \Delta C_{L_{max}} \quad (7.7)$$

The high-aspect ratio method will be used to determine the wing stall angle and maximum lift coefficient since the aspect ratio is larger than the number as determined in equation 7.6 with  $C_1$  equal to 0.4 for a taper ratio of 0.4. (Oliviero 2017a) The high-aspect ratio method in equation 7.7 shows that the fraction is equal to 0.9 for an untwisted constant-airfoil-section wing with a sweep angle of 0° at leading edge.  $\Delta C_{L_{max}}$  takes into account the compressibility effects occurring at higher velocities than 0.2 Mach, though at a velocity of 0.267 Mach these are deemed insignificant. This results in a  $C_{L_{max}}$  of 2.2, for a  $C_{l_{max}}$  of 2.4.

### Drag coefficient

There are three methods available for estimating the drag, all of increasing accuracy. These are in order of increasing accuracy: the class 0 early conceptual design phase very fast estimation of zero lift drag from Raymer (Raymer 2012), class I fast estimation of zero lift drag, and the class II component drag build-up method.

A very fast estimation of the class 0 zero-lift drag in clean configuration can be determined from the wetted aircraft area ( $S_{wet}$ ), reference wing area ( $S_{ref}$ ), and the equivalent skin friction coefficient ( $C_{f_e}$ ). This relation is shown in equation 7.8.

$$C_{D_{0,class0}} = C_{f_e} \frac{S_{wet}}{S_{ref}} \quad (7.8)$$

For the aircraft as considered in this report, a light twin-engine aircraft is considered for which  $C_{f_e}$  equals 0.0045 and  $\frac{S_{wet}}{S_{ref}}$  3.8. This resulted in a  $C_{D_0}$  of 0.0171.

A fast estimation of the class I zero-lift drag (in clean configuration) for a propeller plane is given by equation 7.9.

$$C_{D_{0,class1}} = \frac{1}{S_{ref}} \sum_c C_{D_c} A_c + C_{D_{misc}} \quad (7.9)$$

In this equation  $S_{ref}$  is the reference surface area of the wing, which is 60  $m^2$  in this case. This resulted in a  $C_{D_0}$  equal to 0.013. Each component and  $C_{D_{misc}}$  are given in table 7.3.

The earlier mentioned class I fast estimation of zero-lift drag can be expanded to a class II drag estimation, using the component drag build-up method. This method can be found in equation 7.10.

$$C_{D_{0,class11}} = \frac{1}{S_{ref}} \sum_c (C_{f_c} \cdot FF_c \cdot IF_c \cdot S_{wet_c} + C_{D_{misc_c}}) \quad (7.10)$$

This method estimates subsonic parasite drag for each aircraft component using the flat plate skin friction coefficient ( $C_f$ ), component form factor (FF) and interference factor (IF) for the component friction drag, pressure drag due to viscous separation and effect of each component drag on each other, respectively. The miscellaneous drag component includes in this case just the fuselage base drag.  $C_f$  depends strongly on the type of boundary layer, from empirical data for general aviation for smooth molded composites, 25% of the flow over the fuselage and 50% of the flow over the wing and tail are laminar at cruise speed and altitude. (Oliviero 2017a, p. 44) The remainder is turbulent flow, for which one can find the following formulas for subsonic flight. The Reynolds number for which this is estimated is unknown, though can be estimated to be around  $1 \cdot 10^7$ . The total  $C_f$  is the weighted average of the sum of the laminar and turbulent component (equation 7.12). The Reynolds number is also quite important here, as it relates directly to the flat plate skin friction coefficient. The Reynolds number is the minimum of the actual Reynolds number and the empirically established cut-off Reynolds number, as shown in equation 7.11.

$$Re_{subsonic} = \min(Re_{actual}, Re_{cut-off}) = \min\left(\frac{\rho V l}{\mu}, 38.21 \left(\frac{l_{fus}}{k_{surface}}\right)^{1.053}\right) \quad (7.11)$$

$$C_{f_{laminar}} = \frac{1.328}{\sqrt{Re_{subsonic}}}, C_{f_{turbulent}} = \frac{0.455}{(\log_{10} Re_{subsonic})^{2.58} (1 + 0.144 M^2)^{0.65}} \quad (7.12)$$

The surface smoothness coefficient ( $k_{surface}$ ) equals  $0.052 \cdot 10^{-5}$  for smooth molded composite. The component form factor ( $FF_c$ ) depends strongly on the respective surface, for wing, tail, strut, and pylon, referred to as  $FF_{wing}$  this is given in equation 7.13. For the fuselage, referred to as  $FF_{fuselage}$  and given in equation 7.14, where  $f_{fuselage}$  is the fuselage slenderness factor.

$$FF_{wing} = \left[1 + \frac{0.6}{(x/c)_m} \frac{t}{c} + 100 \left(\frac{t}{c}\right)^4\right] [1.34 M^{0.18} (\cos \lambda_m)^{0.28}] \quad (7.13)$$

$$FF_{fuselage} = \left(1 + \frac{60}{f_{fuselage}^3} + \frac{f_{fuselage}}{400}\right) \quad (7.14)$$

$$f_{fuselage} = \frac{l_{fuselage}}{\sqrt{(4/\pi) S_{fuselage_{max}}}} \quad (7.15)$$

Several components can have an effect on each other. Therefore the interference drag should be considered as well. This is for example caused by boundary layer interaction at the connection of two components, resulting in a thicker boundary layer. Additionally, a component is immersed in the super-velocity around another component. Super-velocity is the accelerated local velocity due to the disturbance of the flow by an object. As the velocity is higher the dynamic pressure increases, resulting in an increased drag for any component within that flow. For the wing the interference factor is 1, as the aircraft comprised of a mid-wing configuration. Assumed here is that the fairing is carefully designed. For the horizontal and vertical tail, the interference factor is equal to 1.08 as it most closely resembles an inverted H-tail from the A-10 Warthog. The interference factor for the fuselage is equal to 1.0.

The fuselage base drag is defined as the drag that occurs from not smoothly finishing the trailing edge of the fuselage, which causes a wake. Via equation 7.16 the corresponding drag polars can be found and are plotted in figure 7.10.

$$C_D = C_{D_0} + \frac{C_L^2}{\pi A e} \quad (7.16)$$

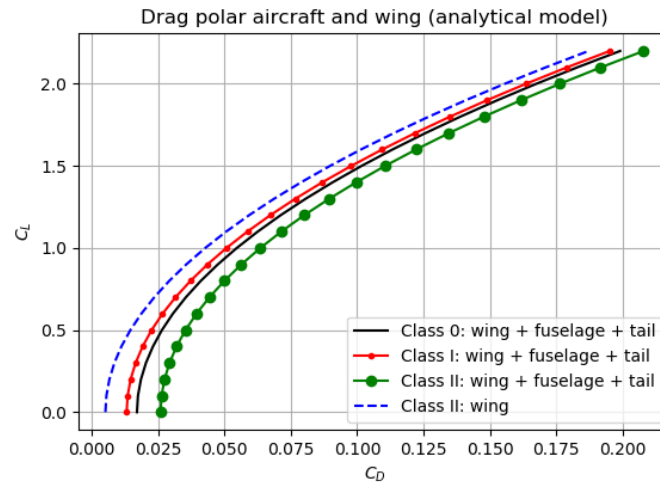


Figure 7.10: The drag polars for the class 0, I, and II drag estimates for the full aircraft (black, red small-dotted, and green large-dotted) and the class II drag estimate for only the wing (blue striped).

### 7.2.6. Stall characteristics

The stall characteristics for the EHAC8431 airfoil and the respective wing-layout have been determined using a pressure-coefficient plot as can be seen in figure 7.11 and visual inspection from figure 7.12. In figure 7.11 one can see that at an angle of attack of  $12^\circ$  the airflow at the tip is losing attachment around  $x = 0.8$  m and is restored around  $x = 1.2$  m. This can be confirmed from visual inspection with figure 7.11, the streamlines in purple show detached behaviour. At around  $17^\circ$  complete stall occurs, where the flow is completely detached from the airfoil. Though at an angle of attack of  $12^\circ$  trailing edge detachment starts occurring, which is shown with the side view of the wing in figure 7.13. The tip stall and trailing edge flow detachment is visible with respectively arrow 2 and 1 from figure 7.14. So from this analysis it is clear that trailing edge stall occurs, which is usually more gradual than leading edge stall and therefore the preferred stall-mode.

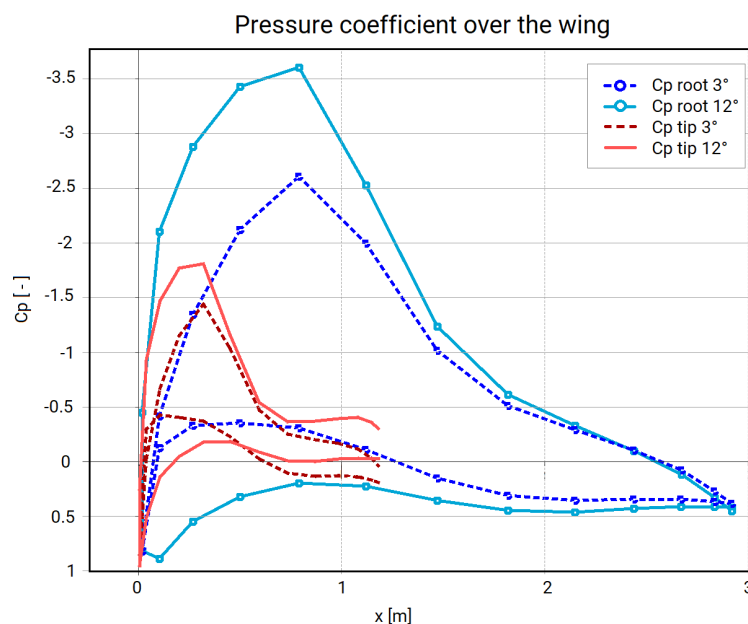


Figure 7.11: The pressure distribution using pressure coefficients over the chord and tip of the wing, at  $3^\circ$  and  $12^\circ$ .

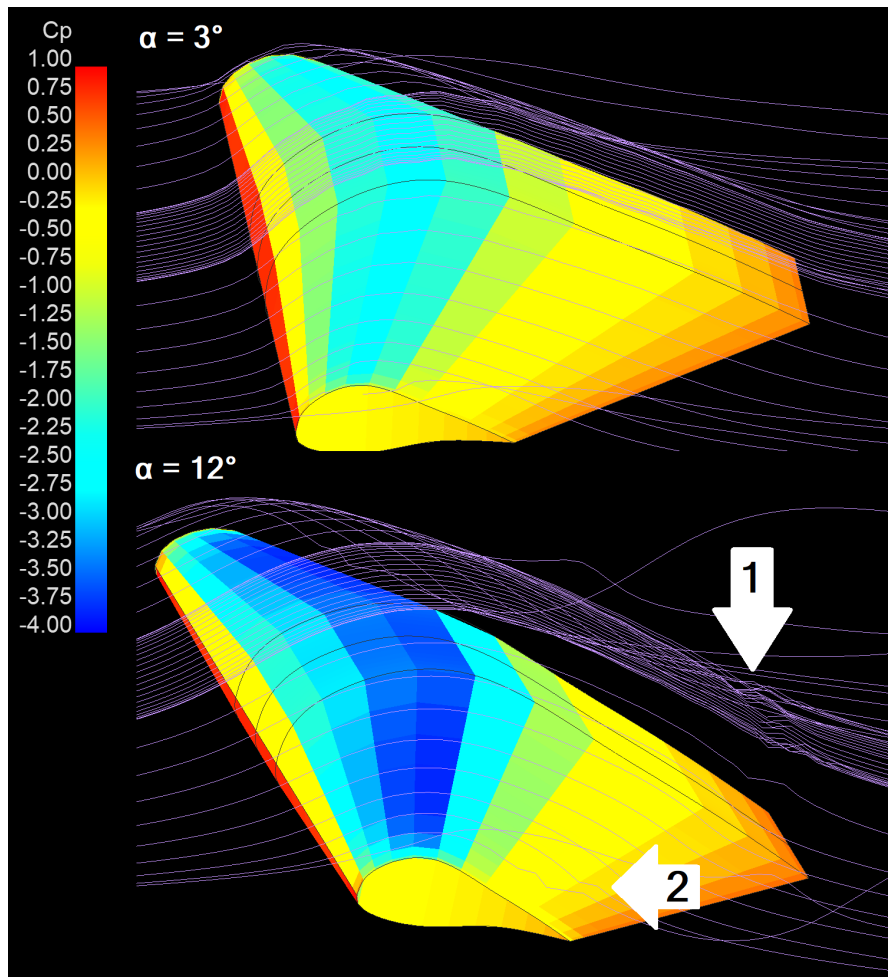


Figure 7.12: The pressure distribution over the wing at  $3^\circ$  and  $12^\circ$ ; the streamlines are shown in pink. With white arrow 1 and 2 the beginning of trailing edge stall is shown and tip stall. The background is black in order to improve contrast for the reader. The image is produced with XFLR5 at a Mach number of 0.267. The leading edge is on the left, while the trailing edge is on the right side of the image.

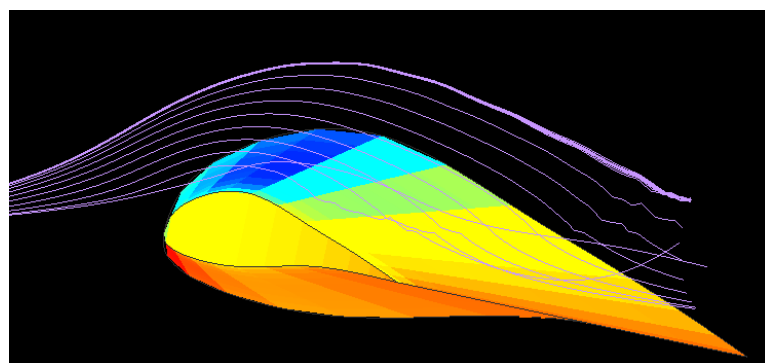


Figure 7.13: The pressure distribution over the wing at  $12^\circ$ ; the streamlines are shown in pink. In this image it is clear to see that trailing edge separation is about to occur, due to the turbulent behaviour of the flow. The image is produced with XFLR5 at a Mach number of 0.267. The leading edge is on the left, while the trailing edge is on the right side of the image.

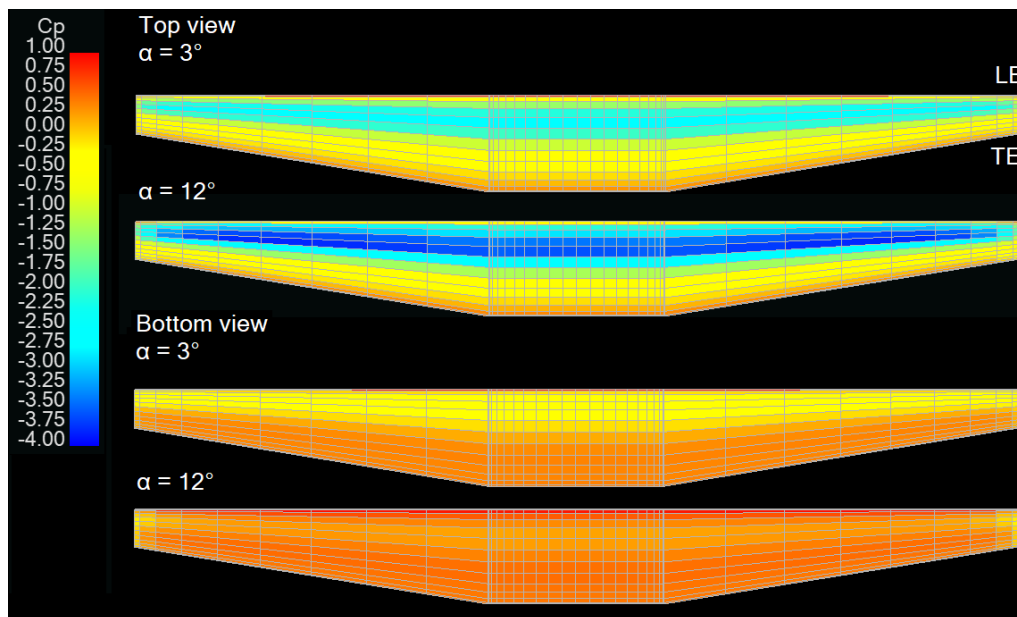


Figure 7.14: The pressure distribution over the top and bottom of the wing at 3° and 12°. The background is black in order to improve contrast for the reader. The image is produced with XFLR5 at a Mach number of 0.267. The leading edge is on the top of the figure, while the trailing edge is on the bottom of the figure.

## 7.3. Glider layout

After sizing the wing, the glider can be sized. Once again, one must bear in mind that this process is not chronological, but iterative. Input and output values of this section determine the performance of the glider as a whole, and cannot be optimised in this section alone. Hence, it is important to note that the output parameters of this section are a culmination of the full numerical model. This section describes the effect of the wing design on the following glider subsystems; fuselage(s), empennage, control surfaces, propulsion, and landing gears.

### 7.3.1. Overview of the layout

The overview of the layout by means of technical drawings can be found in appendix H in figure H.1 and is explained in the following sub-sections. A render of the drawing is shown in figure 7.15.

### 7.3.2. Fuselages

The fuselages of the glider have two main functions. One is to support the aerodynamic loads on the empennage and to connect it to the wing. The other is to carry subsystems such as the landing gear, engines, on-board batteries, and the communication subsystem, while withstanding their associated loads with as little structural weight as possible.

The fuselages are designed to have favourable aerodynamic characteristics. This results in a circular cross section of as small a diameter as possible to perform its functions, to minimise its wet area. The nose and tail shape are rounded such to also decrease separation, meaning they flow smoothly into the central tube and that the tail has a high fineness ratio (the length of the tail divided by the diameter of the central tube) (Vos, Melkert, and Zandbergen 2018); the nose cone fineness ratio depends on the engine dimensions.

The final dimensions of the fuselages are determined to be 12.65 m length from class I size estimations (Eijkelhof 2019) and a circular fuselage with a maximum radius of 1.06 m (Vos and Melkert 2018).

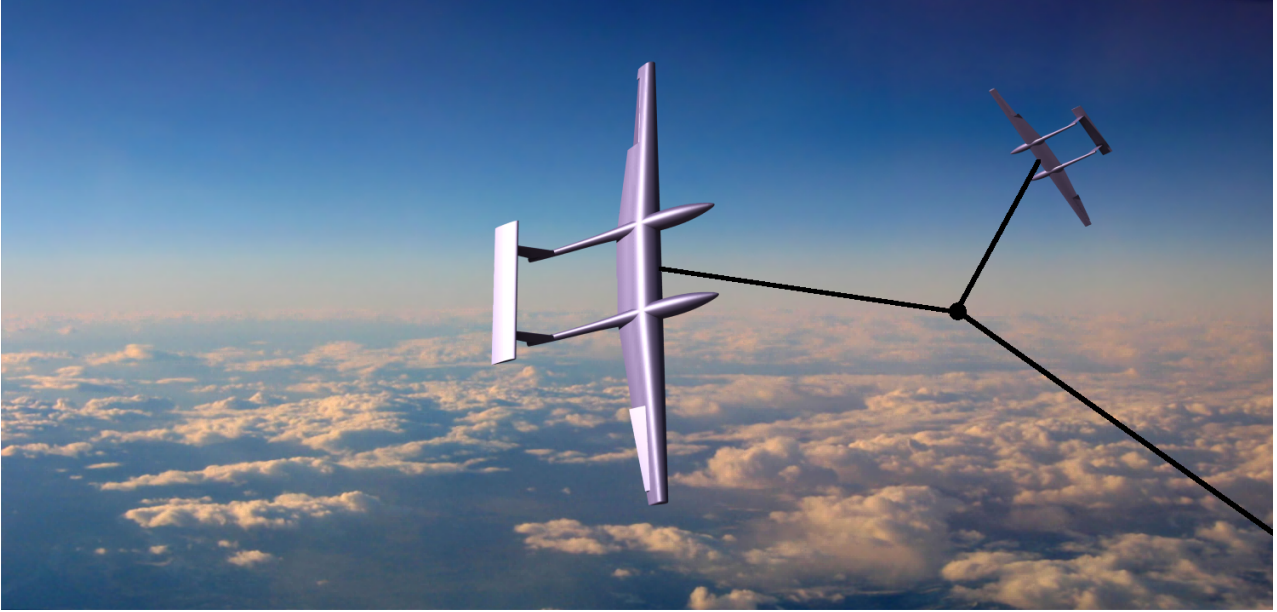


Figure 7.15: Renders of the combined gliders including tether, a specific flight path is not considered for this image.

### 7.3.3. Empennage

The empennage is designed in such a way to ensure longitudinal and yawing stability by correctly using the horizontal and vertical tailplane, respectively. In case of this design, the horizontal tail is most important for longitudinal stability. For a certain increase in angle of attack, the aircraft should have a pitching-down moment exerted on its nose. This is achieved by obtaining a moment coefficient gradient with respect to  $\alpha$  of  $C_{m_\alpha} < 0$ . Increasing certain parameters such as the horizontal tail area as well as the distance from centre of gravity to tail aerodynamic centre will make the  $C_{m_\alpha}$  more negative and thus more stable.

For determining the horizontal tail size, first the aerodynamic centre without the tail was determined in XFLR5 to be 6.032 m from the nose. After this, the centre of gravity was estimated using Class I weight estimation using reference aircraft and was found to be 6.15 m from the nose of the fuselages. From this, the amount of lift and moment arm was calculated to counter-act the pitch-up moment induced by the aerodynamic centre of the wing and the distance between the aerodynamic centre and the centre of gravity. This lead to a horizontal tailplane with a surface area 15 m<sup>2</sup>.

For profile selection of the tailplane, a symmetrical airfoil with a thickness-to-chord ratio of 9 to 12% is the most applied airfoil (Torenbeek 1982). In this case, the NACA0012 airfoil is chosen. The longitudinal positioning of the centre of gravity of the tail was determined from reference aircraft and was at 95% of the length of the fuselage taken from the nose. The change in downwash angle with respect to angle of attack can be calculated with use of equations 7.17, 7.18, and 7.19 (Vos, Melkert, and Zandbergen 2018)

$$K_{\epsilon_\Lambda} = \frac{0.1124 + 0.1265\Lambda + 0.1766\Lambda^2}{r^2} + \frac{0.1024}{r} + 2 \quad (7.17)$$

$$K_{\epsilon_{\Lambda=0}} = \frac{0.1124}{r^2} + \frac{0.1024}{r} + 2 \quad (7.18)$$

$$\frac{d\epsilon}{d\alpha} = \frac{K_{\epsilon_\Lambda}}{K_{\epsilon_{\Lambda=0}}} \left( \frac{r}{r^2 + m_{tv}^2} \frac{0.4876}{\sqrt{r^2 + 0.6319 + m_{tv}^2}} + \left[ 1 + \left( \frac{r^2}{r^2 + 0.7915 + 5.0734m_{tv}^2} \right)^{0.3113} \right] \left\{ 1 - \sqrt{\frac{m_{tv}^2}{1 + m_{tv}^2}} \right\} \right) \frac{C_{L_{\alpha_{wing}}}}{\pi A} \quad (7.19)$$

where  $r$  and  $m_{tv}$  are defined as the distance from the aerodynamic centre from the wing to the tail and the distance between the horizontal tailplane and the vortex shed plane, respectively. Both variables are

defined as a fraction of the half wing span ( $r = \frac{l_h}{b/2}$ ) Using this, the horizontal tail is placed 2 m above the fuselage to reduce the downwash (wake) induced by the airflow over the wing. For the sizing and positioning of the vertical tail, it directly is derived from reference aircraft and the vertical positioning of the horizontal tail, respectively (Eijkelhof 2019). This lead to a vertical tail span of 1.8 m.

#### 7.3.4. Control surfaces

Three different control surfaces are used in the glider, one on the wing and two on the empennage. The ailerons are placed on the wing and the elevators and rudder are placed on the empennage. Reference aircraft AT-802 and Fokker 100 (Sadraey, M. 2012) were used to size the control surfaces, as they were close to the system in terms of wingspan or take-off weight and engine type and placement. No reference data on double-fuselage aircraft was available.

##### Aileron

Fist of all, the aileron sizing. The aileron-to-wing-chord ratio, the aileron-to-wing-span ratio, and the up and down deflection angle are determined according to the reference aircraft. The aileron-to-wing-chord ratio indicates at which length of the chord the aileron is placed. For the glider this ratio is 0.24. The aileron-to-wing-span ratio indicates at which length of the span the aileron is placed. This requires two values, one for the begin point of the aileron and one for the end point. These values are 0.6 and 0.94, respectively. Then the deflection angles, the maximum aileron deflection angle is 25°. This is because of flow separation that will occur if the aileron is further deflected, which will cause the ailerons to loose there effectiveness. So for the glider the aileron deflection angles will be 25° upwards and 20° downwards according to the reference aircraft (Sadraey, M. 2012). A render with the right aileron deployed downwards and the left one upwards is included in figure 7.16.

##### Rudder

The ratio of the area and root chord of the rudder with respect to the vertical stabilizer and the deflection angle are determined according to the reference aircraft. From this the first mentioned ratio is 0.23 and the second is 0.28 for each rudder. The maximum deflection in both directions is 20° (Sadraey, M. 2012).

##### Elevators

The ratio of the area and root chord of the elevator with respect to horizontal stabilizer and the up and down deflection angle are determined according to the reference aircraft. As the fuselages of the glider are comparable in length to the AT-802, this is taken as reference. Then the ratio of the area of the elevator with respect to the horizontal stabilizer is 0.36 and that of the root chord 0.31. the maximum downwards deflection is 15° and the upward deflection is 29° (Sadraey, M. 2012). A render of the aircraft with control surfaces can be seen in figure 7.16.



Figure 7.16: CATIA-render of the control surfaces

#### 7.4. Flight performance of tethered rigid kites

This section is predominantly based on analytical relations found in the Airborne Wind Energy textbook (Schmehl et al. 2013, ch. 2). A model was created to calculate the aerodynamic properties. This model consisted of analytical and numerical calculation methods and was a type of Python file. The wind velocity is assumed to be uniform, constant, and parallel to the ground plane. The apparent wind speed is related to the kite speed and the wind speed as shown in equation 7.20. The wind velocity vector points in the positive x-direction only. Note that gliders fall under the category of kites.

$$\mathbf{v}_a = \mathbf{v}_w - \mathbf{v}_k \quad (7.20)$$

As can be seen in figure 7.17, the kite speed is a result of the radial and tangential component of the speed as shown in equation 7.21.

$$\mathbf{v}_k = \mathbf{v}_{k,r} + \mathbf{v}_{k,\tau} \quad (7.21)$$

When substituting equation 7.21 into equation 7.20 and writing it down as a vector equation in spherical coordinates as described in figure 7.23, the following two equations follow.

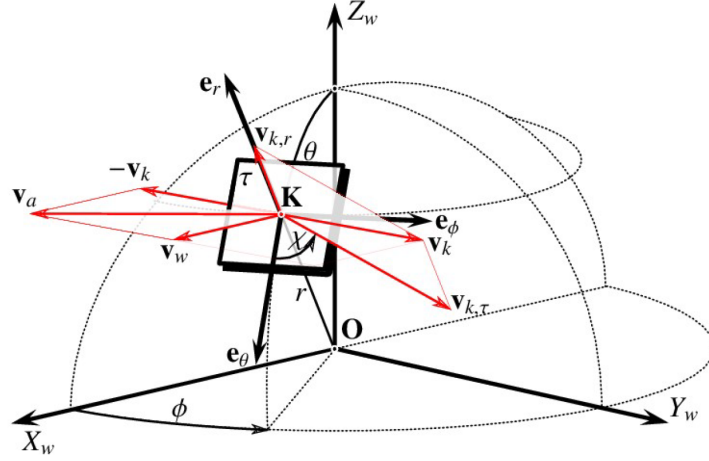


Figure 7.17: Glider velocity vector directions in spherical coordinates (Schmehl et al. 2013)

$$\mathbf{v}_a = \mathbf{v}_w - \mathbf{v}_{k,r} - \mathbf{v}_{k,\tau} \quad (7.22)$$

$$\mathbf{v}_a = \begin{bmatrix} \sin(\theta)\cos(\phi) \\ \cos(\theta)\cos(\phi) \\ -\sin(\phi) \end{bmatrix} v_w - \begin{bmatrix} 1 \\ 0 \\ 0 \end{bmatrix} v_{k,r} - \begin{bmatrix} 0 \\ \cos(\chi) \\ \sin(\chi) \end{bmatrix} v_{k,\tau} \quad (7.23)$$

As seen in figure 7.17, there are three components to the spherical coordinates;  $r$ ,  $\theta$ ,  $\phi$ . The radius  $r$  is the shortest distance between the glider and the generator on the ground. The angle  $\theta$  is defined as the polar angle and is related to the elevation angle ( $\beta$ ) in the following way:  $\beta$  is  $90^\circ - \theta$ . The angle  $\phi$  is the azimuth angle. For the sake of the coordinate system, the model used the polar angle. Another relevant angle is the course angle ( $\chi$ ), which is the angle between the tangential kite speed velocity  $\mathbf{v}_{k,\tau}$  and the local base vector  $\mathbf{e}_\theta$ . The three main scenarios this model takes into account are; horizontal flight ( $\chi = 90^\circ$  or  $270^\circ$ ), upwards flight ( $\chi = 180^\circ$ ), downwards flight ( $\chi = 0^\circ$ ).

Following equation 7.23, the output is the apparent wind speed in spherical coordinates which are converted back to Cartesian coordinates using equation 7.24.

$$\begin{bmatrix} r \\ \theta \\ \phi \end{bmatrix} = \begin{bmatrix} \sin(\theta)\cos(\phi) & \sin(\theta)\sin(\phi) & \cos(\theta) \\ \cos(\theta)\cos(\phi) & \cos(\theta)\sin(\phi) & -\sin(\theta) \\ -\sin(\phi) & \cos(\phi) & 0 \end{bmatrix} \begin{bmatrix} x \\ y \\ z \end{bmatrix} \quad (7.24)$$

The wind speed component,  $\mathbf{v}_w$ , is a function of altitude. This function was determined in the Mid-term report (Arblaster et al. 2019b) and was implemented in the model. At an altitude of 3000 m, the wind speed is approximately 11.5 m/s. After inspecting the transformation matrix for the wind speed in equation 7.23, it is evident that it is the first column of the transformation matrix in equation 7.24. This is because the Cartesian coordinate system is oriented to align the x-axis and the wind speed direction. Hence, the wind speed only acts in the x-direction. The radial component of the kite speed ( $\mathbf{v}_{k,r}$ ) and the tether velocity are the same if a straight tether is assumed. This is a valid assumption for this equation as the radial component of the kite velocity is an order of magnitude lower than the tangential component of the kite velocity. So magnitude of  $\mathbf{v}_{k,\tau}$  was set to be equal to the reel speed of the tether ( $\mathbf{v}_t$ ).

The final unknown term in the system of equations is the magnitude of the tangential kite velocity ( $\mathbf{v}_{k,\tau}$ ). This was determined using equation 7.25. Where  $\lambda$  is the tangential velocity factor.

$$\lambda = \frac{v_{k,\tau}}{v_w} \quad (7.25)$$

The tangential velocity factor can be defined by equation 7.26.

$$\lambda = a + \sqrt{a^2 + b^2 - 1 + \left(\frac{L}{D}\right)^2 (b - f)^2} \quad (7.26)$$

$$a = \cos(\theta)\cos(\phi)\cos(\chi) - \sin(\phi)\sin(\chi) \quad (7.27)$$

$$b = \sin(\theta)\cos(\phi) \quad (7.28)$$

$$f = \frac{V_t}{V_w} \quad (7.29)$$

The tangential velocity factor, by definition, cannot be negative. If one observes equation 7.26, with the condition that  $\lambda$  cannot be less than zero, it can be seen that the following constraint can be found for the azimuth angle and elevation angle.

$$\sin(\theta)\cos(\phi) < \frac{\sqrt{1 + \left(\frac{L}{D}\right)^2(1 - f^2)} + f\left(\frac{L}{D}\right)^2}{1 + \left(\frac{L}{D}\right)^2} \quad (7.30)$$

Crosswind theory dictates that the maximum apparent wind speed occurs when the azimuth angle is zero. At this condition, the maximum elevation angle can be found to be:

$$\beta_{max} = \cos^{-1}\left(\frac{\sqrt{1 + \left(\frac{L}{D}\right)^2(1 - f^2)} + f\left(\frac{L}{D}\right)^2}{1 + \left(\frac{L}{D}\right)^2}\right) \quad (7.31)$$

The inverse cosine is used due to the fact that the elevation angle  $\beta$  is  $90^\circ - \theta$ . Hence,  $\sin(\theta)$  is equal to  $\cos(\beta)$ . Having calculated these values, the apparent wind velocity could be found using equation 7.23. It is then transformed into an apparent velocity vector in Cartesian coordinates using equation 7.24.

With the apparent wind velocity calculated, the net tether force could be calculated. A local coordinate system was used to find the net force within the tether, where the z-axis points in the direction of the lift generated, and the x-direction is parallel to the drag generated by each gliders. The gliders generate a certain lift, which is calculated using the standard lift equation in equation 7.32.

$$L = C_L \frac{1}{2} \rho v_a^2 S \quad (7.32)$$

The lift coefficient was determined using figure 7.6. But the corresponding angle of attack remained in question. The effective angle of attack seen by the wings are the global x and y-components of the apparent wind speed. The global z-component of the apparent wind speed contributes to slip and was accounted for in a different way in equation 7.35. The effective angle of attack was calculated using equation 7.33. The direction of this lift force is parallel to the tether and the tether tension force. The tension force is not equal to the lift force, as there are other forces that partially counter the lift force generated (parasitic forces); glider weight, tether weight, slip force, bank angle losses.

$$\alpha_{eff} = \arctan\left(\frac{V_{a,x}}{V_{a,y}}\right) \quad (7.33)$$

The weight of the tether acts, at the point of connection onto the gliders, parallel and opposite to the lift force. The weight of the glider points towards the ground, so it has a component in the local z-axis and a component in the local x-axis.

$$W_{g,x} = m_{glider} \cdot g \cdot \cos(\beta) \quad (7.34)$$

For the net tether force, the glider weight component in the local z-direction was used as it is parallel and opposite to the lift force as well.

The glider predominantly moves in the  $y$ - $z$  plane. Vertical drag comes from the fact that the apparent wind velocity is a 3D vector. In the local coordinate scheme, the global  $z$ -component of the apparent wind velocity acts like drift for conventional aircraft and causes the glider to move towards the ground. This drift component is a force that also has a component in the local  $z$ -direction. It is called the slip force and was calculated using equation 7.35. In equation 7.35, the effective slip wind speed is solely in the  $z$ -direction due to the fact that the  $x$  and  $y$ -components are taken into account for headwind velocity and the effective angle of attack. The projected fuselage side surface area ( $S_f$ ) is the surface area that the slip wind speed will see. The value  $\beta$  is the side slip angle, and  $\gamma_f$  is the lateral drag coefficient of the fuselage.

$$F_{slip} = \frac{1}{2} \cdot \rho \cdot v_{a,z}^2 \cdot S_f \cdot \beta \gamma_f \quad (7.35)$$

Finally, the gliders fly in a circular flight path and must continuously have a bank angle to maintain the shape of the flight path. This having a bank angle reduces the useful lift generated and contributes to a component of the lift force acting in the local  $y$ -axis. This lift component losses can be approximated using equation 7.36 as seen in figure 7.18.

$$L_{l,\phi} = L \sin(\phi) \quad (7.36)$$

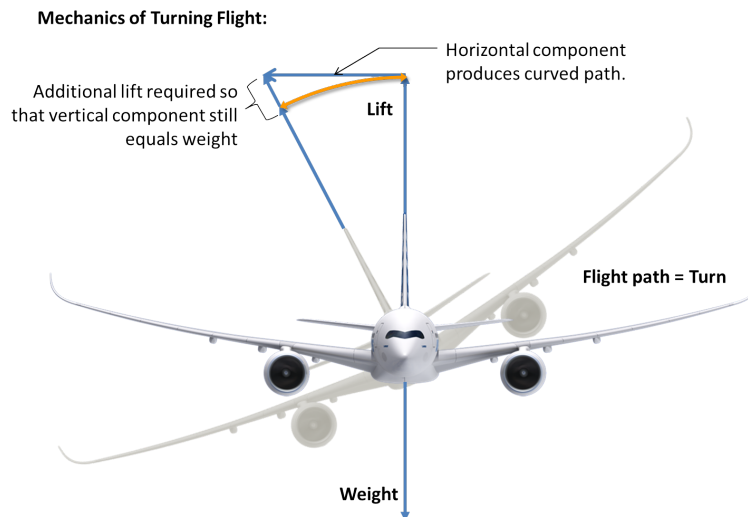


Figure 7.18: Lift losses when the glider has a certain roll angle<sup>3</sup>

### 7.4.1. Flight path

#### Reel-out phase

As mentioned in the previous section, the gliders fly in a circular flight path. This can be seen in the bottom right image in figure 7.19. For a tether with a single glider, the roll angle during operation is derived from the elevation angle (as seen in figure 7.17). At an elevation angle of  $0^\circ$ , the glider would touch the ground. The roll angle needed at that elevation angle would be  $90^\circ$ . So at a desired elevation angle, the glider roll angle would be:

$$\Phi_r = 90 - \beta \quad (7.37)$$

Now consider a dual glider system on a tether. There would not only be an elevation angle, but also an angle between the upper tethers and the stationary tether. In order for each glider to generate a pulling force

<sup>3</sup><https://www.icao.int/safety/LOCI/AUPRTATablet/index.html>

in line with the attached upper tether, the roll angle would have to be further adjusted to accommodate for this change. So for a certain angle between the two gliders (the Y-tether angle), the roll must amend by half of the Y-tether angle. This angle changed depending in the course angle. However, the elevation angle that the glider sees is the elevation angle of the glider with respect to the Y-connection of the tether. So essentially, the elevation angle of the stationary tether has a very weak correlation with the elevation angle of the upper tether.

The flight radius is calculated using the re-arranged centripetal force formula. The radius of the flight path is defined as the effective glider mass multiplied by the apparent wind speed, divided by the tether force in the upper tether. The effective mass that each glider sees is the mass of the glider, the mass of the upper tether connected to the glider, and a fraction of the stationary tether mass. The magnitude of the glider velocity perpendicular to the flight radius is the relevant speed for the centripetal force formula. Finally, the net tether force in the upper tether is reduced by the glider roll angle. Hence, only the local horizontal force (in line with the tether length) is used for this calculation.

$$R_{flight} = \frac{(m_{glider} + m_{t,u} + \frac{m_{t,l}}{n_{glider}}) \cdot v_k^2}{F_{t,net} \cdot \sin(\Phi_r)} \quad (7.38)$$

The flight path is a circle, and is at an angle to the global x-z plane. This means that the glider's apparent wind speed decreases as the glider makes its way to the top of the circle, and increases as it flies towards the bottom of the circle. This is just a simple conversion of gravitational potential energy into kinetic energy. When the glider has upward or downward flight (course angle  $\chi$  is  $0^\circ$  or  $180^\circ$ ), the relative altitude difference from the centre of the flight path circle is zero. Thus, there would be no velocity added or lost. For a elevation angle of the tether and a certain course angle, the change in the glider speed would be found using equation 7.39.

$$\Delta V_k = \sqrt{2 \cdot g \cdot R_{flight} \cdot |\sin(\chi)| \cdot \cos(\beta)} - \frac{\sin(\chi)}{|\sin(\chi)|} \quad (7.39)$$

It is clear that the added velocity is a function of the flight path radius, but the flight path radius is a function of glider speed. So in the numerical model, a form of iteration was used to ensure that the model would converge to a singular glider speed, based on the position of the glider along the flight path and the nature of the flight path.

### Reel-in phase

The reel-in procedure is a simple spiral/helix. The reel-in speed requirement of the drum winch, mentioned in chapter 8, was set to be 25 m/s. The landing procedure, just like the take-off path, involves vertical reeling in. The gliders have a glide ratio of approximately 11.9. This means that for every altitude loss of 25 m in the global z-direction, the glider in cruise conditions would fly approximately 300 m in the global x-z plane. The glider spiral total length is a function of the radius of the spiral, the change in altitude after each rotation, and the total change in altitude. The total length of the spiral is determined by equation 7.40<sup>4</sup>.

$$L_{spiral} = N \cdot \sqrt{H_{2\pi}^2 + (2\pi R_{spiral})^2} \quad (7.40)$$

The radius of the spiral is assumed to be the same as the radius of the take off flight path (300 m). The parameter  $H_{2\pi}$  is the loss of altitude for full rotation of the spiral. For the given flight radius, the circumference of the circle C is approximately 1885 m. With the glide ratio of 11.9, this would result in an altitude loss of 158 m for each full rotation. However, this does not take the angle of attack into account. For a certain angle of attack (or climb angle) at a constant glider speed and glide ratio, the total gain/loss in altitude

<sup>4</sup><https://sciencing.com/calculate-helical-length-7808380.html> [cited 7 January 2020]

after one revolution around the spiral can be quantified using equation 7.41.

$$H_{2\pi} = C \cdot \tan(\alpha) + \frac{C}{\left(\frac{L}{D}\right)} \quad (7.41)$$

The iteration for this reel-in phase was done by assuming a certain flight path radius, winch reel-in speed, and glider speed. This gave an output of what the angle of attack needed to be; 12°. At an angle of attack of 12°,  $H_{2\pi}$  would be approximately 559 m. So, there would be less than one and a half full rotations before the desired altitude drop is needed. The value N is therefore equal to 1.43. Thus, the total length of the spiral L is approximately 2,814 m. The generator can only reel in 25 m/s of the tether, taking approximately 32 seconds to complete the reel-in phase.

#### 7.4.2. Effects of weather

There are four main weather conditions that affect the performance of the system; rain, snow/hail, frost, wind gusts. The effect of the first three are difficult to quantify and can only be approximated using prior research data. The research data, while available, is limited for the following reasons; it is applicable to wings only, the reference wing parameters differ to the gliders' wing parameters, and the flight conditions differ. These parameters affect the lift coefficient and drag coefficient, and therefore the glide ratio, causing a large drop in performance.

Zhenlong Wu conducted the aforementioned research into clean and iced airfoils and how rain affected their aerodynamic performances (Zhenlong et al. 2016). He concluded that rain was largely influential for angles of attack under 9°, and that rain affected clean wings more than wings with ice on them. It was estimated that the maximum decrease of the lift coefficient is 24% and 7% for clean and iced wings respectively. The maximum increase of the drag coefficient is 108% and 6% for clean and iced wings respectively. Heavy rain and ice cause significant aerodynamics performance degradation, but ice causes worse aerodynamic performance. Wu estimates that ice formation on the wing is the equivalent to heavy rain when it comes to aerodynamic performance. Assuming a maximum  $C_L$  decrease of 24% and a maximum  $C_D$  increase of 108%, the apparent wind speed seen by each glider would decrease by 29.6 m/s and would cause a power decrease to 475 kW.

Wind gusts can be quantified by simply changing the value of the wind speed component in the apparent wind speed calculations. Based on the ISA model used to define the average wind speeds at a certain altitude (Arblaster et al. 2019b). At 3 km altitude, the average wind speed is approximately 11.5 m/s. Based on real-time data provided hour-by-hour by Ventusky's weather tracking site<sup>5</sup>, the wind speeds at that same altitude varied throughout the day from 10 m/s to 20 m/s. For wind gust analysis, wind speed ranges from 5-25 m/s were taken (increments of 5 m/s) to quantify the power loss or gain. It is evident that having a wind speed of 0 m/s would mean that there would be no cross wind flying possible. But according to the glider model created, the glider speed would still generate some power. This is because the model is based on instantaneous scenarios in the flight path, and not quasi-transient state. For zero wind speed at quasi-transient state conditions, the glider would continuously lose its speed until it fell to the ground. Therefore, the effect of gusts on the gliders were analysed at the moment of the wind speed change. If the wind speeds instantaneously change to 0, 5, 10, 15, 20, 25 m/s, then the apparent wind speeds change by -1.08, -0.86, 0.40, 1.91, 3.68 m/s respectively. For those same wind speeds, the instantaneous changes in power would be -18.5 kW, -14.8 kW, 6.9 kW, 33.4 kW respectively. At this stage it is still unknown what the presence of rain and ice are. The glider permanently flies at temperatures below 0°C but the water vapour not necessarily freezes on the wings or fuselage and the rain

## 7.5. Performance analysis

To evaluate how the glider performs, it is vital to look into the take-off and landing and flight path, as these can teach a lot about the power output and ground area needed for the glider. In this section they will be

<sup>5</sup><https://www.ventusky.com> [cited 17 January 2020]

evaluated.

### 7.5.1. Take-off and landing

There are two options for the take-off procedure, either the conventional take-off or a rotational take-off procedure. A straight runway take-off procedure is not convenient for the dual glider system since it would require the gliders to pull up the entire weight of the tether. This means that tether would significantly increase the drag during take-off. Due to this problem a rotational take-off procedure was chosen. Other advantages of the rotational procedure are the infinite length of the runway, which means that ground run distance is not an important factor. And that the glider system can be launched in an arbitrary direction, which is not possible for a straight runway take-off approach (Rapp et al. 2018).

The rotational take-off procedure requires a circular runway. The two gliders connected by the Y-tether accelerate until take-off speed is achieved. The stationary tether is connected to the stationary ground station and will reel out when the gliders have detached from the ground. When the gliders have reached the desired altitude they will rotate the stationary tether towards the wind direction, as shown in figure 7.19. Next, the elevation angle of the stationary tether is set, and the stationary tether stands still. Now the rotation of the gliders is sustained by auto-rotation thanks to the wind, the motors will be used as generators for on board power requirements (Cherubini 2017).

For the take-off the tether has to be attached to the tip of the wing. This will provide stability during the take-off due to the pulling force on the tether. However, after take-off the tether should be connected in the centre of gravity of the glider for the crosswind flight. For this reason an extra attachment point of the tether on the wingtip is made which will disconnect when the glider has reached a safe altitude to start banking. This will transfer the pulling force of the tether from the wing tip to the centre of gravity of the glider.

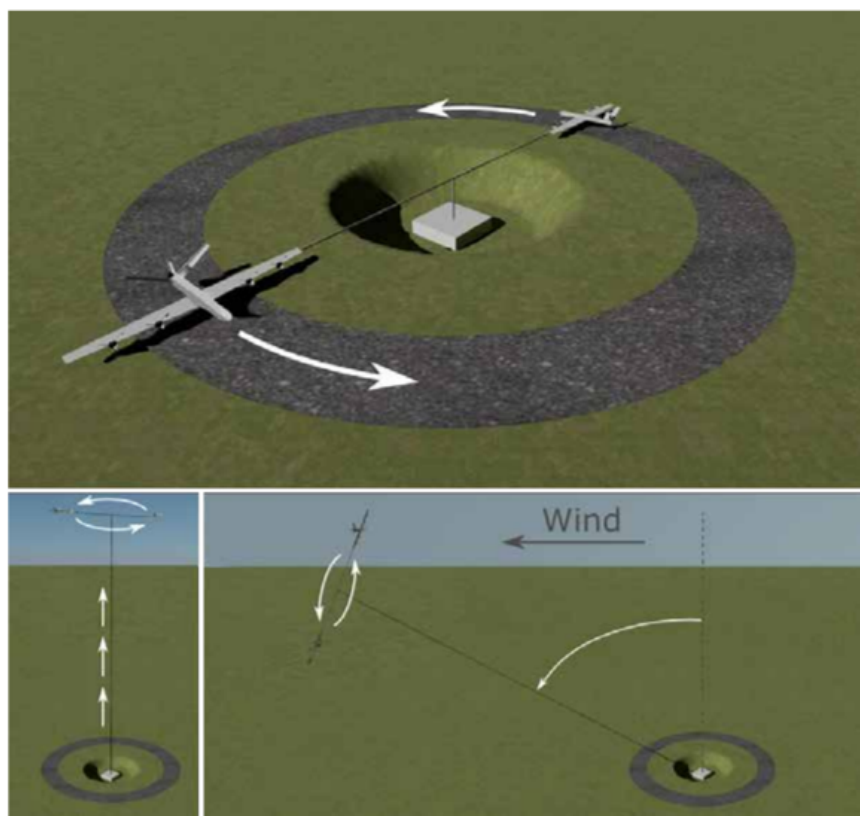


Figure 7.19: Vertical take-off procedure (Cherubini 2017)

The radius of the circular runway is determined by the minimal ground spacing of the systems. The runway is sized to fit within this spacing and the tether sag was taken into account. The tether sag can be neglected for a tether of 300 m, but not for a much longer tether. Therefore the runway will have a radius of 300 m. Since the radius of the runway is smaller than the length of the upper tether a solution has to be found to be able to keep the tether under tension. This will be done by rolling up the tether, so the rotating joint can still be used during take-off. The rolled up tether will slowly be released when the gliders are airborne. How this technically is done is outside the scope of this project.

The landing procedure is different from the take-off procedure. During the landing the gliders will disconnect the tethers, which will fall down using a parachute. The tethers will be reeled in with the same velocity as with which they are falling down. The gliders will then be able to land safely on the ground, where no runway is required.

### 7.5.2. Propulsion

For take-off a propulsion system is needed. Simplified models were used to calculate the required thrust from the aerodynamic drag. Data from literature on the performance of the electric engine and propeller was used to calculate the engine power and weight from the required thrust. The aerodynamic drag was calculated from the main wing and tether drag. A safety factor of three was included to cope with other sources of aerodynamic drag. The required engine power is calculated according to equation 7.42.

$$P = \frac{TV}{\eta} \quad (7.42)$$

T is the thrust and V the flight speed of the aircraft. The propeller efficiency  $\eta$  is set at 85% according to reference data (Gur 2013). This would lead to a total power capacity of almost 600 kW and an engine mass of 46 kg, according to an ambitious project of NASA (Jansen et al. 2017). If 600 s is taken as the duration from take off to the operation distance, a total storage of 100 kWh is needed, which results in a battery mass of 526 kg (Ibrahim et al. 2008). The batteries should be charged on ground before the flight can take off.

To mitigate the drag of the propellers during crosswind flight, the blades are retracted in the fuselage during this flight stage. The propeller is used again during reel-in flight, to charge the on-board battery.

### 7.5.3. Landing gears

Because the wing of the glider is positioned towards the nose, and because the glider has a propeller engine, it makes sense to place the main landing gear under the wing, in front of the centre of gravity, while placing the secondary landing gear towards the tail. Given the weight of the glider, a main gear with a single wheel per fuselage is sufficient (Vos and Melkert 2018). To limit the structural weight of the fuselages, the tail gears are designed to carry the minimum weight required for it to be able to steer. This results in the assumption that the tail gears each carry a minimum of 4% of the static load of the glider while on the ground (Vos and Melkert 2018).

The next step in undercarriage design is determining what load classification number (LCN) is desired for the aircraft. To allow the glider to land on grass or hard sand, a pressure of 300 kPa is selected (Vos and Melkert 2018). Combined with the amount of tires chosen, this means that – to carry a static load of 1,533 kg (based on a glider mass of 3,333 kg) per wheel of the main gear – main gear wheels with a diameter of 68.6 cm and width of 22.2 cm are selected (Vos and Melkert 2018). The tail wheels carry a lower load (133 kg each) and can thus be much smaller, with a diameter of 8.89 cm and a width of 7.62 cm. These wide wheels are required to allow for landing on unprepared surfaces without sinking into the ground or damaging the surface. The load factor on the landing gears is assumed to be 2 (Al-Hussaini 2013), which means that the main landing gear struts each carry a load of 38.8 kN, while the rear landing gear struts each carry 3.37 kN.

Now, the main gear must be positioned such that the glider can be at a downward angle of 15° from its resting position without the propellers hitting the ground or the glider tipping over, while also having

a lateral overturn angle under  $55^\circ$ . This can be determined by analysing the side view of the fuselage and the centre of gravity of the glider. For this step, it is assumed the positioning of the landing gear does not significantly affect the centre of gravity.

Starting with the downward tipping angle, it is assumed the fuselage has a length of 12.65 m, diameter of 0.7 m, and the propeller diameter is 2 m (with a safety clearance of an addition 1 m diameter); together with a centre of gravity 0.35 m from the bottom of the glider and 6.15 m from the nose. Placing the main landing gear a straight angle with the centre line of the fuselage, its connection to the fuselage must be (less than) 5.7 m from the nose, with the gear itself being 1.3 m long. The tail landing gear can be placed at the very end of the fuselage.

Next, with the lateral angle, it is assumed the wingspan is 26.8 m, and that for the length of the wing, the bottom of the fuselages are flush with the bottom of the wing, and that the centre of gravity is along the centre line of each glider. From basic trigonometry, it follows that the minimum length due to the longitudinal restrictions suffice this turnover angle too, as  $38^\circ$  is less than  $55^\circ$ .

## 7.6. On-board control subsystem

An autopilot has to be used to control the control surfaces, as well as communication from the ground. For airliners the internal power consumption is 0.2% on average from the power generated by the engines and the maximum overall power demand of cabin and cargo system of a modern short to midrange aircraft is around 60 kW and a total mass of 170 kg of the on-board energy infrastructure (Brombach et al. 2012). Large UAV's typically require tens of kilowatts of power (Bertran et al. 2016). The VECTOR autopilot from UAV Navigation was selected, as it is capable of fully automated take-off and landing as well as following the flight-path. It can cope with sensor failure as well as perform emergency landings<sup>6</sup>. The electrical aircraft LSA-02 has a 2.4 kW power requirement for operations apart from propulsion. As the mass of the glider is about 8 times as much as that of the LSA-02. Assuming the power required scales linearly with the mass, the glider requires 20 kW. This seems reasonable compared to the midrange aircraft. A mass of 56 kg for the internal electronics is than required. With a reel-in time of 32 s and a reel-out of 233 s, a minimum storage of 1.3 kWh is required, with a charging power of 165 kW.

The aircraft will be unmanned throughout the entirety of its lifetime. Requiring of the autopilot to support the aircraft for the entire operational period. The operational period consists of four phases: The landing phase, the reel-out phase, the reel-in phase, and the landing phase. These phases define the different modes the autopilot shall operate in. By far the most important task of the autopilot during all modes would be maintaining the right control parameters to prevent any chance of collision of the aircraft or with the tether.

In the take-off mode the autopilot will control the aircraft to perform the take-off. The aircraft will move in a circular motion around the central tether powered by its propulsion. The end of the landing phase the aircraft is guaranteed when the aircraft has reached an altitude of 2600 m. The goal altitude can be adjusted to adjust the operational start altitude to a more optimal altitude for energy harvesting.

Once the required operational altitude is obtained, the reel-out phase is initiated. In the reel-out phase the aircraft shall sustain the described flight path from section 7.5. The phase has a reel-out length of up to 800 m. Ultimately, when the reel-out length has been reached the operational state transfers into the reel-in phase.

In the reel-in phase the aircraft is brought in such a position as to minimise the power required for the reel-in. During reel-in the aircraft still operate in a similar flight path, but do so at a different angle with respect to the ground. The goal altitude is the start altitude of the reel-out phase. Unless the system is required to land, in that case the system will release the tethers from the aircraft and the aircraft will fly back and perform the landing by themselves.

<sup>6</sup><https://www.uavnavigation.com/products/autopilots/vector> [cited 15 January 2020]

## 7.7. Power budget

The highest on-board power consumer is the propulsion system. This requires 600 kW per glider as stated in subsection 7.5.2. On-board digital and physical control and communication systems require 20 kW as stated in subsection 7.6. The landing gear requires 1 kW (Seung 2006). The required for the ground based communications is negligible compared to the required on-board power. The power budget is summarized in table 7.4. The total maximum required power is 621 kW, but during crosswind flight only 20 kW is needed.

Table 7.4: Power budget of one glider

Subsystem	Power [kW]
Propulsion	600
Communication and control	20
Landing gear	1
<b>Total glider</b>	<b>621</b>

## 7.8. Material selection

A vital part of designing an energy harvesting device consists of selecting materials for the glider. It should be lightweight, strong and as sustainable as possible. As the device is on the edge of current technology, high-performance materials are necessary for the design.

### 7.8.1. Structural composites

In Aerospace industry composites are widely used as light-weight strong materials for aircraft design. The lighter our device will be, the better it performs. When looking at materials for the wing box structure, composites are preferred. A good parameter to compare materials on is their yield strength-to-density ratio. This tells a lot about the performance. A table is made to compare the most promising of these materials, taken from CES EduPack (Granta Design Limited 2019) or scientific papers. When a different resource as CES EduPack is used, it will be explicitly stated.

Table 7.5: Material properties of candidate materials for the glider structural parts

Material	Density [kg/m <sup>3</sup> ]	Yield stress [MPa]
Carbon fibre + PEEK	1,560	2,420
Aramid fibre + Epoxy	1,380	1,200
Carbon fibre + cyanate ester	1,650	2,150
Banana fibre (no resin)	1,275	730
Tropical wood	1,190	108
Bamboo fibre + poly-lactic	1,260	223

The first three materials in table 7.5 consist of "regular" composites currently used in aerospace industry. The banana fiber is the most promising natural fibre in terms of strength. However, no attempt at making a bio-composite with it as basis has been made yet, apart from flax and hemp bio composites used in automotive industry. There has been a composite produced with bamboo fibers (Sukmawan et al. 2016). The properties are displayed in the table. A final material selection for the structural members does not yet have to be made in this chapter. When evaluating structures it can be seen which materials can meet the requirements.

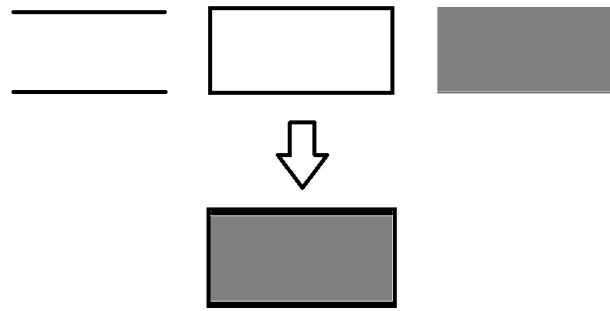


Figure 7.20: Superposition of several wing box elements leads to the wing box properties

### 7.8.2. Structural filler material

In order to strengthen the wing box and take care of shear loads, the wing box will be filled with a material. There is no need to put fuel in the wing, so it does not have to be hollow by definition. Firstly, the strength required will be calculated, afterwards a material will be searched to that requirement in subsection 7.9.1.

### 7.8.3. Skin material

Skin materials need to carry less structural weight in the glider. However, their toughness to resist impacts is important, as the wing should not desintegrate. Furthermore, weather resistance is important. In-detail calculations of the wing skin are for a later design phase. In terms of materials glass-fiber reinforced composites are very good at handling impacts. A natural material with high impact resistance is leather. For the aerodynamic shape of the wing however, the material needs to be stiff and not easy to flex, which is not the case for leather. A lot of the natural materials are not suited for the use as skin due to their difficulties of handling wet circumstances.

## 7.9. Structural analysis

The structural analysis of the gliders consists of investigating different glider components and determining what requirements the structures must meet. For the wing, this is done by designing the wingbox to withstand all loads the gliders will experience. The other components of the gliders – the fuselages, landing gears, and empennage – are not analysed in as much detail as the wing is, due to the limited scope of this project and the fact that – for the purpose of harvesting energy – their optimisation is less interesting than that of the wing.

### 7.9.1. Wing and empennage

The main structural structure of a wing consists of its wing box. The wing box is the structure carrying the wing loads through to the fuselage. Using mechanical/stress relations an analytical model was made to calculate all the stresses and required thicknesses for several parts of the wing box. The assumption is made that the total wing box can, for the time being, be evaluated by adding three parts together as can be seen in figure 7.20. The top and bottom sheet will take care of the bending loads, the outer box takes care of the torsional loads and the filler material takes care of the shear loads. The wing box has no need to be hollow, so it can be filled with a light-weight shear-carrying material to optimise its stress distribution.

The wing box must fit in the aircraft, and therefore the airfoil shape is of vital importance. Figure 7.21 shows the dimensions of the wing box chosen. The dimensions were optimised to have both a high wing box (to cope with bending) and maximum cross-sectional area, to optimise for shear and torque.

The analytical model first calculates all the loads through the wing. This is split in two parts: the tapered wing outside of the fuselages and the straight part of the wing between the fuselages. Both are evaluated separate from each other. An example of a plot of the loads can be seen in figure 7.22. The equations used

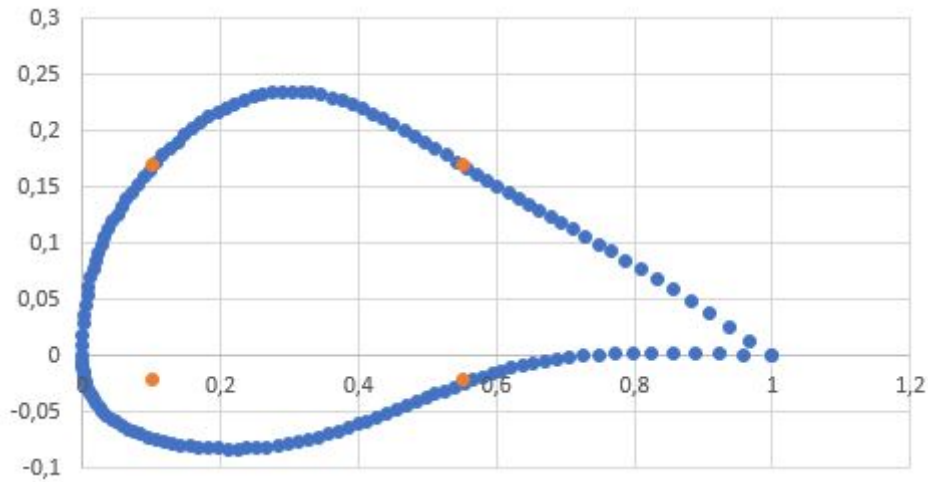


Figure 7.21: Dimensions of the wing box within the airfoil

in the model are given as equations 7.43 to 7.54.

$$K_q = \frac{L}{S} \quad (7.43)$$

$K_q$  is defined as an integration constant later used in the integration giving a ratio between Lift and Surface area.

$$h_{wingbox} = 0.19c_{local} \quad (7.44)$$

$$c_{wingbox} = 0.45c_{local} \quad (7.45)$$

The height and width of the wing box are scaled to the local chord, as described in figure 7.21.

$$q = K_q c_{local} \quad (7.46)$$

The local lift load is determined by having the integration constant multiplied by the local wing chord.

$$q_{drag} = q \frac{D}{L} \quad (7.47)$$

The local drag load is scaled to the local lift load by using the ratio between drag and lift from flight performance

$$S_{i+1} - S_i = \frac{q_{i+1} + q_i}{2} (y_{i+1} - y_i) \quad (7.48)$$

$$M_{i+1} - M_i = \frac{S_{i+1} + S_i}{2} (y_{i+1} - y_i) \quad (7.49)$$

$$T_{i+1} - T_i = \frac{S_{i+1} \cdot d + S_i \cdot d}{2} (y_{i+1} - y_i) \quad (7.50)$$

Integration equations are used to compute the loading over the wing: shear, moment and torsional loading. Boundary conditions were that the shear stress and moment had to be zero at the tip of the wing. The parameter  $y$  describes the spanwise location. These are taken from MIT courses<sup>7</sup>

<sup>7</sup><https://ocw.mit.edu/courses/aeronautics-and-astronautics/16-01-unified-engineering-i-ii-iii-iv-fall-2005-spring-systems-labs-06/sp110.pdf> [cited 28 December 2019]

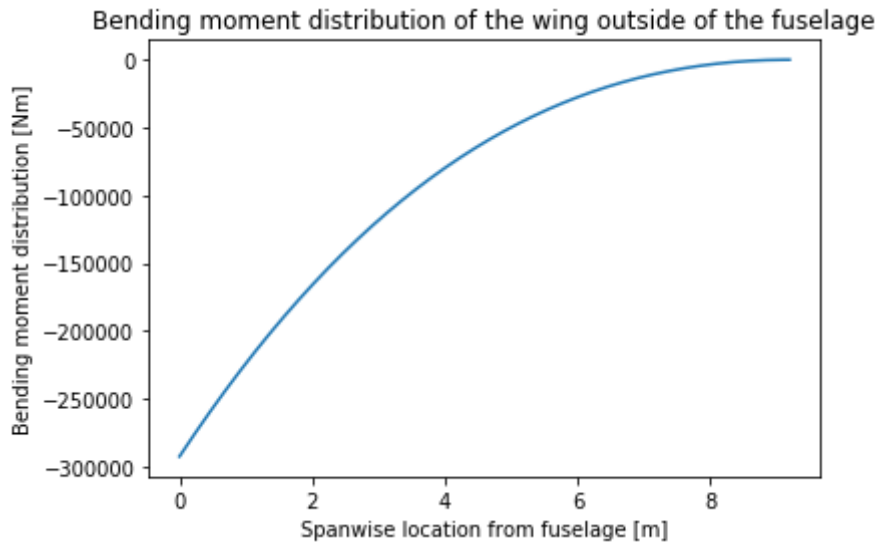


Figure 7.22: Bending moment of the wing outside of the fuselage

$$\sigma_{bending} = \frac{My}{I} \quad (7.51)$$

$$I_{rectangle} = \frac{bh^3}{12} + bhy^2 \quad (7.52)$$

$$\sigma_{torsion} = \frac{T}{2tA} \quad (7.53)$$

$$\sigma_{shear} = \frac{S}{A} \quad (7.54)$$

The equations used to calculate the stress are the final ones used in the structural wing analysis. The inertia is calculated based on rectangular sections and their Steiner term with distance to the neutral axis. The neutral axis is based on symmetry. For the torsion the area in the wing box is used, as for the shear equation.

These distributions were calculated for shear stress and bending moment due to lift, torque and shear stress and bending moment created by the drag loading. These loads were then used to calculate the thickness of the composite structure of the wing box required to stay under the yield strength of the material with a safety factor of 3. Giving a material, the program outputs a weight, which could be used in the flight performance analytical scripts. To find a suitable filler, the required shear strength of the filler material was computed. The program runs both for the centre section, between the two fuselages, with constant cross-section, and the outer section, the part of the wing outside of the fuselages. The values for the current configuration are shown in table 7.6. These values are the calculated values for a material of aramid fibers with PEEK. The natural materials, when inputted, would give structures that either did not fit in the wing anymore, or would become too heavy for the flight performance model to give positive power output values. Structurally, current natural materials don't have good enough properties yet to be used for a structural component of the glider. Current developments should get their yield strength-to-density ratio up, in order for them to become a viable alternative for current composites.

The required thickness, for the outer section, is taken at the location of the wing where the required thickness is biggest. This is at the root, due to the bending forces being strongest there. An example graph of the required thickness is shown in figure 7.23. It shows the thickness required is highest at the root. For

Table 7.6: Structural performance values of the glider

Property	Unit	Value
Wing box height, centre section	m	0.56
Wing box chord, centre section	m	1.32
Wing box tip height	m	0.22
Wing box tip chord	m	0.53
Sheet thickness for bending, outer section	mm	22
Sheet thickness for torsion, outer section	mm	1.3
Wing box mass, outer section	kg	836
Required yield strength filler for shear, outer section	MPa	0.100
Filler mass	kg	355
Sheet thickness for bending, centre section	mm	36
Sheet thickness for torsion, centre section	mm	2.2
Required yield strength filler for shear, centre section	MPa	0.142
Wing box mass, centre section	kg	837
Total wing box mass	kg	2,019

Table 7.7: Properties of possible filler materials for the wing box structure

Material	Density [kg/m <sup>3</sup> ]	Shear strength [MPa]	Environmental comments
Expanded PS foam	50	0.9	Recyclable
PVC cross-linked foam	65	0.5	Recyclable
Balsa wood	100	2.5	Natural
Synbra biofoam	35	0.14	CO2-neutral
Biobased structural epoxy foam	85	0.15	Natural

convenience in manufacturing and calculations, the thickness is kept constant at that highest value over the entire wing box. Later iterations and improvements could save weight by sectioning the wing box in sections and decreasing the thickness throughout.

The required yield strength of the filler for shear is at max 0.142 MPa. This can be used to find a lightweight filler material, preferably lightweight. To do this, table 7.7 was set up, giving different materials from CES Edupack (Granta Design Limited 2019), using a datasheet of a company<sup>8</sup>, or based on research paper (Mazzon et al. 2020). Instead of the yield strength the shear strength of the materials was taken for evaluation. Loading in shear causes a lower shear strength than yield strength in many cases. A safety factor of 3 is applied to ensure safeness of the structure. Therefore the material should have a higher shear strength than 0.426 MPa in order to be a viable solution.

The shear strength of biobased structural foams was not found to be high enough for application in the glider. However, another biobased material, namely balsa wood, shows great potential. Although a bit redundant in strength, it shows good shear-to-density relations. Instead of filling the wing box with balsa wood, it can be used to make ribs, decreasing the weight. If half of the wing box is filled with balsa wood, it is lighter than the PS and PVC foams mentioned in the table, but still stronger. This gives a density of 50 kg/m<sup>3</sup>, which will be used in the weight estimation. Cutting wood is sustainable, when other trees are planted to replace the cutted trees.

The empennage structure will be similar to the structure of the main wing. It will use the same materials as well. The equations previously applied to the wing structure apply for the tail wing as well. They are supplemented with simply distributed loaded clamped beam equations, such as equations 7.55, in which

<sup>8</sup><https://www.synbratechnology.com/media/11720/tds-biofoam-v91-2017-03.pdf> [cited 17 January 2020]

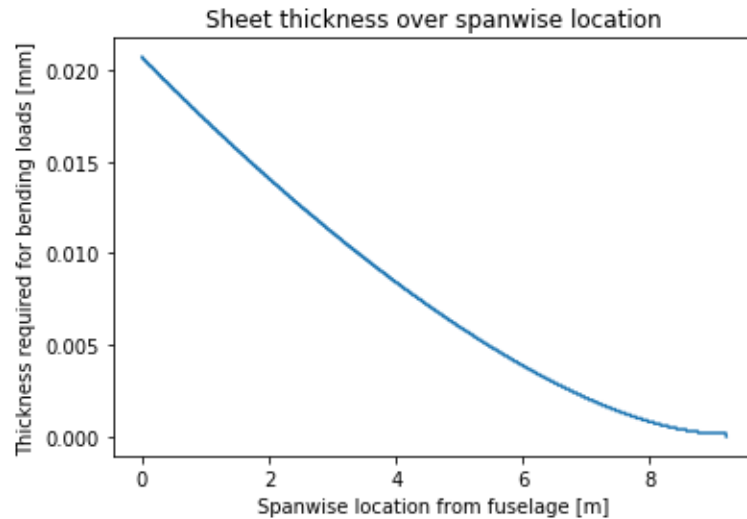


Figure 7.23: Sheet thickness required to cope with the bending loads of the wing outside of the fuselage

the moment at the clamped side of the beam is determined.

$$M = \frac{-qL^2}{12} \quad (7.55)$$

The variable  $q$  is the distributed load strength, and  $L$  is the length of the "beam". This combined renders a required thickness of wing box material of 2 mm, resulting in a weight (filled with the balsa wood filling) of 68 kg.

### 7.9.2. Fuselages

The fuselages must be able to carry the loads it might encounter. The main loads that must be designed for are the wing and empennage loads, as well as the loads when landing and propulsive loads during take-off. This means that there must be support in lateral and longitudinal direction, as well as a skin to carry shear loads. Space must be left for both the main and rear landing gears as well. A circular cross section is convenient for aerodynamic properties. No windows or other cut outs are necessary for the gliders, other than for the engines and the landing gear.

A fuselage is generally divided into three sections: the forebody, aftbody, and centrebody (Niu 1988). These sections denote the sections forward, aft, and between the forward and aft main frames. The forward and aft main frames are located by the wing and fuselage intersection, which is the most highly loaded section of the fuselage.

The frames mainly maintain the shape of the fuselage and carry the loads from the wing and empennage. They must be especially strong in and around the centrebody and towards the end of the aftbody. Longerons attach to the frames and transfer the skin loads to the frames. Stringers, in between the frames are used for additional support in longitudinal direction.

The wing can run through the fuselage, preventing heavy forging to attach two wings to either side of the fuselage. The typical wing-to-fuselage connection is done by bolting the two main frames to front and rear spars of the wingbox (Niu 1988). This is usually the most effective attachment method, though this connection must be designed to sustain fatigue loads due to the wing bending. Similar attachment is to be used for the empennage.

### 7.9.3. Mass budget

For flight performance it is important to have a more in-depth estimation of the weight of the glider. The wing box structure weight and tailplane wing box weight were calculated before. Parts missing are the wing

skin, fuselage, and fuselage content (engine/propellor, battery, other systems).

For an estimation of the mass of wing and fuselage skin a few assumptions are made:

- The skin consists of a glass-fiber reinforced polymer with 1 mm thickness
- Fixing/securing mechanisms of the skin are not taken into account
- Glass-fiber reinforced polymer with a density of  $1910 \text{ kg/m}^3$  is used (Granta Design Limited 2019)

The total wetted area is estimated based on the CATIA model as an estimation. This is approximately  $260 \text{ m}^2$ . Multiplied with the thickness and density this gives a skin weight of 497 kg.

According to Virginia Tech<sup>9</sup> the landing gear takes about 4% of the MTOW of an aircraft. This is in our case about 120 kg.

The fuselage content is mainly determined by engine, battery, electronics and propeller. These add up to about 628 kg based on the analysis in section 7.6. An overview of all the weights is given in table 7.8. This also gives a mass estimation of the total glider, which is 3,333 kg.

Table 7.8: Mass budget of one glider

Subsystem	Weight [kg]
Wing box	2,019
Empennage box	69
Fuselage content	628
Landing gear	120
Skins	497
<b>Total glider</b>	<b>3,333</b>

## 7.10. Sensitivity analysis

The used airfoils were optimized for a range of surface areas between 20 and  $100 \text{ m}^2$  and velocities between 80 and 120 m/s. Slight differences can be spotted in  $C_L/C_D$  within the aforementioned ranges, though these are insignificant. The figure 7.24 shows the effect of the aspect ratio and apparent wind speed on  $C_L/C_D$ .

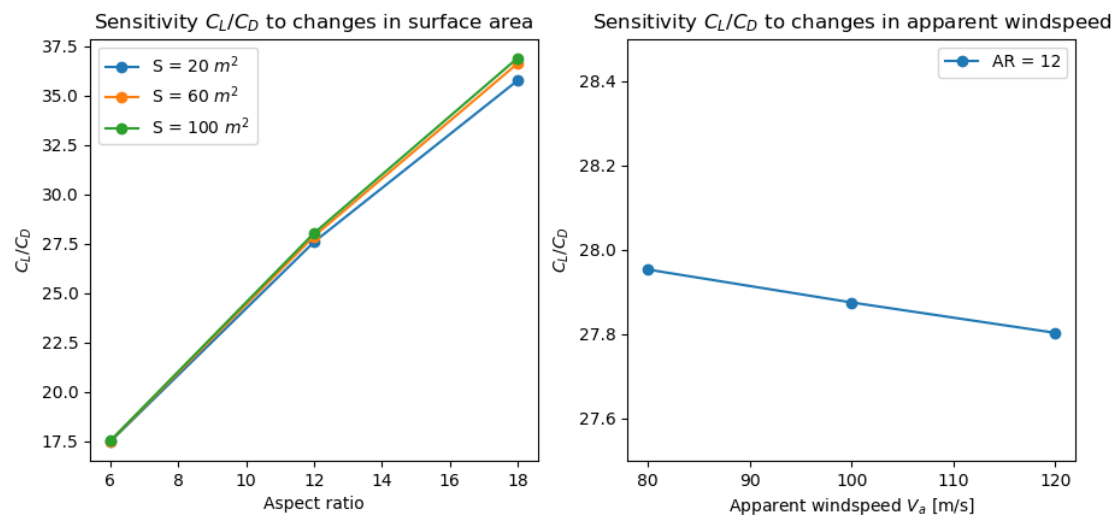


Figure 7.24: The effect of changes in aspect ratio of the wing and apparent windspeed to the lift-over drag ratio. In the left plot the effect of a changing aspect ratio can be seen, while in the right plot the effect of a changing apparent windspeed is depicted.

<sup>9</sup>[http://www.dept.aoe.vt.edu/~mason/Mason\\_f/M96SC08.pdf](http://www.dept.aoe.vt.edu/~mason/Mason_f/M96SC08.pdf) [cited 18 January 2020]

To see how the entire glider responds to changes can teach a lot about the convergence of the codes and the robustness of the design. If big changes in output values can be seen after changing the inputs slightly, the design will be very prone to changes. If the system reacts more insensible, it is less likely that parameters of the glider will change massively. Furthermore, sensitivity analysis can show if a design is poorly optimized, if it's performance increases once you change some input parameters.

To perform the sensitivity analysis, the inputs of the design had to be defined. There were only a few inputs that could be used to "play with". The four main ones identified were number of gliders per tethered system, aspect ratio, surface area and the operating altitude. Other identified, but not thoroughly calculated design inputs could be the densities of some materials and reel-out speed, which was already optimised.

In table 7.9 the results of the big sensitivity analysis is shown. The left column describes the input, and the values used as inputs. The rest of the columns show their effect on the outputs: weight per glider, power per system and flight path radius.

Table 7.9: Results of sensitivity analysis after changing some of the input variables slightly

Inputs Outputs	Weight per glider	Power per system	Flight path radius
#Gliders per system (2, 3, 4)	(0%, -8.64%, -21.0%)	(0%, +20.9%, +13.4%)	(0%, +44.4%, +71.7%)
Aspect ratio (10, 12, 14)	(-6.9% , 0%, +12.2%)	(N.A. , 0%, +8.5%)	(N.A. , 0%, +10.5%)
Surface area (60, 65, 70 m <sup>2</sup> )	(0%, +13.6%, +29.6%)	(0%, +7.4%, +14.6%)	(0%, +5.2%, +9.7%)
Altitude (2.5, 3, 3.5 km)	(-6.2%, 0%, N.A.)	(-27.7%, 0%, N.A.)	(-6.9% , 0%, N.A.)

If the amount of gliders per system is increased, the weight per glider decreases (note that to obtain a stationary tether, a minimum of two gliders is required). The power per system increases as well, mainly for having three gliders per tether. The increase in total system mass due to the step to three gliders is bigger than the extra power output. Furthermore, flight path radii increase sharply, whereas they already were a problem. Sticking to two gliders is thus the result. As this is a design choice, there is only a slight chance it will ever change.

If the aspect ratio is decreased to 10, the system plummets from the sky and does not produce any energy at all. The same holds for lowering the surface area. Therefore the aspect ratio and surface area should in all cases not be decreased. Increasing the surface area and aspect ratio adds more mass than it adds power per system. Furthermore it increases the flight path radius, which is problematic for the take-off and landing.

Finally, the response to altitude is evaluated. By going higher to 3.5 km, the tether mass and drag become too big for the system to stay airborne at all cases, thus that is not an option. By going to lower altitudes, the power per system is sharply decreased, whereas the weight only slightly decreases. The altitude should thus stay at 3 km.

## 7.11. Verification

The numerical and analytical models for the airfoil and wing as defined in sub-section 7.2.5 and 7.2.4, produced  $C_{L\alpha}$  and  $C_L/C_D$  plots.

From the analytical model it became clear that using the DATCOM method from equation 7.5,  $C_L$  should increase 0.1 per angle of attack. From the numerical model using XFLR5, this can indeed be verified within an error margin of 10%. According to figure 7.6  $C_L$  changes between 0 and 10 °from 0.8 to 1.8. This means that the error between the analytical and numerical model is equal to 0%. Therefore the verification of the numerical model with the analytical model is performed successfully.

For the drag several analytical analyses are performed, ranging from class 0 to class II. It is interesting to see from figure 7.10 that the more accurate the analytical analyses became, the higher the drag was. This may be counter intuitive, due to the fact that the aircraft has a very small fuselage. As there are not many reference aircraft for said aircraft, it is not unlikely that the drag coefficient of the entire aircraft may

be larger than initially anticipated. Luckily, this is not a large problem as the largest drag comes from the tether and not the aircraft. The numerical model is provided by in-depth analysis using XFLR5 and plotted in figure 7.7. The reader is encouraged to compare figure 7.10 and 7.7. From the analytical and numerical model two points are picked per model for the verification, at  $C_D = 0.05$  and  $C_D = 0.15$ . The results are shown in table 7.10: the error between the analytical and numerical model for  $C_L/C_D$  is around 12.5%. This could be due to

Table 7.10: Comparison of  $C_L/C_D$  between the analytical and numerical model.

	$C_D = 0.05$	$C_D = 0.15$
$C_L$ (analytical model)	1.15	1.95
$C_L$ (numerical model)	1.3	2.25
<b>Error</b> [ $\Delta C_L$ ]	0.15	0.3
<b>Error</b> [%]	12	13

The structural script is verified by hand-computing one loop of all the loops. This way multiple mistakes were spotted and corrected in the code. Currently all the loops are correct. Equations were checked with TU Delft courses like Structural Analysis and Mechanics of Materials to see if they correspond. Finally, plots of all the data were subject to a sanity check. The bending moment graph should for instance be approximately quadratic, which it was. Simplified calculations (like simple beam equations) were used to make an estimate of what order of magnitude of number should come out of the script. These orders of magnitudes all corresponded.

To verify the assumption that the gliders have no interference on each other, one can consider the time which one glider takes to obtain the circular position of the second glider. With a flight radius of 466 m and a circular flight speed of 87.72 m/s, it takes 16.7 seconds for the gliders to get to the position of the other glider. This is sufficiently large to state that the gliders have negligible interference on each other and thus that the assumption is verified.

The verification of the glider flight model was conducted in a similar manner to the way the structural models were done. At first the code gave incorrect apparent wind speed magnitude values, and then then it gave incorrect apparent wind speed vector directions. To rectify this, and to ensure that the iteration process would be correct, a single iteration of the model was done by hand. The equations were verified using the Airborne Wind Energy textbook (Schmehl et al. 2013, ch. 2) and sensitivity analysis was done to check whether the general trends they followed were intuitively correct. For example with a lower glide ratio, there would be a smaller apparent wind speed, which would lead to less power being produced. The relation between the glide ratio and the apparent These parameters corresponded with the values in the analytical mode, and so the system was considered to be verified.

## 7.12. Conclusions

From this chapter the general wing planform, glider layout, flight path and corresponding net cycle power output, structural performance, and on-board control system can be concluded. In the subsections below, the conclusions are given.

### 7.12.1. Wing and glider layout

The optimisation resulted in a wing surface area of 60 m<sup>2</sup>. The wing span is 26.8 m with an aspect ratio of 12 and zero sweep at the leading edge. A taper ratio of 0.4 is chosen in order to get a quasi-elliptical lift distribution which lead to a trailing edge being under an angle. Since the glider flies at an apparent angle of attack of 3°, during energy production, the  $C_L/C_D$  at this angle of attack of the wing is 27.4.

After sizing the wing, the glider dimensions could be determined. A double fuselage is chosen for bending relief and to carry subsystems such as landing gear. The length of the fuselage is 12.65 m with a maximum radius of 1.06 m. The empennage is designed for stability with a surface area of 15 m<sup>2</sup> and a symmetric airfoil is chosen. The height of the vertical tail plane is determined by down wash computations. As control surfaces, two ailerons are placed on the main wing and the empennage carries the rudder and elevators. The configuration results in a total  $C_L/C_D$  of 11.9 at an apparent angle of attack of 3°.

### 7.12.2. Flight path and net cycle power

Since two gliders are attached to a single main tether, the flight path of each glider must be circular in order to counteract the force of the other glider. The flight path is optimised for maximum net cycle power. In order to determine the flight path and its corresponding net cycle power output, two phases are separately assessed; the reel-out phase and the traction phase. The reel-out phase generates electricity on the ground which needs to be maximised whereas the traction phase consumes energy which has to be minimised. The optimisation lead to an operating altitude of 3,000 m at an elevation angle of 40° and an azimuth angle of 0°. Calculations on the apparent wind speed concluded an apparent angle of attack of 3°, as mentioned before. By determining an optimal reel factor, a reel-out speed of 3.44 m/s was found which lead to a power output during the reel-out phase of 635 kW. The tether length that is reeled out during one cycle is 800 m and the optimal flight radius is 466 m. The reel-out time is 233 s and the reel-in phase is 32 s given a reel-in speed of the drum of 25 m/s.

The influence of weather is also researched and calculated. It is concluded that rain and ice cause a maximum lift decrease of 24% while the drag could increase up to 108% causing a maximum power production reduction of 475 kW. However, at this stage it is still uncertain what the influence of ice, rain and water vapour formation is on the gliders. Currently, the possible lift reduction and drag increase are not taken into account. Gusts affect the system as well ranging from a decrease and increase in power of -18.5 kW and 33.4 kW, respectively.

### 7.12.3. Take-off and landing

For take-off an electric on-board propulsion system is needed. The total energy needed for take-off is 100 kWh which results in a battery weight of 526 kg as stated in subsection 7.5.2. The propellers are attached to both fuselages and to mitigate the drag of the propellers during crosswind flight, the propellers are retracted. During the reel-in phase, the propellers are used again for extra on-board power generation. A rotational take-off procedure is used on a circular runway. Once the two gliders are at the desired altitude, they will rotate the tether towards the desired operation angle. For the landing procedure, the tethers are disconnected and each glider lands separately on the circular runway.

The main landing gear is positioned under the wing, just in front of the centre of gravity and the rear landing gear is positioned towards the tail. The diameter of the wheels is 68.6 cm and the width is 22.2 cm such that it can land on unprepared surfaces. It is positioned 5.7 m from the nose of the glider with a length of 1.3 m.

### 7.12.4. Structural performance and materials

For the material selection and the structural analysis of the glider, the main focus is on the wing and its wing box. For the wing box, balsa wood is used for the ribs. The wing box is 2 mm thick and is made of carbon fiber + PEEK which has a high yield strength. The skin of the wing has to be further analysed but for current calculations, glass fiber is used as a reference material. The wing runs through the fuselage decreasing structural weight.

Based on the structural calculations of the wing box, skin of the wing and empennage and some assumptions from literature study, the glider weight is estimated to be 3,333 kg, including payload.

### 7.12.5. On-board control system

The VECTOR autopilot is chosen as it is capable of automated take-off, landing, and flight. The total power the glider requires is 20 kW and a minimum storage of 2.3 kWh is required. The total payload mass for the control system is 56 kg.

### 7.12.6. Glider parameters

After combining the individual scripts for the glider, the numerical model could be optimised for the parameters mentioned in section 7.10. The model was optimised to give maximum power outputs and minimal flight path radii. The optimised parameters for the system can be seen in table 7.11.

Table 7.11: Optimised system parameters

Parameters	Symbol	Value	Units
Apparent wind speed magnitude	$V_a$	87.72	m/s
Average operating altitude	-	3,000	m
Tether reel-out speed	$V_{reel, out}$	3.44	m/s
Wind speed	$V_w$	11.47	m/s
Tether elevation angle at ground station	$\theta$	40	°
Glider elevation angle at Y-connection	$\beta$	20	°
Power generated at each ground station	$P_{drum}$	635,042	W
Flight path radius	$R_{flight}$	466.5	m
Total tether mass	$m_{tether}$	2,292	kg
Lift generated by each glider	$L_{glider}$	228,981	N
Tether force at connection to glider	$F_{tether}$	106,518	N
Tether diameter	$D_{tether}$	1.49	cm
Tether length	$L_{tether}$	4,809	m
Number of units	$n_{sys}$	19	-
Duration of reel-out phase	$t_{out}$	232	s
Duration of reel-in phase	$t_{in}$	32	s
Length of reeled tether	$l_{reel}$	800	m
Spacing between ground stations	$d_u$	1,296	m
Radius of runway	$r_{runway}$	300	m
Mass of each glider	$m_{glider}$	3,333	kg
Diameter of fuselage	$d_{fuselage}$	106	cm
Nominal angle of attack	$\alpha_{nom}$	2	°

## 7.13. Recommendations

The recommendations can be split into the following subsections: wing, glider layout, aerodynamic performance, materials & structures, on-board control & communication.

### 7.13.1. Wing

The use of winglets can increase the effective aspect ratio by 20%. This would increase glide performances as the  $\frac{C_L}{C_D}$  is increased. However, increasing the effective aspect ratio also greatly increases the need for structural reinforcement at the root of the wing due to the increase in bending moment. Furthermore, adding winglets is known to induce fluttering of the wing (Heyson et al. 1977). It therefore has to be analysed carefully whether winglets would increase the flight performance. XFLR5 is unfortunately not able to converge for a wing twist angle of 5 ° to cope with the tip stall and could therefore not be analysed. It is recommended to apply a wing twist angle in order to keep the aircraft controllable at higher angles of

attack. No coatings are taken into account on the effect of the drag. Only in the class II estimate of the drag, the skin surface coefficient for smooth composites is taken into account. This is an average value taken from literature.

Originally XFLR5 is built for model and glider aircraft and not for analysis with high Reynolds numbers, even though it can calculate these values. It is therefore preferred to perform additional numerical analysis using computational flow dynamics. Even though XFLR5 is able to take viscosity into account, these calculations are using a simplified model. With respect to stall, XFLR5 can only analyse stall behaviour until full stall occurs. This means that unfortunately XFLR5 cannot produce (3D)  $C_L - \alpha$  plots where a distinct decrease in  $C_{L\alpha}$  can be seen, so all the plots are straight lines.

From a feasibility point of view the design seems feasible, as wings in the past have been designed with similar characteristics. The airfoil is a special kind and it is not certain whether or not high-lift devices can be attached to the trailing edge.

### 7.13.2. Glider layout

The vertical tail design resembles similar tails in conventional aircraft. Further analysis could be conducted to design vertical tail wings that would perfectly complement the glider design.

A tail wing height was taken to balance the moments of the glider, but it may not have necessarily been the optimal point for the tail wing height. A script was written to determine the effect of down wash on the tail wing, but this can be further elaborated using numerical simulation. Furthermore, class I and II estimations for glider weight and c.g. was done, but class III and IV could also be done to get a detailed analysis of the stability of the glider.

An idea for the glider, for the future, would be to have asymmetric wings. Most conventional aircraft have symmetrical shapes to simplify calculations. The conventional aircraft were used for class I and II estimations for sizing and centre of gravity. However, this need not be the case. Much like NASCAR racing cars only being designed to turn left, the gliders consistently bank to one side and fly in a circular path. The shape of the wings could be further optimised to find the best aerodynamic performance for gliders flying crosswind.

Ice formation on the wing causes poor aerodynamic performance, which could hamper the amount of energy generated by the system. A way to mitigate this risk is to have active heating, especially in the wings.

The take-off procedure requires the propellers to generate enough thrust to lift both the glider and the tether attached to it. One option would be to have a rotating ground station to create centrifugal forces for the gliders and generate enough speed for takeoff. The tethers would also be in tension, causing less drag and increased take-off efficiency. Alternatively, one can pursue vertical take-off and landing. This involves the gliders using their propellers like helicopter blades to ascend until the target altitude is reached. The advantage of this system is a significantly smaller ground area, a key parameter in energy density of an energy system.

Another possible way to improve the take-off procedure is to use one runway for the take-off of all the glider systems instead of a separate runways for each system. A solution will have to be found to transfer of the airborne system to the desired operating location, to free the runway for the next gliders to take-off. Also, the procedure to roll-up the tether to make it the right length to fit the runway has to be further investigated.

### 7.13.3. Aerodynamic Performance

The aerodynamic performance of the glider was limited to the models that were created. The analytical model, designed during the midterm, was a 2D model that gave order-of-magnitude values for the gliders in question. The numerical model was a 3D model that mapped the instantaneous aerodynamic performance of the system. The numerical models in industry are often in a quasi-transient state, leading to a rudimentary form of flight simulation. This is complex to implement and is often already pre-made in

organisations. For more accurate values and sensitivity analysis, a time-based numerical model should be made.

The aerodynamic properties of the glider and tether were taken from analytical equations, and then discretised over their respective lengths and surface areas. Although this is more accurate than a single governing equation, the accuracy of these results would be much less than the accuracy of numerical simulations. Numerical simulations like CFD or FEM analysis would give similar values, but with lower margins of error.

The flight path of the system is circular and at an angle of elevation. To maintain this flight path, the glider must continuously change its roll angle and angle of attack. As mentioned before, a quasi-transient state numerical model would help describe the aerodynamic properties of the glider as a whole, rather than at certain instances.

#### **7.13.4. Materials & structures**

Structural analysis currently involves mainly the structural analysis of the main wing box and tail wing box. In order to reach production phase, the fuselage and vertical tailplane need to be thoroughly calculated, as well as the glider skin and connections points. Natural materials are, for the structural parts, currently not strong and light enough. If, in the future, these materials can come closer to properties of state-of-the-art composites, they can be used more in the glider. Finally, a detailed analysis on material of the skin has to be performed to reach a final design.

## Technical analysis of the ground station

In this chapter the technical analysis of the ground station is done. First, in section 8.1 the main components of the ground station are discussed. In section 8.2 the performance of the systems and the amount of systems required is discussed. How the ground station is anchored can be found in section 8.3. Then the area needed for the ground station is calculated in section 8.4. Verification is briefly discussed in 8.5 and finally a conclusion is given in section 8.6.

### 8.1. Ground station model

In this section the main components of the ground station model are described. These components include the drum to reel the tether in and out, and a generator to generate the energy.

#### 8.1.1. Assumptions

For the technical analysis of the ground station some assumptions were made, these are stated below.

- Skin drag between the tether and the drum is assumed to be negligible for reel-in calculations.
- When reeling in the tether the tension in the cable is assumed to be negligible
- It is assumed that the power loss due to variable wind speeds after absorbing it by the dampers is zero.

#### 8.1.2. Drum

The drum is designed to have a high reel-in speed in order to shorten the reel-in time in which the system is not producing any energy. The drum that is going to be used for this system has a reel-in speed of 25 m/s and a radius of 530 mm<sup>1</sup>. The latter combined with drum length of 3.45 m is chosen to be high enough for a large amount of reeled tether to be stored on the drum. For the drum, a carbon composite (0.65 fiber fraction) with high torsional strength of 1,140 MPa and a density of  $1.5 \cdot 10^3$  kg/m<sup>3</sup> is chosen (Ashby 2011).

The cable length which is reeled in is limited by the amount of cable that can be stored on the drum. In this case the maximum amount would be 800 m. Having a shorter cable length would lead to the reeled cable being in need for maintenance more often, since the reel-out phase would be shorter and thus the cable gets damaged more quickly as the frequency of the reeling cycles is higher. With a reel-in cable length of 800 m, this leads to a reel-in phase time of 32 seconds. For comparison, the reel-out phase has a time of 233 seconds with a reel-out velocity of 3.44 m/s or rotational winch speed of 124 rpm. To calculate how much power the winch needs to reel the tether in, the amount of kinetic energy is calculated with equation 8.1.

$$E = \frac{1}{2} I \omega^2 \quad (8.1)$$

where  $I$  is the moment of inertia of the drum and  $\omega$  the rotational speed of the drum. From this the amount of power can be calculated using equation 8.2.

$$\Delta P = \frac{\Delta E}{\Delta t} \quad (8.2)$$

This leads to a power loss of 5.58 kW due to the winch.

<sup>1</sup><https://fcreate.com/wp-content/uploads/2018/08/AW053series.pdf> [cited 16 January 2020]

### 8.1.3. Generator

To choose a generator, one can compare the glider system to wind turbines, because both will need low-speed generators whereas usually high speed generators are required. Furthermore, much more research has been done on wind turbines than on the glider system. Still, a lot has to be researched about the optimal generator configuration, but known advantages and disadvantages are going to be discussed. It is beneficial and essential that the generator should produce sufficient power with variable speeds, due to the glider not pulling the cable at constant speeds, because of variable wind speeds. For wind turbines, variable speed turbines produce 8 to 15% more power than fixed speed turbines and therefore variable speed is going to have to be accounted for (Shanker et al. 2012).

Up until the 1990s, wind turbine companies have been using generators with gearboxes attached to lower the rotational speed of the shaft because it is cheap and light. However, in recent years a direct drive design has come into the market, which does not need a gearbox and thus increase reliability and consequently reduces the need for maintenance, since gearboxes are known to fail. However, direct drive needs low rotating-speed generators which can then lead to the direct drive being large in size. This can be shown by the equation 8.3 (Laithwaite et al. 1980).

$$P = kDL\omega \quad (8.3)$$

Which relates the power output of the generator  $P$  to a generator constant  $k$ , diameter and length of the rotor  $D$  and  $L$ , respectively, and the rotor rotational speed  $\omega$ . Having a lower  $\omega$  leads to either  $D$  or  $L$  to increase to generate as much power, leading to a bigger and consequently heavier generator. However, there is a difference in application of generators between wind turbines and tethered gliders. The generator for the latter is placed on the ground and can thus be heavier than on a wind turbine, where more generator weight would need more structural strength in the tower. Direct drive generators are therefore used for this application.

The generator which is going to be used for this system is the Permanent Magnet Generator (PMG)<sup>2</sup>. These have advantages over other generators in that they have a higher power density than other generators but at the cost of more complexity and cost due to the necessity of commutators and brushes to extract the generated energy from the armature (stator) (Potgieter et al. 2012). A full comparison between the generators can be found in table 8.1. It is clear to see that Doubly-Fed Induction generators (DFIGs) and PMGs perform considerably better than conventional DC generators. However, grid-support capability and efficiency are considered to be more critical for this system than cost and thus a PMG would be best for this system.

A PMG is a synchronous generator which includes a stator and rotor inside with a rotating magnetic field and static magnetic field on top of the stator and rotor, respectively. These magnetic fields attract each other and the two components can move at equal rotational velocity and thus make the magnetic field have 0 relative angular velocity. This magnetic attraction between the stator and the rotor is enough to keep the angular velocity constant. Because of the permanent magnet on top of the rotor, the electrons will start moving and three-phase power is generated in an alternating manner (AC). Synchronous generators are in this case required to handle variable speeds and therefore need to include dampers and/or springs to maintain exact synchronous speed. If they would move at different speeds, the south poles of the magnetic field will meet other south poles which makes them repel each other, which makes the rotor lose rotational velocity, and the generator will not function optimally.

Due to the variable wind speeds, the frequency of the current is also variable in the windings of the stator. The variable AC therefore has to be converted to fixed frequency DC and then back to fixed frequency AC for the grid (AC-DC-AC conversion).

<sup>2</sup><https://www.greefenergy.com/post/73> [cited 17 January 2020]

Table 8.1: Comparison between Doubly-Fed Induction, Permanent Magnet and Direct Current generators

Performance indicator	DFIG	PMG	DC generators
Grid-support capability	high	very high	low
Efficiency	high	very high	low
Cost	low	high	low
Reliability	high	high	poor
Power supply	partially stator-converter	totally via converters	directly to grid

## 8.2. Performance

In this section it is determined how much power one system produces including the power needed for the winch and generator power loss.

The power needed for the winch has been determined in subsection 8.1.2 and equals 5.58 kW. The amount of power the gliders produces by pulling on the cable equals 635 kW for one system. With a reel-in and reel-out time of 32 and 233 seconds, respectively, this equals an average net power of 558 kW. With an estimated generator efficiency of 97% (Khazdozian et al. 2014) this equals a total net average power output of 541 kW. With the TU Delft energy requirements one would need 19 systems (38 gliders) to provide it with its yearly energy needs.

## 8.3. Anchoring

To ensure the ground station remains in place, either a foundation or counterweights must be used. A foundation would have to be reinforced to withstand the tensile forces due to the generator. Sizing of a foundation is highly dependent on the soil type and therefore not possible to do at this point. A problem with laying a foundation for the generators is that soil must be moved, thereby disturbing the ecosystem.

In the case of using counterweights, the weight of the counterweights (likely concrete) must be enough to counter the vertical force and enough to provide enough static friction to prevent horizontal movement. However, as there is no soil that prevents movement as well, more concrete would be needed.

Concrete manufacturing is responsible for 8-9% of the global human-caused CO<sub>2</sub> emissions, and 2-3% of energy usage (Monteiro et al. 2017). Most of these emissions originate from the production of cement, where limestone and clay are heated to high temperatures, which releases CO<sub>2</sub> (Jonkers et al. 2010). A more sustainable solution must therefore be found. Current developments include the use of coal fly ash and iron blast-furnace slag (industry byproducts), which reduces the amount of cement needed (Monteiro et al. 2017). Additionally, the aggregate used inside the concrete can use recycled aggregate material.

Another approach for more sustainable concrete is the use of more durable concrete. The Civil Engineering & Geosciences faculty of TU Delft is investigating self-healing concrete to repair occurring cracks, thereby increasing the lifetime of the concrete (Jonkers et al. 2010). Nonetheless, it must be noted that concrete exceeding the life-time of the project does not have an additional benefit.

## 8.4. Area needed for ground station

The dimensions for the generators are 4.20x1.65 m or 6.93 m<sup>2</sup> surface area. The drum has a surface area of 3.45x1.20 m or 4.14 m<sup>2</sup>. With a runway area of 364,110.5 m<sup>2</sup> for a total of 19 systems, this leads to a total ground area needed of 364,320.83 m<sup>2</sup>. This is considering the area around the generator and drum and inside the runway fit for use to place, for example, cows of farmers.

With a total power output of 10.59 MW, this leads to a power density of 29.07 W/m<sup>2</sup>. Comparing this to wind turbine power densities of 1.3 MW/m<sup>2</sup> (Baldwin 2009), this is a really low power density. This can be easily explained by the fact that for the power density of the wind turbines, merely the area of the foundation of the wind turbine on the ground is taken, while for the glider system the runway leads to a

very high ground area. For solar panels, the power density is approximately  $42.5 \text{ W/m}^2$  (Williams et al. 2011). So the power density of the glider system is also lower than for solar panels.

## 8.5. Sensitivity Analysis and Verification

Changing certain inputs and then observing whether the outputs would change in an expected manner is to be done for sensitivity analysis.

Changing the reeled cable length to 400 m, instead of 800, would result in a very low difference in amount of systems needed from 18.51 to 18.49. This makes sense as less energy is generated per cycle, but the frequency of the reel-in and reel-out cycles is higher and thus approximately the same net power is generated.

Changing the density of the winch hardly changes the amount of systems needed as well, since the power loss due to the winch is small in general compared to the power generated. Increasing the density will thus increase the winch power loss but will hardly change the amount of systems needed.

For verification of the ground station, the calculations that were done for determining the power needed and therefore the nominal net power generation were redone manually (by hand). These calculations yielded exactly the same results as the computed calculations.

## 8.6. Conclusions

The winch that is going to be used for this system is the AWE winch from FEcreate<sup>3</sup> due to its high reel-in speed. This results in a power needed for the winch of 5.58 kW. This consequently results in a net power (without generator) of A permanent magnet synchronous generator is used due to its high power efficiency. Furthermore, AC-DC-AC converters are used to obtain fixed current frequency with variable wind speeds. Also the power is transformed by a voltage/current transformer to high-voltage power to be received by the grid. Lastly, the generator has an efficiency of 97%. All in all, the average net power during one cycle (one reel-in and one reel-out phase) equals 541 kW. One would then need 19 systems with 38 gliders in total to reach the TU Delft energy needs. The power density of the glider system is calculated to be much lower than wind turbines and also considerably lower than for solar panels on the ground.

## 8.7. Recommendations

The area at which the system is located has multiple villages surrounding it and thus strict noise regulations would naturally apply to the system. In this case, resilient mounting of the generator and converter-side filtering would result in very low noise levels of the generator as a whole (Korsgaard et al. 2019). Noise is investigated further in subsection 9.3.3.

As previously mentioned in chapter 7, decreasing the number of runways from 19 to 1 would greatly reduce the required area needed to  $19,374 \text{ m}^2$  and a power density of  $546.75 \text{ W/m}^2$ . Therefore, having one runway instead of 19 would be greatly beneficial. Possible ways to do this would for example be to transport make the glider take off at the runway with the cable attached to a heavy on-ground transport vehicle. This vehicle would then move to the generator and drum which are already in place and then the cable would be detached and attached on the ground station. While doing all this, the glider will not produce any pulling force for safe transport.

The required 19 systems are for 10 MW nominal power generation. This includes the safety factor of 15% over the 8.75 MW nominal power. Any excess power can be sold directly to third parties on campus.

---

<sup>3</sup><https://fecreate.com/> [cited 17 January 2020]

## Placement and local impacts of the system

It is complicated to place systems, which take up significant portions of land and airspace, in order to minimise their impact yet operate adequately. This chapter delivers a solution found for the system, as well as recommendations for further research and development. First the spacing is addressed in section 9.1, after which the location is given in section 9.2. Derived from this are the impact on both residents and ecology in sections 9.3 and 9.4, respectively. Finally, recommendations regarding the placement of the system are listed in section 9.5.

### 9.1. Spacing of ground stations

Sufficient spacing is needed for safe operations of the system. At the same time, the spacing should be as small as possible for the highest energy yield per area on the ground. Regular wind turbine parks require sufficient spacing for the wake interaction between the turbines. However, as airborne wind energy stations cover a significantly larger airspace, wake interaction effects can be assumed to be negligible (Faggiani et al. 2018). The spacing required between two units is defined by the flight envelope of the units, as described by figure 9.1. It describes the spacing for regular (non-stationary tether) kites, which requires more space than the design used in this project. However, due to cable sag and the two tethers to which the gliders are attached, the same formulation is used for safety.

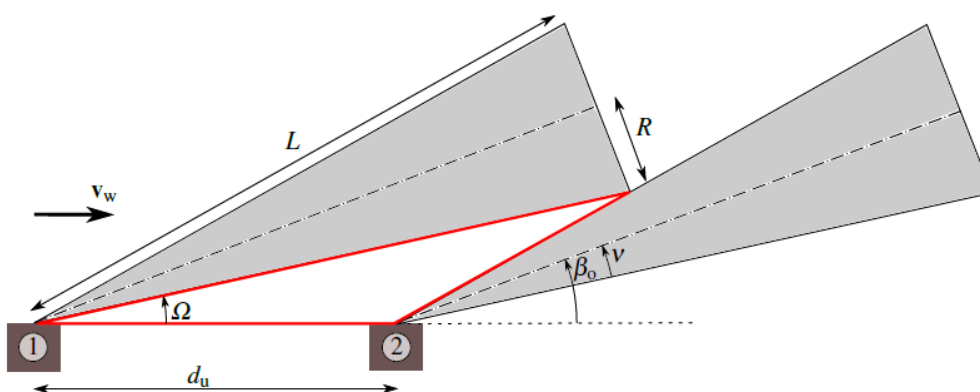


Figure 9.1: Parameters for the spacing between units (Faggiani et al. 2018).

The angle  $\nu$  is variable and dependent on how far the gliders are reeled out from the ground station.  $L$  is the maximum tether length, and is therefore fixed. The distance between the ground stations must be taken to be the maximum for the different  $\nu$ 's. Equation 9.1 determines the minimum spacing between units (Faggiani et al. 2018). For the maximum spacing between units, this means that  $\beta_0 - \nu_1$  and  $\nu_1 + \nu_2$  must be maximised. For a maximum  $\nu_2$ , the second station must be reeled in to its maximum. Similarly,  $\nu_1$  is minimised when the first station is reeled out completely.

$$d_u = \frac{L}{\sin(\beta_0 - \nu_1) \left( \frac{1}{\tan(\beta_0 - \nu_1)} + \frac{1}{\tan(\nu_1 + \nu_2)} \right)} \quad (9.1)$$

Assuming an operation angle ( $\beta_0$ ) of  $40^\circ$ , a maximum operational altitude of 3,000 m, a maximum flight radius of 466 m, and 800 m of tether being reeled in and out,  $v_1 = 3.04^\circ$ . Considering this small angle, it is assumed that  $L$  is equal to the tether length.

Using the computed and mentioned values, the minimum spacing between units is 1,296 m. Wind turbine farms generally operate with a spacing of 7 times the rotor diameter, though it has been found that 15 times the rotor diameter is more economical (Meyers et al. 2012). Considering a rotor diameter of 70 m, this would require a spacing of 490-1,050 m.

The ideal configuration of the ground stations is a hexagon shaped-area, as shown to on the right of figure 9.2. If the farm wishes to expand, or no hexagon-shaped area is available, the configuration can be expanded to an elongated hexagon with minimal decrease in area per ground station.

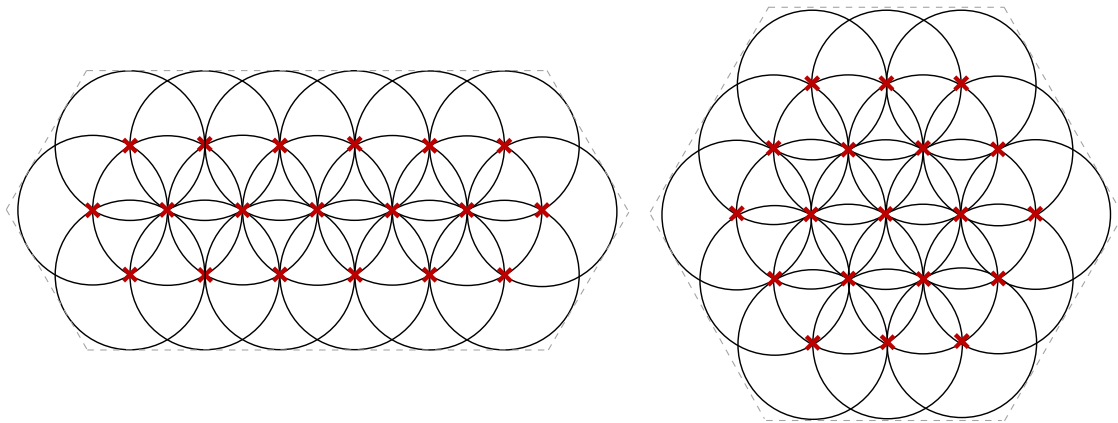


Figure 9.2: Two possible configurations for 19 ground stations (marked with the red crosses): the elongated hexagon (left) and the hexagon (right).

## 9.2. Horizontal positioning of the system

For the horizontal positioning of the system, multiple considerations must be taken into account. First, the system must have sufficient space, therefore population density is taken into account<sup>1</sup>. Then, due to the sustainability requirement of the system, important bird areas are considered (Vreeswijk et al. 2019). Regulations are taken into account by investigating the no-fly zones of the Netherlands<sup>2</sup>. Since operating near Delft is already not a possibility because of those reasons, the high voltage grid and its connection points must be taken into account to minimise losses<sup>3</sup>. Maps of all these considerations are combined and visualised in figure 9.3. As can be seen, most of the south of the Netherlands is not a possibility for the system. Further north, there are fewer high voltage grid connections, as the high voltage grid connections are often located near cities. The best option, as can be deduced from figure 9.3, is the Noordoostpolder in the province of Flevoland. Ideally, the system would be placed as close as possible to the high voltage connection in Ens, south of Emmeloord. Other locations could potentially also be investigated (including the area between Zutphen and Doetinchem, or the area south of Veendam), but this report will focus on the Noordoostpolder, as it appears to be the most promising.

High voltage grid connections are above the ground, so there must be sufficient space between the high voltage station and the tethers; at least one tether length is reasonable. The system has a considerable swept area ( $78.1 \text{ km}^2$ , as calculated in section 9.1), but farming should still be possible underneath the tethers, with safety precautions in place.

<sup>1</sup>[https://www.studioaardrijkskunde.nl/KB1/K02\\_01/3SpreidingbevolkingNL.jpg](https://www.studioaardrijkskunde.nl/KB1/K02_01/3SpreidingbevolkingNL.jpg) [cited 14 January 2020]

<sup>2</sup><https://www.aeret.nl/drone/downloads/Aeret-drone-poster-kaart-verboden-gebieden-kaart.pdf> [cited 14 January 2020]

<sup>3</sup>[https://www.tennet.eu/fileadmin/user\\_upload/Company/Publications/Gridmaps/ENG/Gridmap\\_Netherlands\\_EN\\_2019.pdf](https://www.tennet.eu/fileadmin/user_upload/Company/Publications/Gridmaps/ENG/Gridmap_Netherlands_EN_2019.pdf) [cited 14 January 2020]

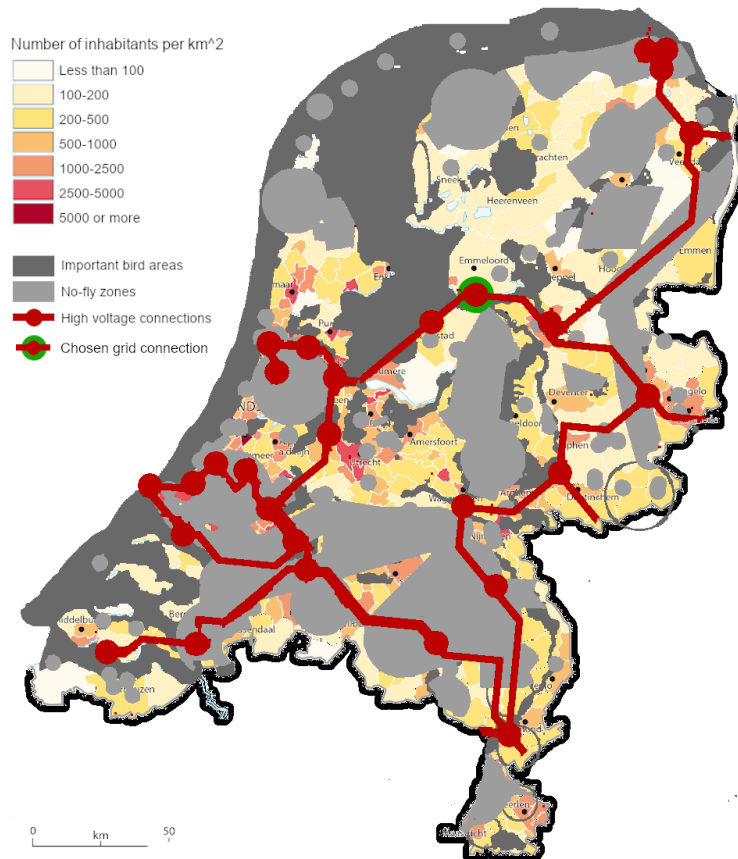


Figure 9.3: Map of the Netherlands considering population density<sup>1</sup>, important bird areas (Vreeswijk et al. 2019), no-fly zones<sup>2</sup>, and high voltage grid connections<sup>3</sup>

Figure 9.5 shows a possible placement for the system, locating it between the villages of Ens and Marknesse. Further justification for this exact area is given in section 9.3. It would fit right between the upcoming routes of Lelystad Airport (Rijksoverheid 2018).

To connect the system to TU Delft, it needs to be connected to the 380 kV connection in Ens (TenneT 2008). A high voltage transformer can be bought of the shelf and have efficiencies of close to 100% (Siemens n.d.). The costs of such a transformer are between 4.5 and 8.8 million euros<sup>4</sup>.

### 9.2.1. Horizontal positioning of factory

For the horizontal positioning of the factory there are a few aspects of importance. First of all, the infrastructure to and from the factory. The factory will require big parts to be imported from all over Europe. That presents the specification of the factory to be well connected to the Dutch infrastructure. Moreover, the factory outputs an entire unit, which is a big and heavy structure. This submits the constraint on the infrastructure between the factory and launch site to be able to accommodate for the transport of the unit.

Secondly, availability of the ground. Flevoland has plenty of area for the positioning of the factory with two big population centres near the launch site, Lelystad and Emmeloord. Thus, finding enough workforce should not pose a complication either.

<sup>4</sup><https://electrical-engineering-portal.com/an-overview-of-large-power-transformer-lpt> [cited 20 January 2020]

### 9.2.2. Horizontal positioning of the maintenance facility

Downtime for maintenance can be a severe cost item of the overall operations. In order to reduce the downtime for maintenance, the maintenance facility should be placed near to the site of operations. Reducing the time of moving the units to and from the maintenance facility would be favorable. Considering the ground space available near the site, the addition of a maintenance facility would only increase job opportunity in the area and not cause any real issues.

## 9.3. Impact of the system on residents

The impact of the system on local residents is also important. As was mentioned in chapter 4, this is taken into account in requirements EHAC-SH-09-01, EHAC-SH-09-02, and EHAC-SH-09-03, which respectively are concerned with regulations regarding light pollution, noise pollution, and visual pollution. Additionally, requirement EHAC-SH-11-07 dictates the system will be safe for humans. However, safety is treated separately, in chapter 10.

### 9.3.1. Light pollution

In the *Midterm Report* (Arblaster et al. 2019b), it was assumed the system would not create any significant light pollution. However, as mentioned at the time, the ecological impact of the system could decrease when the system is clearly visible at night; taking into account that it is not trivial to create a high-visibility structure without simultaneously creating disturbance.

In striking a balance between light pollution, ecological disturbance, and air traffic operations, it appears the current consensus in the wind energy industry is to minimise light pollution as much as possible by using obstruction light control (OLC) technology<sup>5</sup>. This means only turning on obstruction lights when an aircraft is sensed nearby. This trade-off clearly works in favour of residents, while simultaneously not showing a clear advantage nor disadvantage to wildlife.

Because of this, it was decided to design for a low amount of light pollution by also implementing OLC: a ground station monitors nearby air traffic, signaling to the individual gliders when to turn on their navigation lights.

### 9.3.2. Visual pollution impact

Visual pollution caused by wind turbines is strongly linked to people's expectation of the landscape. Notably, a landscape is often experienced as less rural and less scenic when wind turbines are placed (Jensen et al. 2014). This means that the expectations of the people regarding the landscape must be found, to identify to what degree people's experience is affected.

The location for the system proposed here – near the village of Ens in the Noordoostpolder – is known as an agricultural area and is extremely scarcely populated. Of the 455 km<sup>2</sup> of land area that makes up the municipality of Noordoostpolder, 402 km<sup>2</sup> is used for agriculture, while 7.8 km<sup>2</sup> is taken up by residences<sup>6</sup>. As such, interfering with residential areas is not particularly burdensome on the placement of the units.

However, the Noordoostpolder is known for its cultivation of tulips. Figure 9.4 shows a recent overview of tourist attractions in the Noordpolder<sup>7</sup>, notably including the 2019 'tulpenroute' – a scenic route leading visitors along tulip farms. Having the area in which the system will be placed overlap with any of these destinations could be unfortunate for their visitors, but doubly so for the business owners of the area working in the hospitality industry. To minimise this impact, a good area to place the system – while being close to the high-voltage connection near Ens – is the area spanning from Ens to Marknesse, as shown in figure 9.5. An area of the required size can be found which covers but a few tourist attractions, as well as limited coverage of residential areas.

<sup>5</sup><https://www.terma.com/surveillance-mission-systems/wind-farm-solutions/obstruction-light-control/> [cited 13 January 2020]

<sup>6</sup><https://opendata.cbs.nl/statline/#/CBS/nl/dataset/70262ned/table?ts=1579008377710> [cited 14 January 2020]

<sup>7</sup>[https://issuu.com/vvvnnoordoostpolder6/docs/definitieve\\_kaart\\_groot\\_bestand](https://issuu.com/vvvnnoordoostpolder6/docs/definitieve_kaart_groot_bestand) [cited 14 January 2020]

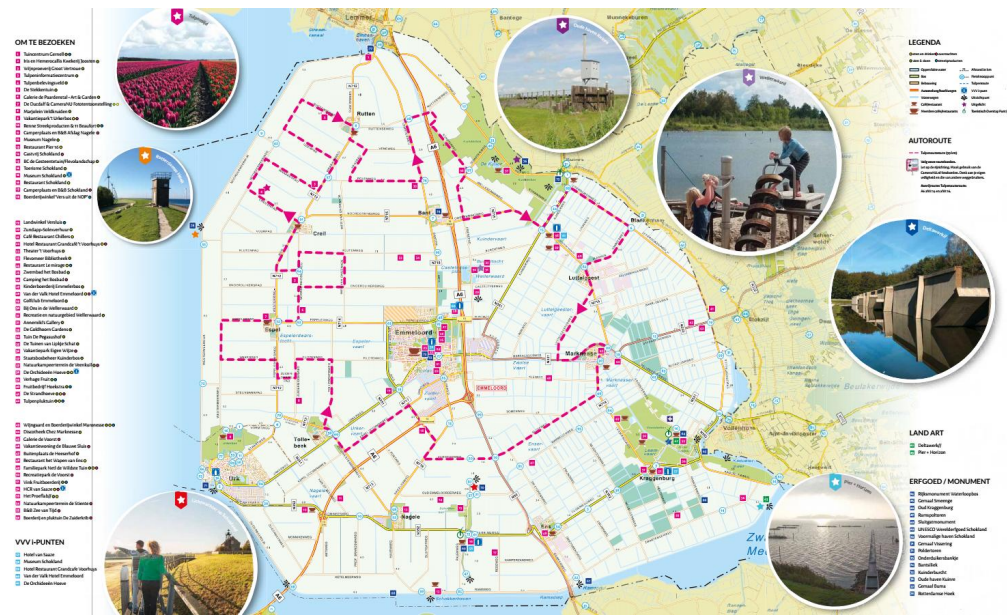


Figure 9.4: A map showing various tourist attractions in the Noordoostpolder<sup>7</sup>

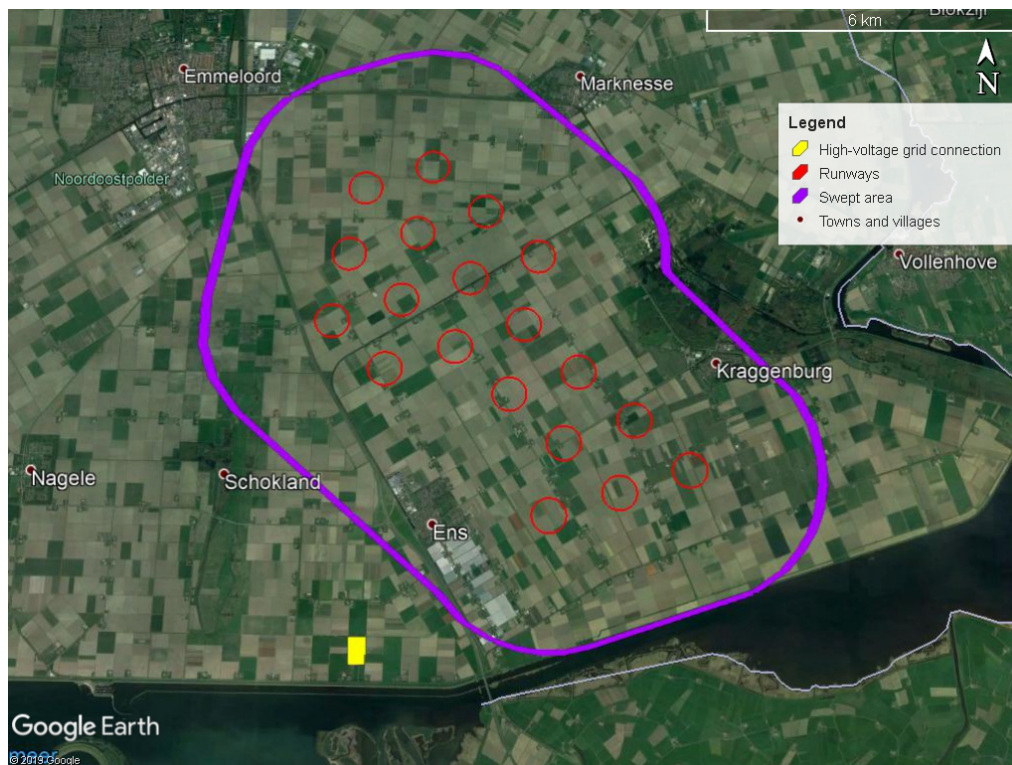


Figure 9.5: A possible location for the system, with 19 individual units – each with its own runway – and a total swept area of 78.1 km<sup>2</sup>. This area is located between several towns and villages in the south-east of the Noordoostpolder. The location of the high-voltage grid connection is also marked.

### 9.3.3. Noise pollution impact

It has been said that gliders used for power generation cause (almost) no noise during operations (Schmehl 2018, p. 485), noting that propellers for on-board power generation to be too small to be impactful. This alone implies AWES have a significant step up compared to conventional wind energy harvesting (European Commission 2011).

For this project, the only noise generation that will be taken into account is the noise the propellers create when used to generate thrust – during take-off and landing, as this is when they use the most power, spin the fastest, and are most audible from the ground. Noise pollution has been called “one of Europe’s biggest health threats”<sup>8</sup> and a growing body of robust research has been developed to analyse, predict, and reduce aircraft noise emissions.

The noise annoyance associated with the glider operations could be predicted. The development of many sound quality metrics<sup>9</sup> can predict how certain aspects of a sound are experienced and how these change with increasing distance from the source. However, the specialisation required for this field is not something that can be explored in-depth within the scope of this project. Of course, this must be investigated during the further development of this project.

Still, without evaluating sound quality metrics for the gliders in great detail, a lot can be said about what regulations these noise levels should adhere to. Dutch regulations regarding wind turbines dictates the day-evening-night level,  $L_{den}$ , shall be below 47 dBA in all noise-sensitive locations. It is clear this is a lenient regulation when compared to neighbouring countries (Nieuwenhuizen 2015).  $L_{den}$  is calculated using equation 9.2 (More 2011).

$$L_{den} = 10 \log_{10} \left[ \frac{1}{24} \left[ 12 (10^{L_d/10}) + 3 (10^{(L_e+5)/10}) + 9 (10^{(L_n+10)/10}) \right] \right] \quad (9.2)$$

In equation 9.2,  $L_d$ ,  $L_e$ , and  $L_n$  are the average A-weighted sound pressure level over an entire year, respectively separated it into day (7:00-19:00), evening (18:00-22:00), and night (22:00-7:00). A-weighted sound takes into account what frequencies humans are sensitive to. To create a very simplistic model, it will be assumed that the average ambient sound is 30 dBA (Gjestland 2008).

Electric aircraft engines are a hot topic right now, but at this time, there have been few experiments regarding their noise on a good level<sup>10</sup>. One study into the noise created by various propeller-driven electric aircraft found that most reference aircraft fall in a range from 50.0 dBA to 70.0 dBA as over-all A-weighted sound pressure level, from a distance at closest approach of about 2.5 km (Pereda Albarrán et al. 2020). Converting these values to those that would be experienced at a distance of 1.0 km (used because, if the runway is at that distance from the nearest residential centre, the distance only increases during a vertical take-off), these values increase by 8.0 dBA using the relation  $20 \log_{10} (R_1 / R_2)$ <sup>10</sup>, arriving at a range of 58.0-78.0 dBA. These numbers can be used to estimate what length of exposure is possible while staying within regulations, which determines the flexibility that facilitates smooth operations.

The average A-weighted sound pressure level required for  $L_{den}$  will be calculated using the above values and equation 9.3.

$$L_{AeqT} = 10 \log_{10} \left[ \frac{1}{T} \left( \sum_{i=1}^n 10^{0.1L_i} \right) \right] \quad (9.3)$$

Here,  $T$  is the averaging time (the length of the period of the day in question) and  $L_i$  is sound level in dBA. Assuming take-offs and landings are spread equally throughout a given 24-hour period, the above

<sup>8</sup><https://www.tudelft.nl/en/2019/lr/postdoc-aircraft-noise-roberto-merino-martinez-wins-clean-sky-academy-award/> [cited 13 January 2020]

<sup>9</sup><https://www.salford.ac.uk/research/sirc/research-groups/acoustics/psychoacoustics/sound-quality-making-products-sound-better/accordion/sound-quality-testing/sound-quality-metrics> [cited 14 January 2019]

<sup>10</sup>Dr.ir. R. Merino-Martínez, private communication, 16 January 2020

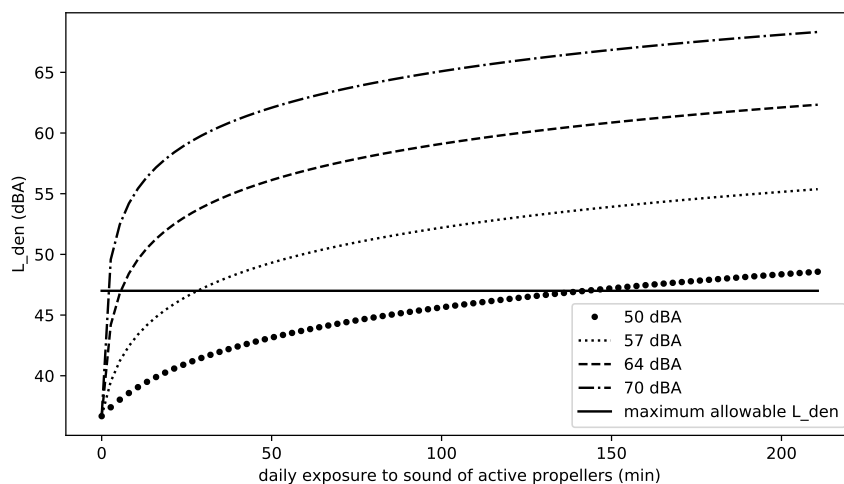


Figure 9.6: A variety of plausible  $L_{den}$  plots, depending on propeller noise

equations give a budget as can be seen in figure 9.6. Assuming a propeller noise of 78 dBA results in an exposure budget of a mere 54 seconds, while 58 dBA results in a budget of around 20 minutes.

From these numbers, it is clear that noise plays an important role in the successful implementation of this system. Its impact interacts closely with the amount of take-offs and landings required on an average day. Assuming a take-off duration of 10 minutes, the most favourable sound estimate means two take-offs can take place from the runways closest to Ens every day (although this does not take into account how the noise fades as the gliders ascend). Given that the gliders should remain airborne unless for scheduled maintenance, this should be sufficient under nominal circumstances.

## 9.4. Impact of the system on ecology

Ecological impact is a broad subject. In the *Midterm Report* (Arblaster et al. 2019b), four impacts on biodiversity were defined according to (Backes et al. 2018):

- **Collision risk:** Birds and bats may collide with some part of the airborne system. Evidence suggests this is heavily linked to how the system is sited with respect to areas important to wildlife.
- **Disturbance and displacement:** Local species are typically displaced by two effects, the first being the human activity related to the construction and operation of the system, while the other is caused by visual, noise, and vibration impacts characteristic to the system.
- **Barrier effect:** Energy farms made up of many systems placed closely together can force birds or mammals to change direction, which becomes a problem during migrations, but also during regular foraging activities.
- **Habitat loss or degradation:** This impact is greatly dependent on the value of a habitat, which is based on how easily it can be replaced – a factor of things such as how rare the habitat is and what role it plays for different species.

Besides the value of biodiversity, these impacts are important to consider in the design process, as Dutch law is particularly strict in the protection of wildlife (Backes et al. 2018). However, the scale of the energy-harvesting system will fall below the threshold of an environmental impact assessment study becoming legally required. In fact, for projects which produce less than 15 MW, whether it could have a significant impact need not even be officially assessed<sup>11</sup> – although it is not unlikely that this system falls outside of

<sup>11</sup><https://wetten.overheid.nl/BWBR0006788/2018-07-01#Bijlage> [cited 15 January 2020]

these regulations and will have to be evaluated independently. Either way, a full environmental impact study regarding biodiversity would be highly beneficial in the precise siting of the system. This report merely dips its toes into this field; such a study is therefore beyond its scope.

As can be seen in figure 9.3, the Noordoostpolder is not an important bird area itself, but the surrounding wetlands are. Directly south of the proposed site, Zwart Meer is located, what 20,000 individuals of various waterbird species call their home during one season or another; this notable includes the Eurasian Spoonbill and Purple Heron, which – although falling within the ‘least concerned’ category of conservation – are threatened on a European level<sup>12</sup>. Following the waterfront to the West, towards the IJsselmeer, the area of Ketelmeer & Vossemeer is found. Every winter, some 20,000-50,000 individuals frequent these lakes, notable including significant congregations of Common Pochard and Tufted Duck, making up over 1% of these species’ global populations<sup>13</sup>.

Further to the east of the system, two more important bird areas are located: De Wieden national park<sup>14</sup>, with the area of Weerribben<sup>15</sup> a bit further north. These are considered to be too far to be directly impacted by the system, but birds leaving or going to these areas could still be affected.

Because of all these nearby areas which contribute to biodiversity, the presence and movement of birds near the system should be carefully taken into account.

#### 9.4.1. Collision risk

In the *Midterm Report* (Arblaster et al. 2019b), it was estimated that – for a tether of 1 km – a stationary tether would claim around eight casualties per year, with bat casualties assumed to be negligibly low. The length of tether beyond 1 km was neglected, as the majority of bird activity takes place below 500 m altitude.

However, it was also noted that the amount of casualties is greatly affected by the bird activity in the area. Given the proximity of the site to important bird areas, it is important that the thousands of birds that pass through those wetlands do not fly through the system’s swept area. This could be prevented in a number of ways, which all boil down to discouraging birds from crossing the swept area of the system; subsection 9.4.3 discusses this further.

#### 9.4.2. Disturbance and displacement

The disturbance and displacement of birds should not affect the important bird areas. Provided the noise limits are met for the residential centres of Ens, Kraggenburg, and Marknesse, they will also be met for Zwart Meer, with the other nearby areas being barely affected. The same holds true for the visual affects of the system, which, under nominal operations, are entirely limited to the swept area of the system.

Another review of the ecological impact of an AWES in a similar setting to this one concluded that the visual and auditory effects of disturbance would be “moderate small” since it’s expected that “local animals will get used to the aircraft in due time” (Schmehl 2018, p. 692). The same conclusion can be drawn here.

#### 9.4.3. Barrier effect

Barrier effect is caused by stimuli that prompt an avoidance response. The disadvantage of this is that the regular flight paths – both for migration and foraging – are disrupted, meaning the affected individuals will have to expend more energy to perform these tasks than they otherwise would.

However, in this case, the barrier effect is desirable: it is preferred that an individual expends more energy – thereby affecting its health and fitness – rather than hitting a tether and its survival being affected that way. This preference stems from the relation between the small area which is affect, compared to the high volume of birds which must be considered; meaning that a lot of birds will have to expend only a bit

<sup>12</sup><http://datazone.birdlife.org/site/factsheet/zwarte-meer-iba-netherlands/details> [cited 15 January 2020]

<sup>13</sup><http://datazone.birdlife.org/site/factsheet/ketelmeer-&-vossemeer-iba-netherlands/details> [cited 15 January 2020]

<sup>14</sup><http://datazone.birdlife.org/site/factsheet/de-wieden-iba-netherlands/details> [cited 15 January 2020]

<sup>15</sup><http://datazone.birdlife.org/site/factsheet/weerribben-iba-netherlands/details> [cited 15 January 2020]

of energy, rather than a lot of birds coming in physical danger. That is to say, the barrier effect limits the total impact on the ecosystem.

In approaching this, research concerned with the ecological impact of power lines can be of interest. A very wide-spread tactic used is applying markers on lines. Markers alone were found to reduce casualties by an average of 74% across 21 studies (values ranging from 55% to 94%) (Bernardino et al. 2018). Based on current knowledge of bird vision, it appears markers using bright colours and high contrasts are most effective (Bernardino et al. 2018). Unfortunately, big markers cannot be applied to the tether, as this would be very detrimental to its aerodynamic performance, but also would prevent the reeling of the tether. Simply marking the tether with bright colours, however, is an option. This can be done by dyeing the fibres of the tether or by changing the composition of its coating.

Another approach that mitigates both collision risk and barrier effects is active habitat management. Imagine birds frequently pass over the area the system's area to go from a feeding area to a roosting site and vice versa. By creating new feeding and roosting areas on one side of the swept area, the amount of crossings could decrease. However, it has been found that this approach is difficult to implement: partially because land use changes are difficult to implement in general, partially because managing bird flight paths in this way has been found hard to achieve, and partially because it may have unforeseen effects on certain species (Bernardino et al. 2018).

#### **9.4.4. Habitat loss and degradation**

The loss of habitat is understood as the destruction of feeding ground by the installation of the system (European Commission 2011). However, this system proposes installing the system on current agricultural land, which in general is not a valuable habitat – especially considering how abundant it is in the region.

### **9.5. Recommendations**

At this stage of the design process, a lot still falls outside of the scope of this project. Several of these elements are important to consider in a next stage, without which the design would be lacking. Several of the shortcomings of the siting of the system and its associated effects are identified here.

#### **9.5.1. Positioning of the system**

With maximising efficiency of the system as the only purpose of the position, the obvious preference would go out to place the system offshore. The most consistent wind speeds are off the coast where, additionally, higher velocities could be achieved. Furthermore, the system would not have to be placed in an already occupied area.

While the system as it is would take up heaps of ground. Once more research into control systems is performed, the unit spacing could be significantly decreased and even, when proven feasible, be placed in crowded sectors. When placed on top of buildings one could consider scaling the system down. Once the system would be proven to be safe and easy to maintain, one could consider placing them on top of tall buildings in urban areas. Allowing for the system to be placed anywhere it is desired. Possibly making it the most versatile wind energy application yet.

Nevertheless, would the system be operating in different countries. A viable option would also be to place it on an elevated area as this would allow for an easier method to achieve preferred altitude in an effortless manner. Resulting in a more efficient take-off, generating more energy per operational cycle.

#### **9.5.2. Impact of the system on residents**

It goes without saying that further development of this project requires analysis of the exact noise characteristics of the takeoff and landing procedures of the gliders. Because the procedure used is still very conceptual, it is likely the precise effects can only be estimated through experimentation. However, basic estimations could already be done to further evaluate the noise annoyance nearby people would experience. The A-weighted sound pressure level used in this report is inadequate, as it does sufficiently account

for annoyance: it is a known phenomenon that the A-weighted sound pressure level from aircraft is experienced as being more annoying than from rail or road traffic (More 2011), meaning using this metric alone would systematically underestimate the impact of the system. As mentioned before, this could be an important influence on the health of the area and should be investigated.

In fact, inadequately accounting for noise emission in the design influences its feasibility. Noise should be investigated further at an early stage, so possible changes to the take-off procedure could be changed, such as switching to some form of ground-powered take-off.

The visual pollution of the system could also be examined further. For example, if the gliders themselves turn out to be experienced as a detrimental element in the landscape, they could be painted blue or a different soothing colour. However, it remains pertinent that the tether is sufficiently visible to birds, so that they might avoid it.

### **9.5.3. Impact of the system on ecology**

Although the system is relatively small and its site might therefore not require an ecological sensitivity assessment, its proximity to important bird areas is striking. In this report, it is estimated that creating a sufficient barrier effect could prevent most of the potential casualties, while otherwise having a limited effect on the well-being of the local species. However, this requires a more expert review, as well as constant monitoring once the system is installed.

One particular gap in knowledge that must be addressed are the nocturnal effects of the system. Both concerning noise and collision risk, the impact of the system on the night life of local ecosystems should be investigated.

## Operations and logistics

In order to explore the application of the system in a real-life environment, one should consider the operation of the system for all scenarios it might face. One method applied to approximate real-life operations is to perform a reliability, availability, maintainability, and safety (RAMS) analysis. In the previous phases of the project, preliminary attempts have been made to analyse the RAMS properties of the system. These aspects have some inter-dependencies, which require a certain order of aspects to be analysed. The availability requires input from both the maintainability and reliability, and the maintainability and safety only require input from the reliability. This informs the ordering of the sections concerning RAMS parameters.

In reality, not all necessities of the system will appear naturally at the desired location. That is where the logistics come in. This chapter is dedicated to the analysis of optimal operational parameters and identify all logistical necessities.

### 10.1. Maintenance plan and replacement of parts

For maintenance, one wishes to decrease the downtime as much as possible without increasing the frequency of unscheduled maintenance. For this reason, as many parts are replaceable as possible. To improve the sustainability of this process, the replaced part will be fixed to be utilised when required by another maintenance cycle.

Naturally, some parts of the system are not replaceable and require for an entire unit to be down for maintenance. This is only applicable to the electric motor and the wing. Both of these items are so critical to the system that their maintenance will result in downtime for an entire unit. The solution is to replace the aircraft requiring maintenance with a stored aircraft. This would minimise the downtime of the system.

### 10.2. Reliability

Firstly, to provide the analyses with the system's failure modes, a fault tree analysis (FTA) can be found in appendix C. The failure modes from the FTA do not supply much more information than what failure modes might cause part failure. Thus, a more thorough method is required to analyse the reliability of the system further. This is where the failure mode, effect, and criticality analysis (FMECA) comes into play. The FMECA can be found in appendix D. Both analyses were applied similarly as suggested in the lecture notes of PM/SE (Hamann et al. 2016).

The reliability is rated as the criticality per item in the FMECA. The criticality per item is acquired from the sum of the criticality numbers of its failure modes. The equation is taken from the lecture notes of PM/SE.

$$C_m = \beta \alpha \lambda_p t \quad (10.1)$$

The criticality for a failure mode is calculated from the failure probability ( $\beta$ ), the failure mode ratio ( $\alpha$ ), failure rate ( $\lambda_p$ ), and operating time ( $t$ ). It can be expressed as in equation 10.1.

With the criticality numbers for each failure mode, the criticality of each item will be obtained with the sum of its individual failure modes. With this knowledge, the more unreliable items can be identified for further analysis. The tether appears to be the most unreliable item within the system with a high criticality number, whereas the landing gear is the most reliable item of the system.

Table 10.1: Maintenance elapsed time factors per item

Maintenance frequency: factors	OBB [h]	EM [h]	Tether [h]	LG [h]	Wing [h]	GC [h]	OBC [h]
Mean time to repair	12	12	2	2	24	2	1
Mean preventive maintenance time	0	2	2	1	6	1	1
Mean time to maintain	1	3	3	2	8	1	1
Mean down time	4	24	4	2	24	2	2

Table 10.2: Maintenance frequency factors

Maintenance frequency: factors	Optimistic (days)	Pessimistic (days)
Mean time between unscheduled maintenance	186	62
Mean time between scheduled maintenance	152	49
Mean time between maintenance	83.6	27.4

### 10.3. Maintainability

Maintainability is investigated in this section by two of its factors, the maintenance elapsed time factor, and the maintenance frequency factor. These factors are all taken from the lecture notes PM/SE (Hamann et al. 2016). The maintenance elapsed time factor is divided in four different factors:

- MTTR: Mean time to repair refers to the time needed to repair or restore the system to its full operational status.
- MPMT: Mean preventive maintenance time refers to the time required to perform preventive maintenance action.
- MTTM: Mean time to maintain refers to the time required to perform both preventive and corrective maintenance action.
- MDT: Mean down time, when besides the active maintenance elapsed times logistic delay times are included, one speaks of the mean down time.

Conventionally, the maintenance elapsed time factors are based on experimental test data. The project is not yet in a test phase of any kind. One could also base the maintainability on test data of similar projects. Unfortunately, there is no test data available of similar cases to this project. For this phase of the project, rough estimates were performed based on engineering sense and previously made assumptions. The different items which were analysed are the on-board battery (OBB), the Electric motor (EM), the tether, the landing gear (LG), the wing, the ground communication (GC), the on-board communications (OBC).

The elapsed times are estimated assuming that, for the most part, the system is minimally affected due to the plan described in section 10.1. The exceptions to this approach are the electric motor and the wing, which would require for the entire system to remain down until repaired fully. Additionally, it is assumed all items can be maintained simultaneously. The second method of quantifying maintainability is done with maintainability frequency factors.

- Mean Time Between Unscheduled Maintenance ( $MTBM_u$ )
- Mean Time Between Scheduled Maintenance ( $MTBM_s$ )
- Mean Time Between Maintenance (MTBM)

$$MBTM = \frac{1}{\frac{1}{MTBM_u} + \frac{1}{MTBM_s}} \quad (10.2)$$

The MBTM is defined as the mean between both the  $MTBM_u$  and the  $MTBM_s$ , which is calculated by equation 10.2. This factor of the maintainability will have the most influence on the system's availability. The estimated values for these factors can be found in table 10.2.

The  $MTBM_s$  would preferably be determined from the optimum maintenance interval. This approach brings down the maintenance cost without losing too much system up-time by return. Moreover, for the

Table 10.3: Availability factors

Availability factors	Optimistic	Pessimistic
Inherent availability	99%	96%
Achieved availability	95%	85%

scheduled maintenance it goes that as little individual systems are taken down as possible in order to achieve the lowest cost. The optimum for maintenance cannot be found without sufficient maintenance data. Currently, the project is not advanced enough to deliver adequate data. Determining the optimum maintenance interval will remain something for the future.

## 10.4. Availability

The availability is the result of the reliability and the maintenance. How availability is determined for this project, is described in this section. To quantify the availability, it is broken down in three factors:

- Inherent Availability ( $A_i$ ): The probability that a system in an ideal support environment will operate satisfactory at any point in time.
- Achieved Availability ( $A_a$ ): A similar probability to the  $A_i$ , in addition, it includes the scheduled maintenance.
- Operational Availability ( $A_o$ ): The probability the system will operate satisfactory when called upon in an actual operational environment, including preventive, corrective maintenance times, and all delay times.

The factors are taken from the lecture notes of PM/SE (Hamann et al. 2016). The operational availability cannot be appropriately quantified as this requires operational data on maintainability, which, for this phase, is inaccessible. The availability of the system is then determined from taking the product of the availability factors of all individual items, which can be found in table 10.3.

$$A_i = \frac{MTBM_u}{MTBM_u \cdot MTTR} \quad (10.3)$$

$$A_a = \frac{MTBM}{MTBM \cdot MTTM} \quad (10.4)$$

The current analysis of availability of the system does not consider any difference between the frequency of failure for a part towards the availability. Not all parts need to be maintained during every maintenance cycle, this assumption makes the availability seem lower than it likely will be.

The most interesting availability factor would be the operational availability, but this can only be derived from operational data on actual performance of the system over time. The system will be analysed for this during its development phase. The operational availability includes also the availability of the generator and the effect of sub-optimal weather conditions on the performance of the system.

## 10.5. Safety

In order to safeguard the security of the people and of the system, the safety of the system must be evaluated. The safety is analysed for failure modes of each item by means of weighing the severity class and multiplying that by the failure rate of each failure mode. The safety risk for each failure mode can be found in the appendix D. The safety risk in the FMECA is followed by the mitigation for the failure mode.

It speaks for itself that the most severe failure modes should be mitigated as well. The first of the most severe failure modes can be prevented by following strict protocol, which would be having no personnel on the landing strip during landing or take-off. The more challenging failure modes to mitigate would be to annihilate the possibility of hostile takeover. The consequences of a malicious takeover could be

catastrophic. Sufficient network protection shall be in place to annihilate any chance of hostile takeover. To reduce the consequences of this takeover, if it would still occur, an additional backdoor overwrite is available at the headquarters. The purpose of the overwrite would be to save human life if necessary.

Furthermore, the system is susceptible to vandalism. The tether, although able to bear loading really well, does not handle out of plane stresses effectively, making a security team a requirement. The sight of the system would preferably be under camera surveillance to support the security team. In case of protests with malignant opinions towards renewable energy, the system's security personnel should be on high alert and employ more personnel in order to ensure safety of the system. In similar sense vandalism can be caused by drones, in order to prevent this a drone no-fly zone will be requested for the area

## 10.6. Effect of RAMS on the design

With the knowledge that the tether is the most likely item to fail during operations, methods had to be thought of to minimise downtime due to maintenance. The method is described in section 10.8. Additionally, the probability of tether failure in the middle of operations demands of the system it can land safely without tether connection. The safety delivered a requirement for the software block diagram, which can be found in section 10.7.4.

## 10.7. Communication systems

In order to control the systems, communication between the gliders, and communication between a glider and the ground station needs to be available. Next to this, for operations, it is required to know the weather conditions in the atmosphere.

As the system allows for a variable harvesting height, an optimal harvesting height can be evaluated when analysing these atmospheric conditions (Bechtle et al. 2019). The optimal locations are where temporally consistent and high wind speeds occur at lowest possible altitudes, to minimise the drag losses of the tether (Bechtle et al. 2019). A model of this optimal harvesting height has to be made in the future, but is not in the scope of this study. Data to make this model can be received from the Royal Netherlands Meteorological Institute (KNMI) as they analyse the atmospheric conditions continuously<sup>1</sup>.

Below, the communication flow diagram and data handling block diagram are depicted, as well as the hardware and software block diagram.

### 10.7.1. Communication flow diagram

The communication flow diagram in figure 10.1 illustrates the flow of data through the system and to and from its environment. The green arrows depict commands given, whilst the red arrows illustrate flows of data.

As can be seen, the KNMI and air traffic control will send relevant data towards the ground station, which will then send commands to the communication subsystems on board of the glider via a transmitter/receiver.

The automatic dependent surveillance-broadcast (ADS-B) is a system in which aircraft continually transmit their identity and GPS- derived navigational information. These transmissions can also be received by other gliders to allow knowledge of nearby traffic. The ADS-B message is a 120 bit transmission that contains the aircraft identification, position, velocity, and status. The message is broadcast with a period that ranges randomly between 0.4 and 0.6 seconds. This randomization function is designed to prevent aircraft from having synchronized transmissions on the same frequency, and thus obscuring each other's transmissions (Francis, Vincent, Noël, et al. 2011).

Navigation lights are added such that the gliders are also visible during night time. Furthermore, a constant signal will be sent to the emergency system, which will activate when the signal is disconnected.

The communication subsystems will send commands to the computer subsystems (of which a second

<sup>1</sup><https://www.knmi.nl/producten-en-diensten/mobiliteit> [cited 13 January 2020]

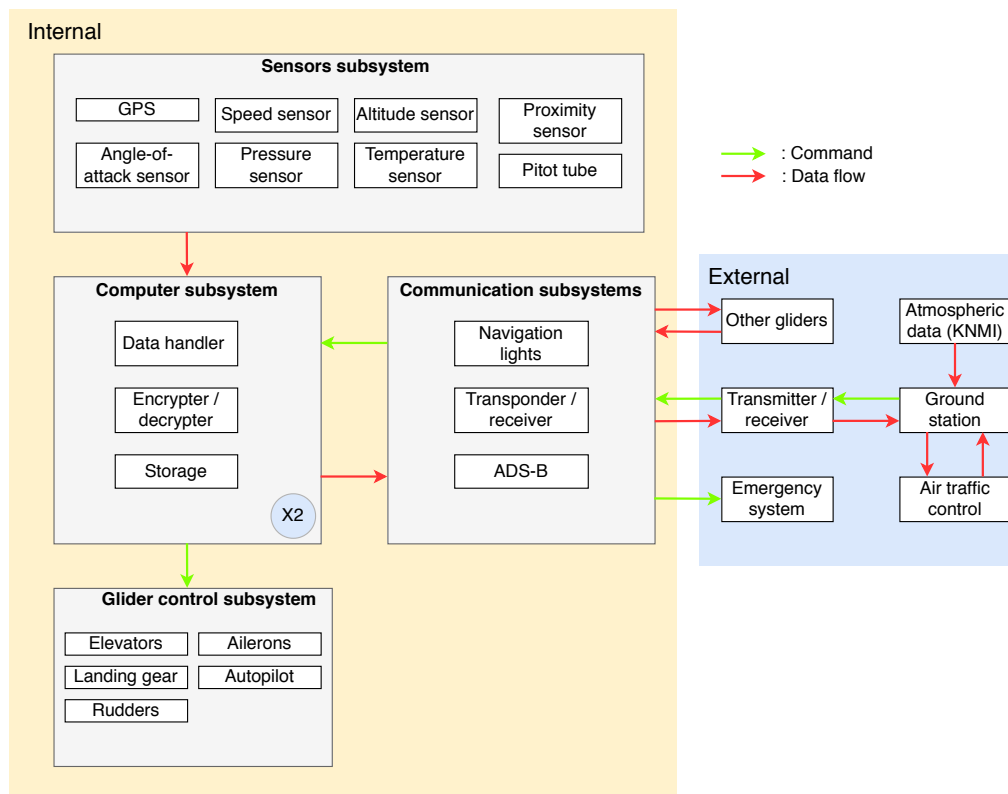


Figure 10.1: Communication flow diagram

one is added in case the first computer fails), which will receive data from the sensor subsystems. To control the glider, the computer subsystems send commands to the glider control subsystems. A back-up computer is added in case the first computer fails.

### 10.7.2. Data handling block diagram

The data handling block diagram shown in figure 10.2 illustrates the components of the data handling of the system. Data flows through the system are depicted by the arrows connecting the subsystems. The thicker arrows denote high-speed data links while low-speed data links suffice for the thinner arrows.

The subsystems are split into six different types: computer, sensor, atmospheric, glider control, electrical power, and communication subsystems. An extra computer is added as a back-up in case the first computer fails. Software for connecting the hardware will have to be made during further research, but is beyond of the scope of this study. A low-power Raspberry Pi 4 would be sufficient for this purpose.

The sensor, atmosphere, and glider control subsystems have got a high-speed data link, because it is important that the aircraft can quickly react to disturbances in the flow. This is especially of importance as both aircraft influence each others motion. Between the data storage and communication subsystems a high-speed data link is placed as well, this is due to the fact that this allows the system to use less energy. If the system would transfer all data at its lowest point in the flight path, less power is needed to transfer data to the surface. In case an anomaly during flight occurs, the warning systems can pick up these signals and warn personnel on the ground.

### 10.7.3. Hardware block diagram

The hardware block diagram as can be seen in figure 10.3, serves to illustrate the components of the system and their mutual relations and interactions. The subsystems are split into six different types: computer, sensor, atmospheric, glider control, electrical power, and communication subsystems. An extra computer

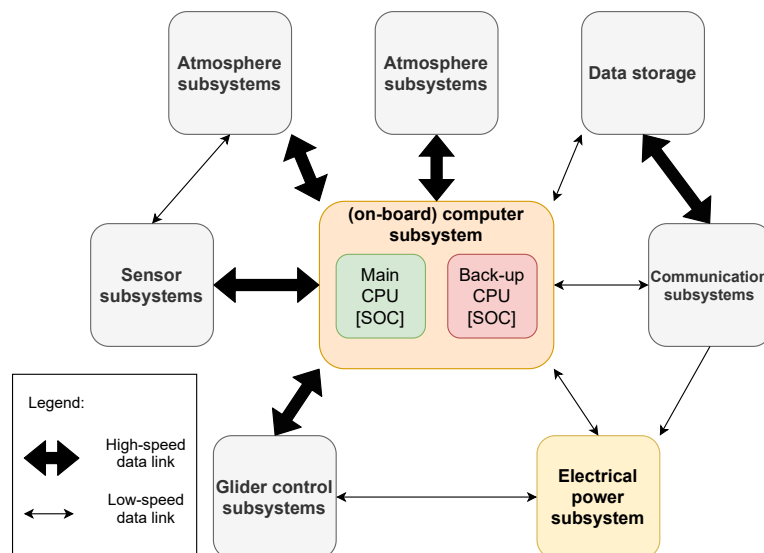


Figure 10.2: Data handling block diagram

is added as a back-up in case the first computer fails.

For the computer subsystem a low-power Raspberry Pi 4 would be sufficient for this purpose, the board uses 15 Watt under full load. The Raspberry Pi 4B consists of a Quad core Cortex-A72 processor, which is a 64-bit system on a chip (SOC) at 1.5 GHz. The SOC comes with 1, 2 or 4GB LPDDR4-3200 RAM. The device has several input/output ports for data handling, e.g. 21 USB 3.0 and 2 USB 2.0 ports. Additionally 40 GPIO header pins are available for sensor read-outs. The device has a Micro-SD card slot for loading the operating system and storing data. The operating system can be a highly reliable version of Linux, an example of an optimized version is the native operating system Raspbian.<sup>2</sup> The operating temperature ranges from 0 to 50°C, but with 15W the processor will most likely produce enough warmth to stay above this temperature. The Raspberry Pi 4B is well-documented, inexpensive at a price of 35 Euros and will remain in production until at least January 2026. The Raspberry Pi 4B is so well-documented that the schematic diagrams, mechanical drawing, and documentation including hardware and configuration are available for free online.<sup>3</sup>

#### 10.7.4. Software block diagram

The software block diagram consists of 4 groups: aircraft, ground station, TU Delft, and storage as shown in figure 10.4. Continuous communication is denoted by solid lines, while optional communication is shown with dashed lines. The aircraft has its status currently monitored, e.g. angle of attack, velocity, heading, altitude, battery power, etcetera. These values are inputs for the autopilot and in case of an emergency the warning & emergency system.

The ground station is also continuously monitored, whereby the information is shown on a screen to the operator via a grid operator interface. In case of an emergency, a warning could be sent out via the warning & emergency system.

TU Delft has energy needs which are constantly monitored, an over- or under capacity can be detected by the system. The power from the aircraft, delivered to the ground station via the tether, is compared with these needs. This allows the flight path to be adjusted in order to generate slightly more or less energy. It's crucial that the connection between these interfaces is secure in order to minimise the possibility of hostile takeover.

Finally, the delivered and required energy is compared and depending on the status of the energy need,

<sup>2</sup><https://www.raspbian.org/> [cited 19 January 2020]

<sup>3</sup><https://www.raspberrypi.org/products/raspberry-pi-4-model-b/specifications/> [19 January 2019]

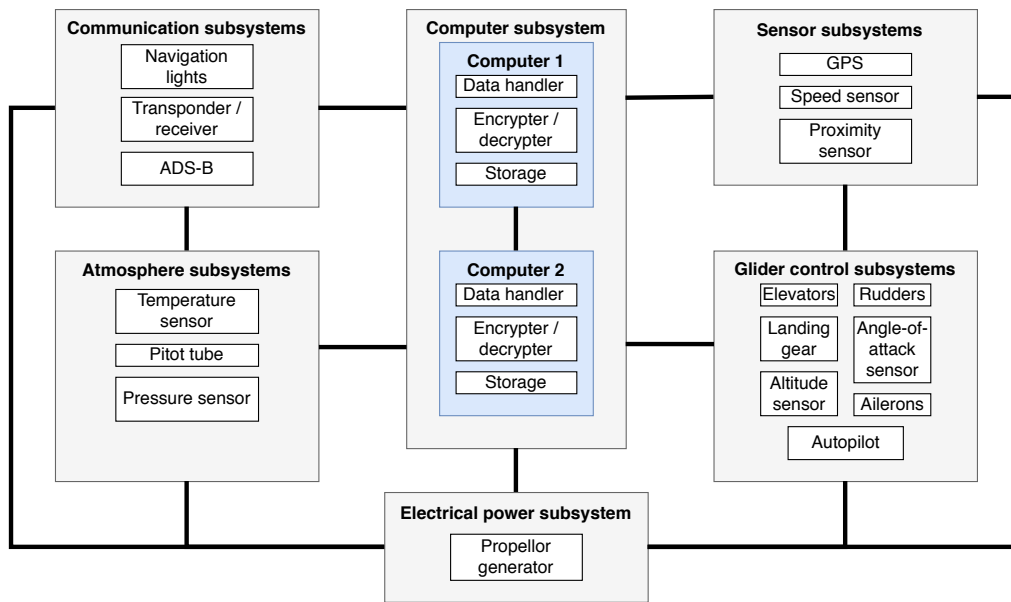


Figure 10.3: The hardware block diagram, where the relations between the hardware are visualised (lines connecting different subsystem blocks represent cabling).

the energy can either be distributed to TU Delft, stored or sold to the grid.

## 10.8. Tether replacement

Due to the high friction and the overall reliability of the tether, the lower part of the tether (which will be reeled in and out in order to generate energy) will need to be replaced regularly. Favourably, only the worn-out part needs replacement, such that costs are reduced. In order to achieve this, a hook mechanism will separate the lower and the remainder of the stationary part of the tether. The replacement procedure goes as follows: first, the worn-out lower tether part is reeled in. Then, a new lower tether part with a hook is connected to the rest of the tether. This lower tether part is connected to a second drum. When the new bottom tether part is connected to the rest of the tether, the system can be reeled out again.

For maintenance it is required to be able to take down the system fully. As the drum is not able to reel in the hook mechanism, it is required to detach the hook. First, the bottom tether part will be reeled in. Then, the hook will be detached and the remainder of the stationary tether part will be connected to a third drum, which will reel in the tether until the y-connection. This drum must have a notch that can accommodate the hook. After that, the gliders will have to land themselves.

## 10.9. Logistics

In order to support the system from cradle to grave, particular aspects of logistics should be explored. The logistics are involved with the take-off and the storage to safely maintain the system during down-time.

### 10.9.1. Take-off

The take-off functional phase is essential for getting the system to its operational phase. The logistical components related to this procedure can be found in figure 10.5. This overview is taken from the logistics flow diagram in the *Midterm Report* (Arblaster et al. 2019b). These functions, combined with the lower level functions from the functional breakdown structure, can also be found in the *Midterm Report* (Arblaster et al. 2019b). The light blocks seen in figure 10.5 are further analysed in this section.

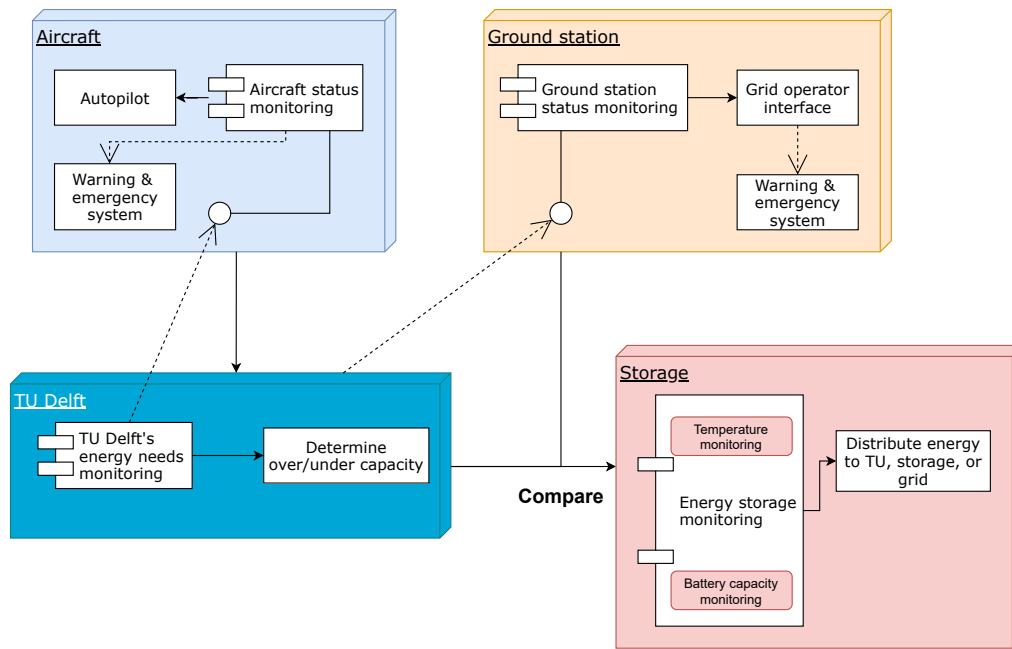


Figure 10.4: The software block diagram, where continuous communication is denoted by solid lines, while optional communication is shown with dashed lines.

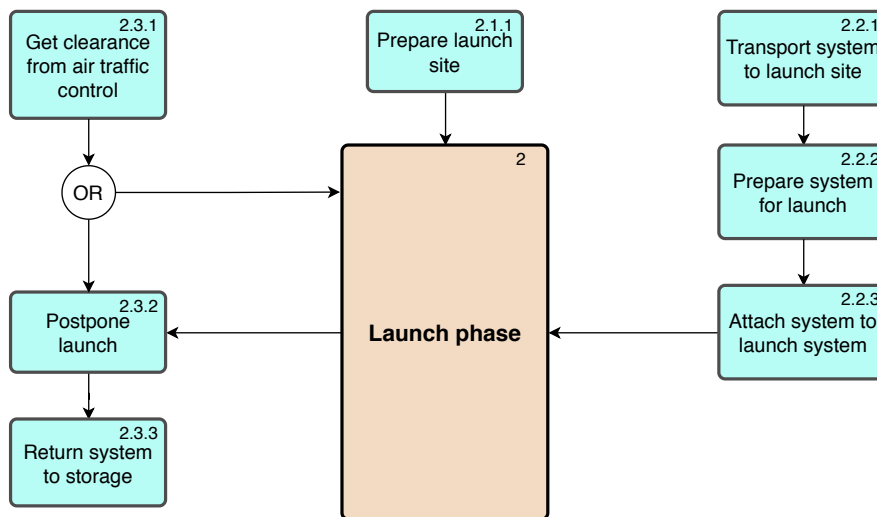


Figure 10.5: Logistical components for take-off

Firstly, block 2.1.1 demands a team to be available at the launch site for the preparation of the launch site. Block 2.2.1 requires a vehicle to transport the aircraft from the storage to the launch site. A carbon neutral vehicle would be the preferred means of transportation. However, when this is not a feasible option, conventional means of transportation will be used. This introduces the requirement for the horizontal positioning between storage and launch site, that the infrastructure in between the storage and launch site suffices for transport of the aircraft. Plenty of space and personnel at the launch site to prepare the aircraft for launch and operational conditions are required by blocks 2.2.2 and 2.2.3. Block 2.2.3 calls for the personnel to be able to also attach the tether. Even though, the operational flight zone will be cleared for the operation of the system, regular contact with air traffic control should be maintained to be aware of the latest developments regarding this airspace. The postponing of the launch does not require much skill of the already available crew or vehicles. The actual storing of the unit following block 2.3.3, however,

would impose a significant cost addition. The extra storage space required could either be rented from nearby airport hangars or back to the storage.

### 10.9.2. Landing

During its operational cycle or during emergencies, the gliders will have to come down periodically. Landing on a circular runway is a very challenging procedure. Therefore, the gliders were designed to land on the ground surface as described in subsection 7.5.3. The gliders can then be transported by a ground based vehicle to be moved to wherever it is required.

Hopefully, a deal can be made with LTO to allow emergency landings on someone's property<sup>4</sup>. The compensation for landowners should not exceed a significant amount.

### 10.9.3. Storage of parts and systems

Planned storage occurs in three phases of the system's lifetime: production, operation, and end-of-life. In addition, there is also unplanned storage. This form of storage can occur at any phase of the system, as errors can occur in any phase of the system's life. The unplanned storage is most influential during its launch and operational phase, because the storage space would have to accommodate for the entire system.

During production, individual parts and assemblies must be stored before use. The factory where the units are assembled must have sufficient storage space for this. Additionally, as two gliders are needed for one unit to operate, two complete gliders must be stored before transport. This same storage should be kept available in case the launch of the unit is postponed.

During operation, it may not be possible to operate the system due to bad weather, maintenance or other reasons. Therefore, the gliders may have to be stored. Maintenance shall be scheduled sequentially to minimise the need for hangar space. During bad weather, or other downtime, the gliders can be stored in the neighbourhood of the generators, as the gliders should be able to withstand weather conditions while stationary. Due to the large spacing between different units, there will be plenty space for the gliders.

Maintenance must also be performed during the operational time of the system. Spare parts must be stored indoors, just like maintenance is to be done inside. As mentioned before, the ground area reserved for the entire system is large enough for a maintenance hangar to be placed. This ground area reserved for the system is a safety measure, but maintenance can be performed within this area with safety regulations in place. In the unlikely event of a system failure, a shelter will be present for safety.

At the end of life, storage must be present before the parts can be reused, recycled, or re-purposed. Parts that will be reused must be stored at the maintenance facility after inspection. Recycled parts will be stored until enough parts have been saved for transport to the recycling facility. Parts that will be re-purposed will be transported to their new destinations.

## 10.10. Energy storage

The energy harvesting system was designed to generate a constant energy output for any given time period. The wind energy farm generates 240 MWh every operating day. In 2018 the highest energy consumption was in December, the consumption was 202 MWh per day<sup>5</sup>. This means every day 38 MWh of energy can be stored, this is equal to 136.8 GJ. Also, this means that when the system has harvested energy for five days it has stored enough energy to be able to provide an extra day of energy.

<sup>4</sup>[https://www.ltonoord.nl/thema/omgeving/schaderegelingen?\\_\\_sw\\_csrfToken\unhbox\voidb@x\bgroup\let\unhbox\voidb@x\setbox\@tempboxa\hbox{v\global\mathchardef\accent@spacefactor\spacefactor}\accent9v\egroup\spacefactor\accent@spacefactoruvBfvccwfFVPsnKiwgTTnM5JGwvQAwg](https://www.ltonoord.nl/thema/omgeving/schaderegelingen?__sw_csrfToken\unhbox\voidb@x\bgroup\let\unhbox\voidb@x\setbox\@tempboxa\hbox{v\global\mathchardef\accent@spacefactor\spacefactor}\accent9v\egroup\spacefactor\accent@spacefactoruvBfvccwfFVPsnKiwgTTnM5JGwvQAwg), cited [24-01-2020]

<sup>5</sup>C.L. Ruts, private conversation, 17 January 2020

There are different possibilities to store the harvested energy. Energy can be stored using an electrical storage method or a thermal storage method. Electrical storage technologies are electrochemical systems (batteries and flow cells), kinetic energy storage (flywheels) and potential energy storage (pumped hydro and compressed air). Thermal storage technologies are based on the sensible and latent heat capacity of materials, they include hot and cold water storage systems, ice storage and phase change materials (Baker 2008b).

First, the electrical storage technologies. The flywheel stores kinetic energy in a rotating drum, conversion to and from electrical energy is done via a motor/generator set. The air friction is minimized by placing the flywheel in a vacuum chamber. This type of storage is mostly used for high-power discharges in a short duration, for example over time periods of several minutes (Baker 2008a). The energy harvested by the gliders needs to be stored for longer periods of time, so this storage technology is not applicable.

Pumped hydro storage uses water reservoirs to store the energy. When the demand is low, the stations use electricity to pump water from the lower reservoir to the upper reservoir. Then, when the demand is high, the water flows out of the upper reservoir and activates turbines to generate electricity for peak hours. This technology needs to be placed in an area with the possibility of different water elevations which makes it a difficult storage solution to apply in large scale in the Netherlands. So, this storage technology is not convenient to use (Ibrahim et al. 2008).

Compressed air energy storage uses large caverns made of high-quality rock deep in the ground, ancient salt mines, or underground natural gas storage caves to compress air in. The air is compressed during off-peak hours using electrical power. Then during peak hours three times the power for the same fuel consumption is produced by expanding the air in a combustion chamber before feeding it into the turbines. Since in this case the energy harvesting system is placed in Flevoland, there will not be any possibilities for underground caverns. Another possibility is small-scale compressed air energy storage in cylinders. However, this will only have an efficiency of 50% (Ibrahim et al. 2008). Thus, compressed air energy storage will not be applicable.

Flow cells consist of two electrolyte reservoirs from which the electrolytes are circulated through an electrochemical cell comprising a cathode, an anode and a membrane separator. An advantage of flow cells is that self-discharge is mitigated by the isolated storage of the electrolyte in the charged state. However, they can only reach efficiencies of 75-85%, which does not come close to batteries (Hall et al. 2008).

Lithium ion batteries have proven to be the most efficient type of battery, reaching an efficiency of almost 100%. The cathode in these batteries is a lithiated metal oxide and the anode is made of graphitic carbon with a layer structure. The electrolyte consists of lithium salts dissolved in organic carbonates. When charging the battery, the lithium atoms in the cathode become ions and migrate through the electrolyte towards the carbon anode where they combine with external electrons and are deposited between carbon layers as lithium atoms. An overview is given in figure 10.6<sup>6</sup>. During discharge this process is reversed. The batteries can store 90-190 Wh/kg and have a self-discharge of approximately 1% per month (Divya et al. 2009).

Next, the thermal storage technologies are taken into account. These technologies are based on either sensible heat or latent heat. Sensible heat is effected by raising the temperature of the storage medium, therefore it desirable for the storage medium to have a high specific heat capacity. This technology can be applied to liquid media, like water, petroleum based oils or molten salts, or solid media, like rocks or metals. Latent heat storage relies on the phase transition temperature of phase change materials, like salt hydrates, metals and alloys or organic compounds like paraffin. Latent heat storage requires a much smaller weight and volume of material to store a certain amount of energy (Hasnaina 1998). Thus, sensible heat storage will not be applied and only latent heat storage will be further investigated.

<sup>6</sup><https://letstalkscience.ca/educational-resources/stem-in-context/how-does-a-lithium-ion-battery-work> [cited 22 January 2020]

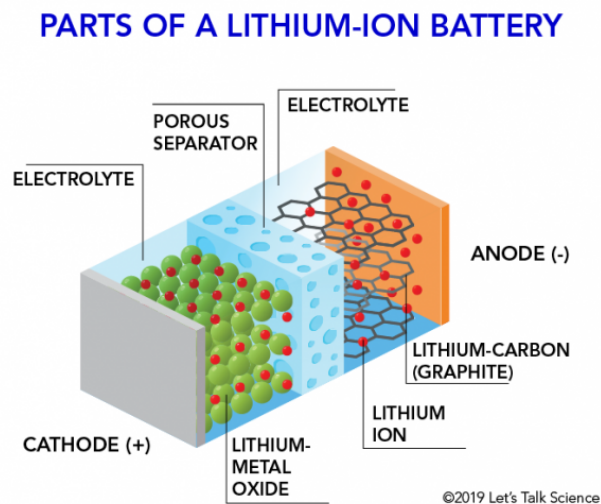


Figure 10.6: Overview lithium ion battery

Latent heat thermal energy storage systems include a heat storage substance that undergoes a phase transition, a container for holding the storage substance, and a heat exchanging surface for transferring heat from the heat source to the phase changing material and from the latter to the heat sink. Latent heat energy storage materials are able to store more kilo Joules per kilogram than batteries. However, due to the high transition temperatures of the materials, this storage method will not be more efficient than using electrical energy storage in the form of a battery (Hasnaina 1998).

So, in conclusion, the lithium ion batteries will be used to store the energy generated by the glider system. These batteries have proven to perform best in this application (Ibrahim et al. 2008). These batteries are able to store up to 190 Wh/kg and they cost between €700 and €1000 per kWh (Divya et al. 2009). Considering the 38 MWh energy that can be stored every day, this would require 200,000 kg of battery mass and a cost of approximately €32 million for each day's worth of energy that must be stored.

For this reason, it was decided to directly deliver the energy to the grid and 'store' it there instead of using an independent storage facility at TU Delft. Since more energy is harvested than consumed, a surplus is created in the grid, this accounts for possible peak demands at TU Delft. It will not be necessary to buy extra energy from the grid. The amount of energy delivered to the grid will be measured at the harvesting site, and the consumed amount will be measured at TU Delft. This will make sure no more energy is consumed than generated.

There will however be a small battery located at the harvesting site to provide energy in case of a blackout. This battery will contain enough energy to keep the harvesting site running and communicate to the gliders that they need to make an emergency landing. The communication system requires 75 W per glider (Francis, Vincent, Noel, et al. 2011) so this is 2,850 W for all gliders. Most likely a blackout will be solved within a couple of hours, however, to be safe, enough energy for 24 hours will be stored in the battery. This will be 68.4 kWh for the communication, and the energy for one household will be added to run the harvesting site which is 11.3 kWh<sup>7</sup>. So the total amount of energy is 79.7 kWh, which will require a battery of 12,996 kg.

## 10.11. Electrical block diagram

In figure 10.7 one can see the electrical block diagram, which gives an overview of all the electrical components in the system and the interaction between these components. Two transformers can be seen in the

<sup>7</sup><https://longreads.cbs.nl/trends18-eng/economy/figures/energy/> [cited 16 January 2020]

ground station which includes one for changing voltage to that of the grid and one for changing voltage which would be compatible for the battery.

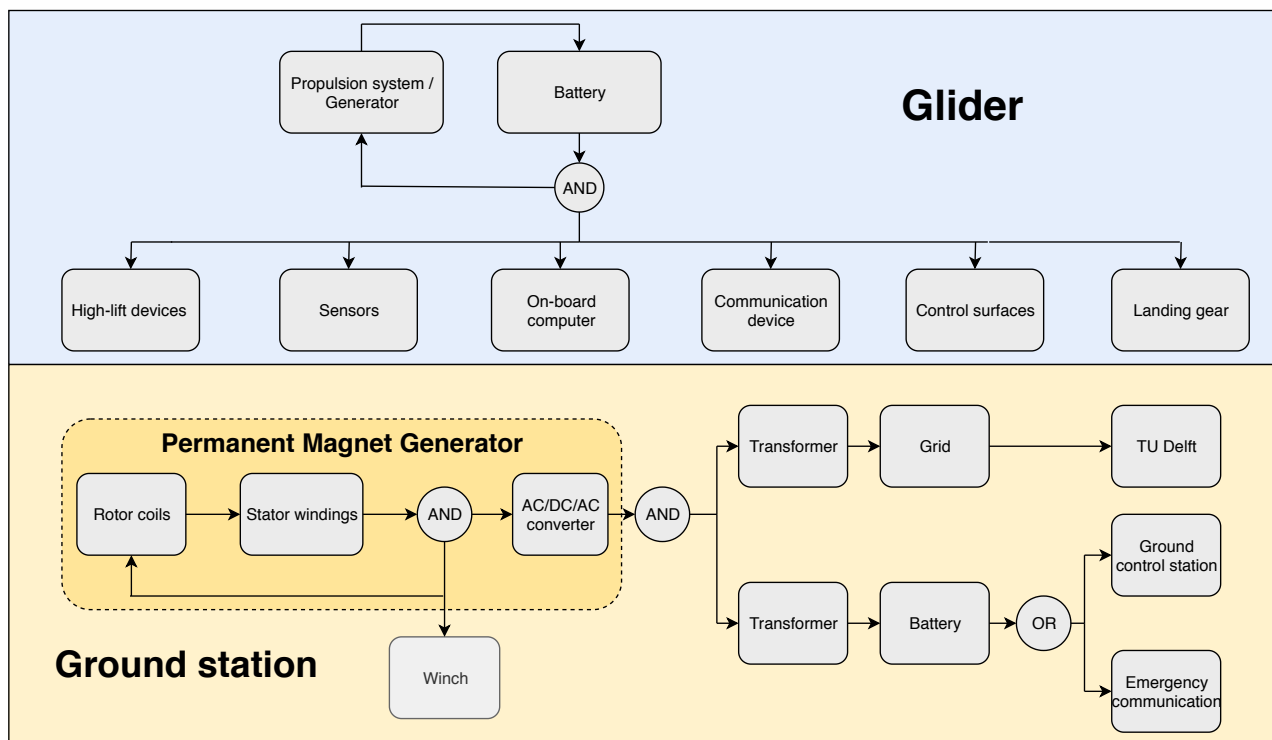


Figure 10.7: Electrical block diagram

## 10.12. Scalability of the system

The system has huge scalability potentials. It consists of many single units. The units could be further developed to accommodate multiple duos of gliders to increase the power output per unit. With improved knowledge of the control of tethered duos of aircraft one could significantly reduce the spacing in between each unit, which in turn would greatly increase the efficiency per ground space.

In addition, the system exists of independent units, which can be added to scale up the system as much as desired. With enough ground space the system can be scaled to provide any power requirement.

## 10.13. Logistics flow diagram

Similarly to the functional flow diagram, the logistics flow diagram is to generate a bigger overview of the entire process concerning the logistics. The logistics flow diagram can be found in appendix E. In this diagram all phases of the lifetime are represented.

## 10.14. Verification

When other instances would share their reliability data, the found data of future research could be verified with other airborne wind energy systems. The same goes for the maintainability and availability of such systems.

## 10.15. Conclusions

Concluding, the operations of the system will prove a challenge. For maintenance, the glider does not consist of too many separate parts. Communications and data handling plans are made and show no difficulty or hard-to-achieve systems. The spacing of ground stations is quite big, however the ground

between them is not occupied, so can still be used. The generated energy can be stored in different ways, but with efficiencies taken into account, lithium-ion batteries are most convenient. Most power will be put in the grid, not stored. Due to the number of devices, scaling is easily done and the system can be scaled to meet virtually any power requirement. The future looks bright for the scalability of the system with a higher power density.

### **10.16. Recommendations**

For further research on similar topics it would be beneficial to partner with an instance which is willing to provide data on the reliability, maintainability, and availability of airborne wind energy systems. This would allow for a verification method of achieved RAMS parameters or when no testing has been done, to assume RAMS properties of similar airborne wind energy systems as applicable to the current system for further development of the project. Furthermore, a model for the optimal harvesting height has to be made, to find the optimal location where temporally consistent and high wind speeds occur, at the lowest possible altitude.

## Production plan

This chapter discusses the production of the final design. The production plan includes the manufacturing, assembly, and integration plan (MAI plan). The MAI plan gives a time ordered outline of the activities required to construct the product from its constituent parts (Garcia 2019).

Figure 11.1 shows the production plan of the final design. In order to make the final assembly, sub-assemblies need to be produced. Some of those sub-assemblies can not be made straight from the parts, but will require a sub-sub-assembly step. In the design, there is the possibility to manufacture or buy parts. An overview of those parts can be seen in table 11.1.

The assembly process of the design is the main part of the production plan, therefore an outline of the assembly process is drawn into the production plan in figure 11.1. The red, horizontal, arrow represents the main assembly line. Sub-assembly lines are added to the main assembly line at specific moments, some can be one simultaneously.

During the manufacturing and assembly process, the lean manufacturing concept will be used in order to reduce the waste during the process. Lean manufacturing is not a method that can be implemented, it is a philosophy, where lean thinking is a dynamic, and knowledge-driven process, through which all people continuously eliminate waste with the goal of creating value (Sinke 2014). One of the waste items is the transportation of parts and systems. To reduce the transportation waste, it is important to produce the systems as close to the operation site as possible.

As the skin material is expected to create the most waste, but the glass-fibre reinforced composite cannot be recycled, it is important to minimise the amount of material that is not used for the production to reduce the environmental footprint during the production. Furthermore, the energy that is required for the production of the systems, will be compensated by the renewable energy harvested by the systems when in operation.

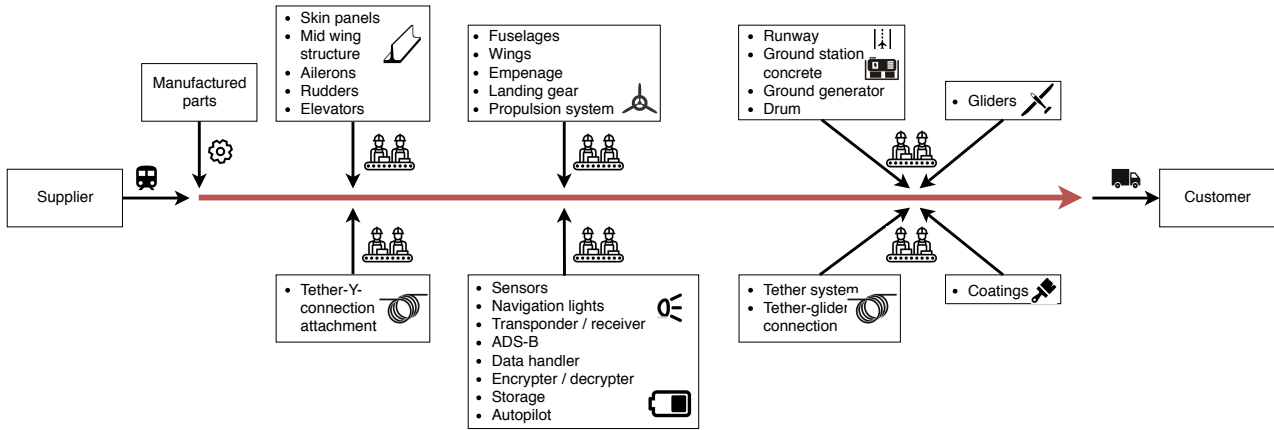


Figure 11.1: Production plan

Table 11.1: Overview of parts and sub-assemblies that are either bought from suppliers or self-manufactured.

Buy		Manufacture
Ground station concrete	Drum	Frames
Generator	Tether	Spars
Y-connection	Tether-glider connection	Skin
Coating	Sensors (8x)	Rivets
Navigation lights	Transponder / receiver	Bolts
ADS-B	Propellor	Ribs
Propellor generator	Data handler	Stringers
Encrypter / decrypter	Storage	
Landing gear	Autopilot	

## Life-cycle assessment

Life-cycle assessment (LCA) is a method used to predict the complete environmental impact a product has throughout (a section of) its lifespan. Here, it will be used to analyse how environmentally sustainable an airborne wind energy system is, in particular to see if it is a reasonable alternative to traditional wind turbines. Requirement EHAC-SH-11-09 states that the energy farm shall have a lower environmental footprint than ground-based renewable energy farms of comparable cost.

Where in other places of the report, the airborne wind energy system is commonly referred to as “the system”, it will be called “the product” in this chapter to avoid confusion.

The first steps in any LCA are to define the goal and scope of the assessment. This was completed in the *Midterm Report* (Arblaster et al. 2019b). One significant change in approach since the Midterm Report is that the EU-guided Product Environmental Footprint will not be utilised, due to a lack of useful data on the matter, given the time constraints of the project. Instead, the only factor which will be analysed at this stage is the global warming potential over a 100 year perspective (GWP100a or simply GWP) of the product – adjusted to the power it produces. To meet requirement EHAC-SH-11-09, the farm must outperform convention wind farms. Additional consideration with respect to the approach are discussed in section 12.1.

### 12.1. System boundary

To result in the full cradle-to-grave EF of the product, the assessment should include all activities associated with its production, use, and disposal. However, due to the constrictive time frame of this project – as well as technical limitations relating to the availability of LCA software and databases – it is not realistic to investigate every component from extraction as raw material onward or to account for the exhaust of employees’ cars anytime they go to inspect a unit. In fact, these restrictions resulted in the most realistic approach being to firmly rely on prior analyses of complete products, rather than individual process streams.

Therefore, a rough estimate of the complete life-cycle will be created by focusing on large-scale flows, based on published LCAs of reference cases. These large-scale flows include: the ground stations (including generator and foundation), the cabling between ground stations, the runways, the tethers, and the gliders. For each of these, the model will focus consider its production (including that of replacement parts). The end-of-life of the product was also considered to be noteworthy – it was previously discussed in chapter 11 – and its impact on the LCA is therefore also briefly discussed in section 12.4.

### 12.2. Resource use and emissions profile

The most time-consuming effort in an LCA is constructing a resource use and emissions profile. As mentioned in section 12.1, this will focus on the manufacturing of the main elements of the product. Because the aerospace materials used for this product were not found in free-use databases, the data used here is based on reference cases, collected and generalised as seen in table 12.1.

The choice was made to scale the reference data according to a variety of factors, depending on what was considered to be suitable for a fair comparison. For the cabling required, the GWP was first normalised to the power generated in the reference, after which the distance of cable assumed in the reference was accounted for. Note that the energy farm is located 50 km away from the grid in the reference, compared to 3.5 km for this project, according to chapter 9. The ground station and glider were scaled in similar

Table 12.1: The global warming potential of each of the five main components considered

	Base GWP [unit]	Scalable value [unit]	Reference
<b>Cabling</b>	1.02 [gCO <sub>2</sub> -eq/kWh]	$4.77 \cdot 10^5$ [kgCO <sub>2</sub> -eq/km]	Schmehl 2018, p. 738-741
<b>Ground station</b>	1.41 [gCO <sub>2</sub> -eq/kWh]	1.36 [kgCO <sub>2</sub> -eq/kW]	Schmehl 2018, p. 738-741
<b>Glider</b>	0.21 [gCO <sub>2</sub> -eq/kWh]	0.14 [kgCO <sub>2</sub> -eq/kg]	Schmehl 2018, p. 738-741
<b>Tether</b>	14.4 [kgCO <sub>2</sub> -eq/kg]	14.4 [kgCO <sub>2</sub> -eq/kg]	DSM Dyneema 2013
<b>Runway</b>	$2.2 \cdot 10^5$ [kgCO <sub>2</sub> -eq/km]	$2.2 \cdot 10^5$ [kgCO <sub>2</sub> -eq/km]	Milachowski et al. 2011

ways. However, the GWP of the ground station is assumed to scale according to the amount of power being produced, while the GWP of the glider is assumed the scale with its weight. These relations are all assumed to be linear. The road used as runway is already expressed as a function of its distance (Milachowski et al. 2011), meaning this number does not need to be scaled, given that the reference road has a representative width. The same goes for the tether material – Dyneema, the GWP of which is provided per 1 kg of rope (DSM Dyneema 2013).

Having obtained the values of table 12.1, the flows are evaluated using the dimensions:

- a total length of cabling of 27 km (using the layout shown in figure 9.5);
- a total of 19 units;
- each unit producing an average of 635 kW;
- two gliders per unit, each with a mass of 3,333 kg;
- each unit having a total tether mass of 2,291 kg;
- each unit having a runway with a circumference of 1.88 km.

These values for a road use the GWP for an average road constructed in Germany. As discussed in subsection 7.5.3, the gliders are able to comfortably take-off and land on a variety of unprepared surfaces, meaning that even an average road is likely too extreme of a measure. However, as it is expected that the construction relating to launch and landing has a heavy impact on the overall LCA (Schmehl 2018, p. 741), this value is used for now.

For the LCA of the maintenance of the system, only the replacement of parts is considered. The maintenance of the runway is not taken into account, as studies on this subject generally do not analyse this, except when combining it with the LCA of the regular traffic, making a comparison to this case unrealistic. In the replacement of parts, only the lifespan of the tether (7 weeks as examined in section 6.5) will be considered to be critical. As with the runway, it is assumed the cabling will not need replacement and that the small repairs the gliders and ground stations will need is small enough to be negligible. For the purpose of this analysis, it is assumed the energy farm operates for 20 years before being decommissioned. This is in line with other LCAs (Schmehl 2018, p. 739).

### 12.3. Impact assessment

With all relevant numbers being collected in section 12.2, the impact of the product can be assessed. Using basic addition and multiplication, a total lifetime GWP of  $2.56 \cdot 10^8$  kgCO<sub>2</sub>-eq is obtained. Assuming a constant production of energy of 635 kW per unit over 20 years, this results in 121 gCO<sub>2</sub>-eq/kWh. The distribution across elements is shown in figure 12.1.

As can be seen, the total LCA is dominated by two things: the construction of the runway, as well as the regular replacement of the tether. It is worth noting that both of these effects are highly speculative. As mentioned in 6.3, studies on the lifetime of reeled tethers for AWES vary by orders of magnitude, making it unclear what values would be representative of the actual design. Compared to lifetimes of several year (Schmehl 2018), a lifetime of seven weeks is extremely conservative. Looking at the runway construction, this contribution to the LCA is unacceptable – maybe this would be different if they could be used for other purposes, but as it stands, they are solely use for energy generation, making their construction under these values counterproductive.

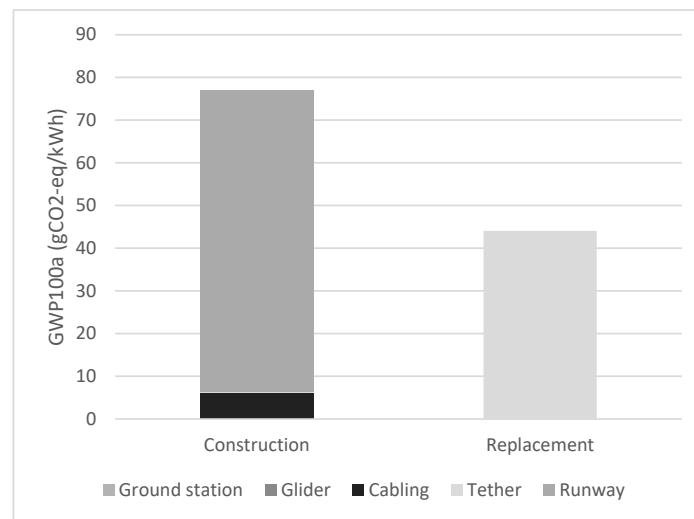


Figure 12.1: GWP of the energy farm over 20 years

Reassessing the LCA of the product, the lifetime of the tether is increased to half a year. The construction of the road is reduced in accordance with the weight of the glider compared to the weight of a fully-loaded – a factor of 10. This change results in a total GWP of 25.4 gCO<sub>2</sub>-eq/kWh, as shown in figure 12.2. Comparing this value to the reference case – 5.611 gCO<sub>2</sub>-eq/kWh – this number seems a lot more realistic than the initial estimate of 121 gCO<sub>2</sub>-eq/kWh, although it still deviates with a factor of ±4. This does not suggest that the GWP of the product is in fact this low, but rather reaffirms that a lot of further investigation must be done on the durability of the tether, in particular.

## 12.4. End-of-life

The end-of-life of the system has already been treated elsewhere, but it is worthwhile to discuss what its implications are for the LCA of the system. With the exception of certain subsystems of the glider with a long lifespan, very little elements can be reused at all. Recycling also becomes an issue for the most part, as the composite fibres used are more suited for energy recovery than recycling (DSM Dyneema 2013). Luckily though, a lot of metals are also used – both in the ground station, as the cabling, as (to some extent) in the glider. Metals are often salvageable to be revitalised in another form.

## 12.5. Conclusion

Analysing the LCA of the airborne wind energy farm, an initial estimate revealed a GWP of 121 gCO<sub>2</sub>-eq/kWh. By adjusting the tether durability to more closely resemble values found in literature, as well as assuming savings could be made on the runway, a GWP of 25.4 gCO<sub>2</sub>-eq/kWh was achieved. This is still considerably higher than the value found in literature of 5.611 gCO<sub>2</sub>-eq/kWh. This can be accounted for in two ways: (1) the LCA in the reference assumes a novel launch and landing system which does not require a paved runway; (2) the glider in the reference is lighter than the one designed in this report, while also generating considerably more energy.

It was established that the farm must outperform convention wind farms, which have been found to have a GWP of 5–45 gCO<sub>2</sub>-eq/kWh – conventionally established as 20.85 gCO<sub>2</sub>-eq/kWh for onshore wind farms (Schmehl 2018, p. 746). Taking all this into consideration, it seems likely that an AWES as was designed in this report could be constructed in a more sustainable way than a conventional wind farm on

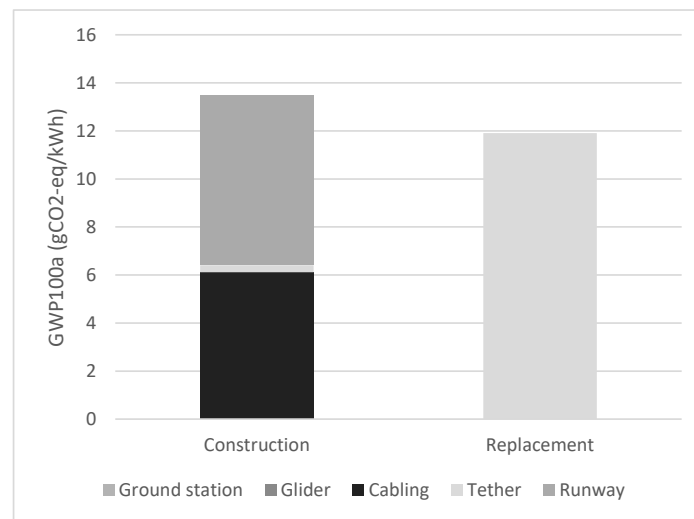


Figure 12.2: GWP of the energy farm over 20 years with adjusted values

the same (onshore) location. However, requirement EHAC-SH-11-09 is stated as a function of cost. Using the numbers found in chapter 13, the cost of energy from this farm comes out at \$0.063/kWh, which is slightly more than the global weighted average price for onshore wind, which is \$0.057/kWh. This means the current design is not on track to meet requirement EHAC-SH-11-09. However, these numbers are certainly promising. Further investigation and a more detailed design could improve this aspect of the performance of the energy farm, especially given the optimistic numbers found in literature.

## 12.6. Recommendations

This chapter gave a very rough estimation of the GWP of an airborne wind energy farm. First of all, it is not desirable to evaluate the environmental impact of a product on global warming potential alone (European Commission 2013): other impact factors should also be considered in future research.

In the analysis performed in this chapter, a lot of known elements of the product were not incorporated. The hydrophobic coating used on the tether, for example, or the materials used within the wing structure. Judging by the results, it seems highly unlikely that these would have had a significant impact on the GWP of the product, but it surely warrants further investigation. Similarly, the maintenance and end-of-life of the product could already be analysed at this stage in the design, given the right LCA tools.

It is unclear whether the GWP of the product would be positively influenced if all of these factors are incorporated. However, one area that would lead to improvement is the use of more sustainable construction materials/methods for the runway and ground station. Recent developments were already brought up in subsection 8.3, but were not implemented here.

This chapter discusses the cost analysis of the system. It contains all cost elements of the post-DSE project activities. Section 13.1 gives an overview of the breakdown of all cost. In section 13.2 a budget is depicted and the return of investment is calculated.

### 13.1. Cost breakdown structure

The costs associated with the project were divided in two main categories: direct costs and indirect costs. Direct costs are all costs related to the production of the product itself, while the indirect costs come with the organisation around the product. Within those two categories, sub-categories were defined as shown in table 13.1. The cost items for each sub-category can be seen in the cost breakdown structure in appendix F.

Each of the sub-categories may have an investment cost and a yearly cost associated with it. For example, the software licenses within the development category have an acquisition cost and a yearly fee as well. The most notable costs will be explained in further detail in section 13.2.

Table 13.1: The sub-categories of direct and indirect costs.

Direct costs	Indirect costs
Start up costs	Grid connection
Subsystems	Salaries
Manufacturing	Insurances
Operations	Energy use
Maintenance	Rent
Infrastructure	
Sales & marketing	
Development	

### 13.2. Operational profit and return of investment

A number of values were taken from wind turbine cost breakdowns (Beurskens et al. 2018). These costs are published in euro's per kW or per kWh, so those costs assume that the values are similar for land based wind turbines. For foundations and installation, a total value of 1,150 €/kW is reported, but this also includes infrastructure, connection to the grid and insurances. For 10 MW of power, that means €11,500,000. The grid connection has a cost of €3,000,000<sup>1</sup>, and it is assumed that the infrastructure and insurances take 35% of the remainder. This leaves €5,545,000 for foundations and installation. Furthermore, as stated in section 9.2 the high voltage transformer can be bought for approximately €5,000,000, and thus the total cost for connection tariff is €8,000,000.

Yearly costs for insurances and maintenance of infrastructure are estimated to be 12.3 €/kW. It is assumed that insurances will be 60% of the cost, at €73,800 per year. Similarly, rental of the farmland is said to cost 0.0029 €/kWh per year, so for 70,000 MWh this comes to around €200,000 per year. This assumes

<sup>1</sup><https://www.tennet.eu/electricity-market/connecting-to-the-dutch-high-voltage-grid/costs-of-a-grid-connection/> [cited 17 January 2020]

Cost analysis					
1. Direct cost			2. Indirect cost		
1.1 Startup cost		Yearly cost	Investment cost	2.1 Connection to grid	
1.1.1 Foundations & installation			€ 5'525'000.00	2.1.1 Connection tariff (incl. transformer)	
1.1.2 Commissioning & qualification			€ 3'000'000.00	2.1.2 Periodical connection charge	
1.1.3 Patent			€ 10'000.00	2.1.3 Transmission tariff	
1.2 Subsystems			2.2 Salaries		
1.2.1 Glider			€ 19'000'000.00	2.2.1 Manufacturers	
1.2.2 Tether			€ 51'243.00	2.2.2 Operators	
1.2.3 Generator			€ 5'344'782.61	2.2.3 Maintainers	
1.2.4 Drum			€ 950'000.00	2.2.4 Installers	
1.2.5 Propulsion			€ 743'478.26	2.2.5 Legal	
1.2.6 Coating			€ 33'750.00	2.2.6 Sales&marketing	
1.3 Manufacturing			2.2.7 Management		
1.3.1 Quality control			€ 200'000.00	2.2.8 Engineers	
1.3.2 Machinery			€ 3'000'000.00	2.2.9 R&D	
1.4 Operations			2.2.10 Guards		
1.4.1 Parts and product transportation		€ 60'000.00		2.2.11 Development engineers	
1.4.2 Safety measures			€ 2'000'000.00		€ 1'800'000.00
1.4.3 External contact		€ 24'000.00		2.3 Insurance	
1.5 Maintenance			2.3.1 Casco		
1.5.1 Quality control			€ 400'000.00	2.3.2 Exploitation	
1.5.2 Misc parts replacement		€ 1'600'000.00		2.3.3 Liability	
1.5.3 Runway		€ 40'000.00		2.3.4 Disability	
1.5.4 Infrastructure		€ 20'000.00		2.3.5 Legal	
1.5.5 Website		€ 2'000.00		2.3.6 Goods and stock	
1.5.6 Patent		€ 1'400.00		2.3.7 Business stagnation	
1.5.7 Bottom tether replacement		€ 367'536.00		2.3.8 Health	
1.5.8 Upper tether replacement		€ 331'312.50		2.3.9 Pension	
1.6 Infrastructure			2.4 Energy use		
1.6.1 Roads/railways			€ 2'975'000.00	2.4.1 Operations	
1.6.2 Ops/maintenance building			€ 400'000.00	2.4.2 Maintenance/manufacturing building	
1.6.3 Runway			€ 5'730'400.00	2.4.3 Testing	
1.7 Sales&marketing			2.4.4 Office		€ 3'600.00
1.7.1 Website			€ 20'000.00	2.4.5 Office development phase	
1.7.2 Marketing analysis			€ 20'000.00		€ 36'000.00
1.8 Development			2.5 Rent		
1.8.1 Software licenses			€ 41'000.00	2.5.1 Office	
1.8.2 Test models			€ 1'000'000.00	2.5.2 Land	
1.8.3 Software licenses (yearly)		€ 2'000.00		2.5.3 Office development phase	
1.8.4 Software licenses development phase			€ 20'000.00		€ 1'300'000.00
			Total cost		€ 3'971'648.50
					€ 62'883'653.87

Figure 13.1: Cost analysis

similar spacing as land wind turbines, which is not the case. However, the land underneath the flying gliders can be cultivated; only the generator itself cannot be used for farming purposes.

The manufacturing of the gliders, including the internal sub-systems, are estimated by studying existing gliders. The most extensive gliders cost €250,000 and are used for the glider cost estimation<sup>2</sup>. Since it is assumed that the internal sub-systems are included in the glider cost, it is estimated that each glider is twice as expensive as the most extensive existing glider, thus equal to €500,000. With two gliders per system and 19 systems in total, this gives a total glider cost of €19,000,000.

In order to estimate the cost of the generators required for the systems, the main cost factors of generator systems have been evaluated. On average, the total cost of a generator system equals €1,875,000<sup>3</sup>. Taking out the other parts of the wind turbine, it results to €575,000. Thus, 30,67% of the total cost are generator cost, and thus 13,467 kWh/€. As a total of 87,600,000 kWh is required for the systems, a total of €5,344,782.61 will be spent on the generators.

The tethers are a large recurring cost, as they must be replaced regularly. It was determined in chapter 6 that part of the tether after the hook must be replaced every seven weeks. The bottom tether, the part up to the hook, was assumed to be replaced each week. Dyneema rope of 1.5 cm thickness can be bought for €0.31 per meter<sup>4</sup>. It was assumed that the weatherproof coating adds another 50% to this price. With a tether of 4,800 m, this leads to a complete tether price of €51,243. Taking into account the tether length of the upper and lower sections and the frequency of replacement, the yearly costs of tether replacements

<sup>2</sup><https://www.acnistelrode.nl/prijs-zweefvliegtuig/> [cited 17 January 2020]

<sup>3</sup><https://ieeexplore.ieee.org/stamp/stamp.jsp?tp=&arnumber=1677663> [cited 17 January 2020]

<sup>4</sup>[https://linysyntetyczne.pl/dyneema\\_rope\\_1,5mm\\_uncoated\\_per\\_meter](https://linysyntetyczne.pl/dyneema_rope_1,5mm_uncoated_per_meter) [cited 17 January 2020]

adds up to €698,848.50 per year.

As can be seen in subsection 7.9.3, the weight of each glider equals 3,333 kg, which is more than 10 times lower than the maximum weight of a truck. Therefore, the strength of the runway can be lower than the strength of a highway. Normal asphalt will be strong enough, and is thus considered for the cost analysis. As the length of each runway is 1,885 km, and the width equals 10 m, the surface of each runway equals 18,850 m<sup>2</sup>. Each m<sup>2</sup> of asphalt cost €12-16<sup>5</sup>. The better asphalt has been taken for the runway, thus the asphalt runway cost per runway equals €301,600. As 19 runways are required, this gives a total of €5,730,400.00 for the construction of the runways.

Salaries were estimated based on profession as well as the number of people needed. Manufacturers and installers are a one time cost once the project is launched. Similarly, the development is assumed to take ten years of three engineers before the system can be launched. It is assumed that the office team consists of one person on legal affairs, one person on sales and marketing, one person in management, three engineers and one R&D scientist. On the field there are four operators taking shifts, three people maintaining the system, and two guards at all times.

All the above mentioned cost as well as smaller costs are shown in figure 13.1. This shows that the total investment cost is €62,883,653.87, and the yearly cost once the system is operational is €3,971,648.50.

To investigate the financial sustainability of the project, the energy use of the TU Delft must be investigated. In 2018, TU Delft budgeted 8.851 million euro's for energy use (*Financieel Jaarverslag 2018 2019*). Assuming a development time of ten years for the product, the energy prices are expected to rise by 13% by 2030 (Bani 2019). This would mean that the TU Delft would be spending €10,001,630 each year on its energy, assuming a consistent energy use of approximately 70,000 MWh, or 14.29 cents per kWh.

As the system is meant to be run by TU Delft, there is no profit. However, considering the cost analysis, the yearly savings add up to €6,029,981.50 each year, or a difference of €0.0861 per kWh.

Using the yearly savings of €6,029,981.50 and the investment of €62,883,653.87, the return of investment is 10.43 years. However, considering that this system can provide energy at the low price of 5.67 cents per kWh, TU Delft could consider expanding and selling the excess energy at a higher price.

---

<sup>5</sup><http://www.asfaltering.nl/asfalteren-prijzen/> [cited 17 January 2020]

To bring the system effectively on the market, the target market and potential for further opportunities should be analysed beforehand. With the right clients the further development of the project becomes feasible. This chapter discusses the steps to be taken regarding branding and the market in sections 14.1, 14.2 and 14.3.

### 14.1. Branding

Besides TU Delft there are other possible clients interested in the system. For marketing it is essential to consider the branding of the product, but possibly more important a company name is essential for governmental registration of the company. Without this registration it would be impossible to start up a company in the Netherlands. The name allows for advertising at relevant sites. The company would also partake in several green innovation start-up competitions and other innovation competitions to rake up more funding.

The name Greenhyve was picked by the team. The name consists of two elements: green and hyve. Green demonstrates the sustainability related ambition of the project, whereas hyve comes from idea of the wind park working together as a hive mind to achieve its goals. The 'y' in hyve comes from the concept of the Y-tether. The entire park would be referred to as the Greenhyve, with multiple hyves spread out over the wind park area. A hyve consists of the ground station, the tether set-up, and two gliders.

### 14.2. Current market

Currently, Greenhyve does not yet outperform wind turbines in nominal power output. It does outperform wind turbine parks in availability. Greenhyve is less reliant on wind speeds due to its high altitude and flexibility in operational altitude to always maximise efficiency. Making it a good renewable solution to the supply gap caused by conventional wind energy systems.

Furthermore, the energy transition goals of the Dutch government are very ambitious resulting in an increased demand for innovative methods for renewable energy generation. For 2030, 70% of all generated energy is aspired to be renewable in the Netherlands <sup>1</sup>, which is currently only 16% <sup>2</sup>. Achieving this goal proves a challenging task as there is not adequate available ground space to place most conventional renewable energy generating system. This is where Greenhyve comes in. Greenhyve allows for ground underneath the flying area to be used for activities, which do not require airspace. Another huge challenge the Netherlands is facing, is getting a reliable power output using renewable energy sources. Solar and wind energy show big fluctuations in their availability. The availability of high-altitude winds is way higher. Therefore Greenhyve could provide a big solution to what one of the biggest challenges of the 21st century.

Current (global) renewable electricity costs are portrayed in table 14.1, as well as their percentage change in costs. As can be seen, prices are dropping fast, mainly due to the fast developments in the industry. As shown in chapter 13, Greenhyve produces energy at 0.0567 €/kWh, or approximately 0.063 \$/kWh. This

<sup>1</sup><https://www.rijksoverheid.nl/onderwerpen/duurzame-energie/documenten/publicaties/2016/01/20/energie-in-nederland-verduurzamen> cited [14-01-2020]

<sup>2</sup><https://opendata.cbs.nl/statline/#/CBS/nl/dataset/82610NED/table?ts=1579688232422> cited [16-01-2020], and <https://opendata.cbs.nl/statline/#/CBS/nl/dataset/84575NED/table?ts=1579688319308> cited [16-01-2020]

Table 14.1: Costs of comparable renewable power sources and their price change (Anuta et al. 2019)

Energy type	Global weighted average cost (\$/kWh)	Change in cost 2017-2018
Bioenergy	0.062	-14%
Geothermal	0.072	-1%
Hydro	0.047	-11%
Solar photo-voltaics	0.085	-13%
Concentrated solar power	0.185	-26%
Offshore wind	0.127	-1%
Onshore wind	0.057	-13%
Greenhyve	0.057	NA

means that Greenhyve falls in a cheaper category of renewable energy sources currently available. Especially once the tether wear is investigated in further depth, these costs per kWh can drop significantly. Therefore, Greenhyve will be more cost efficient than other renewable energy types.

### 14.3. Market opportunities

Greenhyve would be available anywhere in the world, although the availability of high-altitude winds is smaller around the equator. The most prone market is the European one. The European Union recently announced to commit 1 trillion euro to 'The European Green Deal Investment Plan and Just Transition Mechanism'<sup>3</sup>. Greenhyve is currently designed to be deployed in the Netherlands, however, with the European plan other less prosperous European states become attractive for deployment as well.

Unlike conventional wind turbines, Greenhyve is similarly efficient inland as offshore due to its high altitude of operation. Making it an efficient renewable energy source for many European states without vast coast lines.

Eventually, when Greenhyve performs on par with a cutting-edge wind turbine farm, it becomes a sustainable and cheap alternative to offshore wind turbine farms. The structural components require significantly less material than wind turbines and the materials are more easily replaced by sustainable alternatives. Individual hyves are much easier to upgrade to a more modern version as it does not concern such colossal structures. Each section of hyve could individually be upgraded to increase the efficiency of a readily placed hyve to keep even old hyves relevant.

<sup>3</sup>[https://ec.europa.eu/commission/presscorner/detail/en/qanda\\_20\\_24](https://ec.europa.eu/commission/presscorner/detail/en/qanda_20_24) cited [14-01-2020]

In this chapter, the phase after the DSE project is described. Section 15.1 shows the design & development logic, illustrated by a block diagram. The sub-tasks of each block in the design & development logic are written in the project Gantt chart, as can be seen in section 15.2.

### 15.1. Design & development logic

In this section, the project design & development logic for the post-DSE period is described. This comprises the steps which need to be taken to bring the product to the market. It gives a good indication of the specialisms and resources needed for the follow-up steps. The project design & development logic is given in figure 15.1.

Once the DSE has been completed, a lot still has to happen to develop and market the design. First of all, an office needs to be acquired, and staff needs to be hired. At the same time, negotiations should start with the different partners required for the system to work.

After this, a prototype of the design needs to be developed, which will be used to test the system. During this development, the prototype needs to be tested, verified and validated. It is reasonable to say that a few iteration loops will be needed during this period.

When the design is finished, it needs to be certified by a variety of instances, regarding the airworthiness of the design, its potential impact on its surroundings, and its connection to the grid. In the meantime, a definite site needs to be located which can appropriately host the system.

Once certification is complete, insurance companies can be contacted to provide insurance in case something goes wrong with the system. Finally, the operation site will be set up and the end product will be produced. After, the system can enter the market.

### 15.2. Project Gantt chart

The design & development logic leads to the Gantt chart. The Gantt chart shows when tasks are planned and how much time they should take. Some tasks run parallel and have links; those tasks require close collaboration to make sure the content is updated regularly. The Gantt chart is shown in appendix G.

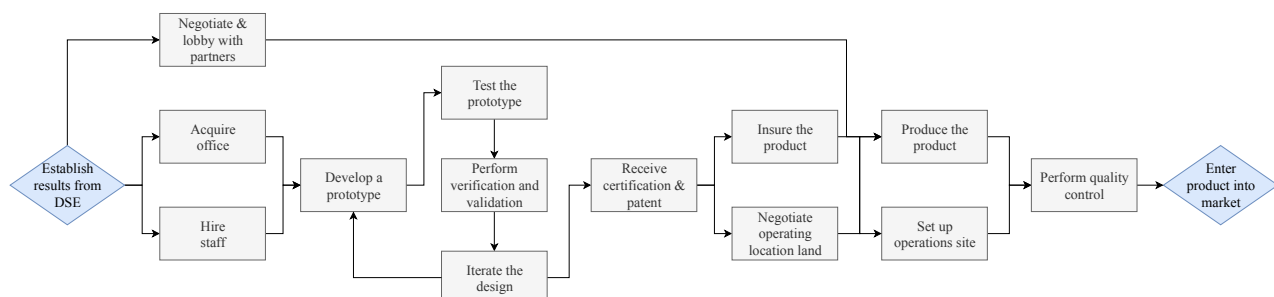


Figure 15.1: Flow diagram of tasks to be completed after the DSE.

## Requirement compliance matrix

This chapter contains the requirement compliance matrix. This matrix is an overview of the set requirements and shows whether the requirements are met. If not, the reason for that is explained at the end of the chapter. At an early stage some requirements were identified as being important to the system, but were later discovered to be beyond the scope of this study. These are noted by a '-'.

First, the mission requirements, which are stated below, are analysed. All three have been met in the design of the system. EHAC-MIS-01 is met, since the system produces 38 MWh more than the TU Delft energy needs, daily. As the system flies above 2 km, where the lower clouds are positioned, EHAC-MIS-03 and EHAC-MIS-04 are both met.

- **EHAC-MIS-01:** The system shall provide the TU Delft with its yearly energy needs.
- **EHAC-MIS-03:** The system shall be located above the clouds.
- **EHAC-MIS-04:** The system shall be able to fly.

Tables 16.1 and 16.2 give an overview of all stakeholder and system requirements set.

Table 16.1: The stakeholder requirements with a stakeholder linked to the requirement (first column) and the unique identifier of the requirement (second column)

Stakeholder	Identifier	Stakeholder requirement	Met?
Primary customer: TU Delft	EHAC-SH-11-01	The system shall be constructed using renewable materials only.	×
	EHAC-SH-11-02	The system shall harvest renewable energy.	✓
	EHAC-SH-11-03	The system shall provide energy more cost efficient than comparable methods on the ground surface do.	✓
	EHAC-SH-11-04	The systems return on investment shall be 10 years.	✓
	EHAC-SH-11-05	The system shall be able to sell excess energy to third parties.	✓
	EHAC-SH-11-06	The system shall be safe for birds.	✓
	EHAC-SH-11-07	The system shall be safe for humans.	✓
	EHAC-SH-11-08	The system shall produce more energy than others of comparable surface area.	×
	EHAC-SH-11-09	The system shall have a smaller environmental footprint than methods on the ground surface of comparable costs.	×
	EHAC-SH-11-10	The system shall use technologies that are at least TRL 3	✓
Airports	EHAC-SH-01-01	The energy harvesting system shall not interfere with airport operations.	✓
Airspace regulators	EHAC-SH-02-01	The system shall get a certificate of airworthiness.	-
	EHAC-SH-02-02	The system shall not compromise safety for airspace users.	✓

Emergency services	EHAC-SH-03-01	All EROs of the system shall have ERO certification.	✓
	EHAC-SH-03-02	The system shall be able to be shut down by emergency services.	✓
	EHAC-SH-03-04	The emergency services shall reach the launch site within 15 minutes.	✓
Environmental organisations	EHAC-SH-04-01	The system shall be sited 1 km away from migration paths of birds.	×
	EHAC-SH-04-02	The system shall meet the drop shadow regulations.	✓
	EHAC-SH-04-03	The system shall not be placed in a Natura 2000 area.	✓
	EHAC-SH-04-04	The system shall not produce any greenhouse gasses.	✓
	EHAC-SH-04-05	The system shall not produce any harmful radiation.	✓
	EHAC-SH-04-06	The system shall not produce any toxic byproducts.	✓
Grid operators	EHAC-SH-05-01	The system shall comply with grid operation requirements.	✓
	EHAC-SH-05-02	The system shall have an average voltage of 380 kV.	✓
	EHAC-SH-05-03	The system shall have a peak voltage of <td> V.	-
	EHAC-SH-05-04	The system shall have an average current of <td> A.	-
	EHAC-SH-05-05	The system shall have a peak current of <td> A.	-
	EHAC-SH-05-06	The system shall have an average power of <td> W.	-
	EHAC-SH-05-07	The system shall have a peak power of <td> W.	-
	EHAC-SH-05-08	The system shall have an electrical efficiency of <td> %.	-
	EHAC-SH-05-09	The system shall have an electrical frequency of <td> Hz.	-
	EHAC-SH-05-10	The system shall have <td> electric phases.	-
Local government	EHAC-SH-06-01	The system shall fit within the municipality's destination plan.	×
National governmental organisations	EHAC-SH-07-01	The system shall fit within the national environmental regulations.	✓
	EHAC-SH-07-04	The system shall not interfere with foreign airspace	✓
	EHAC-SH-07-05	The system shall promote the Dutch field of engineering.	✓
	EHAC-SH-07-06	The system shall not interfere with international shipping routes	✓
Production partners	EHAC-SH-08-01	The system shall be produced in a hazard-free environment.	✓
Residents	EHAC-SH-09-01	The system shall meet the light pollution regulations.	✓
	EHAC-SH-09-02	The system shall meet the noise pollution regulations.	✓
	EHAC-SH-09-03	The system shall meet the visual pollution regulations.	✓
	EHAC-SH-09-04	The system shall have a maximum impact area of <td> m <sup>2</sup> .	-
	EHAC-SH-09-05	The system shall have an impact more than 100 m away from buildings and crowds of people.	×
	EHAC-SH-09-06	The system shall have a maximum impact energy of <td> J.	-

Transportation partners	EHAC-SH-10-01	The system shall be moved via currently existing infrastructure.	✓
-------------------------	---------------	--	---

Table 16.2: The system requirements with a system linked to the requirement (first column) and the unique identifier of the requirement (second column)

System	Identifier	System requirement	Met?
Energy	EHAC-SYS-EN-01	The system shall power the in-flight operations of the system.	✓
	EHAC-SYS-EN-02	The system shall be able to store 500 kW on-board.	✓
	EHAC-SYS-EN-03	The system shall be able to store 50 kWh on the ground.	✓
	EHAC-SYS-EN-04	The system shall transfer energy at a rate of <td> W.	-
	EHAC-SYS-EN-05	The system shall be able to deliver a peak power value of <td> kWh.	-
Flight performance	EHAC-SYS-FP-01	The system software shall control the system entirely.	✓
	EHAC-SYS-FP-02	The system shall be able to be launched.	✓
	EHAC-SYS-FP-03	The system shall be able to maintain flight.	✓
	EHAC-SYS-FP-07	The system shall be statically stable.	✓
	EHAC-SYS-FP-06	The system shall be dynamically stable.	✓
	EHAC-SYS-FP-05	The system shall be able to perform controlled landing.	✓
Operations	EHAC-SYS-OP-07	The system shall be able to communicate relevant data to the ground station.	✓
	EHAC-SYS-OP-02	The system shall include maintenance facilities.	✓
	EHAC-SYS-OP-03	The system shall include on-ground servicing facilities.	✓
	EHAC-SYS-OP-06	The system shall not come down uncontrollably in case of a subsystem failure.	✓
	EHAC-SYS-OP-09	The system shall be able to function in wet conditions.	✓
	EHAC-SYS-OP-10	The system shall not fail due to thunderstorms which happen in the Netherlands.	✓
	EHAC-SYS-OP-08	The system shall consist of components that are all either fail-safe or safe-life.	✓
Structures	EHAC-SYS-ST-04	The system shall consist of available materials.	✓
	EHAC-SYS-ST-05	The system shall consist of structures that are producible with current production methods.	✓
	EHAC-SYS-ST-06	The system shall be able to withstand wind speeds up to 20 m/s.	✓
	EHAC-SYS-ST-08	The materials of the system shall not deteriorate to a degree in which it will fail before maintenance is done.	✓
	EHAC-SYS-ST-07	The system shall be able to withstand wind gusts up to 20 m/s.	✓
	EHAC-SYS-ST-09	The system shall be able to withstand all temperatures between -73 to -23 and 120 to 140 °C.	✓
	EHAC-SYS-ST-10	The system shall be able to withstand temperature difference rates of <td> °C/s.	-

There are six requirements which have not been met. An explanation is given below.

- **EHAC-SH-11-01:** Due to low TRL and currently insufficient material characteristics, it has been decided that for now, non-renewable materials are used to benefit the production of green energy. Once renewable materials are discovered with sufficient material characteristics, it can be decided to use those.
- **EHAC-SH-11-08:** As stated in 8.4, the system will not generate more power than an existing energy harvesting system with comparable surface area, due to a higher output power of an onshore wind turbine than the output power of a glider system, and since the onshore wind turbines require a smaller area. However, as mentioned in the recommendations of chapter 7, there is a possibility to use one runway for all systems. This would highly reduce the needed area, in case this recommendation is pursued, this requirements will be met.
- **EHAC-SH-11-09:** As was discussed in chapter 12, the global warming potential of the system is higher than that for a standardised model of onshore wind turbines. Given that energy from the system is in similar price range to that from onshore wind turbines, it can be concluded that the requirement is not met.
- **EHAC-SH-04-01:** Since the ideal position for the energy was decided to be in the Noordoostpolder, a lot of important bird areas are nearby. These areas are a popular winter destination to tens of thousands of birds each year. Although the system is located nearby migration routes, the ecological impact of the system can be mitigated in various ways, as discussed in section 9.4.
- **EHAC-SH-06-01:** The municipality's destination plan is difficult to change, and there is a low change that the people living in the area will agree to making place for the harvesting site.
- **EHAC-SH-09-05:** As the system will be build in a place where houses are located, it can not be ensured that the place of impact in case of system failure will have a distance of at least 100 m away from buildings or people.

## Verification procedure

This chapter is about an important part of any technical project, verification. Most projects must do verification and validation, but the DSE is about building a conceptual design. Conceptual designs can be verified in many ways, and this chapter summarises the verification done on the models created. Verifica-

tion of the tether sag computations was done by first verifying the catenary cable equations. The source of the equations (Federal Highway Administration of the USA) is considered reliable, and cites a journal paper from *Transactions of the American Society of Civil Engineers* for these equations. These equations are mainly used for the stay cables of bridges, but bridges are at this point of the development of this project one of the closest comparisons. Once the equations are verified, the code written for the tether sag had to be verified. The code was written in multiple definitions, thereby simplifying the verification process. Other than using engineering intuition, the computations were verified by hand. Plots and print functions were also used to visualise the results for mid-way calculations to verify that all inputs and outputs of the definitions were consistent and plausible. Further verification of the tether sag cannot be performed, as similar tethers do not exist, so no comparable data is available.

Verification of the tether drag calculations was also done by hand, comparing the drag of the elements at various sections of the cable. Also hand calculations were performed on a generalisation of the entire cable (analytical model) in order to verify the order of magnitude of the outcomes of the integration of the cable segments in the code.

Numerical and analytical models were created for the airfoil and wing characteristics. Their outputs were  $C_{L\alpha}$  and  $C_L/C_D$  plots. From the analytical model it became clear, after using the DATCOM method, that the  $C_L$  should increase 0.1 per degree of angle of attack. From the numerical model using XFLR5, this can indeed be verified within an error margin of 10%. In the midterm report, the acceptable verification margin of error was said to be 10% (Arblaster et al. 2019b). The error between the analytical and numerical model was calculated to be equal to 0%. Therefore the verification of the numerical model with the analytical model is performed successfully.

For the glider drag, several analytical analyses were performed (class 0 to II). One trend that was noticed was that the more accurate the analytical analyses became, the higher the calculated drag became. This is predominantly down to the fact that the fuselage is much smaller than conventional aircraft, and so the analytical expressions (based on reference data) would have significant margins of error. This is not too much of an issue, as the largest drag comes from the tether and not the aircraft. The numerical model is provided by in-depth analysis using XFLR5. From the analytical and numerical model two points are picked per model for the verification, at  $C_D = 0.05$  and  $C_D = 0.15$ . The error between analytical and numerical model for  $C_L/C_D$  was found to be around 12.5%.

The structural script is verified by hand-computing one loop of all the loops. This way multiple mistakes were spotted and corrected in the code. Currently all the loops are correct. Equations were checked with TU Delft courses like Structural Analysis and Mechanics of Materials to see if they correspond. Finally, plots of all the data were subject to a sanity check. The bending moment graph should for instance be approximately quadratic, which it was. Simplified calculations (like simple beam equations) were used to make an estimate of what order of magnitude of number should come out of the script. These orders of magnitudes all corresponded.

The verification of the glider flight model was conducted in a similar manner to the way the structural models were verified. At first, the code gave incorrect apparent wind speed magnitude values, and then it gave incorrect apparent wind speed vector directions. To rectify this – and to ensure that the iteration process would be correct – a single iteration of the model was done by hand. The equations were verified using the *Airborne Wind Energy* textbook (Schmehl et al. 2013) and sensitivity analysis was done to check whether the general trends they followed were intuitively correct. For example, with a lower glide ratio there would be a smaller apparent wind speed, which would lead to less power being produced. This relation corresponded with the values in the analytical mode, and so the system was considered to be verified. In the next stage, a numerical model for the glider flight should be created that could be verified by the analytical model before creating numerical simulations.

Operations and logistics had comparatively fewer calculations, yet still needed to be verified. However, this field of study is very new and there is insufficient research into the operations and logistics side of airborne wind energy. Therefore, when new research is conducted by other members in this field, their data could be used to verify this system. The same goes for the maintainability and availability of such systems.

The verification of this system has been at a lower level than other projects at this stage of development simply due to the fact that projects of this kind are still in early development stages. Ideally, verification would involve acquiring experimental data from reputed sources (i.e. scientific journals) and testing the models with the data. The discrepancies would be noted, and a reasoning behind the errors would have to be documented. Next, the margins of error would have to be calculated.

The next stage of development would be to have numerical simulations. Numerical simulations, if conducted properly, have significantly higher orders of accuracy. This could be compared to the analytical model and numerical model in order to be verified. This would be the final stage of the design process before production.

After production, the system can be tested. The test data can then be compared with the numerical model and the numerical simulation. If they are within an acceptable margin of error, the models are said to be validated. Furthermore, the system outputs would be compared to the original system requirements. If the system does meet the key system requirements, the system is said to be fully validated. Only after this, can the system be patented, marketed, and distributed.

## Conclusion and recommendations for further research

The overall conclusion is given in section 18.1 and further recommendations are given in section 18.2.

### 18.1. Conclusion

The goal of the project was to have a set of energy systems that would provide enough energy to power TU Delft. As this project draws to its close, it is time to summarise exactly how this goal was met. There were four main aspects to designing an energy harvesting glider system; structures, energy, operations, and flight performance. Although it may seem that these departments have little correlation, the tiniest change on one of the design aspects, would result in a snowball effect that would affect the entire system. Hence, it was vital all the departments collaborated when designing individual subsystems. For many subsystems, rough analytical models were created to provide a sanity check and give approximate values for the more detailed design phase. A numerical model was then created, as a team, to find the optimal configuration and design of the energy harvesting system. After the design was completed, the system was proudly named “Greenhyve”. The following paragraphs will give the outcomes of this design phase.

The primary requirements of this project are; to provide TU Delft with its yearly energy demands, to operate above the clouds, and to be able to perform unaided flight. After an initial design phase, three system concepts were procured for the final design trade-off. These three options were; free-floating balloons, tethered gliders, tethered wind turbines. After each concept was assessed for various important trade criteria, the tethered glider option was chosen as the final concept that the group would pursue. This design option was modified to create a more efficient and unique concept. Modifications included; having multiple gliders on each tether, and having twin-fuselage gliders. Hardware block diagrams, software block diagrams, and electrical block diagrams were created to give a development vision to the team.

Sustainability played a prominent role in the design of the project. There are two philosophies we could have followed when designing the system; performance or sustainability. When designing a system for performance, it becomes very difficult to replace unsustainable parts with sustainable parts. As the goal of this project is to have a sustainable energy harvesting system, the latter philosophy was chosen as the team ethos. The sustainability of the glider was not simply limited to the materials, it included the entire life cycle.

With any energy production system, there are plenty of risks. In addition to conventional energy farm risks, this system would deal with many more risks, such as; manufacturing risks, operations & logistics risks, end-of-life risks, and sustainability risks. Risk mitigation strategies were implemented to ensure this system would get off the ground.

The tethers play a critical role in the operations and performance of the glider. The tether is in fact a Y-tether. The upper part of the tether, after the Y-connection is called the upper tether, while the lower part of the tether is called the stationary tether. The Y-connection of the tether consists of the thrust ball bearing with a basic dynamic load rating of 364kN, which would accommodate for a safety factor of 2. The model 51160 M of SKF would be able to bear these loads.

Dyneema was selected as the tether material. It is not sustainable, which is a pro of banana fibre, the alternative. Banana fibre would however require a thicker and heavier tether, which would make the design unfeasible. Hydrophobic coating is needed to maintain correct material properties during operation. A parachute is added to the cable as an emergency feature.

The aerodynamic drag of each Y-tether is 16 kN in the negative direction of the tangential flight speed. The aerodynamic forces on the stationary cable are 0.45 kN in positive wind direction and 1.2 kN downwards. If the entire tether would move instead of just the Y-tethers, the drag increases by 400%. This would lead to no power output.

As previously mentioned, a numerical model was created and the code was optimised for a certain system size. Each glider has a wing surface area of 60 m<sup>2</sup>. The wing span is 26.8 m with an aspect ratio of 12 and zero sweep at the leading edge. A taper ratio of 0.4 is chosen in order to get a quasi-elliptical lift distribution which lead to a trailing edge being under an angle. Since the glider flies at an apparent angle of attack of approximately 2°. A double-fuselage glider was chosen to relieve bending stress and to house subsystems (i.e. landing gear, propellers, engines). The length of the fuselage is 12.65 m with a maximum radius of 1.06 m. The empennage is designed for stability with a surface area of 15 m<sup>2</sup> and a symmetric airfoil was chosen. The height of the vertical tail plane is determined by down wash computations. As for control surfaces, two ailerons were placed on the main wing, while the empennage carries the rudder and elevators. This configuration results in a total glide ratio of 11.9.

The gliders should be able to operate 24/7, but will occasionally need to take off the ground after maintenance or emergency groundings. For take-off an electric on-board propulsion system is needed. The total energy needed for take-off is 100 kWh which results in a battery mass of 526 kg. The propellers are attached to both fuselages and to mitigate the drag of the propellers during crosswind flight, the propellers are retracted. A rotational take-off procedure is used on a circular runway. Once the two gliders are at the desired altitude, they will rotate the tether towards the desired operation angle. For the landing procedure, the tethers are disconnected and each glider lands separately on the circular runway. The main landing gear is positioned under the wing, just in front of the center of gravity and the rear landing gear is positioned towards the tail. The diameter of the wheels is 68.6 cm and the width is 22.2 cm. It was designed to be able to land on unprepared surfaces. It is positioned 5.7 m from the nose of the glider with a length of 1.3 m.

One of the major problems airborne wind energy systems face is tether drag, especially at the conditions we operate at. One way to mitigate this issue is to have a single longitudinally stationary tether, that splits into separate moving tethers. With this, the primary source of tether drag would be the relatively short tether between the Y-connection and the glide. Based on drag calculations, this tether design would reduce tether drag by up to five times. Since two gliders are attached to a single main tether, the flight path of each glider must be circular in order to counteract the force of the other glider. The flight path is optimised for maximum net cycle power. In order to determine the flight path and its corresponding net cycle power output, two phases are separately assessed; the reel-out phase and the traction phase. The reel-out phase generates electricity on the ground which needs to be maximised whereas the traction phase consumes energy which has to be minimised. The optimisation leads to an average operating altitude of 3,000 m at an elevation angle of 40° and an azimuth angle of 0°. Calculations on the apparent wind speed concluded an apparent angle of attack of 2°, as mentioned before. By determining an optimal reel factor, a reel-out speed of 3.44 m/s was found which leads to a power output during the reel-out phase of 635 kW per ground station generator. The tether length that is reeled out during one cycle is 800 m and the optimal flight radius is 466 m. The reel-out time is 233 s and the reel-in phase is 32 s given a reel-in speed of the drum of 25 m/s.

The influence of weather was also researched and calculated. It was concluded that rain and ice cause a maximum lift decrease of 24% while the drag could increase up to 108% causing a maximum power production reduction of 475 kW. However, at this stage it is still uncertain what the influence of ice, rain and water vapour formation is on the gliders, as well as the probability of either of them occurring at any given point in time. Currently, the possible lift reduction and drag increase are not taken into account. Gusts affect the system as well ranging from a decrease and increase in power of -18.5 kW and 33.4 kW, respectively.

For the material selection and the structural analysis of the glider, the main focus was on the wing and its wing box. For the wing box, balsa wood was used for the ribs. The wing box is 2 mm thick and is made of carbon fiber + PEEK which has a high yield strength. The skin of the wing has to be further analysed but for current calculations, glass fiber is used as a reference material. The wing runs through the fuselage decreasing structural weight. Based on the structural calculations of the wing box, skin of the wing, and empennage, the glider weight was estimated to be 3,333 kg, including payload. The VECTOR autopilot was chosen as it is capable of automated take-off, landing, and flight. The total power the glider requires is 20 kW and a minimum storage of 2.3 kWh is required. The total payload mass for the control system is 56 kg.

The winch that is going to be used for this system is FEcreate's AWE winch, due to its high reel-in speed. The winch demands 5.58 kW of power during the reel in phase. A synchronous generator with permanent magnets was used due to its high power efficiency (97%). Furthermore, AC-DC-AC converters are used to obtain fixed current frequency with variable wind speeds. The power is transformed by a voltage/current transformer to high-voltage power to be received by the grid. The average net power during one cycle (one reel-in and one reel-out phase) is 541 kW. One would then need 19 systems with 38 gliders in total to reach the TU Delft energy needs. This includes the safety factor of approximately 15% (10 MW nominal power instead of 8.75 MW that is required for the TU Delft).

The system is challenging to operate, but definitely feasible. For maintenance, the glider consists of not too many separate parts. Communications and data handling plans are made and show no difficult or hard-to-achieve systems. The spacing of ground stations is significant, however the ground between them is available for alternate uses. The generated energy can be stored in different ways, but with efficiencies taken into account lithium-ion batteries are most convenient. Most power will be put in the grid, not stored. Due to the number of devices, scaling is easily done and the system can be scaled to meet virtually any power requirement.

The spacing of the ground stations is more than the spacing of offshore wind turbines. However, this system generates more power than individual wind turbines. The 'hyve' of systems was set up in hexagonal positions, to minimise the ground space needed. It would be placed in Noordoostpolder, to have better grid access and to use largely unused areas of land.

Analysing the LCA of the airborne wind energy farm, an initial estimate revealed a GWP of 121 gCO<sub>2</sub>-eq/kWh. By adjusting the tether durability to more closely resemble values found in literature, as well as assuming savings could be made on the runway, a GWP of 25.4 gCO<sub>2</sub>-eq/kWh was achieved. This is still considerably higher than the value found in literature of 5.611 gCO<sub>2</sub>-eq/kWh. This can be accounted for in two ways; the LCA in the reference assumes a novel launch and landing system which does not require a paved runway, and the glider in the reference is lighter than the one designed in this report, while also generating considerably more energy.

It was established that the farm must outperform convention wind farms, which have been found to have a GWP of 5–45 gCO<sub>2</sub>-eq/kWh – conventionally established as 20.85 gCO<sub>2</sub>-eq/kWh for onshore wind farms (Schmehl 2018, p. 746). Taking all this into consideration, it seems likely that an AWES as was designed in this report could be constructed in a more sustainable way than a conventional wind farm on the same (onshore) location. However, requirement EHAC-SH-11-09 is stated as a function of cost. Using the numbers found in chapter 13, the cost of energy from this farm comes out at 0.063 \$/kWh, which is slightly more than the global weighted average price for onshore wind, which is 0.057 \$/kWh. This means the current design is not on track to meet requirement EHAC-SH-11-09.

Verification and validation was difficult to do on such a conceptual system. Verification by hand or using analytical equations from reputed sources was done on the various models that were created. However, not enough data is available to compare the models to research. Furthermore, validation is only possible after a prototype is created and tested.

## 18.2. Recommendations

In this section multiple recommendations for further research will be discussed. These can either be opportunities to get better designs or parts of the design that need further investigation.

### 18.2.1. Tether

As stated in chapter 6, a lot of the vibrations of such long tethers under tension force are still unknown. This could have a big influence on the drag and thus on the flight performance. Current research is not far enough to predict these. This means extensive testing has to be performed to understand the behaviour of the tethers. Furthermore, the length and altitude of tethers makes that not enough research or tests are done to predict the durability of the tether effectively, especially if combined with the unknown vibrations. This means testing on these has to be performed on that part as well. The tether material is currently chosen to be non-natural, as the natural materials have not reached sufficient properties yet. In the future, more research on these materials is necessary to get them useful for state-of-the-art applications as our design. A big barrier for banana fibers were the rope properties. It was out of our scope of this study to investigate what exactly happens in combining different materials for one rope. In that application, the banana fiber could already be feasible, but not in the current 12-strand uniform material braiding method. Tether durability has not been tested during this project, and a lot on it is unknown, mainly on how the coating will react to the constant reeling in and reeling out.

### 18.2.2. Glider

Weight is crucial for the glider, as all weight compromises the power output on the ground. The gliders currently are limited in their aspect ratio, and thus effectiveness, by structural weight. If lighter and stronger materials can be made, the aspect ratio can increase, making a more effective flying glider. A lot of components of a good center of gravity location are unknown. However, they are quite playable by moving for instance the batteries in the glider. An optimal configuration for that still has to be found. Control surfaces are currently based on reference aircraft, which might cause differences for the double-fuselage configuration. Detailed numerical calculations should give better insight in the behaviour of the aircraft.

It is recommended to apply a wing twist angle in order to keep the aircraft controllable at higher angles of attack. Due to limitations in the numerical analysis software the effects of a wing twist angle could not be analysed yet. Further analysis should be performed to determine the optimum angle for which lift is hardly affected and stall properties are more favourable.

The wing box material is currently not natural or easily renewable. The non-natural materials have the properties needed for this edge-of-technology application. Therefore they are the only options for now. If more research is performed on natural or bio-based composites they could become an option in the future. The material of glider skin has to be researched in more detail, with a material trade-off. The structures of the aircraft, mainly the wing box, are kept at constant thickness. If this can be changed to a variable thickness, there could be serious weight reductions, causing better performance of the glider.

The current design of the glider is based on a symmetrical glider, as are most current aircraft. This allows for more accurate calculations for this phase, but chances are it is not the most optimal configuration. Asymmetrical aircraft could work better for this application, as during the entire operational phase the aircraft is in a constant turn. If it is designed such that it flies stable in the required angle, it will have less losses due to the constant turning.

More elaborated investigations have to be made to the use of winglets, the effect of weather coatings on drag, the attachment of high-lift device actuators, highly-advanced CFD computations of the wing, the vertical tail, downwash CFD computations, movable ground stations, active de-icing, a time-based numerical model, FEM analysis of the structures and connection points.

### 18.2.3. Ground Station

The take-off procedure has a difficulty in the landing gear radius. The Y-split of the tether is quite low, causing a runway radius of about one kilometer. This of course is way too high, and therefore the tether has to be shortened for the take-off. The detailed design of how this will work is outside of the scope of this study, and thus still needs to be performed. Furthermore using other materials than asphalt for the runway can ensure lower environmental footprint of the system. Using one runway for multiple systems by moving the generators or designing a moving system can reduce the ground space needed and the environmental footprint of the design.

The generators are currently using copper as stator windings. Copper is not a renewable material, and thus is not sustainable. In future other materials that can work for this use can be investigated. Noise cancelling of the generator has to be considered if the system would ever be placed close to densely-populated areas.

### 18.2.4. Other

Safety of the system is currently not investigated in detail yet. The system should be extremely reliable, such as aircraft, so it can fly above inhabited grounds. If this is not achieved, the ground spacing needed for the system is too big to be an economical choice. This means many tests and certifications have to be performed, as well as deep verification and validation of all failure modes and control systems. Emergency situations should not result in casualties. Advanced research on this could even lead to the system being placed on top of buildings. Placing the system in hilly or mountainous areas could get the system to its operating altitude easier, thus increasing the efficiency of the system. In the Netherlands this is not possible due to the geography. More expert reviews on the well-being of local birds is necessary to avoid bird collisions, mainly at nocturnal times.

Reference data on RAMS parameters was scarce. Partnering up with instances which do have this data can lead to a more accurate RAMS description.

A detailed control system for the glider is a big challenge, and will take a lot of time and resources to design. A model to take the current weather circumstances and translate them to an optimal harvesting altitude and flight path still has to be written.

Currently, the runway puts a big environmental footprint on the system. More research on ecological runways can be performed to mitigate this footprint. It is doubtful whether asphalt or concrete is necessary for the runway, which could be the topic of further investigation.

The required 19 systems are for 10 MW nominal power generation. This is 29% higher than the actual average power that the TU Delft requires, which is 7.75 MW<sup>1</sup>. Excess energy will be sold to third parties on campus which need approximately 1.7 MW (Blom et al. 2017).

---

<sup>1</sup><http://emonitor.tudelft.nl/index.php/campus/> [cited 20 January 2020]

# Bibliography

- Anuta, H., P Ralon, and M. Taylor (2019). *Renewable Power Generation Costs in 2018*. URL: [https://www.irena.org/-/media/Files/IRENA/Agency/Publication/2019/May/IRENA\\_Renewable-Power-Generations-Costs-in-2018.pdf](https://www.irena.org/-/media/Files/IRENA/Agency/Publication/2019/May/IRENA_Renewable-Power-Generations-Costs-in-2018.pdf).
- Arblaster, T.P.S., X.F. Van Beurden, H.H.J. De Goeijen, L.M. De Klerk, T.S. Lokken, P. Madabhushi, A.D.P. Schoon, M.G.M. Van de Ven, W.A.J.G. De Vries, R.M. Vrouwens, and C.F. Van Winkel (2019a). *Baseline Report*. TU Delft.
- (2019b). *Midterm Report*. TU Delft.
- Ashby, M.F. (2011). *Materials Selection in Mechanical Design*.
- Backes, C.W. and S. Akerboom (2018). *Renewable energy projects and species law — a legal comparative research*.
- Baker, J. (2008a). *New technology and possible advances in energy storage*.
- (2008b). “New technology and possible advances in energy storage”. In: *Elsevier, energy policy* 36.12, pp. 4368–4373. DOI: 10.1016/j.enpol.2008.09.040.
- Baldwin, Peter Michael Iain (2009). “Long Term Performance of Mono-pile Supported Offshore Wind Turbines”. PhD thesis.
- Bani, M. (Oct. 2019). *Is woningverduurzaming een rendabele investering of een kostenpost?*
- Bechtle, P., M. Schelbergen, R. Schmehl, U. Zillmann, and S. Watson (2019). “Airborne wind energy resource analysis”. In: *Renewable Energy* 141, pp. 1103–1116. ISSN: 0960-1481. DOI: <https://doi.org/10.1016/j.renene.2019.03.118>.
- Bernardino, J., K. Bevanger, R. Barrientos, J. Dwyer, A. Marques, R. Martins, J. Shaw, J. Silva, and F. Moreira (June 2018). “Bird collisions with power lines: State of the art and priority areas for research”. In: *Biological Conservation* 222. DOI: 10.1016/j.biocon.2018.02.029.
- Bertran, E. and A. Sánchez-Cerdà (2016). *On the Tradeoff Between Electrical Power Consumption and Flight Performance in Fixed-Wing UAV Autopilots*.
- Beurskens, L., E. Mast, and I. Pisca (May 2018). *Conceptadvies SDE+ 2019. Windenergie op land*.
- Blom, T. and A.A.J.F. van den Dobbelsteen (2017). *CO<sub>2</sub>-roadmap TU Delft*.
- Brombach, J., T. Schröter, A. Lücken, and D. Schulz (2012). *Optimizing the Weight of an Aircraft Power Supply System through a +/- 270 VDC Main Voltage*.
- Cherubini, A. (2017). *Advances in Airborne Wind Energy and Wind Drones*.
- Cherubini, A., A. Papini, R. Vertechy, and M. Fontana (2015). *Airborne Wind Energy Systems: A review of the technologies*, pp. 1461–1476.
- Corporaal, D.R. (Dec. 2017). 6.2.1 *De lierstart*. Zweefvlieg opleiding. Friesland.
- Deperrois, A. (2019). *XFLR5*. Version 6.47. URL: <https://xflr5.tech/>.
- Divya, K.C. and J. Ostergaard (2009). *Battery energy storage technology for power systems - An overview*, pp. 511–520.
- Doshi, A. (2017). *Banana fiber to fabric process optimization for improving its spinnability*.
- DSM Dyneema (Feb. 2013). *Customer Information Sheet: DSM Dyneema protects people and the environment*.
- Eijkelfhof, D. (2019). *Design and Optimisation Framework of a Multi-MW Airborne Wind Energy Reference System*. Delft.
- European Commission (2011). *Wind energy developments and Natura 2000. EU Guidance on wind energy development in accordance with the EU nature legislation*. Publications Office of the European Union. DOI: 10.2779/98894.

- European Commission (2013). "Commission recommendations of 9 April 2013 on the use of common methods to measure and communicate the life cycle environmental performance of products and organisations". In: URL: <https://eur-lex.europa.eu/legal-content/EN/TXT/?uri=CELEX:32013H0179>.
- Faggiani, P. and R. Schmehl (2018). "Airborne Wind Energy". In: Springer-Verlag Berlin Heidelberg. Chap. 16: Design and Economics of a Pumping Kite Wind Park.
- Financieel Jaarverslag 2018* (Apr. 2019). Delft.
- Francis, R., R. Vincent, J. Noël, P. Tremblay, D. Desjardins, A. Cushley, and M. Wallace (Aug. 2011). *The Flying Laboratory for the Observation of ADS-B Signals*.
- Francis, R., R. Vincent, J.M. Noel, P. Tremblay, D. Desjardins, A. Cushley, and M. Wallace (2011). *The flying laboratory for the observation of adsb signals*.
- Garcia, S.J. (Oct. 31, 2019). *Project guide design synthesis exercise. harvesting energy from high up*. Delft University of Technology. Delft.
- Gjestland, T. (June 2008). *Background noise levels in Europe*.
- Granta Design Limited (2019). *CES EduPack 2019*. Cambridge, United Kingdom. URL: <https://grantadesign.com/education/ces-edupack/>.
- Gur, O. (Jan. 2013). *Practical Propeller Efficiency Model*.
- Hall, P.J. and E.J. Bain (2008). *Energy-storage technologies and electricity generation*, pp. 4352–4355.
- Hamann, R.J. and M.J.L. van Tooren (Jan. 2016). *Systems engineering & technical management techniques - part II*.
- Hasnaina, S.M. (1998). *Review on sustainable thermal energy storage technologies, part 1: heat storage materials and techniques*.
- Heyson, H.H., G.D. Riebe, and C.L. Fulton (1977). *Theoretical parametric study of the relative advantages of winglets and wing-tip extensions*.
- Al-Hussaini, A.A. (2013). *Aircraft Design*.
- Ibrahim, H., A. Ilinca, and J. Perron (2008). *Energy storage systems – Characteristics and comparisons*.
- Jansen, R.H., C. Bowman, A. Jankovsky, R. Dyson, and J.L. Felder (2017). *Overview of NASA Electrified Aircraft Propulsion Research for Large Subsonic Transports*.
- Jensen, C., T. Panduro, and T. Lundhede (Nov. 2014). "The Vindication of Don Quixote: The Impact of Noise and Visual Pollution from Wind Turbines". In: *Land Economics* 90, pp. 668–682. DOI: 10.3368/le.90.4.668.
- Jiang, G., L. Chen, S. Zhang, and H. Huang (2018). "Superhydrophobic SiC/CNTs Coatings with Photothermal Deicing and Passive Anti-Icing Properties". In: *ACS Applied Materials & Interfaces* 10.42, pp. 36, 505–36, 511. DOI: 10.1021/acsami.8b11201.
- Jonkers, H.M., A. Thijssen, G. Muyzer, O. Copuroglu, and E. Schlangen (2010). "Application of bacteria as self-healing agent for the development of sustainable concrete". In: *Ecological Engineering* 36 (2), pp. 230–235. DOI: <https://doi.org/10.1016/j.ecoleng.2008.12.036>.
- Khazdozian, H., R. Hadimani, and D. Jiles (Nov. 2014). *Size reduction of permanent magnet generators for wind turbines with higher energy density permanent magnets*, pp. 1–6. DOI: 10.1109/NAPS.2014.6965439.
- Korsgaard, S., A.B. Kjaer, S.S. Nielsen, and L. Demsa (Sept. 2019). *Acoustic Noise Analysis of a Magnetically Geared Permanent Magnet Generator*. DOI: 10.1109/ECCE.2019.8912892.
- Kumarasena, S., N.P. Jones, P. Irwin, and P. Taylor (Feb. 2005). *Wind-Induced Vibration of Stay Cables*. URL: <https://rosap.ntl.bts.gov/view/dot/38398>.
- Laithwaite, E.R. and L.L. Freris (1980). *Electrical power: its generation, transmission and use*.
- Mazzon, E., P. Guigues, and J.P. Habas (2020). "Biobased structural epoxy foams derived from plant-oil: Formulation, manufacturing and characterization". In: *Industrial Crops and Products*.
- Meyers, J. and C. Meneveau (2012). "Optimal turbine spacing in fully developed wind farm boundary layers". In: *Wind Energy* 15.2, pp. 305–317. DOI: 10.1002/we.469.

- Milachowski, C., T. Stengel, and C. Gehlen (2011). *Life cycle assessment for road construction and use*. European Concrete Paving Association. URL: [https://www.eupave.eu/wp-content/uploads/eupave\\_life\\_cycle\\_assessment.pdf](https://www.eupave.eu/wp-content/uploads/eupave_life_cycle_assessment.pdf).
- Monteiro, P., S. Miller, and A. Horvath (2017). "Towards sustainable concrete." In: *Nature Matter* 16, pp. 698–699. DOI: <https://doi.org/10.1038/nmat4930>.
- More, S.R. (July 2011). "Aircraft Noise Characteristics and Metrics". PhD thesis. Partnership for AiR Transportation Noise and Emissions Reduction.
- Nieuwenhuizen, E. (2015). *Differences in noise regulations for wind turbines in four European countries*.
- Niu, M.C.Y. (1988). *Airframe Structural Design. Practical Design Information and Data on Aircraft Structures*. Conmilit Press Ltd.
- Oliviero, F. (2017a). *ADSEE II: Aircraft aerodynamic analysis - lift & drag*. Delft.
- (2017b). *ADSEE II: Aircraft aerodynamic analysis-fundamentals*. Delft.
- Pereda Albarrán, M.Y., M. Kreimeier, W. Enders, and E. Stumpf (Jan. 2020). "Noise evaluation of battery powered small aircraft". In: *CEAS Aeronautical Journal* 11.1, pp. 125–135. ISSN: 1869-5590. DOI: 10.1007/s13272-019-00404-2. URL: <https://doi.org/10.1007/s13272-019-00404-2>.
- Potgieter, J. and M. J. Kamper (2012). "Design of new concept direct grid-connected slip-synchronous permanent-magnet wind generator". In: *IEEE Transactions on Industry Applications* 48.3, pp. 913–922.
- Rapp, S. and R. Schmehl (July 2018). *Vertical Takeoff and landing of flexible ing kite power system*.
- Raymer, Daniel (2012). *Aircraft design: a conceptual approach*. American Institute of Aeronautics and Astronautics, Inc.
- Rijksoverheid (Feb. 2018). *kaarten vliegroutes Lelystad Airport*.
- Sadraey, M. (2012). *Aircraft Design: A System Engineering Approach*. Wiley Publications. Chap. Chapter 12, Design of control surfaces.
- Schmehl, R. (2018). *Airborne Wind Energy. Advances in Technology Development and Research*. Springer-Verlag Berlin Heidelberg. DOI: 10.1007/978-981-10-1947-0.
- Schmehl, R., M. Diehl, and U. Ahrens (2013). *Airborne Wind Energy*. Springer-Verlag Berlin Heidelberg. DOI: 10.1007/978-3-642-39965-7.
- Seung, T. (2006). *Ultimate ower optimizing for a 'stand alone' landing gear system of more electric aircraft*.
- Shanker, T. and R.K. Singh (2012). "Wind energy conversion system: A review". In: *2012 Students Conference on Engineering and Systems*. IEEE, pp. 1–6.
- Siemens (n.d.). *Transformers*.
- Sinke, J. (May 2014). *Lean manufacturing, chapter 10*.
- Sukmawan, R., H. Takagi, and A.N. Nakagaito (2016). "Strength evaluation of cross-ply green composite laminates reinforced by bamboo fiber". In: *Composites Part B Engineering*.
- TenneT (Dec. 2008). *Aansluiten op het Nederlandse hoogspanningsnet*.
- Torenbeek, E. (Dec. 1982). *Synthesis of subsonic airplane design*.
- Volat, C., M. Farzaneh, and A. Leblond (June 2005). "De-icing/Anti-icing Techniques for Power Lines: Current Methods and Future Direction". In:
- Vos, R. and J.A. Melkert (2018). *ADSEE I: Landing Gear and Empennage Design*. Delft.
- Vos, R., J.A. Melkert, and B.T.C. Zandbergen (2018). *ADSEE I: The Design of the Fuselage*. Delft.
- Vreeswijk, T. van, M. van Roomen, E. van Winden, H. Dotinga, and N. Korporaal (2019). *Important Bird Areas in the Netherlands 2019. A revision of the national IBA inventory*. Vogelbescherming Nederland and Sovon Dutch Centre for Field Ornithology.
- Williams, B.J. and B.A. Raymis (Nov. 2011). *Solar power array with maximized panel power extraction*. US Patent 8,053,929.
- Yu-xing, P., C. Xiang-dong, Z. Zhen-cai, W. Da-gang, G. Xian-sheng, Z. Sheng-yong, S. Shi-sheng, and X. Wen-xue (2016). "Sliding friction and wear behavior of winding hoisting rope in ultra-deep coal mine under different conditions". In: *Wear* 368-369, pp. 423–434. ISSN: 0043-1648. DOI: <https://doi.org/>

10.1016/j.wear.2016.10.012. URL: <http://www.sciencedirect.com/science/article/pii/S004316481630463X>.

Yoon, J.N. (2007). *Air Force Fighters & Tailhooks*. URL: <https://www.rijksoverheid.nl/documenten/rapporten/2016/02/15/operationele-energie-strategie>.

Zhenlong, w. and Yihua C. (2016). "Numerical simulation of airfoil aerodynamic performance under the coupling effects of heavy rain and ice accretion". In: *Advances in Mechanical Engineering* 8, pp. 1–9. DOI: 10.1177/1687814016667162.

Functional flow diagram

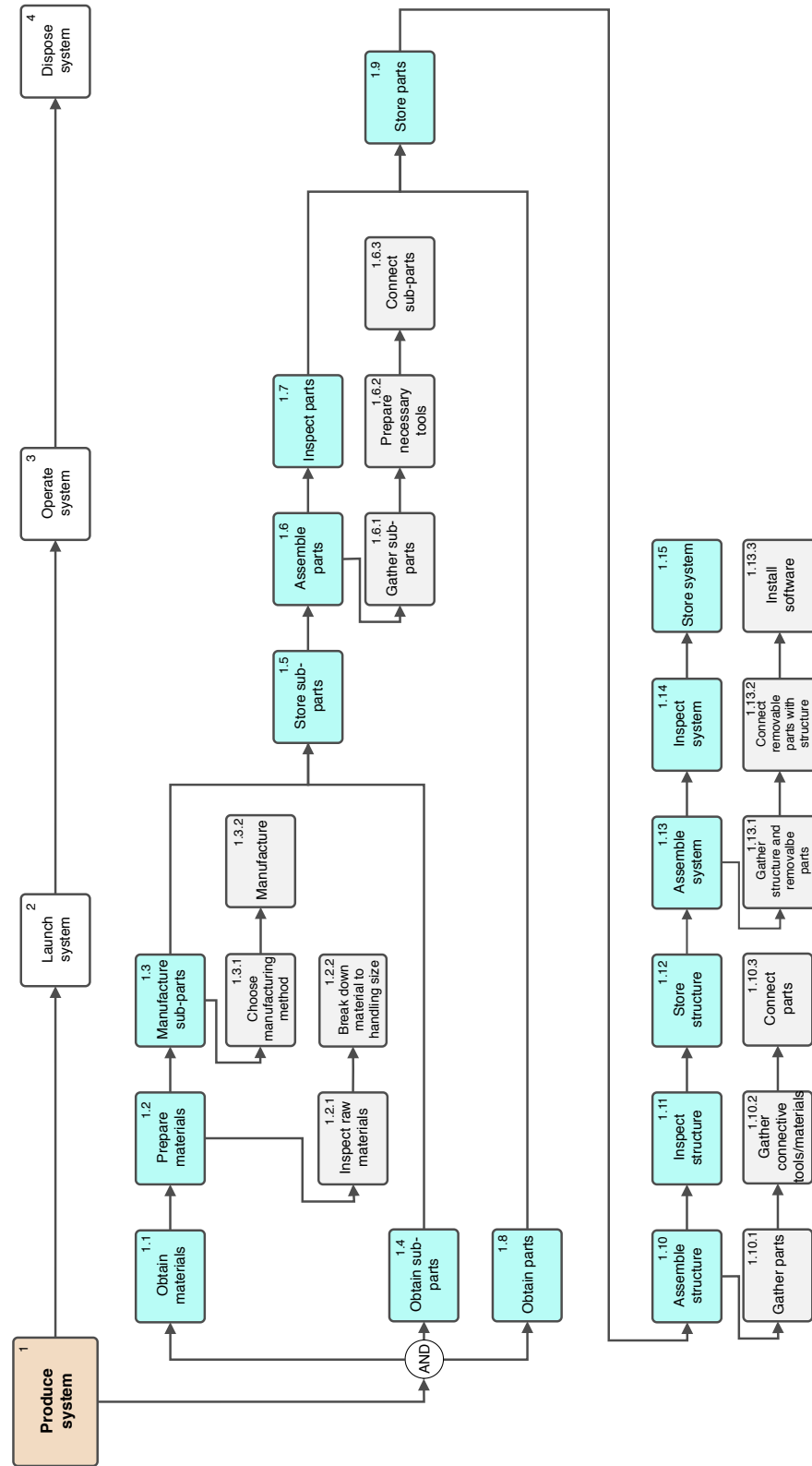


Figure A.1: Functional flow diagram for the production phase of the system.

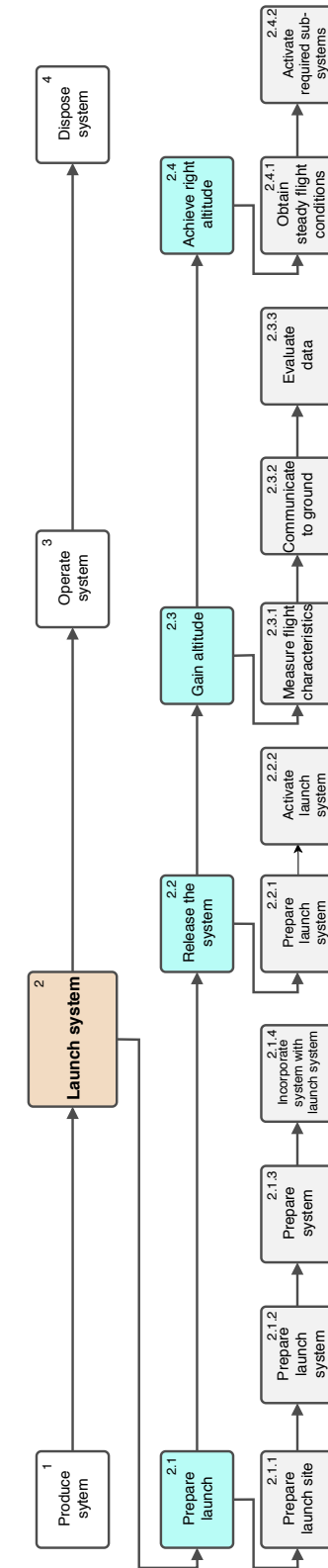


Figure A.2: Functional flow diagram for the launch phase of the system.

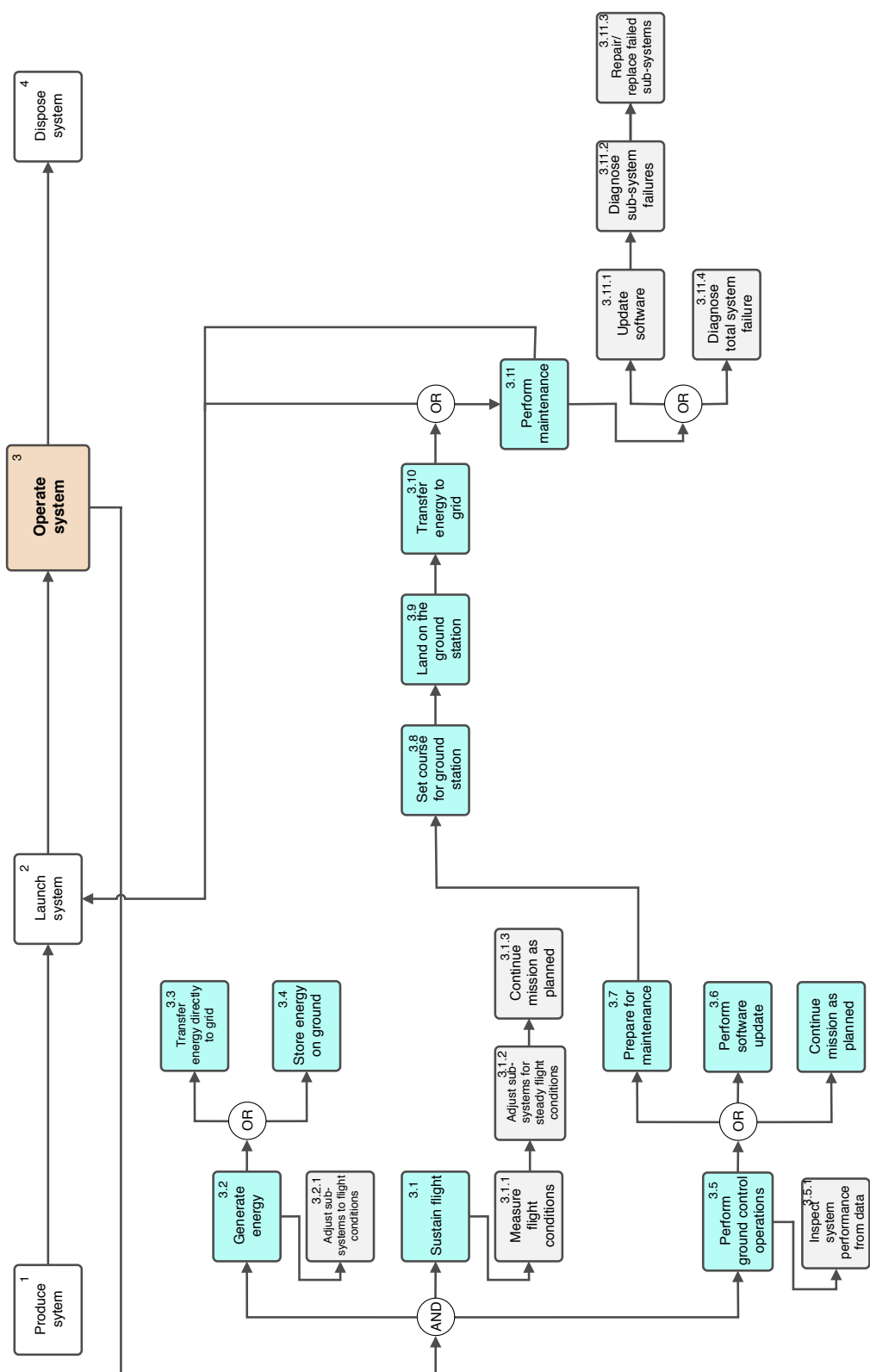


Figure A.3: Functional flow diagram for the operations phase of the system.

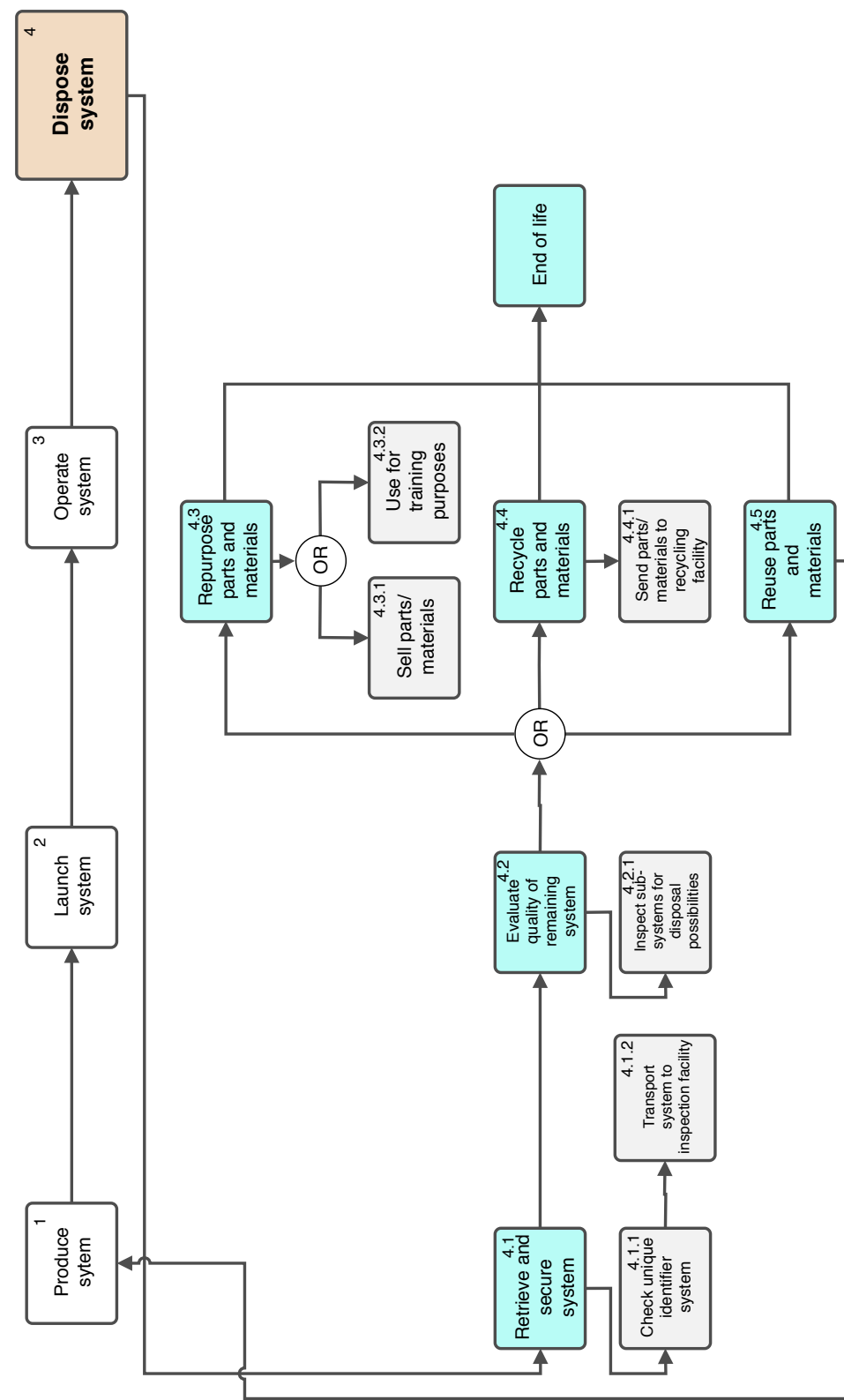


Figure A.4: Functional flow diagram for the disposal phase of the system.

# Functional breakdown structure

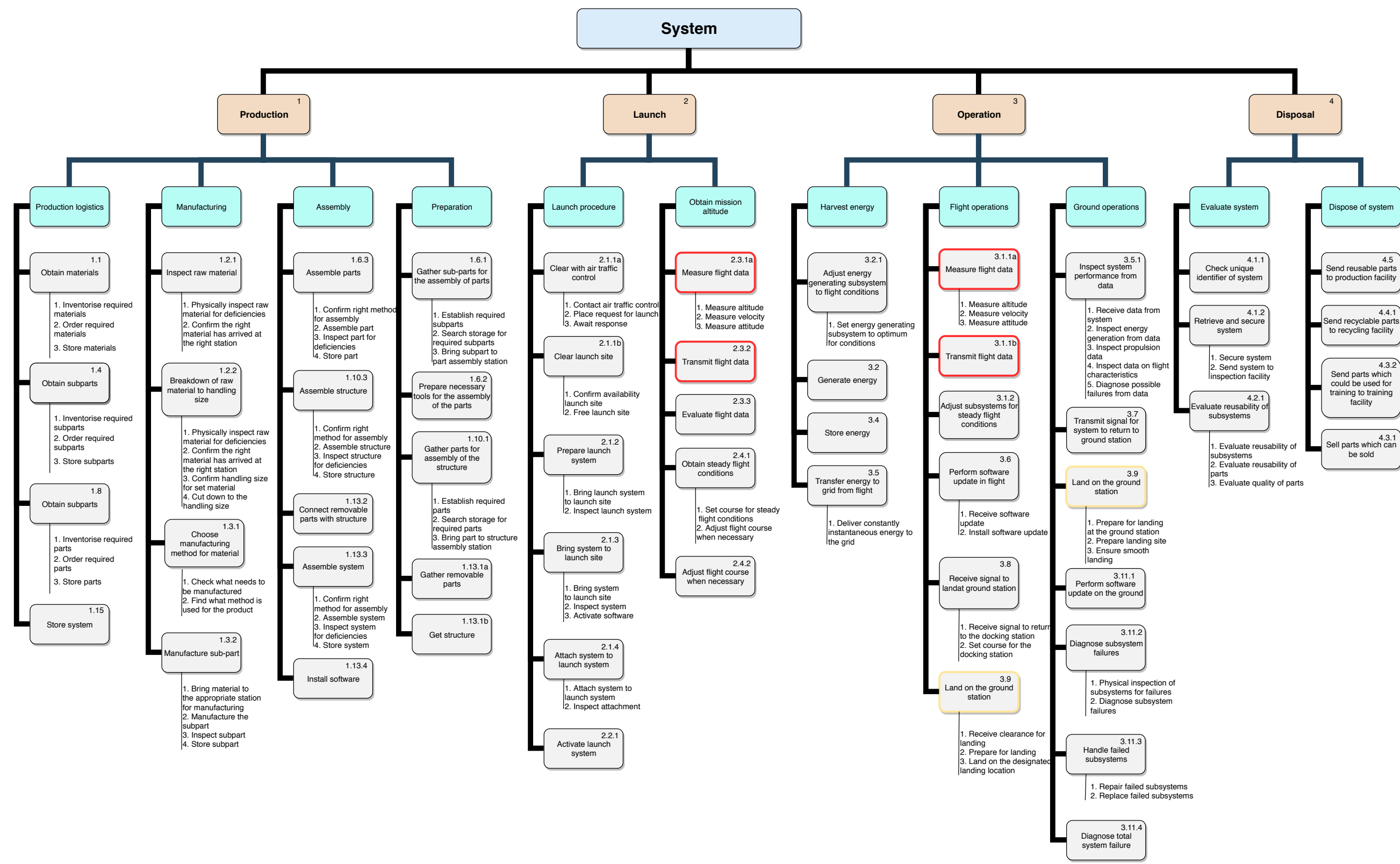


Figure B.1: Functional breakdown structure of system

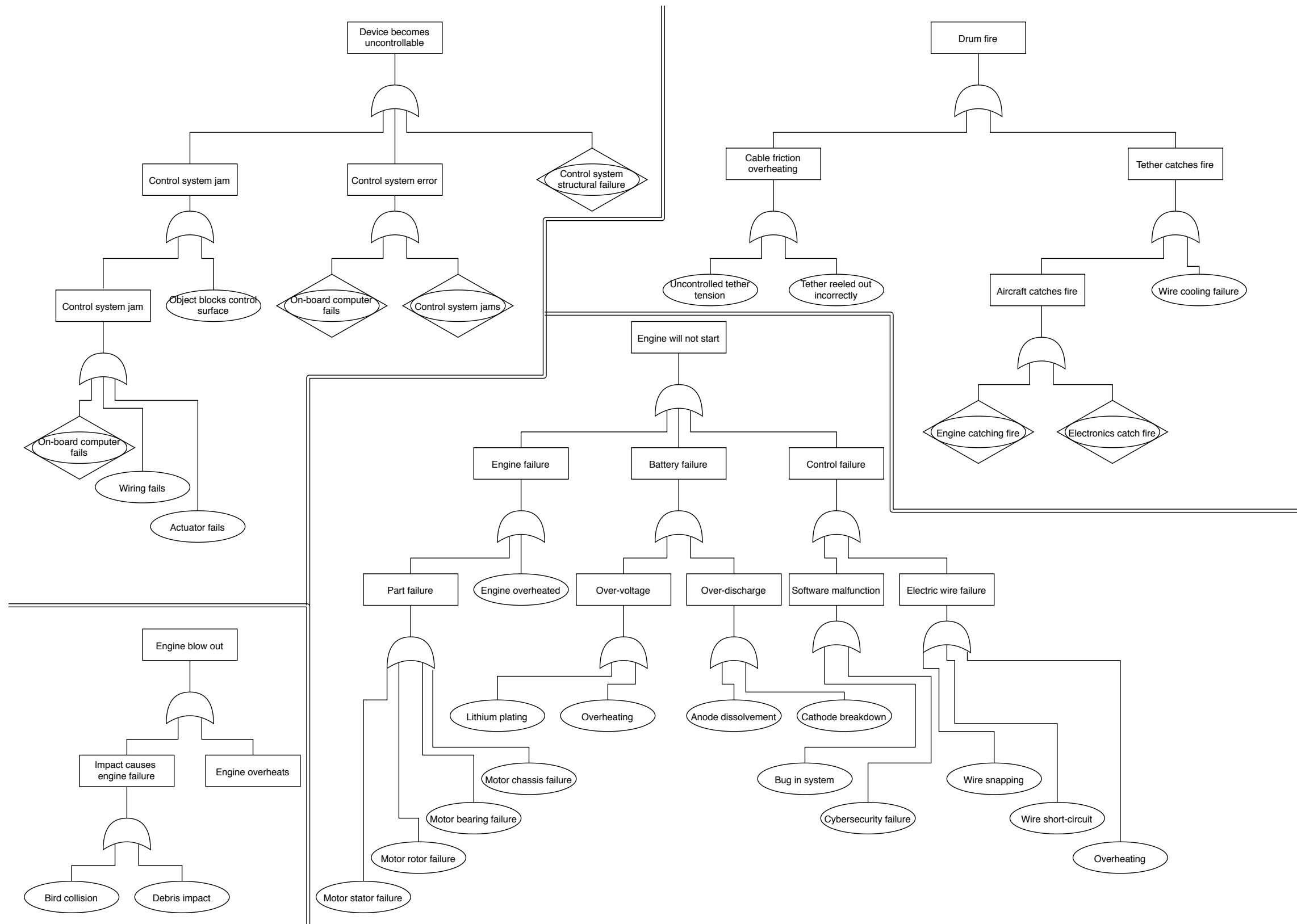


Figure C.1: Fault Tree Analysis

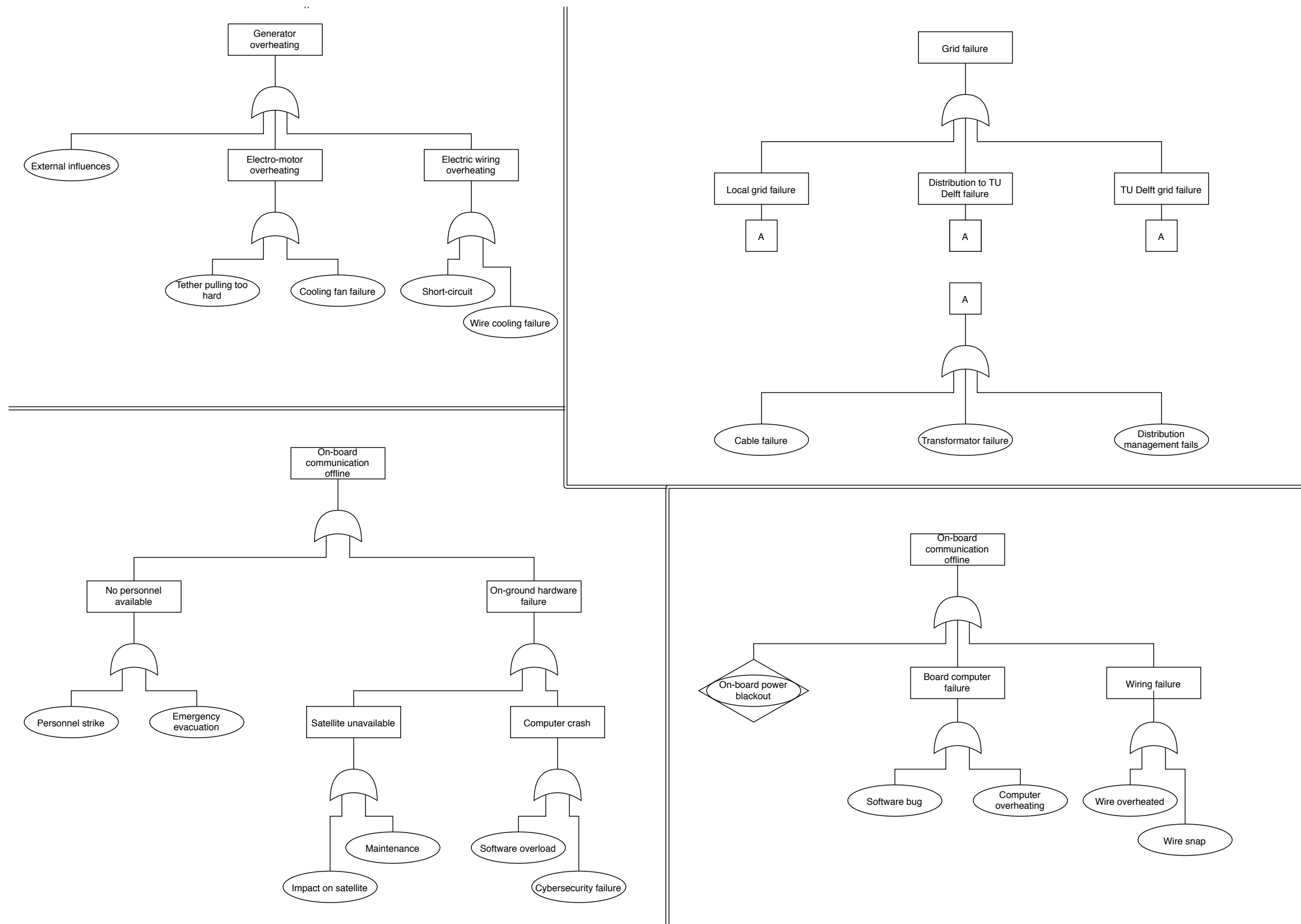


Figure C.2: Fault Tree Analysis

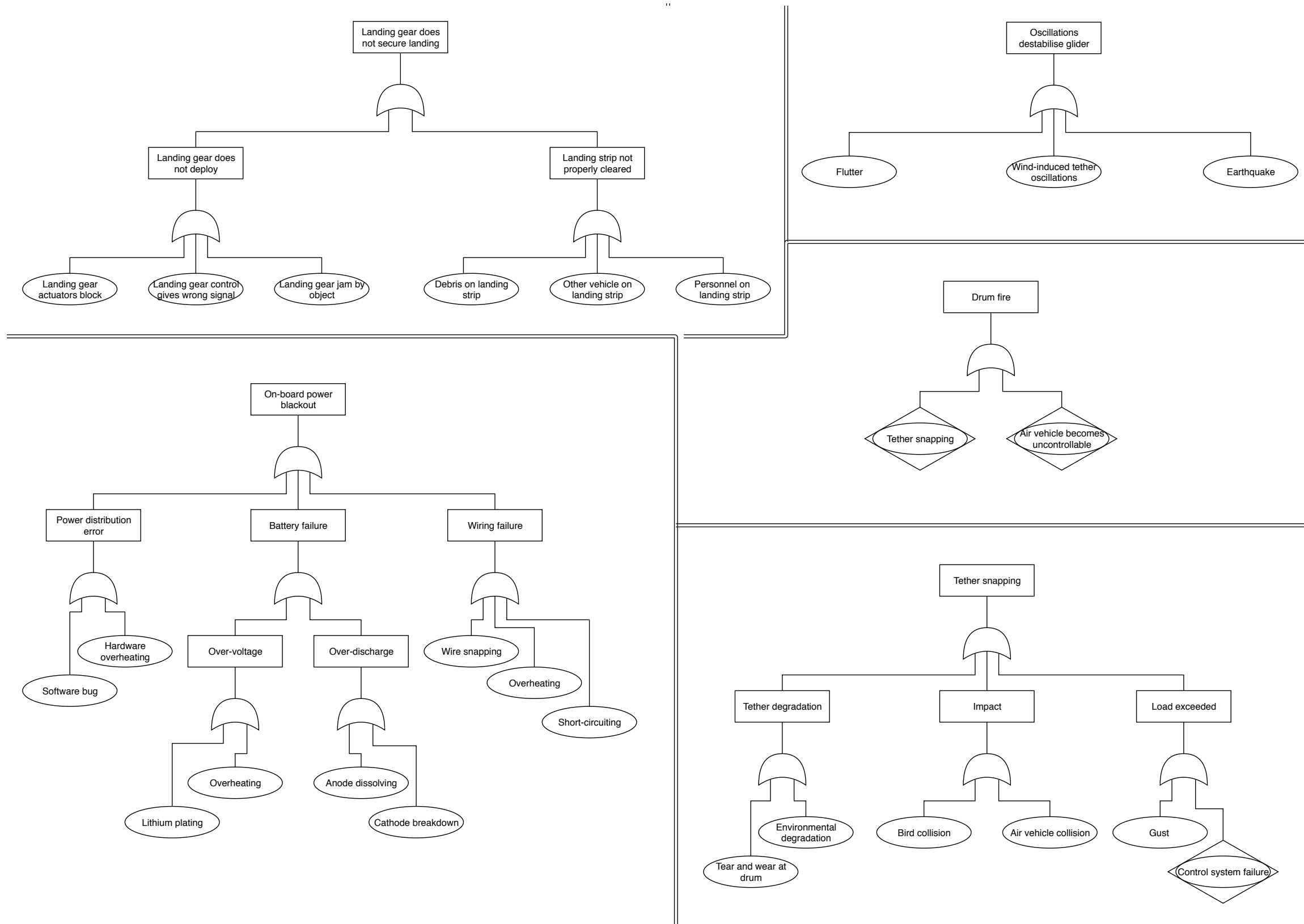


Figure C.3: Fault Tree Analysis

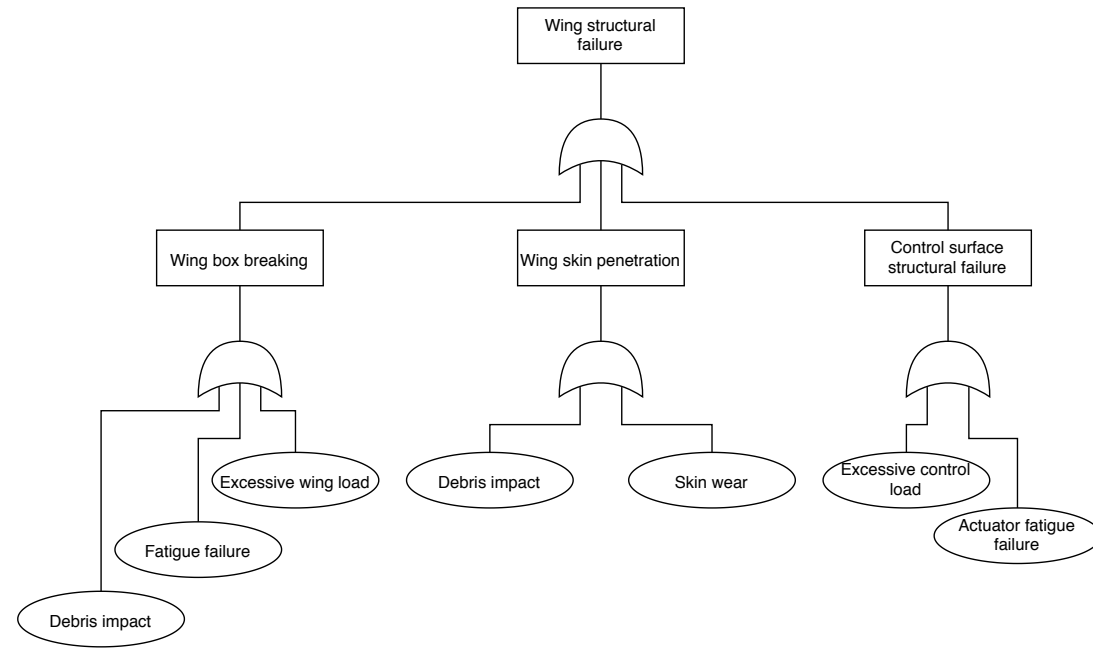


Figure C.4: Fault Tree Analysis

# D FMECA

Identification number	Item/functional identification	Function	Failure mode & causes	Severity class	Failure probability	Failure effect probability	Failure mode ratio	Failure rate	Operating time	Failure mode criticality	Item criticality	Safety risk	Risk mitigation
EHAC-FMEA-01-A	On-board battery	Provide power to on-board electronics	Lithium plating	4	D	D	0.25	0.005	1	6.25E-06	5.73E-04	1.00E-03	Prevent overvoltage of batteries
EHAC-FMEA-01-B			Overheating	2	D	B	0.25	0.15	1	1.88E-04		3.00E-03	Provide cooling and measure battery temperature
EHAC-FMEA-01-C			Copper anode dissolves in electrolyte	4	D	A	0.25	0.3	1	3.75E-04		1.00E-03	Never completely discharge the system
EHAC-FMEA-01-D			Cathode breakdown	4	E	A	0.25	0.3	1	3.75E-06		1.00E-05	Never completely discharge the system
EHAC-FMEA-02-A	Electric motor	Propel aircraft	Motor stator fails	4	D	A	0.2	0.3	0.2	6.00E-05	1.21E-04	1.00E-03	Regular scheduled preventive maintenance
EHAC-FMEA-02-B			Motor rotor fails	4	D	A	0.2	0.3	0.2	6.00E-05		1.00E-03	Regular scheduled preventive maintenance
EHAC-FMEA-02-C			Propellor blade structural failure	3	E	A	0.1	0.3	0.2	3.00E-07		2.00E-05	Regular scheduled preventive maintenance
EHAC-FMEA-02-E			Motor bearing fails	2	E	A	0.06	0.3	0.2	1.80E-07		3.00E-05	Regular scheduled preventive maintenance
EHAC-FMEA-02-F			Debris collision	3	E	C	0.04	0.05	0.2	2.00E-08		2.00E-05	Take system down when risk of debris collision arises
EHAC-FMEA-02-G			Cooling fails	3	E	B	0.25	0.15	0.2	3.75E-07		2.00E-05	Temperature measurements at the motor
EHAC-FMEA-02-H			Bird collision	3	D	B	0.15	0.15	0.2	2.25E-07		2.00E-03	Make individual system unattractive for birds and include scarecrow
EHAC-FMEA-03-A	Tether	Connect aircraft to ground station	Tether degradation due to weather	4	C	B	0.25	0.15	1	1.88E-03	8.82E-03	1.00E-02	Apply protective coating and take down system during high risk weather scenarios
EHAC-FMEA-03-B			Air vehicle collision	2	D	A	0.01	0.3	1	1.50E-05		3.00E-03	Develop emergency escape plan for aircraft
EHAC-FMEA-03-C			Tether tears at drum	4	C	A	0.45	0.3	1	6.75E-03		1.00E-02	Aircraft can land without tether
EHAC-FMEA-03-D			Bird collision	2	C	E	0.07	0.00005	1	1.75E-07		3.00E-02	Make individual system unattractive for birds and include scarecrow
EHAC-FMEA-03-E			Load exceeds max load due to wind gusts	4	D	C	0.07	0.05	1	1.75E-05		1.00E-03	Measure wind speeds at altitude
EHAC-FMEA-03-F			Excessive load due to control malperformance	3	D	C	0.05	0.05	1	1.25E-05		2.00E-03	Emergency plan for remainder system
EHAC-FMEA-03-G			Tethers tangling up	2	D	A	0.1	0.3	1	1.50E-04		3.00E-03	Decoupling option at aircraft
EHAC-FMEA-04-A	Landing gear	Support aircraft retrieval	On-board computer does not activate landing gear	3	E	B	0.3	0.15	0.005	1.13E-08	2.96E-06	2.00E-05	Back-up overwrite system
EHAC-FMEA-04-B			Object blocking landing gear	3	E	A	0.1	0.3	0.005	7.50E-09		2.00E-05	Enable landing without landing gear
EHAC-FMEA-04-C			Landing gear actuator structurally fails	3	D	A	0.35	0.3	0.005	2.63E-06		2.00E-03	Regular scheduled preventive maintenance
EHAC-FMEA-04-D			Load at landing exceeds max load	3	D	C	0.25	0.05	0.005	3.13E-07		2.00E-03	Design landing gear to be fail safe
EHAC-FMEA-05-A	Landing strip	Accomodate safe landing space	Other vehicles on landing strip	2	D	B	0.4	0.15	0.005	1.50E-06	3.25E-06	3.00E-03	Clear landing strip way ahead of time
EHAC-FMEA-05-B			Debris on landing strip	3	D	C	0.2	0.05	0.005	2.50E-07		2.00E-03	Always have a clean up crew available when landing
EHAC-FMEA-05-C			Personnel on landing strip	1	D	B	0.4	0.15	0.005	1.50E-06		4.00E-03	Strict rules regarding clearing personnel fom strip
EHAC-FMEA-06-A	Power grid	Conduct energy to the TU Delft	High-voltage cable snapping	4	E	D	0.1	0.005	1	2.50E-08	1.35E-05	1.00E-05	On-site storage
EHAC-FMEA-06-B			Net blackout	4	E	A	0.45	0.3	1	6.75E-06		1.00E-05	On-site storage
EHAC-FMEA-06-C			Transformer station overheating	4	E	A	0.45	0.3	1	6.75E-06		1.00E-05	On-site storage
EHAC-FMEA-07-A	Wing	Provide lift	Impact	2	D	C	0.35	0.05	1	8.75E-05	3.17E-04	3.00E-03	Add scarecrow to the system and do not fly when high impact risk occurs
EHAC-FMEA-07-B			Fatigue	3	E	B	0.15	0.15	1	1.13E-06		2.00E-05	Regular scheduled preventive maintenance
EHAC-FMEA-07-C			Excessive loads	2	E	A	0.2	0.3	1	3.00E-06		3.00E-05	Land system when excessive load scenario occurs
EHAC-FMEA-07-D			Skin wear	3	D	B	0.3	0.15	1	2.25E-04		2.00E-03	Regular scheduled preventive maintenance
EHAC-FMEA-08-A	Ground communication	Provide ground station with data	National communication system blackout	3	E	A	0.15	0.3	1	2.25E-06	9.75E-06	2.00E-05	Autopilot to land
EHAC-FMEA-08-B			Software overload	4	E	B	0.3	0.15	1	2.25E-06		1.00E-05	Autopilot is able to operate for safe time
EHAC-FMEA-08-C			Hostile take-over	1	E	A	0.15	0.3	1	2.25E-06		4.00E-05	Back-up overwrite system
EHAC-FMEA-08-D			Personnel evacuation	4	E	B	0.1	0.15	1	7.50E-07		1.00E-05	Autopilot is able to operate for safe time
EHAC-FMEA-08-E			Personnel strike	4	E	B	0.3	0.15	1	2.25E-06		1.00E-05	Secure PR well
EHAC-FMEA-08-A	On-board communications	Manage on-board apparatus	On-board wire snaps from impact	4	E	C	0.1	0.05	0.5	1.25E-07	6.56E-05	1.00E-05	Add scarecrow to the system and do not fly when high impact risk occurs
EHAC-FMEA-08-B			Short circuit	3	D	C	0.5	0.05	0.5	6.25E-05		2.00E-03	Regular scheduled preventive maintenance
EHAC-FMEA-08-C			On-board computer overheats	3	E	A	0.4	0.3	0.5	3.00E-06		2.00E-05	Temperature sensors at computer

Logistics flow diagram

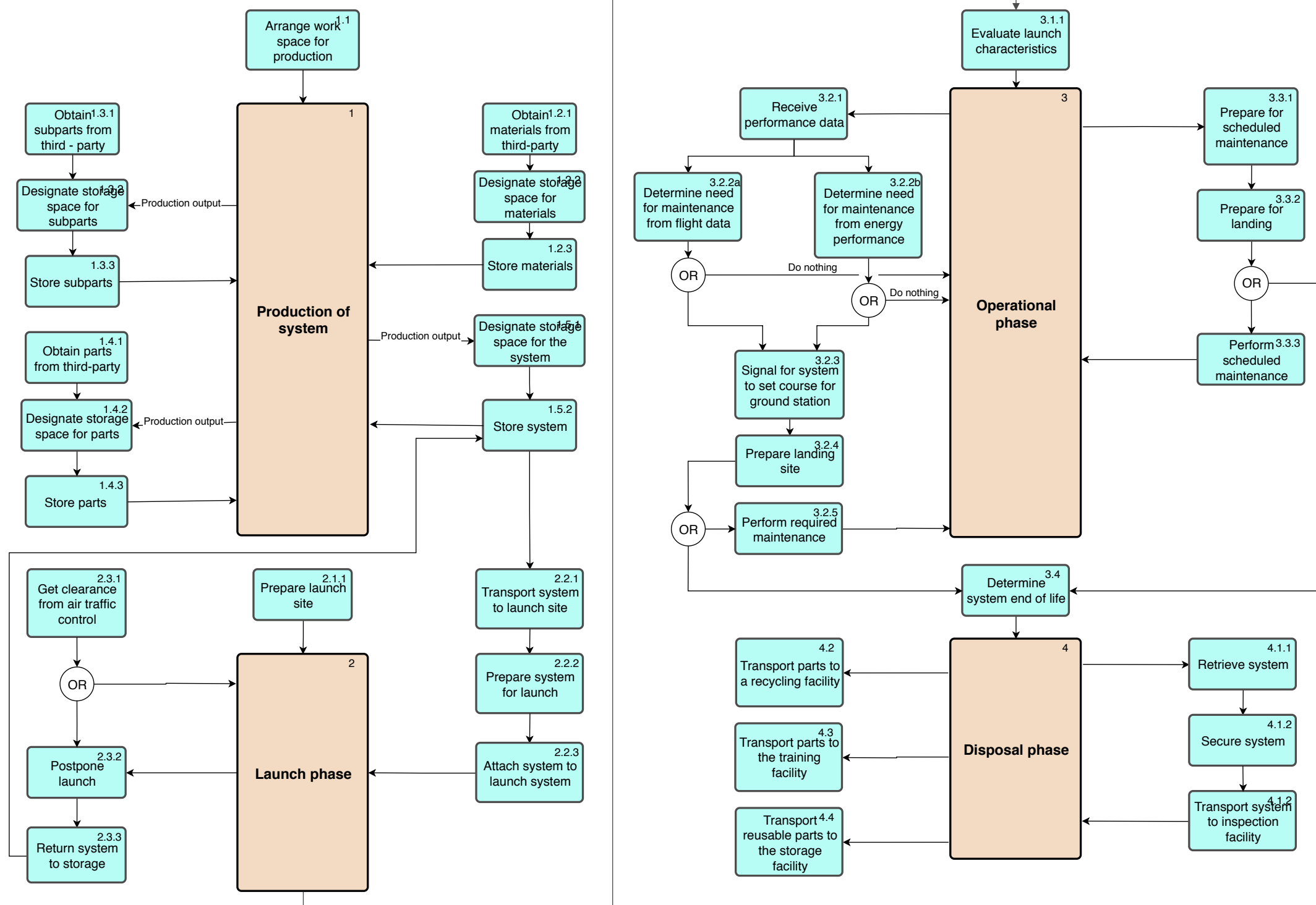


Figure E.1: Logistics flow diagram of system

Cost breakdown structure

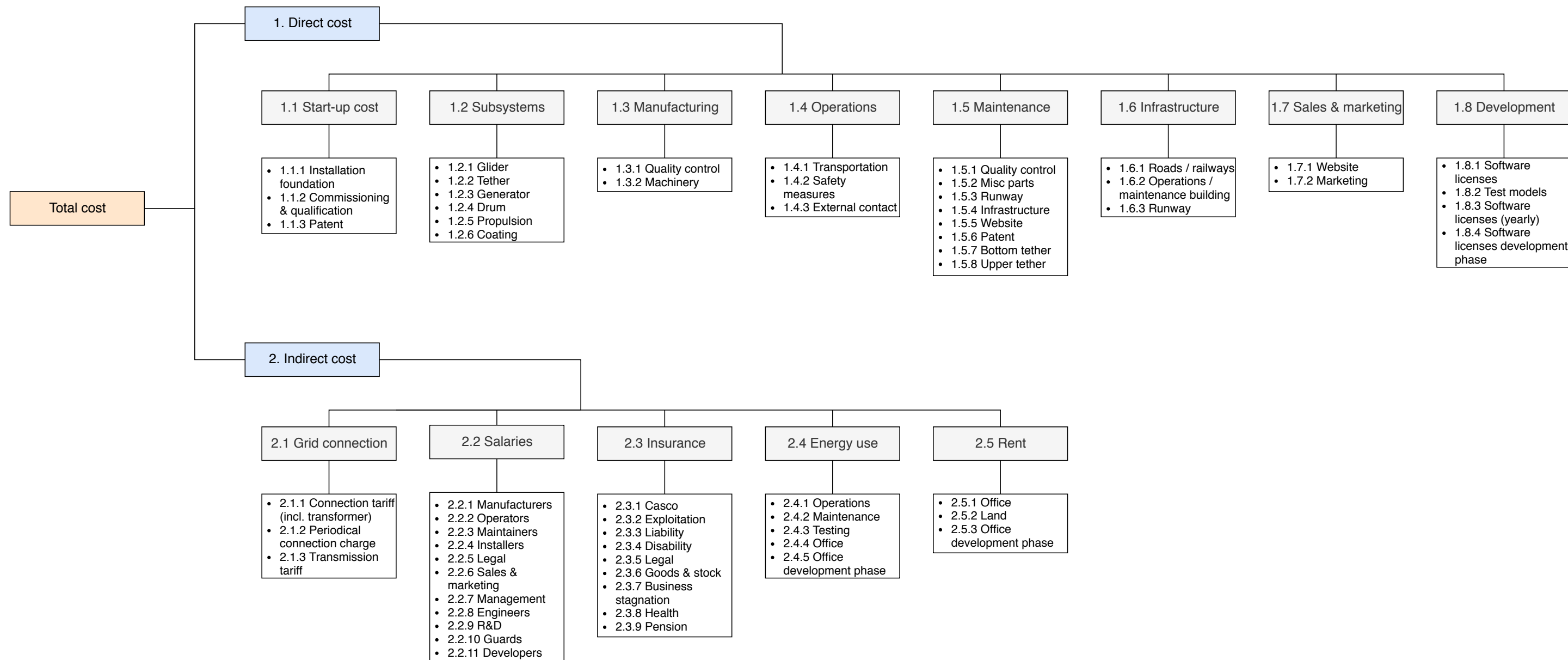


Figure E1: Cost breakdown structure

Table G.1: Project Gantt chart

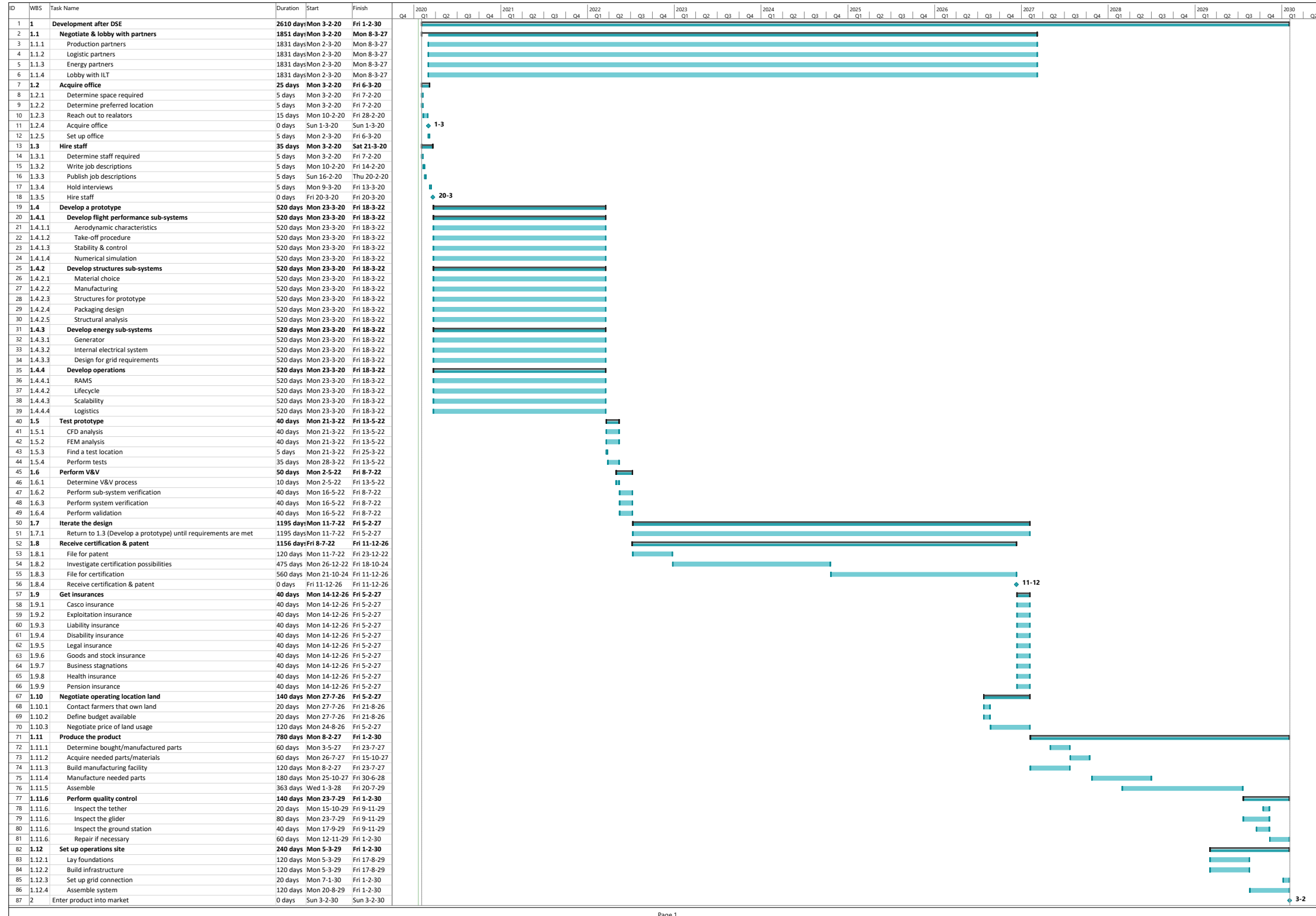


Figure H.1: Technical drawing of the glider using CATIA

